A Centrifugal Microfluidic Platform for Capturing, Assaying and Manipulation of Beads and Biological Cells

Robert Burger (Dipl. Ing.)

Thesis submitted in partial fulfillment of the requirements for the degree of

Doctor of Philosophy

July 2012

Research Supervisor: Prof. Jens Ducrée

Co-Supervisor: Dr. Nuno Reis

Biomedical Diagnostics Institute / School of Physical Sciences

Dublin City University

Declaration

I hereby certify that this material, which I now submit for assessment on the programme of study leading to the award of Doctor of Philosophy is entirely my own work, that I have exercised reasonable care to ensure that the work is original, and does not to the best of my knowledge breach any law of copyright, and has not been taken from the work of others save and to the extent that such work has been cited and acknowledged within the text of my work.

Signed: _____ Date: _____

(Robert Burger, ID: 58121463)

Abstract

Microfluidics is deemed a field with great opportunities, especially for applications in medical diagnostics. The vision is to miniaturize processes typically performed in a central clinical lab into small, simple to use devices – so called lab-on-a-chip (LOC) systems. A wide variety of concepts for liquid actuation have been developed, including pressure driven flow, electro osmotic actuation or capillary driven methods.
This work is based on the centrifugal platform (lab-on-a-disc). Fluid actuation is performed by the forces induced due to the rotation of the disc, thus eliminating the need for external pumps since only a spindle motor is necessary to rotate the disc and propel the liquids inside of the micro structures. Lab-on-a-disc systems are especially promising for point-of-care applications involving particles or cells due to the centrifugal force present in a rotating system. Capturing, assaying and identification of biological cells and microparticles are important operations for lab-on-a-disc platforms, and the focus of this work is to provide novel building blocks towards an integrated system for cell and particle based assays.
As a main outcome of my work, a novel particle capturing and manipulation scheme on a centrifugal microfluidic platform has been developed. To capture particles (biological cells or micro-beads) I designed an array of V-shaped micro cups and characterized it. Particles sediment under stagnant flow conditions into the array where they are then mechanically trapped in spatially well-defined locations. Due to the absence of flow during the capturing process, i.e. particle sedimentation is driven by the artificial gravity field on the centrifugal platform, the capture efficiency of this approach is close to 100% which is notably higher than values reported for typical pressure driven systems. After capturing the particles, the surrounding medium can easily be exchanged to expose them to various conditions such as staining solutions or washing buffers, and thus perform assays on the captured particles. By scale matching the size of the capturing elements to the size of the particles, sharply peaked single occupancy can be achieved. Since all particles are arrayed in the same focal plane in spatially well defined locations, operations such as counting or fluorescent detection can be performed easily. The application of this platform to perform multiplexed bead-based immuno-assays as well as the discrimination of various cell types based on intra cellular and membrane based markers using fluorescently tagged antibodies is demonstrated. Additionally, methods to manipulate captured particles either in batch mode or on an individual particle level have been developed and characterized. Batch release of captured particles is performed by a novel magnetic actuator which is solely controlled by the rotation frequency of the disc. Furthermore, the application of this actuator to rapidly mix liquids is shown. Manipulation of individual particles is performed using an optical tweezers setup which has been developed as part of this work. Additionally, this optical module also provides fluorescence detection capabilities. This is the first time that optical

tweezers have been combined with a centrifugal microfluidic system.
This work presents the core technology for an integrated centrifugal platform to perform cell and particle based assays for fundamental research as well as for point-of-care applications.
The key outputs of my specific work are:

1. Design, fabrication and characterization of a novel particle capturing scheme on a centrifugal microfluidic platform (V-cups) with very high capture efficiency (close to 100%) and sharply peaked single occupancy (up to 99.7% single occupancy).

2. A novel rotation frequency controlled magnetic actuator for releasing captured particles as well as for rapidly mixing liquids has been developed, manufactured and characterized.

3. The V-cup platform has successfully been employed to capture cells and perform multi-step antibody staining assays for cell discrimination.

4. An optical tweezers setup has been built and integrated into a centrifugal teststand, and successful manipulation of individual particles trapped in the V-cup array is demonstrated.

List of Publications

Journal Publications

[1] R. Burger, N. Reis, J. Garcia da Fonseca and J. Ducrée. Plasma Extraction by Centrifugo-Pneumatically Induced Gating of Flow. *Journal of Micromechanics and Microengineering*, **Preparation of Revised Manuscript (to be re-submitted October 2012)**.

[2] R. Burger, H. Cayron, N. Reis, J. Garcia da Fonseca, and J. Ducrée. Centrifugally actuated mixing based on siphon-induced droplet break off and phase shifting. **to be re-submitted**.

[3] C. E. Nwankire, D. S. Chan, J. Gaughran, T. O'Connell, R. Burger, R. A. Gorkin III, and J. Ducrée. Full integration and automation of whole-blood bioassays by centrifugo-pneumatically actuated dissolvable film valves. *Lab on a Chip*, **Under Review (Submitted June 2012)**.

[4] N. Godino, R. Gorkin III, A. V. Linares, R. Burger, and J. Ducrée. Comprehensive Integration of Homogeneous Bioassays via Centrifugo-Pneumatic Cascading. *Lab on a Chip* **(Under Review (Re-Submitted June 2012))**

[5] D. Kirby, J. Siegrist, L. Zavattoni, R. Burger, and J. Ducrée. Centrifugo-magnetophoretic particle separation. *Microfluidics and Nanofluidics*, DOI: 10.1007/s10404-012-1007-6, 2012

[6] R. Burger, D. Kirby, M. Glynn, C. E. Nwankire, M. O'Sullivan, J. Siegrist, D. Kinahan, G. Aguirre, G. Kijanka, R. A. Gorkin III, and J. Ducrée. Centrifugal microfluidics for cell analysis. *Current Opinion in Chemical Biology*, 2012.

[7] R. Burger and J. Ducrée, Handling and analysis of cells and bioparticles on centrifugal microfluidic platforms. *Expert Reviews of Molecular Diagnostics*, 12(4):407-421, 2012.

[8] R. Burger, P. Reith, V. Akujobi, and J. Ducrée. Rotationally controlled magneto-hydrodynamic particle handling for bead-based microfluidic assays. *Microfluidics and Nanofluidics*, DOI: 10.1007/s10404-012-0994-7, 2012

[9] R. Burger, P. Reith, G. Kijanka, V. Akujobi, P. Abgrall, and J. Ducrée. Array-based capture, distribution, counting and multiplexed assaying of beads on a centrifugal microfluidic platform. *Lab on a Chip*, 12(7):1289-1295, 2012.

[10] S. Häberle, L. Nägele, R. Burger, F. Von Stetten, R. Zengerle, and J. Ducrée. Alginate bead fabrication and encapsulation of living cells under centrifugally induced artificial gravity conditions. *Journal of Microencapsulation*, 25(4):267-274, 2008

Conference Publications

2012

[1] R. Burger, Dirk Kurzbuch, Robert Gorkin, Orla Sheils, John O'Leary, Macdara Glynn, Gregor Kijanka, Jens Ducré, Laser-Based Manipulation and Fluorescent Detection of Individual, Centrifugally Arrayed Bioparticles, *Accepted for the 16th International Conference on Miniaturized Systems for Chemistry and Life Sciences (μTAS 2012)*

[2] M. Czugala, D. Maher, R. Burger, K. J. Fraser, J. Ducrée, D. Diamond and F. Benito-Lopez, Portable Lab-on-a-Disc System Integrating Photo-Switchable Micro-Valves for In-Situ Aquatic Environmental Monitoring, *Accepted for the 16th International Conference on Miniaturized Systems for Chemistry and Life Sciences (μTAS 2012)*

[3] D. Kirby, G. Kijanka, J. Siegrist, R. Burger, and J. Ducrée. Immunomagnetic purification of cancer cells from whole blood on a centrifugal microfluidic platform. *Accepted for the 16th International Conference on Miniaturized Systems for Chemistry and Life Sciences (μTAS 2012)*

[4] N. Godino, R. Gorkin III, A. V. Linares, R. Burger, and J. Ducée, A centrifugo-pneumatic cascade for fully integrated and multiplexed biological analysis. In *Proceedings of the 25th IEEE International Conference on Micro Electro Mechanical Systems (MEMS 2012)*, 989-992.

2011

[5] R. Burger, G. Kijanka, O. Sheils, J. OLeary, and J. Ducrée, Arrayed capture, assaying and binary counting of cells in a stopped- flow sedimentation mode. In *Proceedings of the 15th International Conference on Miniaturized Systems for Chemistry and Life Sciences (μTAS 2011)*, 538-540

[6] R. A. Gorkin, R. Burger, D. Kurzbuch, G.G. Donohoe, X. Zhang, M. Czugala, F.B. Lopez, S. ODriscoll, M. Rook, C. McDonagh, D. Diamond, R. OKennedy, and J. Ducrée, Efficient Development Kit for Well-To-Chip Customization and Detection of Colorimetric and Fluorescence Based Microfluidic Immunoassays, In *Proceedings of the 15th International Conference on Miniaturized Systems for Chemistry and Life Sciences (μTAS 2011)*, 924-926.

[7] J. Siegrist, G. Donohoe, M. Sommers, D. Kurzbuch, R. Burger, S. Hearty, J. Murrell, C. Martin, L. Barrett, C. McDonagh, R. OKennedy, and J. Ducrée, *A Centrifugo-Microfluidic Cartridge with Integrated Detection Optics Towards Automated At-Line Bioprocess Monitoring of Immunoglobulin G*, In *Proceedings of the 15th International Conference on Miniaturized Systems for Chemistry and Life Sciences (μTAS 2011)*, 194-196.

[8] J. Siegrist, R. Burger, D. Kirby, L. Zavattoni, G. Kijanka, and J. Ducrée, Stress-Free Centrifugo-Magnetic 2D-Separation of Cancer Cells in a Stopped-Flow Mode, In *Proceedings of the 15th International Conference on Miniaturized Systems for Chemistry and Life Sciences (μTAS 2011)*, 1915-1917.

[9] R. Burger, J. Siegrist, P. Reith, L. Zavattoni, D. Kirby, R. Gorkin, G. Kijanka, and J. Ducrée. Multi-force particle handling and detection strategies on centrifugal microfluidic platforms, In *Proceedings of IEEE-Sensors 2011*, pages 802-804

[10] R. Gorkin, C. Nwankire, J. Siegrist, R. Burger, J. Gaughran, and J. Ducrée, Rotationally Controlled Centrifugo-Pneumatic Valving Utilizing Dissolvable Films, In *Proceedings of IEEE Transducers 2011*, 1276-1279.

[11] J. Siegrist, L. Zavattoni, R. Burger, and J. Ducrée, 2-Dimensional Separation Of Biomimetic Particles By Stopped-Flow Centrifugo-Magnetophoresis, In *Proceedings of IEEE Transducers 2011*, 278-281.

[12] R. Burger, P. Reith, P. Abgrall, J. Ducrée, Integration of High-Efficiency Capture and Magneto-hydrodynamic Retrieval of Particles on a Centrifugal Microfluidic Platform,In *Proceedings of the 24th IEEE International Conference on Micro Electro Mechanical Systems (MEMS 2011)*, 1147-1150.

[13] R.Burger, P. Reith, P. Abgrall, G. Kijanka, J. Ducrée, Multiplexing of highly reproducible, bead-based im- munoassays on a centrifugal microfluidic platform, In *Proceedings of the 24th IEEE International Conference on Micro Electro Mechanical Systems (MEMS 2011)*, 1170-1173.

2009

[14] R. Burger, I.K. Dimov, J. Ducrée, Highly Efficient Single Cell Capturing Under Stagnant Flow Conditions on a Centrifugal Microfluidic Platform, In *The 13th International Conference on Miniaturized Systems for Chemistry and Life Sciences (μTAS 2009)*, 490 492

[15] R. Burger, N. Reis, J.G. Fonseca, J. Ducrée, Blood Separation Based on Pressure Driven Membrane Deflection, In *The 13th International Conference on Miniaturized Systems for Chemistry and Life Sciences (μTAS 2009)*, 122 - 124

[16] G. Kijanka, I. K. Dimov, R. Burger and J. Ducrée, Minimizing stress exposure to cells using novel micro-fluidic cell capture devices. Presented at *Medical Physics and Biomedical Engineering, World Congress 2009, Septem- ber 7-12, Munich, Germany.* (Poster Presentation)

[17] R. Burger, N. Reis, J.G. Fonseca, J. Ducrée, Droplet Mixer Based on Siphon-Induced Flow Discretization and Phase Shifting, In *Proceedings of the 22th IEEE International Conference on Micro Electro Mechanical Systems (MEMS 2009)*, 443-446.

2007

[18] S. Häberle, S. Pausch, R. Burger, S. Lutz, F. von Stetten, R. Zengerle, J. Ducrée, Integration, Automatisierung, und Parallelisierung von Silika-basierten Nukleinsaure-Extraktionen mit dem virtuellen Coriolis-Schalter, In *Proceedings of Mikrosystemtechnik-Kongress 2007, Dresden, Germany*, 465-468.

[19] S. Häberle, S. Pausch, R. Burger, S. Lutz, F. von Stetten, R. Zengerle, and J. Ducrée, Automation of nucleid acid extraction by a coriolis-force actuated droplet router, In *Proceedings of the 11th International Conference on Miniaturized Systems for Chemistry and Life Sciences (TAS 2007)*, 1231-1233.

[20] S. Häberle, L. Naegele, R. Burger, R. Zengerle, J. Ducrée, Alginate Microbead fabrication on an cen- trifugal microfluidics platform, In *Proceedings of the 20th IEEE International Conference on Micro Electro Mechanical Systems (MEMS 2007)*, 497-500.

Book Chapter

[1] R. Burger, M. Kitsara, C. Nwankire and J. Ducrée. Automation of Immunoassays Through Centrifugal Lab-on-a-Disc Platforms, *Novel Approaches in Immunoassays*, Future Science Group, **To be published 2012**

[2] G. Kijanka, R. Burger, I. K. Dimov, R. Padovani, K. Lawler, R. O'Kennedy and J. Ducrée (2011). Recent Developments in Cell-Based Microscale Technologies and Their Potential Application in Personalised Medicine, *Advanced Biomedical Engineering*, Dr. Gaetano Gargiulo (Ed.), ISBN: 978-953-307-555-6, InTech,

Patents

[1] J. Ducrée and R. Burger, A centrifugal capture system. Patent document 12/855,579 (Dublin City Univer- sity), August 12, 2010

[2] R. Burger, J.G. Fonseca, N. Reis, Jet Deflection Device, WO 2010047609

[3] R. Burger, J.G. Fonseca, N. Reis, Liquid Handling, UK Patent P46374GB

Contents

List of Figures

List of Tables

List of Abbreviations

BSA	Bovine serum albumin
CCD	Charge-coupled device
CD	Compact disc
CTC	Circulating tumor cell
DEP	Dielectrophoresis
DF	Dissolvable film
DFR	Dry film resist
DNA	Deoxyribonucleic acid
DVD	Digital versatile disc
ESR-1	Estrogen receptor α
FITC	Fluorescein isothiocyanate
HIV	Human immunodeficiency virus
IgG	mmunoglobulin G
IR	Infrared
LOC	Lab on a chip
MRSA	Methicillin-resistant *Staphylococcus aureus*
NA	Numerical aperture
OTS	Octadecyltrichlorosilane
PBS	Phosphate buffered saline
PC	Polycarbonate
PCR	Polymerase chain reaction
PDMS	Polydimethylsiloxane
PI	Propidium iodide
PMMA	Poly(methyl methacrylate)
POC	Point of care
PS	Polystyrene
RNA	Ribonucleic acid
RPM	Rotations per minute

Chapter 1

Introduction

1.1 Overview

In the past number of decades, miniaturization had a dramatic impact on virtually every aspect of life. The development of the first transistor by Shockley, Bardeen and Brattain at the Bell Labs at the end of the 1940s paved the way to modern microprocessors which enable personal computers capable of performing millions of operations per second. In much the same way as miniaturization in microelectronics brought the computing power of room-sized computer to typical laptops, microfluidics holds the promise to enable highly integrated lab-on-a-chip (LOC) devices which integrate all the steps typically performed in a central lab into a small cartridge. Of particular interest are so called point-of-care (POC) devices which allow testing close to the patient. Application scenarios include self-testing at home (e.g. for the monitoring of chronic diseases), in a general practitioners office or in emergency settings.

There are several motivations to develop POC systems:

1. de-centralized testing (i.e. no need for central laboratories).
2. Applications in resource poor regions such as developing countries where infrastructure is poor and sample transport to centralized facilities is not feasible.
3. Short sample-to-answer time, allowing faster treatment of patients
4. Low sample and reagent consumption.
5. Improved reliability due to automation.
6. Overall cost reduction.

One of the most successful POC diagnostic products today are glucose test strips to measure the glucose level in blood. This rather simple test drastically improves the quality of life for diabetic patients since it enables them to monitor their glucose level and administer the appropriate dose of insulin. Another very successful POC device is the i-STAT system by Abbott [1, 2]. i-STAT is comprised of a handheld reader and disposable cartridges to measure parameters such as electrolytes, blood gases or cardiac markers. Another commercially successful POC system is

the GeneXpert analyzer developed by Cepheid which offers tests for MRSA, *C. difficile* and tuberculosis. A lab-on-a-disc based platform for veterinary as well as for medical diagnostic applications has been developed by Abaxis [3]. Fig. 1.1 shows the i-STAT and Abaxis systems. Furthermore start-up companies such as Radisens [4] and Biosurfit [5] are currently developing lab-on-a-disc based tests.

Figure 1.1: a) shows the i-STAT hand held POC analyzer [6]. b) shows the Piccolo express reader developed by Abaxis [3]

This is only a small section of the current activities in the point-of-care market, and according to a recent review by Chin and colleagues there are at least 32 companies currently active in this field [7].

1.2 Towards an Integrated Point-of-Care System for Cell Analysis

There is a clear need for automated POC systems to perform cell based analysis for applications in medical diagnostics as well as for research settings. In order to develop an integrated POC system, several fluidic "building blocks" are necessary which need to be compatible with each other. The work presented in this thesis is part of an ongoing effort in the Biomedical Diagnostics Institute (BDI) to develop next generation POC systems. In particular research currently focuses on three aspects:

1. Cell separation, concentration and purification

2. Novel valving schemes

3. Cell capture, assaying and counting

1.2.1 Cell Separation, Concentration and Purification

Separating target cells from a background population is a common first step in the cell analysis process chain. Differences in cell-densities are routinely used to separate cell populations. For example, Ficoll density gradient medium is used to separate lymphocytes from erythrocytes using standard centrifuges. One of the cell separation methods currently being developed in our group uses a density gradient based separation method in a microfluidic disc to separate white blood cells from whole blood and provide purified and concentrated cells for subsequent analysis steps [8] Another method uses magnetic micro beads coated with antibodies to specifically label target cells and separate them under stagnant flow conditions using an on-disc magnet [9] (this method is described in more detail in Appendix C.1.

1.2.2 Valving Schemes

Valving is one of the most fundamental operations necessary to integrate complex assays on a fluidic platform. Samples and reagents typically have to be pro-loaded on the disc and sequentially released in a controlled manner without user interaction. The fact that on a centrifugal platform all liquid volumes on the disc are simultaneously exposed to the same artificial gravity field generated by the rotation of the disc makes valving more challenging than in typical pressure driven systems. An ideal valving technology for centrifugal platforms should be actuated without adding complexity to the instrumental setup, in best case being solely controlled by the rotation frequency of the disc and work over a wide range of rotation frequencies, while at the same time yielding at sharply defined burst frequencies.

Very common and simple to implement valving schemes on centrifugal platforms are so-called hydrophobic or hydrophilic valves (passive valves). Hydrophobic valves consist of a constriction of a microchannel which exhibits a hydrophobic surface, thus preventing the liquid from entering the constriction. Hydrophilic valves, on the other hand, consist of a sudden expansion of the channel and the capillary pres-

sure prevents the liquid from advancing into the expansion common to both valving schemes is that the liquid flow resumes once a certain threshold frequency is exceeded [10].

Siphon based valves are also very commonly used on centrifugal platforms due to their robust working principle and ease of fabrication [11, 12]. Compared to the previous valving methods, siphon valves are closed at high rotation frequencies and open when the disc is stopped or spinning below a certain threshold frequency. Common valving concepts are shown in Fig. 1.2

Our group recently developed a novel centrifguo-pneumatic valving scheme. Here

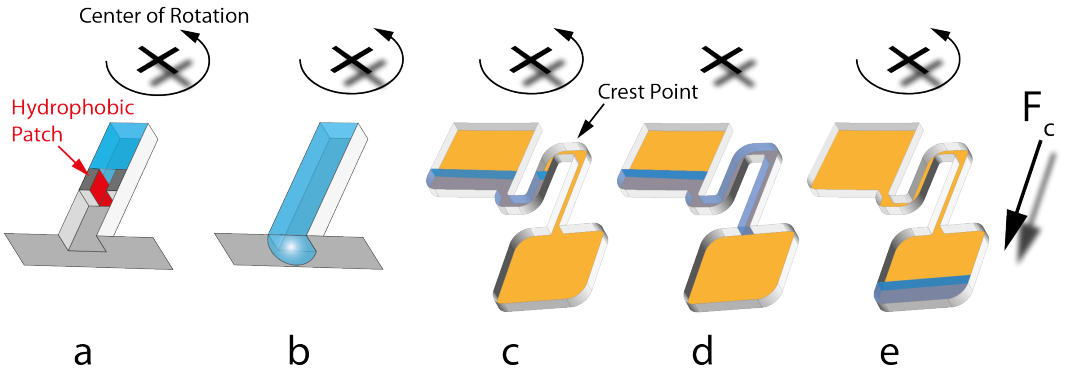

Figure 1.2: Valving schemes for centrifugal microfluidic platforms. a) shows a hydrophobic valve. A hydrophobic constriction in the channel stops the liquid from advancing. To overcome the valve a critical "burst frequency" needs to be exceeded. b) shows a hydrophilic or geometic valve. The advancing liquid stops at a sudden expansion of the channel and only passes when the disc is accelerated beyond the "burst frequency". c – e) depicts the working principle of a siphon based valve. While the disc is spinning, the liquid level in the reservoir and the siphon channel are equal (c). When the disc is stopped, the liquid in the siphon channel advances due to capillary forces (e). Once the liquid passed the crest point of the siphon, the disk is accelerated again and all liquid is transferred to the second chamber *via* the siphon channel (f)

liquid is pumped at high rotation frequencies into a chamber connected to an outlet siphon and a dead-end air compression chamber. Due to the high rotation speed the air in the dead-end chamber is compressed. Lowering the rotation frequency below a certain threshold leads to expansion of the previously compressed air, which pushes the liquid past the crest point of the siphon and thus opens the valve. The advantage of this implementation is that no hydrophilic surface is necessary since priming of the siphon does not rely on capillary action. [13] see also Chapter C.2

The major disadvantage of the valving methods discussed so far is that none of them provides a barrier for gases. To overcome this limitation sacrificial valves which are actuated by light, a laser, or heat have been introduced. Benito-Lopez and col-

leagues developed a valving scheme based on ionogels which block liquid flow when not exposed to light, while exposure to light results in shrinking of the gel, thus permitting liquid to pass [14]. Another commonly used sacrificial valving method uses wax barriers to stop liquid. These valves are opened by exposure to infrared light which melts the wax and thus opens the flow path [15, 16]. Additionally, Garcia-Cordero and co-workers used an infra-red laser to connect channels separated by a polymer film [17].

A valving scheme based on water dissolvable films (DF) has recently been developed in our group by Gorkin, Nwankire and co-workers [18] (see also Appendix C.3). The DF valves act as single-use, normally-closed valves as well as vapour barriers. Two channels are separated by a barrier of DF, creating a dead end pocket. At low rotation frequencies the dead end channel is primed, resulting in an inverted gas-liquid stack radially inwards from the DF. Below a threshold speed of rotation, the entrapped air prevents the liquid from reaching and thus dissolving the DF. Above the threshold frequency, the entrapped air is displaced by the liquid which results in wetting and subsequent dissolution of the DF. This in turn opens a barrier-free passage for the liquid. The threshold frequencies can be determined by the design of the fluidic network, especially the volume of the dead-end pocket. The working principle is shown in Fig. 1.3. This valving method has been applied to successfully integrate a multi-step immunoassay on a centrifugal platform, and the dissolution products of the DF had no measurable impact on the outcome of the assay. This valving method is very promising since it does not require any external actuators (such as lasers or heat sources), and in this sense is similar to the previously mentioned passive valves while at the same time providing a barrier for vapor and gases. The fact that the valve dissolves completely and thus provides a barrier-free passage is especially valuable for applications in cell analysis to minimize the risk of cell-loss during transfer.

1.2.3 Cell Capture, Assaying and Counting

Besides separating target cells and gating liquids, another very important operation is to capture, assay and count cells. The development of a novel method to capture

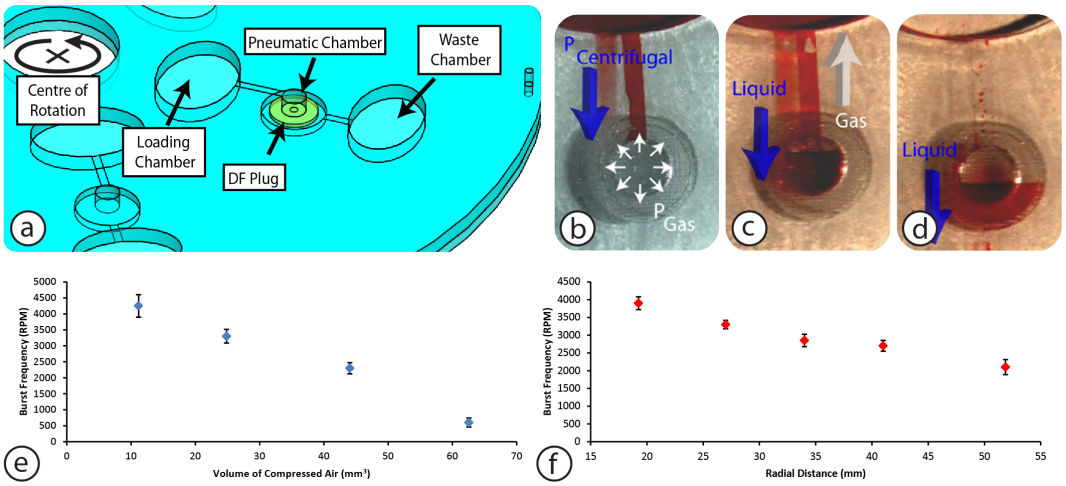

Figure 1.3: Working principle of the dissolvable film (DF) based valving scheme. The design of a valve is shown in (a). A radially inwards loading chamber is connected to a radially outwards waste chamber *via* a channel blocked by the DF. By adjusting the volume of the pneumatic chamber, the burst frequency of the valve can be set. Sequence (b - d) shows the operation of the valve: (a) valve is closed, compressed air prevents liquid from entering; (b) above the burst frequency, liquid enters the chamber and displaces the gas, thus dissolving the DF; (d) liquid passed through the valve. The relationship between pneumatic chamber volume and burst frequency is shown in (e), whereas (f) shows the relationship between radial distance of the valve and burst frequency for a constant chamber volume.(a-d) Adapted from [18]

cells and particles, expose them to various reagents and washing steps and subsequently perform a readout comprising of classification and counting of the cells is the main focus of this work. A detailed overview of the state-of-the-art methods for particle analysis on centrifugal platforms is provided in Chapter 2 and Appendix A, while the V-Cup based method for cell and particle capturing, which has been developed during the course of this work, is described in detail in Chapters 4, 5 and 6.

1.3 Aim of This Thesis

The aim of this thesis is to develop novel methods for the handling of liquids and particles (i.e. biological cells or micro-beads) on centrifugal microfluidic systems to enable the design of integrated point-of-care devices. The ultimate goal is the development of a platform to perform an automated differential cell count. Applications

of this platform could be to perform a differential lymphocyte count from whole blood, or to count cancer cells in a suspension of cells. In particular this work is focuses on:

1. Developing a method for capturing cells and particles in spatially well defined locations within a centrifugal microfluidic system. The capture efficiency is desired to be high in order to allow capturing of small cell numbers and / or to enable a total particle count.

2. Enable the exchange of the medium surrounding the captured particles, so as to expose them to various reagents such as antibodies.

3. Methods to manipulate captured particles either in batch or on a single particle level.

1.4 Thesis Outline

This thesis is structured as follows:

Chapter 2

This chapter reviews the current state-of-the-art in particle handling on centrifugal microfluidc platforms and summarizes the recent advances in operations such as cell removal, filtering, lysis, separation, sorting, encapsulation, trapping, assaying, cytometry and detection; including methods derived from low-cost conventional optical disc drive technologies such as CDs and DVDs.

Chapter 3

In this chapter the fabrication technologies to manufacture the microfluidic structures used in this work are introduced (SU8 lithography and replication in PDMS or PMMA). Furthermore, during the course of this work two generations of centrifugal test stands have been designed and built. Both generations are described in detail in this chapter.

Chapter 4

This chapter introduces the novel V-Cup based particle capturing scheme. The capturing efficiency of this method is close to 100%. Besides the working principle, the application of this platform to perform mulitplexed bead based immuno assays is demonstrated.

Chapter 5

In order to be able to recover captured particle from the V-Cup array, a novel magnetic actuator has been designed. This actuator is solely controlled by the rotation frequency of the disc. At high-speed rotation the actuator is disabled, thus allowing particle capturing. Below a certain threshold frequency the actuator is activated, thus releasing the previously captured beads. Furthermore the application of this actuator for mixing liquids is demonstrated.

Chapter 6

This chapter demonstrates the application of the V-Cup array to capture mixed populations of cells (MCF7, RPMI 8226 and HeLa) and discriminate between different types based on intracellular markers (ESR-1) and membrane based markers (EpCAM).

Chapter 7

In this chapter the manipulation of individual particles trapped in the V-Cup array using a custom built optical tweezers setup is demonstrated. Furthermore, the fluorescence detection capabilities of the optical module are shown. This is the first time that optical tweezers have been combined with centrifugal microfluidics.

Chapter 8

Finally, the conclusion and outlook summarizes the work presented here and outlines the challenges and opportunities lying ahead.

Appendix A

Appendix A contains another own review paper on cell handling on centrifugal platforms which has been published in *Current Opinion in Chemical Biology*

Appendix B

Appendix B contains own publications currently under review.

Appendix C

Co-authored journal publications either already published or currently under review are shown in Appendix C.

Chapter 2

Handling and Analysis of Cells and Bioparticles on Centrifugal Microfluidic Platforms

This Chapter has been published in:

Robert Burger and Jens Ducrée, *Handling and analysis of cells and bioparticles on centrifugal microfluidic platforms*, Expert Reviews in Molecular Diagnostics 2012

Microfluidic systems for cell separation and analysis have attracted increasing research activity over the past decades. In particular, the prospect of integrating all steps from sample preparation to assay readout in a single microfluidic cartridge, which is inserted into a compact, portable and potentially low-cost instrument, bears great promise to leverage next-generation diagnostic products and to advance life-science research with novel cell and particle manipulation, and analysis tools. Within the range of microfluidic actuation principles available, the centrifugal force is exceptionally well suited for cell handling due to its rotationally induced artificial gravity field, which can be varied over several orders of magnitude and which can manipulate bioparticles even in the absence of flow. We will survey how the base centrifugal force has been combined with the hydrodynamic Stokes drag, magnetic, dielectrophoretic and other forces to enable multidimensional separation and manipulation. The same centrifugal microfluidic toolbox has also been applied to investigate particles such as biofunctionalized beads, bacteria and multicellular microorganisms. This review summarizes the significant progress in modular unit operations such as cell removal, filtering, lysis, separation, sorting, encapsulation, trapping, assaying, sensing, cytometry and detection, even derived from low-cost conventional optical disc drive technology (e.g., CD and DVD), towards integrated and automated centrifugal microfluidic platforms for the handling and analysis of cells and bioparticles.

2.1 Introduction

In the past decade, in particular, considerable effort in the microfluidics community has been focused on developing cell and particle handling, and analysis systems for applications in cell research and clinical diagnostics. One main motivation to use microfluidic systems is the potential to reduce costs by integrating a full set of functional modules in cost-efficient (polymer) cartridges, the portability of the instrumentation and the unique capability to create well-defined microhabitats for the cells [19,20]. The number of excellent reviews on different aspects of microfluidic and microfabrication techniques for cell and particle handling convincingly underpins the high relevance of this topic within the scientific community. Manz *et al.*

published a series of reviews dealing with various aspects such as the history, theory and fabrication of micro total analysis systems [21, 22], as well as reviewing standard operations and applications [22, 23]. Whitesides and coworkers reviewed the application of soft lithographic techniques for studying microorganisms [24]. Microfluidic systems for cellomics were reviewed by Andersson and van den Berg [25] while Huh *et al.* reported on microfabricated flow cytometers (FCs) [26]. Erickson and Li covered a wide range of integrated microfluidic devices including systems for cell handling and counting [27]. Andersson-Svahn and van den Berg discussed the potential of performing experiments on single cells as opposed to large cell populations [28]. El-Ali and coworkers also reviewed microsystems for performing cell-based experiments [29]. In their recent work, Lindstrom and Andersson-Svahn surveyed the application of microfluidics for single-cell analysis [30], whereas the review of Yang and coworkers described cell handling and analysis using microfluidic systems in general [31] . Microfluidic solutions for cell separation have been highlighted in the review by Bhagat and colleagues [32]. This work for the first time specifically addresses centrifugal microfluidic systems for particle and especially cell handling utilizing the rotationally induced forces [33,34]. Centrifugal platforms offer many intrinsic advantages for cell handling as compared with typical pump-driven systems. Rotational actuation is simply implemented by controlling the frequency of a spindle motor to rotate the substrate. As the spinning frequency can easily be controlled over more than three orders of magnitude, the range of forces covers approximately six orders of magnitude, which is far superior to common, pressure-driven lab-on-a-chip systems. Another advantage of the centrifugal technology is the far-ranging independence of the fluid actuation from parameters such as viscosity, conductivity and pH. Furthermore, due to the inertia of the disc, the spinning motion is self-stabilizing, thus eliminating jittering known from reciprocating or syringe pumps. This system-intrinsic robustness of centrifugal liquid handling proves to be a major benefit for biological or in vitro diagnostic applications where one of the challenges is the wide variety of fluidic properties. The rotational actuation, which is driven by a basic, low-cost spindle motor also obviates the need for external, pressure- generating pumps and their world-to-chip interfacing. Moreover, the modular nature of

the centrifugal platform fluidically completely separates the instrument-based driving and detection units from the liquid sample and reagents, which are exclusively handled by the microstructured, typically disposable disc. The latter aspects are beneficial for bioanalytical applications since all (potentially infectious) samples can be processed in a fluidically encapsulated system, thus minimizing the risks of sample contamination as well as release of potential, for example blood-borne, biohazards. Centrifugal particle sedimentation has actually been known for centuries; for example, for splitting a blood sample into a cellular pellet and a supernatant for plasma extraction. It is also well known how to separate different cell bands by density gradient media and how to optimize the separation by the Boycott effect in radially inclined vessels. Starting as early as the 1960s, the liquid-handling capabilities have been extended and commercial centrifugal analyzers were even developed by Anderson and coworkers at Oak Ridge National Labs (TN, USA) [35–37]. With the advent of microfabrication, the originally very crude liquid-handling options have been substantially advanced by adding capillary action and high-flow resistances to the microfluidic plumbers toolbox. Mainly in the past decade, a wide range of fluidic structures have been developed in various groups to perform laboratory unit operations such as valving [12, 16, 38–40], metering [41, 42] and mixing [43–47], thus providing a comprehensive toolbox for efficient design of functionally integrated systems. By orchestrating the interplay of capillary and rotationally induced forces and resulting flows via a designated frequency protocol (i.e., frequency as a function of time), a higher level of control and parallelization of liquid handling could be achieved. By now, several academic groups and companies have even succeeded in demonstrating full-fledged, centrifugal microfluidic sample-to-answer systems that include the full scope of the liquid- handling protocol starting at upstream sample preconditioning to downstream detection. Madou *et al.*, as well as Ducrèe and coworkers, comprehensively surveyed centrifugal microfluidic unit operations as well as their applications for biomedical applications [33, 34, 48]. This work for the first time specifically reviews a surge of recent developments on the unique particle-handling capability of centrifugal microfluidic platforms. These specific capabilities make use of stopped-flow batch as well as continuous flow techniques. Also, the

particle-handling capabilities could be significantly enhanced by making use of (laminar) microfluidic conditions and the scale-matching of microstructures with cellular length scales. To keep the focus of this review, we chose to exclude centrifugal particle handling implemented by rapid, merely pressure-driven flow through curved channels [49–56]. We first introduce the basic forces governing the flow of liquids and suspended particles. In the following section, we will report on plasma extraction methods from whole blood. Next, centrifugal systems to determine the total cell concentration are described. The subsequent section covers classical, miniaturized and disc-based versions of flow-based counting, sorting and manipulation of individual bioparticles. We then present centrifugally enabled capturing, assaying, transport, counting and sensing with localized bioparticles before we survey readout methods derived from conventional optical disc drives. Finally, we provide an expert commentary and 5-year view on the anticipated development of the field.

2.2 Centrifugal Hydrodynamics

The cell manipulation presented in this review primarily relies on the three rotationally induced (pseudo) forces acting in the plane of rotation of the disc [33, 34]. A particle or fluid volume density, ρ, on a planar substrate rotating at a distance, r, from a central axis experiences the radially directed centrifugal force density (Fig. 2.1):

$$f_\omega = \rho r \omega^2 \tag{2.1}$$

which scales with the square of the (angular) rotational frequency, ω. Secondary effects, which are induced by the spinning frame of reference (i.e., the disc), are the Euler force density:

$$f_E = \rho r \frac{d\omega}{dt} \tag{2.2}$$

which is directed against a change in fluid velocity and results in swirling currents propelled by rotational acceleration, and the Coriolis force density:

$$f_c = 2\rho\omega\nu \tag{2.3}$$

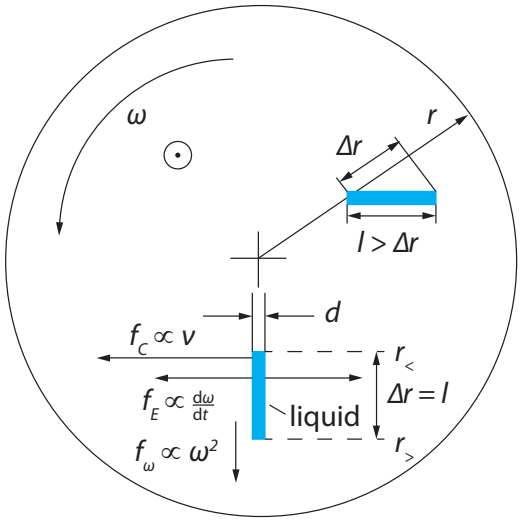

Figure 2.1: Forces acting on a liquid plug with length l and width d, situated between $r_<$ and $r_>$. The plug is traveling at speed v and is exposed to the centrifugal force density f_ω, the Euler force density f_E and the Corriolis force density f_C. (Adapted from [34], this figure is not part of the published review paper)

which deflects objects perpendicular to their direction of motion at the velocity, ν, in the plane of rotation.

Sedimentation of particles in the centrifugally induced field is propelled by the buoyancy force:

$$F_m = \Delta m r \omega^2 \tag{2.4}$$

which depends on the mass difference, Δm, between the particle and the liquid volume it displaces in the suspending medium. The radial motion of the particle driven by F_m is counteracted by the viscous (Stokes) drag:

$$F_d = 6\pi\eta R\nu. \tag{2.5}$$

where R and h denote the radius of the (spherical) particle and the viscosity of the fluid, respectively. Due to the proportionality of F_d to the relative speed, ν, of the particle with respect to the suspending medium, a constant speed of sedimentation will establish over time for a given frequency of rotation w, corresponding to the equilibrium of F_d and F_m.

The so-called shock interface delineates the interface between the particle-free supernatant and the concentrated suspension. The (radial) speed of the shock interface

is given by:

$$\nu_r = \frac{m}{\bar{f}}\omega^2 r(1 - \frac{\rho_{liquid}}{\rho_{particle}}) \tag{2.6}$$

where $\bar{f} \cong 6\pi\eta R\nu$ denotes the so-called friction coefficient, here approximated for a sphere of radius R, while ρ_{liquid} and $\rho_{particle}$ represent the densities of the liquid and the particle, respectively.

2.3 Preconditioning of Cell Suspensions

In this section we will survey methods to remove cells (or bioparticles) from a sample, either by sedimentation or lysis, in order to provide a particle-free supernatant for subsequent analytical steps.

2.3.1 Cell Removal Based on Centrifugally Induced Sedimentation

As mentioned before, one of the unique advantages of centrifugal microfluidics is the dynamically tunable artificial gravity field, which readily lends itself to the implementation of collective, sedimentation-based particle removal. This is comparable to traditional centrifugation schemes where a cell suspension is compacted into a cellular pellet to produce a cell-free supernatant by batch-mode centrifugation in a vial spun by a standard centrifuge. Of particular interest for diagnostic point-of-care applications is the extraction of cell-free plasma from whole-blood samples for subsequent analysis. Steigert *et al.* demonstrated a plasma-metering structure using siphon-based valving to retain the sample in the separation chamber during high-speed cell sedimentation [41]. After separation, the disc is decelerated to prime the hydrophilic siphon by capillary action. Subsequent spinning of the disc transfers a metered amount of plasma to a second chamber for analysis. A similar system was presented by Amasia and coworkers [57]. Häberle *et al.* presented a decanting structure for cell separation based on an azimuthally inclined throttling channel. Their technology yielded plasma with less than 0.11% of remaining cells (Fig. 2.2) [58]. Zhan *et al.* used a curved microchannel on a CD-shaped chip to separate plasma from blood cells and reported a separation efficiency of 99% for diluted blood exhibiting a hematocrit of 6% [59]. Another separation scheme was demonstrated by

Schembri and coworkers [60]. Burger *et al.* presented a blood separation structure based on pressure- driven membrane deflection [61]. Lee and coworkers developed a fully integrated test for hepatitis B virus and Escherichia coli with a blood separation structure as a first process step [62].

2.3.2 Cell Lysis

Another very common sample preparation task is cell lysis; for example, for a subsequent content analysis (e.g., DNA, RNA, proteins and metabolome). The choice of method to be applied primarily depends on the challenge to disrupt the cell membrane. Many cells, for example erythrocytes in whole blood, may be lysed by batch-mode mixing of the cell suspension with the conventional lysis agents using scaled-down volumes as demonstrated by Lutz and colleagues [63]. However, some bacteria are much harder to lyse and typically require harsher conditions.

Kellogg *et al.*, for instance, used a combination of alkaline solution and heat to lyse *E. coli* bacteria [64], while Klepárník and Horky used alkaline-based lysis of cells followed by electrophoretic detection of DNA fragments [65].

Kido and coworkers [66] developed a mechanical cell lysis method using on-disc magnetic actuators akin to the system presented by Grumann and colleagues [45] for the lysis of *E. coli* and *S. cerevisiae* bacteria cells. This concept was later improved by Siegrist *et al.*, who used an on-disc magnet and additional silica particles for bacteria lysis and sample homogenization (Figure 2.2) [67]. In this work, lysis and subsequent PCR-based detection of Bacillus subtilis from clinical samples has been shown. In another work from the same research group, mechanical cell lysis was performed by using microbeads to lyse mammalian (CHO-K1), bacterial (*E. coli*) and yeast (*S. cerevisiae*) cells on a disc in 57 min [68].

2.4 Measuring Total Cell Volumes

While the aim of the previously described methods is to remove or lyse cells, in many cases the volume fraction of cell populations present in a given sample volume is an important indicator. Riegger *et al.* presented a very simple-to-use device to determine the hematocrit that delineates the percentage of erythrocytes in a sample

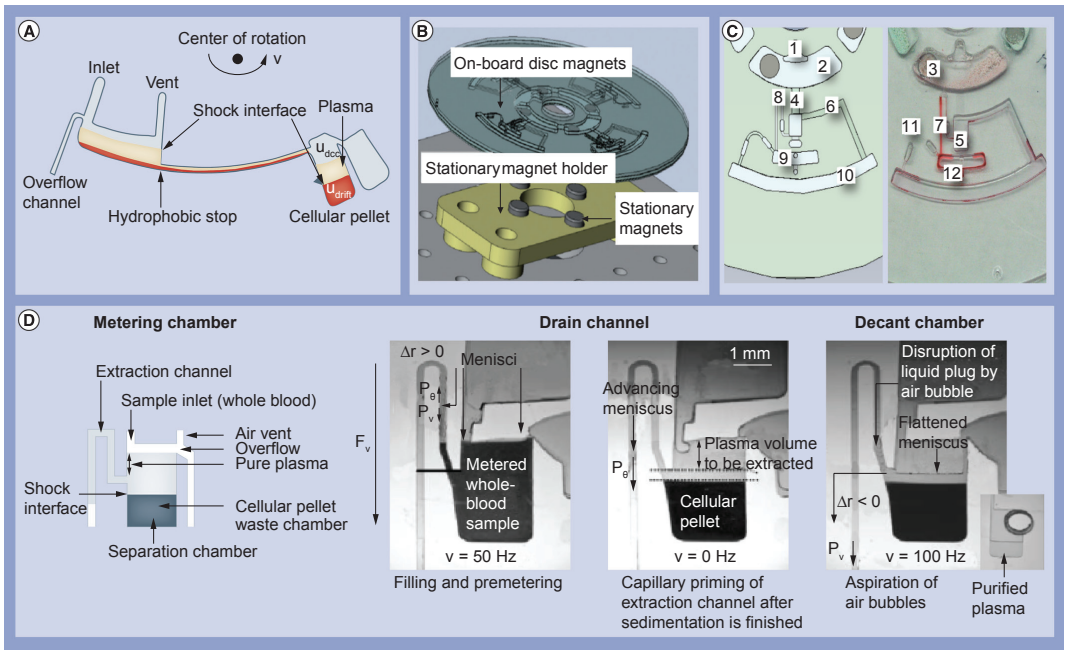

Figure 2.2: Cell removal and lysis. (A) The decanting structure by Häberle *et al.* [58] uses a long azimuthal channel for blood separation. (B & C) The magnetically actuated cell lysis structure by Siegrist *et al* [67]. (C) 1: sample inlet; 2: lysis chamber; 3: magnetic lysis disc; 4: hydraulic capillary valve; 5: clarification (upper) and capture (lower) chambers; 6: volume definition channel; 7: siphon capillary valve; 8: siphon; 9: collection chamber; 10: waste chamber; 11: self-venting channels; and 12: sample collection port. (D) The siphon-based blood separation scheme by Steigert *et al.* performs separation in a reservoir followed by extraction of the plasma via a siphon channel [41]. F_ν: Centrifugal force; P_ν: Centrifugal pressure; P_Θ: Capillary pressure; U_{dcc}: Velocity of the counter current.

of whole blood using a standard CD drive [69]. The hematocrit was determined by measuring the filling height of the cellular pellet in the sedimentation chamber.
A similar method has also been used to measure the concentration of somatic cells as well as the cream content of milk [70]. Cells were collected in a funnel structure and, subsequently, the volume of the pellet containing somatic cells was recorded by a custom-made reader. This device is intended for mobile veterinary point-of-use detection of bovine mastitis.
Schaff and coworkers used a density gradient-based approach to perform a differential white blood cell count. To this end, cultured white blood cells were fluorescently labeled and then separated in two bands under stagnant flow conditions using density gradient media. Subsequently, the fluorescent signal of each cell band was recorded and correlated with the cell concentration [71].

2.5 Flow-Based Counting, Sorting & Manipulation of Individual Bioparticles

While the previously shown methods have been developed to measure the concentration or total number of all cells in a given sample, in many real diagnostic or life-science applications the identification and sorting/counting of target cells in a mixed population is of more relevance and will be covered in the following flow-based schemes.

2.5.1 Conventional Flow Cytometry

Flow cytometry is the work horse for cell counting in life-science and clinical applications; for example, for monitoring the CD4 level of HIV patients. Classical FCs align the flow of a cell suspension by two sheath flows in order to present each suspended cell to a stationary detector. Modern FCs are capable of counting and identifying thousands of cells per second based on a variety of characteristics such as fluorescent markers, scattering and impedance. Although FCs are very versatile and fast, disadvantages such as high cost, large footprint, weight and the need for a trained operator render them unsuitable for applications in areas such as point-of-

care/patient self-testing or global diagnostics.

2.5.2 Flow-Based Cell Counting & Sorting on Miniaturized Devices

In order to address these needs, a plethora of research groups have advanced chip-based FCs [26], some with fluorescence-activated [72], dielectrophoretic [73–75] or magnetically activated cell-sorting [76] capability. In order not to lose the focus of this specific review, we will not discuss these in detail. Another way to achieve cell sorting is to take advantage of specific microfluidic effects. For instance, inertia in combination with microhydrodynamic lift forces [53, 77–79]has been applied to achieve particle focusing without the need for sheath flow. For more information, please consult the reviews mentioned earlier.

2.5.3 Density Gradient Centrifugation

As mentioned before, density gradient centrifugation is a standard method for the separation of cells into subpopulations and commercial products with densities adjusted to specific cells are readily available. Shiono and colleagues presented a centrifugal device for the continuous separation of cells using up to six parallel streams of media with different densities. They demonstrated the separation of cells from whole blood [80,81] as well as the separation of a suspension containing human mast cells and fibroblasts [82]. A separation time of 100 min for a sample volume of 30 ml was reported.

Centrifugal Pinched-Flow Fractionation Another effect used for microfluidic particle sorting is pinched- flow fractionation in a pressure-driven system [83]. A centrifugal implementation of pinched-flow fractionation has recently been shown by Morijiri and coworkers [84]. In this work they demonstrated the size- and density-based separation of a suspension containing polystyrene beads with diameters of 3 and 5 μm as well as 5 μm silica particles into different outlets (Figure 2.3).

Centrifugal Counterflow Elutriation Centrifugal counterflow elutriation is a technique that has been successfully used to separate cells using conventional centrifugal setups [85,86]. A microfluidic implementation of the centrifugal counterflow

elutriation principle using density gradient media has been developed by Seki and coworkers (Figure 2.3) [87]. The group demonstrated the separation of a mixture of polystyrene particles with diameters of 3 and 9.9 μm, followed by the retrieval of the particle-containing fractions [87].

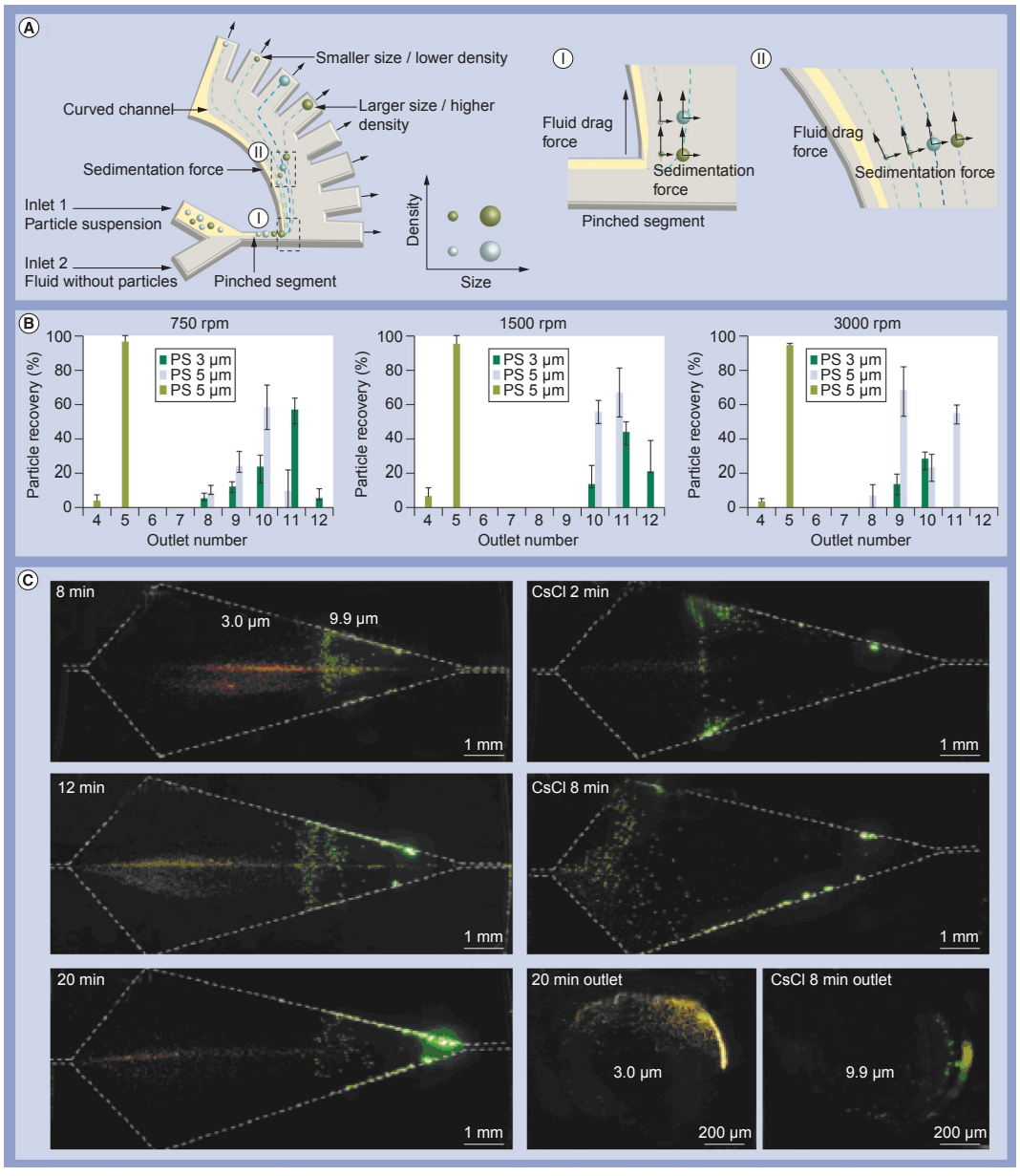

Figure 2.3: Size- and density-based particle separation schemes. Centrifugal pinched-flow particle separation scheme developed by Morijiri *et al.* is shown on the top [84]. (A) The working principle. (B) Separation results for PS and silica beads; error bars show the standard deviation for the particle recovery. (C) A microfluidic counterflow elutriation structure developed by the same group [87]. PS: Polystyrene; rpm: Rotations per min.

Multiforce Sorting in Flow-Based Centrifugal Schemes

While pinched-flow fractionation and centrifugal counterflow elutriation rely on parameters such as size and density of particles, other important parameters to discriminate cells are their morphology and markers expressed on the cell membrane.

Centrifugal Dielectrophoresis Dielectrophoretic cell sorting takes advantage of the difference in dielectric properties between cells, which results from parameters such as size and membrane morphology. Martinez-Duarte *et al.* successfully demonstrated the separation of yeast cells using an array of carbon electrodes on a centrifugal platform [88]. Another dielectrophoretic-based cell separation and routing system using metal electrodes has been presented by Boettcher and co-workers [89].

Centrifugo-Magnetophoresis All methods described so far have been label-free, that is, cells are solely distinguished based on differences in intrinsic physical properties such as density or dielectric properties. Label-based methods, on the other hand, rely on the modification of the cells by attaching, for example, magnetic beads to their surface and hence changing their properties as compared to unlabeled cells. This principle has been very successfully demonstrated in pressure-driven microfluidic systems by Pamme and colleagues [90]. They used this principle to perform bead-based immunoassays [91] as well as for continuous cell sorting [92].
Siegrist *et al.* recently introduced a similar method for cell separation and routing on a centrifugal platform aimed at the detection of circulating tumor cells (CTCs) [93–95]. The separation principle roots in the sedimentation of paramagnetic and nonmagnetic particles under stagnant flow conditions in the presence of a magnetic field perpendicular to the sedimentation direction. While nonmagnetic particles follow a radial trajectory, paramagnetic particles are deflected towards the magnet and can thus be separated. By coating paramagnetic beads with anti-EpCAM IgG (a marker expressed on certain types of cancer cells), the so-functionalized beads bind to the cells which can then be continuously separated from the background of nonmagnetic cells by a co-rotating magnetic field (Figure 2.4).

Chen *et al.* presented a centrifugal device for separating MCF7 breast cancer

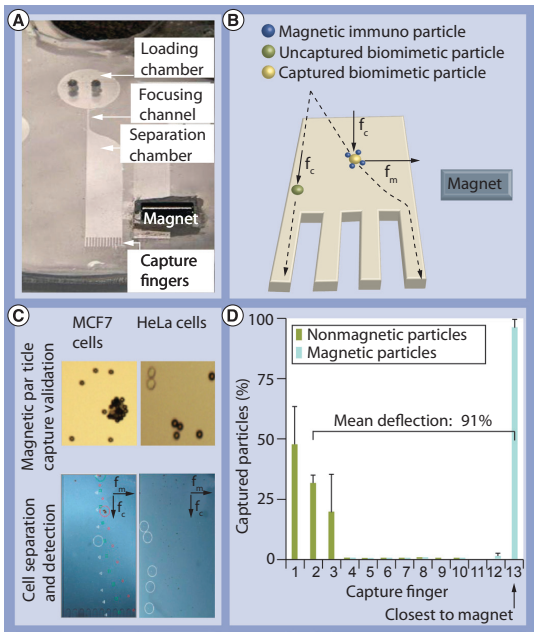

Figure 2.4: Centrifugo-magnetic particle separation scheme. (A & B) The working principle. Particles sediment due to the centrifugal force and magnetic particles are deflected by the perpendicular magnetic field, while nonmagnetic particles follow a straight path. This results in a separation of magnetic and nonmagnetic particles. (C) Magnetically tagged and deflected MCF7 cancer cells and untagged HeLa cells which are not deflected. (D) The separation of magnetic and nonmagnetic particles. The error bars show the standard deviation of the particles deflected to the capturing fingers F_m: Magnetic force; F_n: Centrifugal force. [94]

cells from a population of Jurkat cells (Figure 2.5) [96]. In their work, a negative selection process is used to remove the background cells by binding them to IgG-coated magnetic microparticles. A multistage magnetic setup is then used to retain the magnetic particles with the attached Jurkat cells, so only the target MCF7 cells advance to the radially outmost reservoir. A depletion rate of Jurkat cells of 99.96% and an average yield of cancer cells of 60 ± 10% has been reported.

In a similar setup using positive separation, antibody-coated magnetic beads have been used to isolate circulating endothelial cells from a population of peripheral blood mononuclear [97].

2.5.4 Cell Encapsulation

Häberle *et al.* developed a method for the encapsulation of cells in alginate spheres [98]. HN25 and PC12 cells were suspended in a solution of alginate and dispensed through a micronozzle, leading to the generation of droplets containing cells. These droplets were then collected in a co-rotating vessel containing Ca^{2+} ions. Upon contact with Ca^{2+} ions, alginate was cross-linked, which resulted in hardened droplets.

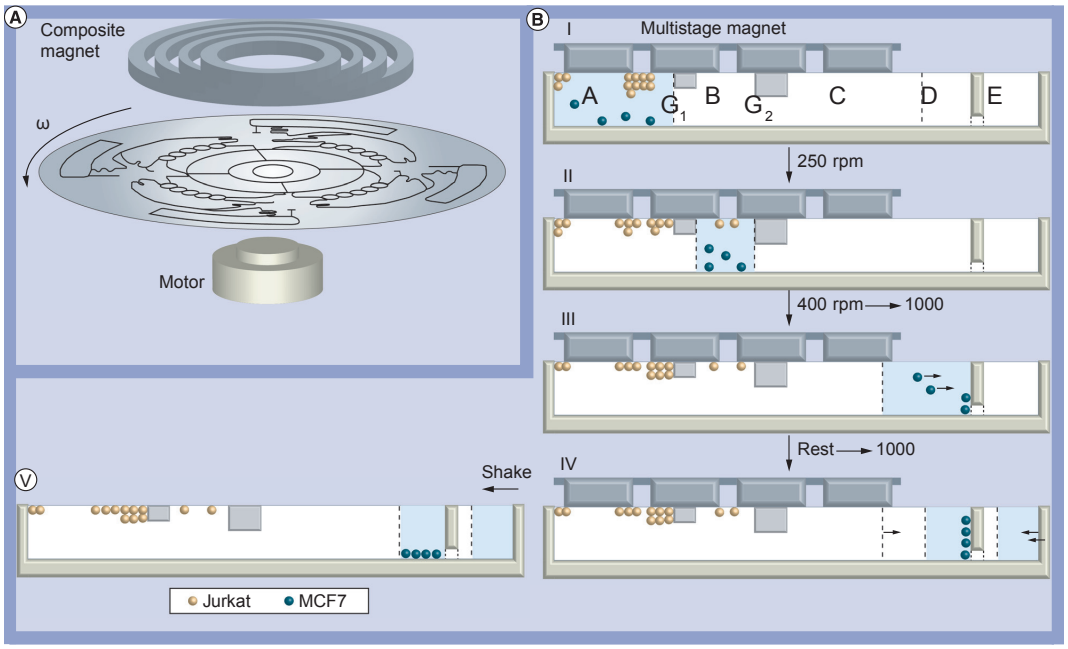

Figure 2.5: Negative cell separation scheme for cancer cells. (A) Setup comprising of motor, disc and magnetic rings for particle retention. (B) The schematic separation process. Jurkat cells are tagged with paramagnetic beads, while MCF7 cancer cells remain unlabeled. Magnetically labeled cells are then retained by the external magnets and only unlabeled cells (MCF7) can progress to the collection chamber, which is positioned radially outwards. (I) Sample is loaded and magnetically labeled Jurkat cells are trapped in the inlet reservoir (A). The chambers are connected by the capillary valves G1 and G2. (II) Trapping in the second trapping area. (III) Further separation and sedimentation of MCF7 cells in the outer reservoir (C) and collection bins (D). (IV) Extraction of liquid into wast reservoir (E). (V) Spreading of MCF7 cells on the bottom for counting. rpm: Rotations per min. [96].

Alginate bead diameters ranging from 180 to 800 μm, depending on the nozzle dimension and spinning frequency, as well as bead production rates of up to 600 beads per second, were demonstrated. Cells remained viable in the alginate beads for up to 7 days.

2.6 Cell Capture & Assaying of Localized Bioparticles

Another important class of devices perform cell assays on disc. These systems address a major shortcoming of FCs, namely their inability to observe the (temporal) response of a given cell upon exposure to environmental conditions or drugs. Therefore, while a FC can only provide a snap shot of a cell, the capability to resolve the reaction of a cell to a stimulus is particularly interesting for drug testing or when only a limited number of cells are available. This is, for example, the case in stem cell research. To enable time-resolved observation of the same cells, they are typically captured in well-defined positions and/or biochemical microenvironments using mechanical traps.

2.6.1 Gravity-Based Trapping & Analysis

Kubo *et al.* designed a cell-trapping structure on a centrifugal platform and demonstrated its application to perform viability assays on Jurkat cells. After being captured in cup-shaped chambers, the cells are stained to assess cell viability [99]. A system to perform apoptosis and cytotoxicity assays on mechanically retained single cells was presented by Lee and coworkers [100]. Cells were trapped in pits aligned on the outer side wall of an inclined microchannel. Each pit was dimensioned to hold a single cell (Figure 5). A suspension of HEK293 cells was then flown through the channel and cells were trapped in the pits with a reported capture efficiency of up to 80%. After trapping, cells were either exposed to UV light to induce apoptosis or to paraformaldehyde for cytotoxicity studies.

Another, pit-based cell capture system was developed by Furutani *et al.* to perform on-disc PCR on single cells (Figure 2.6) [101] . The cell occupancy for each well, which depends on the initial cell concentration, was studied and the selective detection of Salmonella enterica from a mix with *E. coli via* PCR was demonstrated.

Chen *et al.* used spiral channels with trapping holes to capture cells and subsequently immobilize them in agarose to create cell arrays [102]. Riegger and coworkers demonstrated the implementation of a multiplexed immunoassay using on-disc trapped colored beads [103].

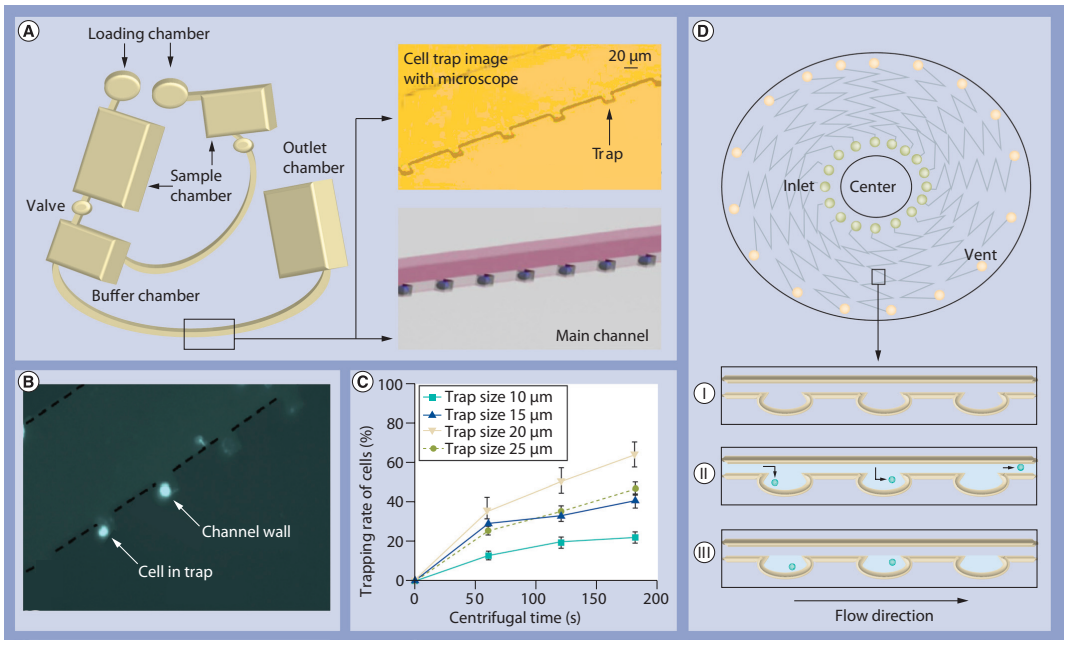

Figure 2.6: Systems for single-cell capturing and assaying. (A) Inclined channel with cell traps in the side walls, (B) with captured cells and (C) capture efficiency; error bars show standard deviation of the cell trapping rate. [100] (D) Furutani *et al.* presented a similar design for single-cell PCR. (I) The disc contains channels with pockets along the side walls. (II) When a cell suspension is flown through, cells sediment into the pockets and get trapped. (III) The liquid in the channel is then replaced with PCR mix and subsequently drained such that the pockets are no longer connected by liquid but form individual PCR vessels [101].

2.6.2 Capture & Assaying in Arrays of Geometrical Traps

Burger *et al.* published a method for capturing individual cells in an array of V-cups [104]. In a dead-end chamber, all cells sediment under the impact of the centrifugal force into an array of scale-matched V-cups, where they are mechanically trapped. Cups are dimensioned such that each cup can only accommodate one cell, which results in a sharply peaked, single-cell occupancy distribution across the array. The advantage of this system compared to pressure-driven systems is the very high capture efficiency close to 100% [104] (for more details see chapter 4). The authors first demonstrated the application of this capturing scheme to perform multiplexed, bead-based immunoassays on disc [105] before implementing the capture and discrimination of cancer cells based on intracellular and membrane-

bound immunomarkers (Figure 2.7) [106]. Furthermore, a mechanism for collective retrieval of bioparticles based on magneto-hydrodynamically induced pumping has been demonstrated [107]. A system for trapping cells and label-free analysis of secreted proteins using surface-enhanced Raman spectroscopy was demonstrated by Cho *et al* [108].

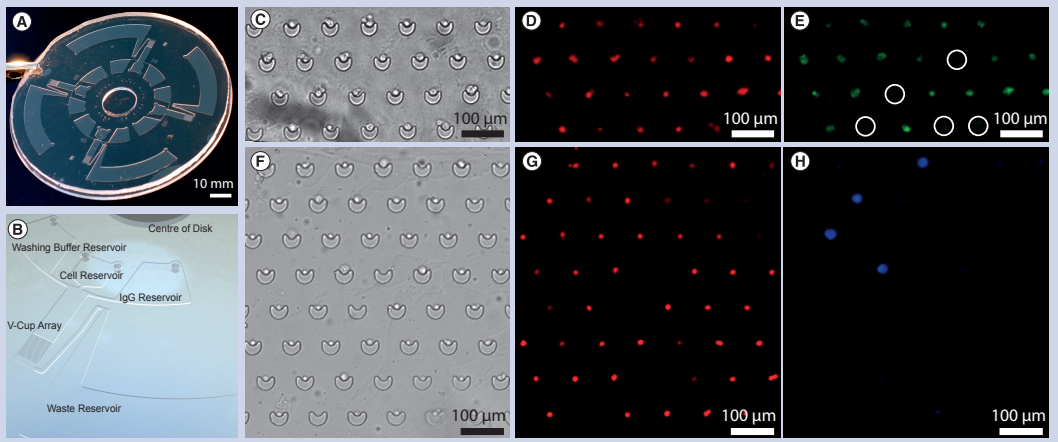

Figure 2.7: Capturing and staining of single cells. (A & B) V-cup-based cell capturing structure. Sequence (CE) shows captured MCF7 and HeLa cells. (E) The white circles indicate the sites where HeLa cells (that do not express ESR1) are trapped. The DNA in all cells has been stained with propidium iodide (D) and only MCF7 cells, which express estrogen receptor a (ESR1), have been stained with anti- ESR1 antibodies (green cells in E). Image sequence (FG) shows captured RPMI 8226 plasma cells and MCF7 cells. DNA has been stained with propidium iodide (G) and MCF7 cells have been identified based on EpCAM, which is present on the membrane of cancer cells (cells in H) [106].

2.6.3 Cells as Sensors

Owing to their sensitivity to environmental conditions, modified cells can also be used as sensors to detect, for example, the presence of toxins such as arsenite. Rothert and colleagues reported on the development of a centrifugal platform using *E. coli* cells that were modified to produce green fluorescence protein upon exposure to arsenite and antimonite [109]. Later, a spore-based system for the detection of arsenite and zinc using the same platform was presented [110].

2.6.4 Investigation of Mulitcellular Organisms

An automated platform for the cultivation and observation of (multicellular) Caenorhabditis elegans worms on disc was demonstrated by Kim and coworkers [111]. This platform performs automatic feeding and waste removal, and up to 20 cultivation

chambers can be integrated on a disc. Furthermore, the breeding of three generations of *C. elegans* on disc within 2 weeks has been demonstrated.

2.7 Detection by Optical Disc Drive-Derived Instrumentation

All previously described methods only share the disc shape and a rotation-based actuation with optical data storage media such as CD-ROMs or DVDs. However, optical disc drives such as CD drives offer further advantages that make them promising platforms for point-of-care devices. The most striking advantages are the large installation base (almost every computer contains an optical disc drive), the very favorable price due to mass production and the high resolution (data is represented in submicron features). The application of standard pick-up units from CD-ROM drives to build an optical profilometer [112,113] as well as the use of pick-ups to build a cytometer [114] have already been demonstrated (although not in the context of a centrifugal microfluidic system).

2.7.1 Cell Detection

Imaad and coworkers presented a cytometer based on a standard data CD utilizing a conventional optical disc drive for readout [115]. To this end, a suspension of cells or polystyrene particles is introduced into a microchannel close to the data track of the disk. The data on the disc is then read using a conventional CD drive of a PC. Since the laser of the CD drive has to pass through the cell suspension, it is scattered by the cells, which results in readout errors. The amount of readout errors has proven to be proportional to the concentration of particles in the channel (Figure 2.8).

2.7.2 Other On-Disc Bioassays

The detection of biomolecules such as proteins, DNA or antibodies is also a very important operation and in many cases follows the separation or stimulation of cells. Since this review is focused on cell handling we will only briefly describe some

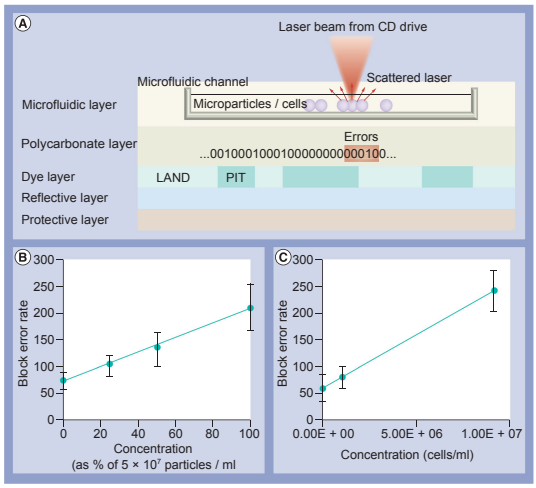

Figure 2.8: Cell counting using standard optical disc technology. (A) Working principle: a microfluidic channel is created on top of the polycarbonate layer of a standard CD. Introducing a cell suspension into the channel results in light scattering, which in turn produces readout errors. (B & C) The block error rate is directly proportional to the concentration of particles or cells in the microfluidic channel [115].

noteworthy publications on the integration of bioassays.

Chen *et al.* used a double-spiral setup to generate DNA arrays on disc [116]. La Clair and Burkart presented a method to screen the interaction between ligands immobilized on standard CDs and biomolecules. The data on the CD was then read out in a PC CD drive and the binding of the biomolecules was assessed by detecting the error rate induced by the scattering of the laser beam [117]. Morais *et al.* also used a standard CD and a modified CD-ROM drive to perform a competitive immunoassay [118]. Lange and colleagues also used a conventional CD drive to detect the binding of biomolecules [119]. Barathur *et al.* reported on the integration of DNA microarrays in centrifugal systems and readout using standard CD drives [120] . Methods for the immobilization of biomolecules on standard CD surfaces have been reviewed by Yu [121]. Bosco and colleagues reported on a centrifugal platform for label-free detection of biomolecules using cantilever chips and a DVD pick-up for readout. Binding of the analyte molecules to the cantilever resulted in a deflection, which was then measured using the DVD pick-up [122].

2.8 Expert Commentary

Centrifugal microfluidic systems have attracted much interest from academia as well as from industry over the last decades. Early research was overwhelmingly directed

towards the development of basic liquid-handling operations such as valving, metering and mixing. By now a comprehensive liquid-handling toolbox is available to solve major challenges of sample preconditioning and integration with (optical) detection (e.g., for molecular diagnostics or immunoassays).

Cell handling has so far mostly been considered for providing filtered, that is, particle-free analytes, at the beginning of a process chain; for example, for plasma extraction from whole blood for subsequent assay steps. Only in recent years has research on centrifugal systems for the specific investigation of cells started to attract broader interest. We are firmly convinced that cell manipulation and analysis will significantly grow over the near-term future. This is because centrifugal liquid handling offers a few unique selling points compared with conventional microfluidic actuation principles such as pressure-driven flow. These are:

- Force control by simple spindle motor
- Jitter-free force fields and flow propulsion by rotationally stabilized actuation
- Force can be scaled over more than six orders of magnitude
- Option for modular, multipurpose setup due to force transmission without fluidic interface
- Option for particle sedimentation and band extraction (e.g., for cell subpopulations)
- Option for particle handling in absence of flow
- Option for simple instrumentation including actuation and detection akin to optical disc drives

Among the challenges specific to the centrifugal microfluidic platforms are:

- The unidirectional nature of the centrifugal field
- The limited realestate available to concatenate liquid-handling operations along the radial direction
- The simultaneous exposure of all on-board liquids to the same, rotational actuation

- The interfacing (e.g., fluidic, electrical or optical) between the rotating substrate and the stationary instrument (e.g., for actuation, transfer of signal and power and detection)

However, solutions and work-arounds to these issues have been demonstrated by the various players in the field. Overall, the centrifugal microfluidic platform has now been taken to a very high level of technological maturity. The platform also boasts one of the earliest and still ongoing commercial avenues in the lab-on-a-chip community. As is common in emerging technologies, the road is flanked by successes as well as failures. A prominent example of a commercial stakeholder is Abaxis Inc. (CA, USA), who have been providing point-of- care systems for medical and veterinary diagnostic applications since the mid-1990s [3]. A few years later, companies such as Tecan (Mannedorf, Switzerland; based on an acquisition of Gamera Biosciences) [123], Burstein Technologies (CA, USA), Bayer (Leverkusen, Germany) [124], Boehringer Ingelheim Microparts (Ingelheim, Germany) [125], Roche Diagnostics (Basel, Switzerland) [126] and SpinX (Geneva, Switerland) have created a comprehensive portfolio of intellectual property. Gyros AB (Uppsalas, Sweden)presently commercialize an immunoassay platform primarily for the biopharmaceutical industry [127]. In Asia, one of the major optical disc drive manufacturers, Samsung (Seoul, South Korea) [128], have recently launched a centrifugal assay platform. Furthermore, a few start-ups are seeking to enter the market. Examples are the Portuguese spin-out Biosurfit (Lisbon, Portugal), who are currently developing a label-free, surface-plasmon-resonance-based point-of-care device for multiparameter blood-based test panels [5], and the Irish start-up Radisens Diagnostics (Cork, Ireland), who have reached an agreement on licensing Tecans microfluidics patent portfolio [4].

2.9 Five-Year View

Considering the enormous increase in publications on handling of particles, especially for the analysis of cells, we believe centrifugal microfluidic cell handling will pick up significant momentum in the near-term future. One major driving factor will be the increasing demand to detect rare cells in biological samples such as blood

with high accuracy. Considerable research effort has been directed at the detection of CTCs [129–132]. This is a needle-in-a-haystack challenge as the CTCs are extremely rare and, to be of diagnostic relevance, systems are assumed to require a detection limit better than five CTCs per several milliliters of blood in a background of billions of normal blood cells. Some promising technologies to tackle this challenge are magnetic cell separation [94,96,97], hydrodynamic separation [84,87] or liquid recirculation [133]. It will be interesting to benchmark centrifugal systems against state-of-the-art microfluidic and conventional systems for CTC detection. A particular benefit of centrifugal systems might be the prospect of full integration into a sample-to-answer system. In addition, a new generation of powerful research tools for cell and cancer research - for example, for investigating cell exposure to external stimuli, cell embedding into well-defined biochemical microenvironments or intracellular communication might well be leveraged by the unique selling points of centrifugal microfluidics. Another major driver for centrifugal cell platforms will be the emerging demand for very cheap and highly user-friendly diagnostic platforms for counting cell subpopulations; for example, complete blood counts and CD4 counts in HIV diagnostics. While such cell counts can be routinely performed in the well-established central laboratory infrastructures of the developed world, there is a clear need for robust, portable and extremely low-cost point- of-use devices in resource-poor, global diagnostic settings, and possibly also for enabling more frequent routine screening and companion diagnostics in personalized medicine/theranostics. We believe that these decentralized applications in particular will benefit from the adoption of mature optical disc drive technology for readout. A centrifugal point-of-care system for cell detection, possibly combined with other plasma- or lysate-based parameter panels, and costing less than US$100 (cost of goods) appears to be within reach. In 5 years, market entry of the first centrifugal sample-to-answer systems performing decentralized, accurate cell counts and assays (e.g., for white blood cell populations, CD4 or cell-based drug testing), will have already taken place or will be imminent. It needs to be seen whether sophisticated, multistage and cell-handling systems will enable simplified and more accurate rare-cell counting, such as for CTC detection in cancer patients. Furthermore, the combination with standard cell manipulation

and analysis tools such as optical tweezers and patch-clamp might be investigated. From a more technical, liquid-handling point of view, options for counting or allotting absolute cell numbers might also have some promising application. It will also be interesting to see whether adding centrifugal multiphase microfluidics [134,135] to the cell-on-a-disc technologies presented here will open further application options.

Chapter 3

Fabrication Methods and Experimental Setup

This chapter describes the methods used to fabricate the microfluidic discs used in this work, and also the experimental setup for testing the discs. Masters of the microfludic disc were fabricated by photo lithography in SU8 and subsequently replicated in Polydimethylsiloxane (PDMS) or in Poly(methyl methacrylate) (PMMA) by hot embossing. During the course of this work several centrifugal microfluidic test stands have been developed and built. Design and function of these test stands will also be described in this chapter. For the first time an optical tweezers / fluorescence detection module has been integrated in a centrifugal test stand.

3.1 Fabrication of Microfluidic Discs

3.1.1 Master Fabrication by Lithography

Masters for the microfluidic structures used in this work have been fabricated in SU8 (Microchem, USA) by photolitography. SU8 is a negative tone, epoxy based photo resist, allowing the creation of thick layers (up to several hundreds of μm) which has been developed by IBM [136]. SU8 allows the fabrication of permanent structures with high aspect ratios (10:1) and near vertical side walls. Besides being used as a structural material to create microfluidic and micromechanical structures [137,138], SU8 has been widely used for the fabrication of tools to replicate microstructures in PDMS by casting, or in rigid polymers by hot embossing.

Masters have been manufactured using two different protocols:

1. SU8 and Dry Film Resist (DFR)
2. SU8 only

The advantage of the process using a combination of SU8 and DFR is that it is faster and easier to generate thick (i.e. $> 100\,\mu$m) layers which are especially useful for generating reservoirs. However, the adhesion and resolution of the DFR layer is inferior compared to the SU8-only process. Therefore the SU8-only process has been used for generating hot embossing masters.

SU8 and Dry Film Resist

For this process one or more layers of DFR have been laminated on top of a first layer of SU8. The first level typically containing small features such as V-cups was manufactured in SU8. The second layer, containing only fluidic reservoirs was manufactured using WBR 2100 dry film resist (DFR) (DuPont, USA). The process parameters are summarized in table 3.1.

SU8-Only

The SU8-only process delivers masters with better resolution and durability compared to the previous process, and also allows user-defined thicknesses of the second layer. The process parameters are shown in table 3.2

Layer	#	Step	Parameters
1. SU 8 3025	1.	Clean Wafer	DI water and IPA, dry with N2
	2.	Spin Coating	2500 RPM, 30 s $\Rightarrow \approx 25$ μm thickness
	3.	Soft Bake	14 min. @ 95 °C on Hot Plate
	4.	Exposure Level 1	Exposure Engergy: 280 mJ cm^{-2}
	5.	Post Exposure Bake	3 min @ 95 °C
	6.	Develop	10 min.
	7.	Rinse	Rinse with fresh Developer
	8.	Rinse	IPA, dry with N2
	9.	Hard Bake	1 min. @ 150 °C on Hot Plate
	10.	UV Plasma	Activate Surface in O2 Plasma for 2 min (700 mTorr, 29.6 W).
2. WBR 2100	11.	Laminate WBR 2100 (2x)	Roll Temperature: 95 °C
	12.	Align 2nd layer and Exposure	Exposure Energy: 440 mJ cm^{-2}
	13.	Post Exposure Bake	55 s @ 100 °C
	14.	Develop	20 min. in 1.6% K_2CO_3
	15.	Rinse	DI Water

Table 3.1: Process parameters for two level master for PDMS casting

Layer	#	Step	Parameters
1. SU 8 3025	1.	Clean Wafer	DI water and IPA, dry with N2
	2.	Spin Coating	2500 RPM, 30 s $\Rightarrow \approx 25$ μm thickness
	3.	Soft Bake	14 min. @ 95 °C on Hot Plate
	4.	Exposure Level 1	Exposure Energy: 280 mJ cm^{-2}
	5.	Post Exposure Bake	3 min @ 95 °C
	6.	Develop	10 min. in EC Solvent
	7.	Rinse	Rinse with fresh Developer
	8.	Rinse	IPA, dry with N_2
2. SU 8 3050	9.	Spin Coating	1500 RPM, 30 s $\Rightarrow \approx 80$ μm thickness
	10.	Soft Bake	20 min. @ 95 °C on Hot Plate
	11.	Spin Coating	Spin Coating @ 1500 RPM, 30 s $\Rightarrow \approx 80$ μm thickness
	12.	Soft Bake	20 min. @ 95 °C on Hot Plate
	13.	Align 2nd Level and Exposure	Exposure Energy: 300 mJ cm^{-2}
	14.	Post Exposure Bake	6 min @ 95 °C
	15.	Develop	10 min. EC Solvent
	16.	Rinse	Rinse with fresh Developer
	17.	Rinse	IPA, dry with N_2
	18.	Hard Bake	90 min. @ 150 °C on Hot Plate

Table 3.2: Process parameters for two level master for PDMS casting or hot embossing

3.1.2 Surface Coating

In order to facilitate demoulding of the PDMS or PMMA from the litographically structured mould, the surface was treated with a hydrophobic coating. To this end, the wafer was immersed in a solution of 400 μM Octadecyltrichlorosilane (OTS) (Sigma Aldrich, Ireland) in anhydrous Heptane (Sigma Aldrich, Ireland) for 2 hours. Subsequently, the wafer was sonicated for 5 min. in pure Heptane The wafer was then rinsed with Methanol followed by Isopropanol and dried with N_2. Finally the wafer was baked on a hot plate at 100 °C for 20 min. This surface treatment resulted in a water contact angle > 100 °.

3.1.3 Replication of Microfluidic Chips

Replication in PDMS and Bonding to PMMA Discs

PDMS is a very commonly used material for the fabrication of microfluidic devices which has been pioneered by the Whitesides group in the late 1990s [139, 140]. The advantage of PDMS is that it is very simple and fast to replicate micro features from a master. Furthermore PDMS is non-toxic, elastic and can be easily bonded to PDMS or glass.

Chips were fabricated by mixing PDMS (Dow Corning, USA) in a ratio of 5 : 1, base to curing agent. The PDMS mixture was then poured onto the mould (Typically 25 g of PDMS mix was used per 4" wafer) and degassed under vacuum for at least 20 min the mould was then placed in a level oven at 70 °C for 30 min to cure the PDMS. Subsequently the PDMS was cut from the mould and access holes were punched. A second batch of PDMS was then mixed in a ratio of 20 : 1 (base to curing agent), degassed and spin coated on blank PMMA (Radionics, Ireland) disc at a rotation speed of 1000 RPM. The spin coated PDMS was cured in the oven at 70 °C for 40 min. The disc was then exposed to an O_2 plasma (700 mTorr, 29.6 W, 5 min). The structured PDMS part was subsequently aligned to the PMMA base disc and placed in the oven for at least 3 hours to perform bonding [141]. In order to enable complete filling of structures such as the V-Cup arrays with liquid, PDMS discs were kept under vacuum for at least 30 min prior to use [142]. The fabrication process is illustrated in Fig. 3.1.

Replication in PDMS and Bonding to Glass

Chips for experiments involving particle manipulation using the optical tweezers setup were manufactured in PDMS and bonded to glass cover slips (25 x 60 mm, thickness # 1 (130 – 160 μm), VWR, Ireland). This is necessary to enable trapping using the optical tweezers (see 3.3.2). To this end PDMS was mixed in a ratio of 10 : 1, base to curing agent and processed as described above. After cutting of the chips and punching of the access holes, chips and glass slips were activated using O_2 plasma (700 mTorr, 29.6 W, 5 min). Following plasma activation chips were immediately bonded to glass and placed in the oven at 70 °C for at least 2 hours.

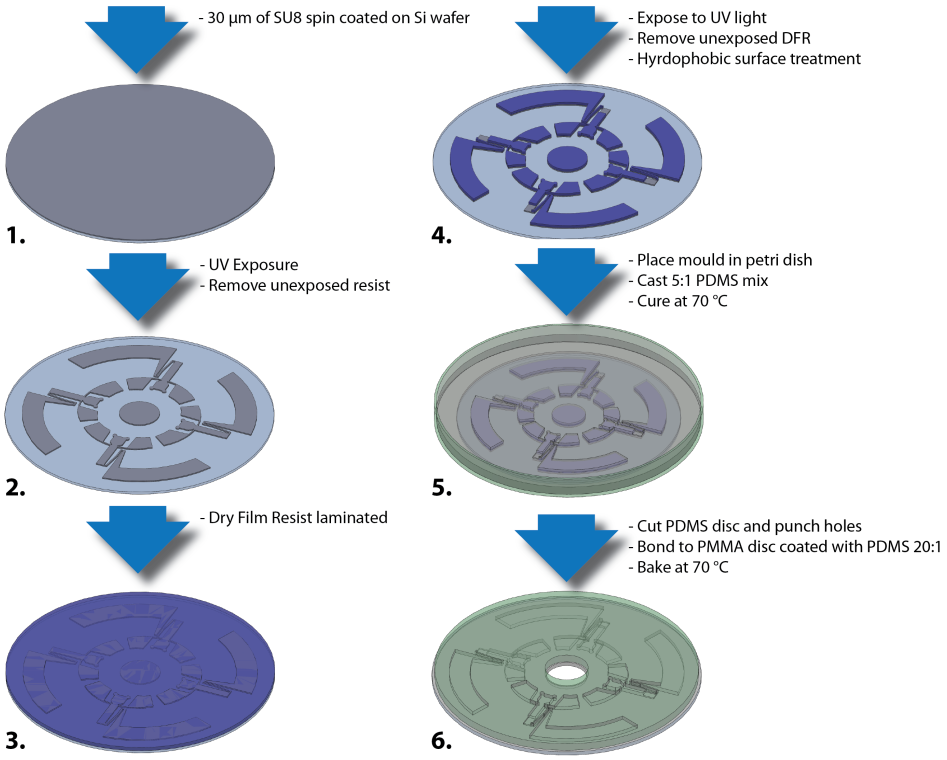

Figure 3.1: Summary of fabrication process. Fabrication of mould using SU8 and dry film resist (1 - 4). PDMS is cast on the mould (5.) and the disc subsequently assembled (6.). [104]

This method resulted in irreversible bonding of PDMS to glass. The chips where then attached to a custom made holder to enable mounting in the centrifugal test stand.

Hot Embossing

Hot embossing enables the rapid replication of microfluidic structures in rigid polymers such as PMMA. To this end, the polymer is heated above its glass transition temperature (T_g) and then a stamp with the negative of the microstructures is pressed into the softened polymer. After the pattern has been transferred, stamp and polymer are cooled below T_g while a constant pressure is applied. After cooling below T_g, stamp and polymer substrate can be separated. Hot embossing offers a fast and efficient method for manufacture of small to medium numbers of microfluidic chips in typical polymers such as PMMA, Polycarbonate (PC) or Topas. Since masters can be easily manufactured on silicon wafers by lithography hot embossing offers much more cost efficient replication (for small numbers of chips) than for example injection moulding. Embossing has been performed using a Hex-02 hot embosser (Jenoptik, Germany). The typical process parameters used in this work are shown in table 3.3.

#	Step	Parameters
1.	Bringing polymer and master in contact	F = 300 N
2.	Heating above T_g	T = 123 °C
3.	Apply embossing force	F = 23.5 kN
4.	Transfer pattern into PMMA	t = 6 min.
5.	Cooling below T_g and demoulding	T = 96 °C

Table 3.3: Process parameters for hot embossing in PMMA from a 4" silicon master

The total cycle time of this process is approximately 15 minutes. After embossing the structured PMMA substrate is cut to disc shape and access holes are created using a CO_2 laser cutter (Epilog, USA). Subsequently, discs are sealed by bonding to a plain PMMA disc using pressure sensitive adhesive (Adhesive Research, Ireland).

3.2 The Centrifugal Test Stands

During the course of this work, two generations of centrifugal test stands have been designed and built. The first test stand provides basic functionality for spinning discs and observing the movement of particles and liquids within the fluidic network, while the second generation stand offers additional fluorescence detection and optical tweezers based particle manipulation capabilities. In this work for the first time, centifugal microfluidics has been combined with the unique capabilities provided by optical tweezers. In the next section, the 1^{st} generation version will be described first, followed by the 2^{nd} gen. test point.

3.2.1 The 1^{st} Generation Centifugal Test Stand

The basic functionality which needs to be offered by a centrifugal test stand is to spin discs according to a user definable program and observe the behavior of particles and fluids in the disc. Two 1^{st} generation test stands have been built, whereas the components are essentially identical except for the cameras used and the strobe lights. The differences in terms or performance are highlighted in table 3.4. The test stand comprises of the following main components:

1. Motor with optical encoder (4490H024B, Faulhaber, Germany)
2. Motor controller (MCBL 5004, Faulhaber, Germany)
3. Strobe light illumination (Drelloscope 3244, Drello, Germany / BVS-II, Polytec, Germany)
4. Camera (Sensicam qe (monochrome) / Pixelfly qe (color), PCO, Germany)
5. Motorized zoom lens (12x motorized zoom 1-51188, Navitar, USA)
6. Linear stage for radial positioning (T-LSR150, Zaber Inc, Canada)
7. Delay box for azimuthal positioning (in-house built)
8. Computer for image acquisition and process control

One of the test stands built during the course of this work is shown in Fig. 3.2, while a schematic representation of all components is shown in Fig. 3.3.

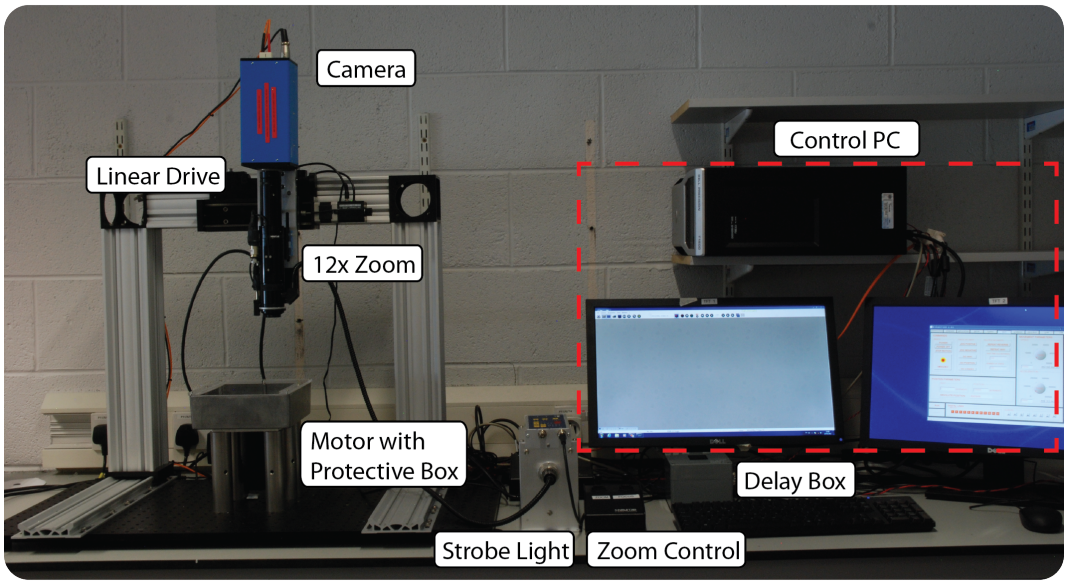

Figure 3.2: The first generation test stand and its main components

The test stand works as follows; the user sets the rotational frequency of the motor using software on the control PC (Winmotion, Faulhaber, Germany). When the motor is spinning, it sends two signals to the delay box (position and reset). On the position signal line, the motor sends 1000 impulses per revolution, while sending one pulse per revolution on the reset line. A digital counter in the delay box counts the impulses on the position line and compares them with a user defined value between 0 and 999, while the signal on the reset line is used to reset the counter once per revolution. When the counted impulses are equal to the user defined position value, the delay box sends a TTL pulse which triggers the strobe light and camera. The radial position for image acquisition is selected by moving the camera using a linear drive. This setup allows imaging of any position on the disc, with a radial position resolution of a few μm and an azimuthal resolution of 0.36 °. Images can then be directly recorded to the hard drive of the control PC. The camera is attached to a 12x motorized zoom lens, and several lens attachments (0.5x and 1.5x) and adapters (0.67x and 2x) are available to adjust the magnification of the optical system. This setup allows the observation of micron-sized objects such as beads or cells even under high rotation frequencies. Since images are always recorded at the

Maximum Rotation Frequency	160 Hz
Maximum torque	191 mNm
Field of view (depending on lens configuration)	72 mm (0.25x lens attachment + 0.67x adapter, min zoom) – 0.52 mm (1.5x lens attachment + 2x adapter, max zoom)
Resolution limit (theoretical)	33.33 μm – 1.12 μm (for the configuration shown above)
Objective working distance	341 - 50 mm
Minimum exposure time	0.5 μs (Sensicam qe), 5 μs (Pixelfly qe)
Maximum frame rate	10 fps
Resolution	1376 x 1040 (Sensicam qe),1392 x 1040 (Pixelfly qe)

Table 3.4: Technical specifications of the centrifugal test stands

same radial and azimuthal position, the images appear steady to the observer. The key-specifications of this system are summarized in table 3.4

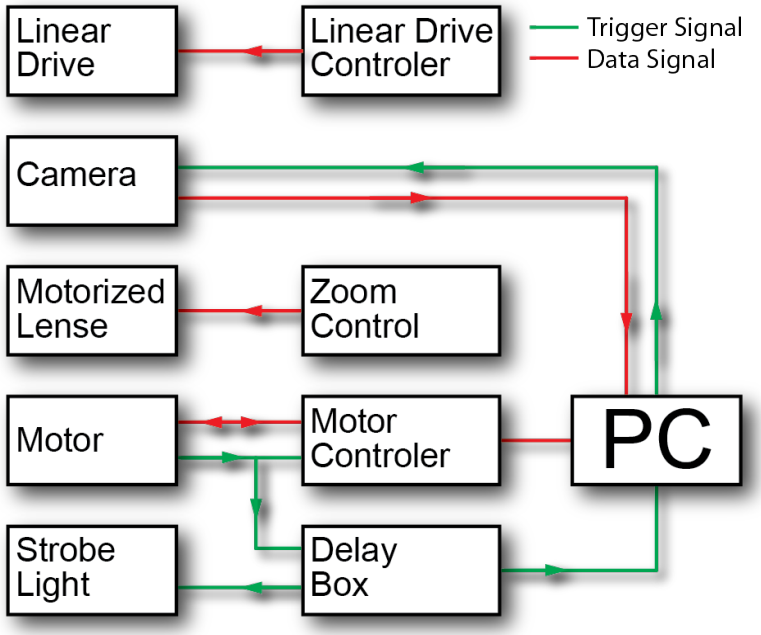

Figure 3.3: Diagram of the centrifugal test stand

3.2.2 The Advanced Centrifugal Test Stand (2^{nd} Generation)

Based on the 1^{st} gen. centrifugal test stand, a more advanced version has been developed which allows multi-color fluorescence detection and single particle manipulation using an optical tweezers setup. First the setup of the second generation

test stand will be discussed, followed by an explanation of the working principle of optical trapping (see 3.3).

In addition to the components of the 1^{st} generation test stand, the second generation incorporates a custom built optical module. The setup used in this work comprises of a 1064 nm IR laser with a power of 1 W (Roithner Lasertechnik, Austria). The laser beam is widened by a beam expander comprising of two lenses in order to fill the back aperture of the microscope objective. The laser beam is then focused through a 40x oil immersion microscope objective with a high numerical aperture of NA = 1.3 (CZ Plan Neofluar 40x/1.3 OIL PH3, Zeiss, Germany). A CCD camera (TXG 14f Mono, Baumer, Germany) is attached such that it allows observation of the manipulation performed by the optical tweezers as well as fluorescence imaging. An infrared filter is attached to the camera in order to protect the CCD chip from reflected laser radiation which would have a negative effect on the imaging quality. Fluorescence excitation is performed by a 250 W halogen lamp (KL 2500 LCD, Schott, Germany) with an attached band pass filter (485 ± 10 nm). The second generation test stand and the optical module are shown in Figs. 3.4 and 3.5.

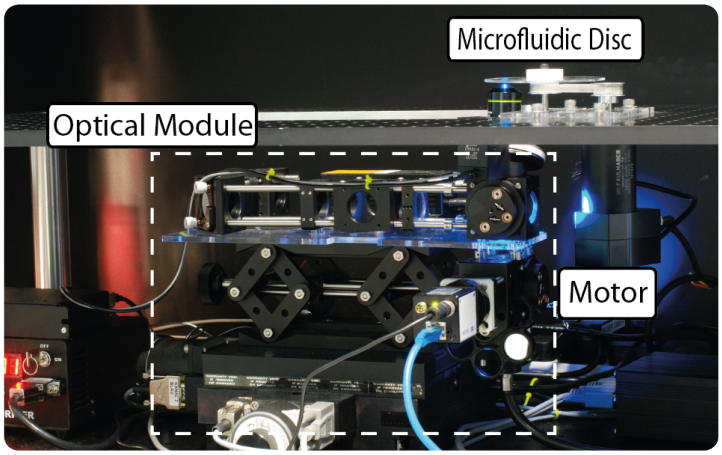

Figure 3.4: Second generation centrifugal test stand with optical module

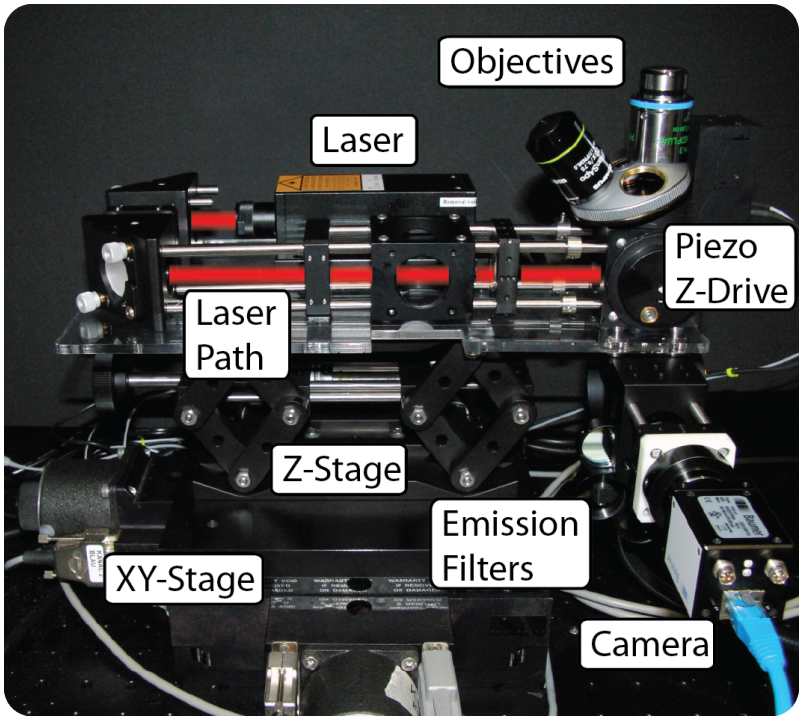

Figure 3.5: Optical module of the second generation test stand which provided optical tweezers as well as fluorescence detection capabilities

The schematic of the optical module is shown in Fig. 3.6. The complete optical module is mounted on a computer controlled XY table.

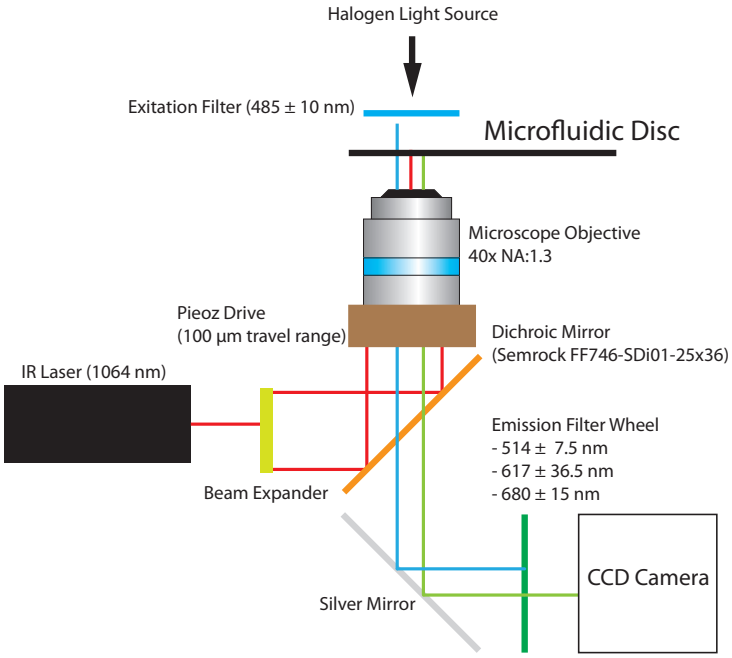

Figure 3.6: Schematic overview of the module providing optical tweezers and fluorescence detection capabilities

3.3 Particle Manipulation using Optical Tweezers

3.3.1 A Brief History of Optical Particle Manipulation

Optical tweezers employ a tightly focused laser beam to trap and manipulate particles in the range of a few nanometers up to several micrometers. The use of lasers to capture and manipulate particles was pioneered by Ashkin at the AT&T Bell Labs in the 1970s. In his first work he demonstrated that particles can be accelerated using a laser, and the stable capturing of particles in a trap comprising of two counterpropagating laser beams [143]. Later Ashkin and Dziedzic demonstrated levitation of 20 μm glass beads in air as well as in vacuum using a single laser beam and gravity as a counteracting force [144]. The first single beam optical tweezers setup, which didn't need gravity as a counteracting force but solely relied on light induced forces, was presented by Ashkin, Chu and co-workers in 1986 [145]. The invention of the single beam setup was a significant step forward and this is the type of trap still widely in use today, and is also used in this work.

Optical tweezers have been used for a wider range of applications, such as stretching single DNA strands [146], study of molecular motors [147] as well as DNA and RNA polymerases [148, 149]. The most relevant applications of optical tweezers in the context of this work is the manipulation of cells and micro beads. The first work demonstrating the capabilities of optical tweezers to capture living cells was published by Ashkin and co-workers [150]. Since then optical tweezers have been employed for various applications in cell sorting and identification [151–153]. A wide range of excellent reviews has been published over recent years, giving an overview of the various areas of applications for optical tweezers [154–157]

3.3.2 Working Principle of Optical Tweezers

Depending on the diameter of the particle $d_{Particle}$, two different models can be applied to describe the forces acting on the particle. In the case where $d_{Particle}$ is much smaller than the wavelength λ of the laser used for the optical trap, the so-called Rayleigh regime, the particles act as dipoles. The force exerted on a dipole by the laser divides itself in two components, the scattering force which points in the direction of the incident light and the gradient force, pointing in the direction of the intensity gradient of the incident light. Chaumet at al. derived an expression to calculate the total time averaged force exerted by an electromagnetic field on an dipolar sphere in the Rayleigh regime [158]. In the case where $d_{Particle} \gg \lambda$ (Mie scattering regime) the working principle can be explained using a classical ray optics model [159]. Since the size of biological cells typically satisfies this requirement, the working principle will here be described using the ray optics approach. When a transparent dielectric particle with refractive index n_p, surrounded by a medium with refractive index n_m (with $n_p > n_m$) is hit by a ray of light with power P, a part of the light is reflected at the interface, while the remaining ray with power P' enters the particle. The reflected component of the light results in a force in the direction of the propagation of the incoming ray (scattering force, F_s). Since $n_p > n_m$, the ray in the sphere is refracted, resulting in a change of momentum. Due to the conservation of momentum, the sphere also experiences a change of momentum of the same magnitude, but in the opposite direction (gradient force

F_g).

The resulting forces through the center O of the sphere can be calculated by [159]:

$$F_Z = F_s = \frac{n_m P}{c}\left(1 + R\ cos2\theta - \frac{T^2[cos(2\theta - 2r) + R\ cos2\theta]}{1 + R^2 + 2R\ cos2r}\right) \tag{3.1}$$

$$F_Y = F_g = \frac{n_m P}{c}\left(1 + R\ sin2\theta - \frac{T^2[sin(2\theta - 2r) + R\ sin2\theta]}{1 + R^2 + 2R\ sin2r}\right) \tag{3.2}$$

where θ and r are the angles of incidence and refraction, respectively. R and T are the Fresnel coefficients for reflection and transmission. c is the speed of light.

First in the case of transparent sphere which is illuminated by a beam of light, the intensity of which increases towards the center is considered (Fig. 3.7). If the center of the sphere is shifted with respect to the maximum intensity of the incoming beam, the sphere is drawn towards the intensity maximum due to the unbalanced gradient forces. However, to achieve stable trapping with this configuration, an external force counteracting the scattering force, e.g. gravity or a second laser, is necessary.

In order to create a stable trap using only one laser, it is necessary to focus the laser, thus creating a 3 dimensional intensity gradient. The forces for this configuration are shown in Fig. 3.8.

3.3.3 Practical Considerations for Designing an Optical Tweezers Setup

After outlining the theory of particle manipulation using optical forces, this section summarizes some practical considerations for the design of an optical tweezers setup. From the previous considerations it is apparent that the refractive index of the particles needs to be higher than the refractive index of the surrounding medium to create a stable trap. If the refractive index of the medium is higher than the refractive index of the sphere, the particle will be pushed away from the focus of the laser. In order to create a stable 3D trap, the gradient forces must dominate over the scattering forces which pushes the particle away from the focal point of the laser. This can be achieved by a very steep gradient of the light, produced by focusing

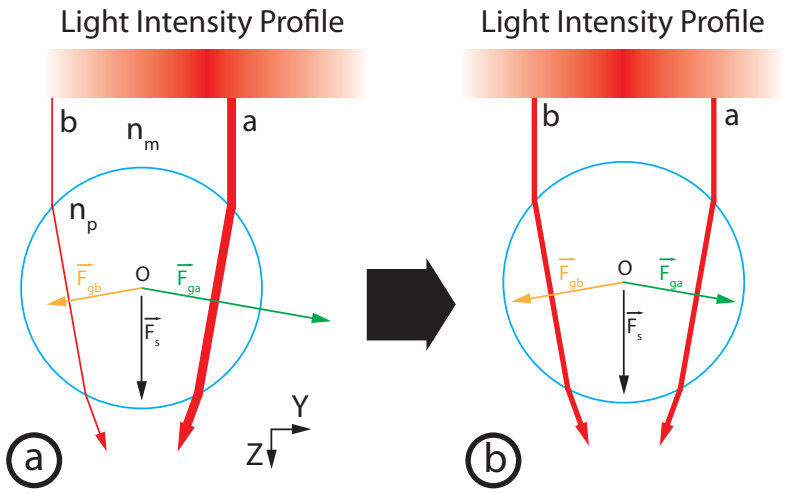

Figure 3.7: Ray optics description of the forces induced in a dielectric sphere due to a nonhomogeneous laser beam. a) A transparent particle is illuminated by a parallel beam of light with an intensity maximum in the center of the beam. Since the particle is shifted towards the left side of the intensity maximum, the right side of the bead is exposed to a ray with a higher intensity than the left side (visualized by the different thicknesses of ray a and b). Since the refractive index n_p of the particle is higher than the refractive index n_m of the surrounding medium, the beams are refracted towards the center of the particle, which in turn changes the momentum of the photons. Due to the conservation of momentum, the particle experiences a change of momentum of equal magnitude but in the opposite direction. This leads to the gradient forces F_{ga} and F_{gb}. Since the intensity of the beam on the left side of the sphere is lower than on the right side $\Rightarrow F_{ga} > F_{gb}$. Hence the resulting force is directed towards the intensity maximum of the laser beam. In addition, the reflected light results in a force in Z direction (scattering force F_s). b) Once the center of the sphere is aligned with the intensity maximum of the laser beam, the resulting force in Y-direction is 0 and only a force in Z-direction is acting on the sphere.

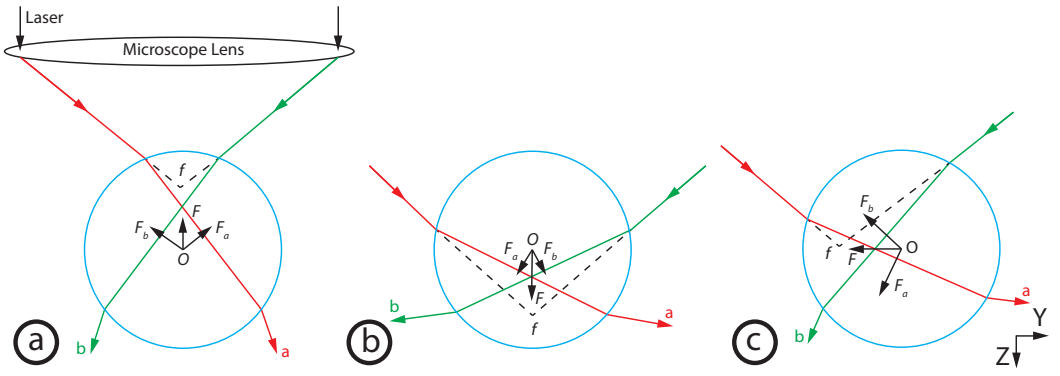

Figure 3.8: Working principle of a single beam optical trap using a focused laser. a) In the case where the center of the particle (O) is located below the focal point f of the laser beam, the resulting gradient forces "pull" the bead towards the focal point. b) shows the forces for the case where O is located above f c) shows the case where the center of the particle is at an arbitrary position with respect to f. In all cases the resulting force F is oriented such that O is drawn towards f. F_a and F_b denominate the forces induced by ray a and b, respectively. F is the resulting force. For the sake of clarity, scattering forces are not considered in this example. Adapted from [159]

the laser using an objective with a high numerical aperture NA. However, high NA objectives have some disadvantages. The focal point is typically very close to the objective which limits the working range in Z-direction. For microfluidic applications this means that the cover used for sealing the channel must be very thin (this is the reason for using glass cover slides to bond the chips for the optical tweezers experiments see section 3.1.3). Another disadvantage of these objectives is that they are comprised of a large number of lenses and transmit only between 32 - 68% of the laser power [160]. Furthermore, high magnification objectives only provide a limited field of view which makes observation of the manipulation more difficult. The configuration selected for this setup results in a field of view of approx. 600 μm diameter. For biological applications the choice of the laser wavelength is critical to avoid damaging the biological material. Typically, a wavelength in the near infrared between $\approx$ 750 - 1200 nm is selected since this is between the region where proteins absorb and where the transmittance of water decreases [156]. Neuman and colleagues examined the photodamage induced for different wavelengths in *E. coli* and Chinese hamster ovary (CHO) cells [160].

For the setup used in this work the following components have been selected:

1. Objective: CZ Plan Neofluar 40x NA 1.3 OIL PH3, working distance = 200 μm (Zeiss, Germany)

2. Laser: 1064 nm, 1W DPSS Laser (Roithner, Austria)

3. PIFOC Piezo Nanofocusing Z-Drive, 100 μm (Physik Instrumente, Germany)

The current setup is capable of manipulating a single particle at a time and is rather bulky due to the laser being mounted on the XY table. In the next revision, the laser could be coupled in using an optical fiber to achieve a more compact footprint. Furthermore, simultaneous multi-particle manipulation could be implemented using movable mirrors or holographic optical tweezers.

Chapter 4

Capture, Distribution, Counting and Multiplexed Assaying of Beads using the V-Cup Platform

This Chapter has been published in:

Robert Burger, Patrick Reith, Gregor Kijanka, Victor Akujobi, Patrick Abgrall and Jens Ducrée, *Array-Based Capture, Distribution, Counting and Multiplexed Assaying of Beads on a Centrifugal Microfluidic Platform*, Lab on a Chip 2012

This chapter presents the fundamental working principle of the V-Cup capturing scheme, developed during the course of this work. Particles sediment under stagnant (i.e. no-flow) conditions into an array of mechanical traps (so called V-Cups) where they get trapped. By scale matching the size of the V-Cups to the size of the particles sharply peaked single occupancy distributions can be achieved. Furthermore it is shown that the capture efficiency of this method is close to 100% and thus much higher than typical pressure driven approaches. This technology offers unique capabilities for cell and particle based applications on centrifugal microfluidic platforms. In this chapter also the application of the V-Cup platform to perform mulitplexed bead based immuno assays is demonstrated.

We present a novel centrifugal microfluidic platform for the highly efficient manipulation and analysis of particles for applications in bead-based assays. The platform uses an array of geometrical V-Cup barriers to trap particles using stopped-flow sedimentation under highly reproducible hydrodynamic conditions. The impact parameters governing the occupancy distribution and capture efficiency of the arrayed traps are investigated. The unique, nearly 100% capture efficiency paired with the capability to establish sharply peaked, single occupancy distributions enables a novel, digital readout mode for color-multiplexed, particle-based assays with low-complexity instrumentation. The presented technology marks an essential step towards a versatile platform for the integration of bead- and cell-based biological assays.

4.1 Introduction

Microfluidic systems offer a manifold of advantages such as short diffusion times and precise control of (laminar) flow and shear rate and therefore have the potential to leverage innovative tools for biological assays and drug discovery [161] Typical applications are cell- and bead-based assays where it is mandatory to capture particles in a well-defined manner and expose them to a variety of conditions [162, 163]. In bead-based assays, specific capture probes are immobilized on the surface of beads which are typically labeled by a unique spectroscopic fingerprint or distinguished by the fluorescent tag of a detection antibody. Using conventional instruments, the handling of the suspended beads in the assay protocol is rather straightforward. However, the spectroscopic identification of the beads and the (simultaneous) readout of the assay signal originating from their surface constitute major microfluidic, optical and instrumental challenges. In most cases a complex and expensive apparatus akin to commercial flow cytometry systems is required for detection. Further issues arise from the miniaturization of bead-based assays. In macroscopic systems, homogeneous assay conditions can be assured by stirring, and reagents can be readily exchanged by using filters or magnetic beads. In miniaturized systems, micro particles can be captured using for example hydrodynamic trapping in meander channels [164, 165]. Furthermore, beads can be embedded in a matrix of a support

material [166] or they can be aggregated, e.g. in step or weir-structures [103, 167] and then exposed to a sequence of reagents in flow-based schemes. Such bead aggregates are very difficult to control in three dimensional microcavities and also lead to a high fluidic resistance. They are commonly prone to display statistical voids and noticeable fractions of the layers may even be missing, in particular at the ceiling of microfluidic channels. Due to the interplay of the laminar flow conditions prevailing in microstructures, the parabolic Poiseuille flow profile and the commonly rather wide pore size distribution in the bead aggregate, a considerable spread between the individual assay conditions for each bead is thus very common. This intrinsic lack of hydrodynamic control severely affects the biochemical assays, e.g. through the total amount of sample passing across the surface of beads, the binding kinetics and the efficiency of washing due to uncontrollable, local variations of fluid shear. In the overall context of (multiplexed) bead- and also cell- based assays, this paper introduces a novel strategy for the capture, retention and treatment of particles which will also facilitate a digital mode for counting and ID of the particle content in a given aliquot. Several methods for bead or cell trapping have been reported in the past. Common methods are dielectrophoretic trapping (DEP) and hydrodynamic trapping. Yang *et al.* [168] showed a setup comprising of two parallel channels separated by a dam structure where cells were trapped due to the flow between the two channels. Di Carlo *et al.* [169] presented an array of capture elements using a pressure driven flow. These capture elements were designed to leave a 2 μm gap in the vicinity of the eventual capture location to promote liquid flow through the capturing elements. Skelley *et al.* advanced this approach to retain two different cells in each capturing site for cell pairing [170]. A similar technique was also used by Khoury *et al.* for on-chip culturing of human stem cells [171]. Kim and coworkers recently published a chip for trapping bacteria from a pressure driven flow [172]. Gravity driven sedimentation approaches to capture cells in microwells have also been investigated in the past [173, 174]. Lee *et al.* developed a system using the artificial gravity created in a centrifugal microfluidic system to trap cells [100]. In their system, a cell suspension was flown through a radially sloped channel with pockets in the side walls where the cells were trapped under the impact of the centrifugal

force. Martinez-Duarte *et al.* showed a DEP filter integrated on a centrifugal microfluidic platform, using carbon electrodes to filter cells [88]. Another centrifugal microfluidic structure using DEP for cell separation was presented by Boettcher *et al.* [89]. Centrifugal microfluidic systems offer unique solutions for sample preparation and liquid handling. Various functions such as valving, metering, mixing, diluting and particle separation have been shown in the past [33, 34, 48]. Furthermore, this technology enables development of low cost point of care devices [69]. In our novel scheme, suspended particles such as 20 μm polymer beads are captured in an array of V-Cups under stopped-flow conditions, i.e. by mere sedimentation, during fast rotation of the disc-shaped substrate. Compared to typical, flow-driven capture schemes, our new method utilizes microfluidic structures which are easier to manufacture (e.g. no vertical gaps are necessary to promote flow through the cups), does not need to connect to periphery such as external pumps, and offers an unprecedented level of capture efficiency. Furthermore, the scheme presented here with beads is also applicable to cells. The influence of the ratio between the particle size and the active capturing zone of the V-Cups on the particle occupancy per cup and the overall capture efficiency are investigated. We found that the particle count distributions can be tuned to a sharp peak at a single occupancy per V-Cup. Such single occupancy distributions introduce highly homogeneous and reproducible assay conditions for bead- and cell-based assays. This novel particle capture scheme is the most critical element towards a comprehensive platform for capturing and analyzing beads and cell populations on a centrifugal platform.

4.2 Experimental Methods & Materials

4.2.1 Device Fabrication

All devices used in this work have been fabricated in PDMS (Sylgard 184, Dow Corning GmbH, GERMANY). Molds for PDMS casting have been manufactured using the method described in chapter 3. To replicate this template, PDMS was mixed in ratio of 5 : 1 (base to curing agent by weight), poured on the mold and degassed under vacuum for 20 min. The PDMS was then partially cured in the oven

at 85 °C for 15 min and removed from the mold. Access holes have been punched into the PDMS slab. The disc was sealed with a blank PMMA disc exhibiting a spin coated layer of PDMS in a ratio 20 : 1 (base to curing agent by weight) on its surface which has been cured in the oven for 20 min. The PMMA-PDMS assembly was eventually baked at 85 °C for 3 h to establish irreversible bonding [141]. Fig. 4.1 shows one of the discs used in this work.

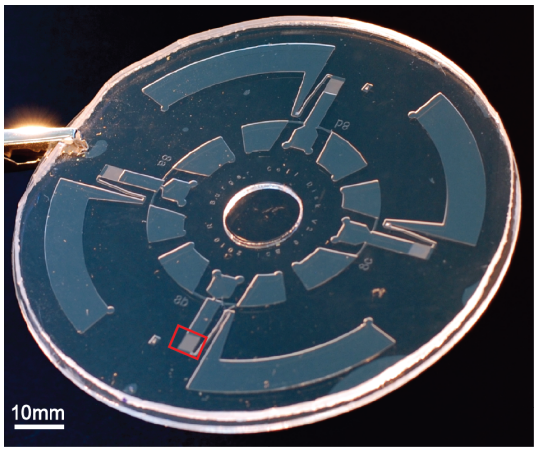

Figure 4.1: PDMS disc with four identical fluidic structures used in this work. The position of one capturing array is marked by the red square.

4.2.2 Preparation of Microfluidic Chip

The microfluidic structures used in this work contain arrays with a density of capturing elements ranging between 180 and 340 elements per mm^2, depending on the size of the V-Cups. Each chamber contains 1350 - 3500 single capture elements. To assure complete and bubble-free filling, the device is placed in a vacuum prior to introducing the liquids [142]. A computer controlled motor (Faulhaber Minimotor SA, SWITZERLAND) sets the spin rate of the disc. Imaging during rotation was achieved using a highly sensitive camera (Sensicam qe, PCO, GERMANY) attached to a motorized 12x zoom lens (Navitar, USA) in a setup similar to the one presented by Grumann *et al.* [175].

4.3 Working Principle

The system presented in this work is based on the sedimentation of particles in a suspending medium due to the influence of the centrifugal force and subsequent

mechanical trapping of the particles in an array of mechanical traps. The array comprises of a staggered arrangement of v-shaped cups with each subsequent line shifted by 1/3 of the center-to-center distance λ between two neighboring cups. This arrangement eliminates free radial pathways between the sample inlet and the bottom of the chamber. Initially, the array is completely filled with pure liquid. Beads are then introduced radially inwards from the cup array. Rotating the disc induces a radially directed sedimentation of the beads which are denser than the surrounding liquid. The capturing chamber is designed such that there is no flow of liquid during the capturing process, i.e. capturing is performed under stagnant flow conditions. When a bead sedimenting into the array hits a cup sufficiently close to its center, the bead becomes mechanically trapped. The capturing and medium exchange process is shown in Figs. 4.2 and 4.3, respectively to illustrate the working principle.

The size of the cups determines the number of beads it can hold and hence the occupancy can be adjusted ranging from single to multi-bead occupancy depending on the ratio $R_c = d_C/d_B$ of the active capturing cross section of the cups d_C and the diameter of the beads d_B. Since the particles sediment in a stagnant liquid, our new method overcomes a major drawback of pressure driven capturing schemes. This drawback is linked to the continuity of streamlines which diverge around obstacles and hence drag the particles around the capturing elements. This effect has previously been suppressed in part by introducing small gaps in the capture elements, e.g. slits or vertical gaps between the top of the trapping structures and the lid [169, 171, 172]. These sieve-like openings are too narrow for the particles to pass, but they do add flow components directed through the center of the capturing elements. However, in particular for small, micron-scale beads, these structures are rather complex to manufacture and tend to result in only a slightly improvement of the capture efficiency. In recent experiments on pressure driven cell capturing, Kim *et al.* reported maximum capture efficiencies of particles as low as 1% [172], whereas our system can be readily configured to achieve a theoretical capture efficiency of 100%. Our experimental results come indeed very close to the theoretical limit. To enable washing, treatment and staining of the captured particles, the medium in the

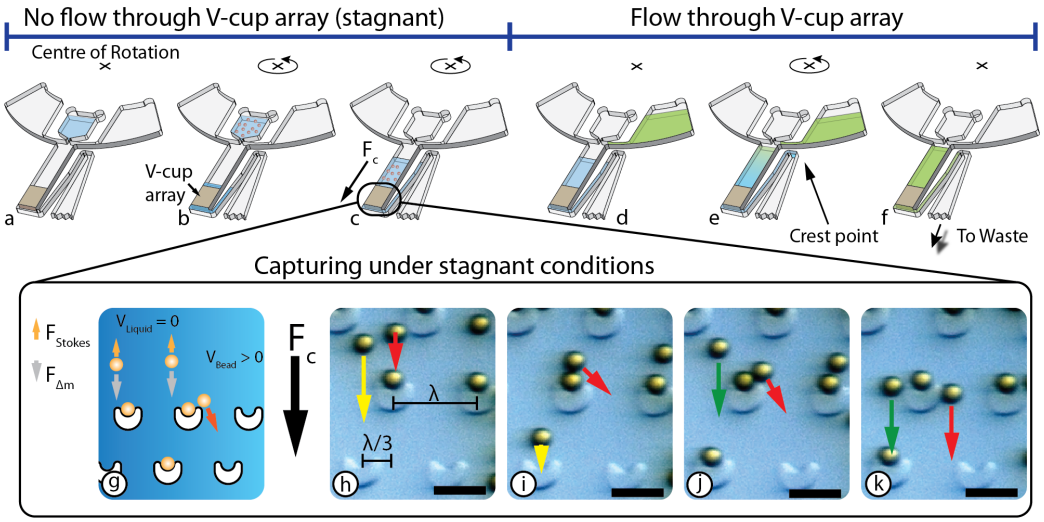

Figure 4.2: Bead capturing and procedure for medium exchange. (a) Introduction of a small volume of liquid to fill the capturing array and to enable particle sedimentation. (b) Particle suspension is filled in the central reservoir and the disc is spun, resulting in a transfer of the particle suspension on top of the liquid in the capturing array and the sedimentation of the beads (b, c) (until this point there is no flow of liquid through the array). The medium in the bead capturing chamber can be displaced by introducing a second liquid in the reservoir and spinning the disc. The liquid flows into the capturing chamber, resulting in the rise of the liquid level above the crest point of the siphon. This leads to a liquid flow into the waste reservoir (d, e). If the volume of the second liquid is larger than the volume of the capturing chamber, the liquid volume in the chamber is exchanged (f). This can be repeated successively in order to expose the particles to different reagents. Image g illustrates the capturing principle and forces acting on the beads while the sequence h – k shows the capturing of 20 μm PS beads in an array of cups with $R_c = 1$. The yellow arrow shows the capturing of a bead in a cup while the red and green arrows show the sedimentation and deflection of beads along their approach of already occupied cups. A video of the capturing process is also available as supplementary information. Scale bars are 50 μm.

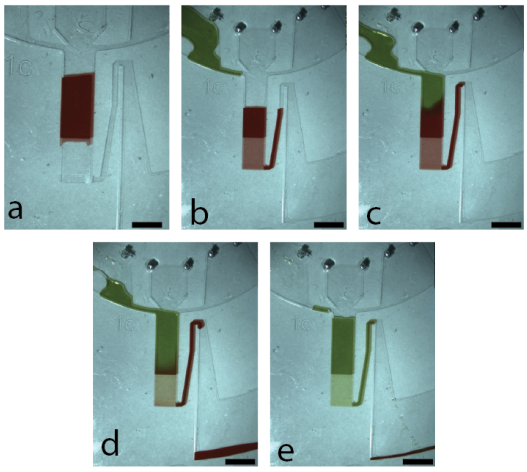

Figure 4.3: Medium exchange in v-cup chamber. The chamber is completely filled with a first liquid (red) (a). The disc is then stopped and a second liquid (green) is introduced (b). Subsequent spinning of the disc transfers the second liquid into the array chamber where the first liquid is completely replaced (c - d). Scale bars are 1 mm.

V-Cup chamber is exchanged via a siphon-based mechanism. The radial position of the crest point of the siphon sets the maximum filling level of the V-Cup chamber. So adding an amount of liquid corresponding to the dead volume of the array chamber will prime the siphon past its crest point and completely replace the original medium surrounding the beads under the prevalent laminar flow conditions in our microfluidic system. While keeping the flow rates during the exchange sufficiently low, the vast majority of beads remain trapped.

4.3.1 Bead-Based Immunoassays

The particle suspensions used for the immunoassays consisted of 20 μm polystyrene beads (Microparticles GmbH, GERMANY) diluted in PBS with 5% Bovine Serum Albumin (BSA) (Sigma-Aldrich, IRELAND) to reduce agglomeration and sticking to the PDMS. All immunoassay experiments have been carried out using three colors of 20 μm polystyrene beads. Each color corresponds to a different IgG coating: mouse anti-ERa IgG (sc-8002, Santa Cruz, USA) (white PS beads), human IgG (MS143, Biomeda corp., USA) (red PS beads) and rabbit Anti-fd Bacteriophage IgG (B2661, Sigma-Aldrich, IRELAND) (blue PS beads). The analyte for the immunoassay contained goat-anti-mouse antibodies (Ab, IgG1) labelled with Alexa Fluor 488 (A11001, Invitrogen, USA), goat anti-human Ab (IgG2) labelled with Alexa Fluor 488 (A11013, Invitrogen, USA) and goat anti-rabbit Ab (IgG3) labelled with Atto 488 (A11008, Invitrogen, USA). For the bead-based immunoassays capture array comprising of cups with an active capture zone diameter of 20 μm have been used in order to induce distributions which are sharply peaked at single bead occupancy. In a first step, the array region has been filled with 2 ml of PBS buffer with 5% BSA. Next 2 ml of bead suspension (2000 beads μl^{-1}) has been filled in the bead reservoir. The disc was immediately spun at 20 Hz in order to transfer the bead suspension in the array chamber and capture the beads in the V-Cups. Shake mode capturing was applied to achieve single bead occupancy per cup. After the capturing step, the disc was stopped and 8 μl of analyte (containing IgG1, IgG2 or IgG3) was pipetted into the sample reservoir. The disc was then rotated again at 20 Hz, leading to a flow of the analyte into the array chamber accompanied by the displacement of

the initial liquid through the siphon channel into the waste chamber. After the full substitution of the first liquid, the disc is stopped and incubated at room temperature for 90 min. Following the incubation step, the array is washed 3 times with 8 μl PBS buffer containing 0.1% BSA to remove all unbound antibodies. Subsequently, the fluorescence of the beads is measured using an inverted fluorescence microscope (IX 81, Olympus, Japan) with a FITC-compatible filter.

4.4 Results and Discussion

4.4.1 Characterization of Particle Capture

To characterize the influence of the ratio of the active capturing cross-section of the V-Cups to the bead diameter on the occupancy distribution of the trapped beads, discs with three different cup sizes (d_c = 14 μm, 20 μm and 32 μm) were prepared and tested with 10 μm and 20 μm diameter particles, respectively. We observed that the spinning frequency does not have a decisive impact on the capture efficiency, but only on the time required for the sedimentation of the particles. Therefore, all subsequent experiments were run at the same rotational frequency of 20 Hz. It was also observed that a shake mode step was advantageous to narrow the occupancy distribution. To this end the following spinning protocol has been used:

1. Bead capturing at 20 Hz
2. Shake mode (acceleration 75 Hz s^{-1}, 40 Hz for 10 s, deceleration 75 Hz s^{-1}, 2 Hz for 10 s, 30 cycles)

The results for 10 μm silica bead experiments show that for a ratio R_c = 1.4, 94% of all occupied cups contain a single bead, while only 0.8% of all cups remained empty. Increasing R_C to 2 leads to a broader occupancy distribution characterized by 57% and 26.6% of single and double occupancy, respectively, and only 2.7% of all cups are left empty. It is to be noted that in particular the number of empty cups also depends on the absolute number of introduced beads. Moving RC further up to 3.2 shifts the maximum of the significantly broadened occupancy distribution to 8 beads per cup. For R_c = 1, 99.5% of all occupied cups contain a single bead.

Increasing R_c to 1.6 leads to a wider distribution where 48.8% are occupied by one bead, 27.7% contain 2 beads and 11% contain 3 beads. The results are shown in Fig. 4.4.

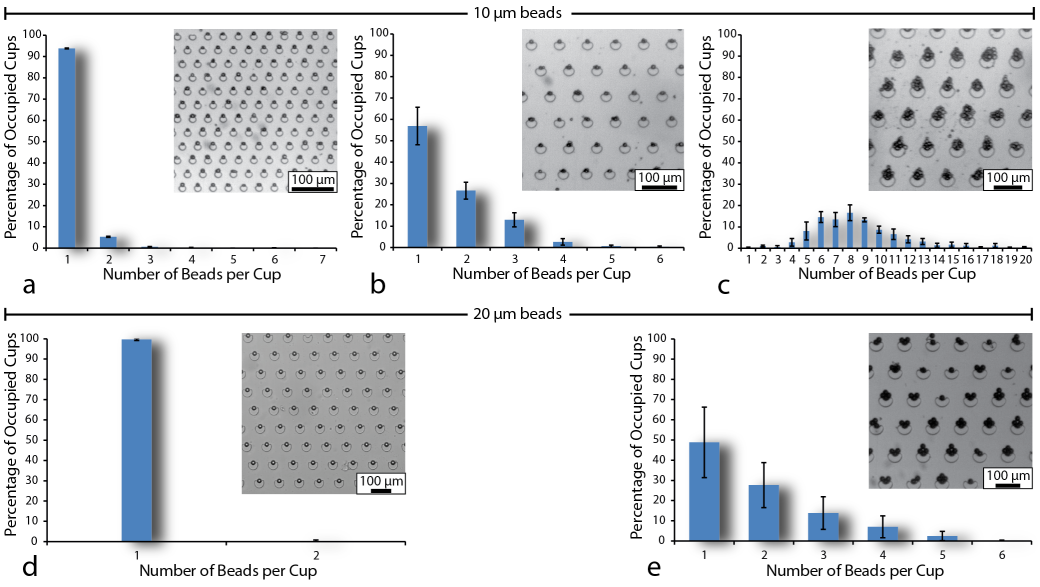

Figure 4.4: Occupancy distribution for different cup sizes with 10 μm silica beads (ac) and 20 μm PS beads (d and e). a) Capture elements with a 14 μm active capturing area. 94% of all occupied cups contain a single bead. Only 0.8% of all cups remained empty. b) Increasing the active capturing area to 20 μm leads to a broader occupancy distribution, and only 2.7% of all cups stayed empty. c) Occupancy distribution for cups with a 32 μm capturing area. The maximum of the distribution shifted to 8 beads per cup, leaving 0.9% of all cups empty. d) $R_c = 1$, 99.7% single occupancy and only 5% of all cups empty. e) $R_c = 1.6$, 48.8% are occupied by a single bead and 27% contain 2 beads. Insets show typical bead distributions in the capture array.

These results demonstrate that it is possible to influence the number of trapped beads per cup by adjusting the ratio between particle diameter and capturing area of the cups. While the occupancy distribution for increasing R_c widens, the distribution shows a sharp peak for R_c values of 1 and 1.4 with 94% single occupancy. This demonstrates that a high percentage of single occupancy can be achieved, even if R_c varies. This is important considering that biological cells are polydisperse, i.e. a population exhibits a wider size distribution. Capturing single particles in well-defined locations is an important capability to enable single-cell or bead-based assays as well as particle counting.

4.4.2 Particle Capture Efficiency

The particle capture efficiency was assessed using 20 μm PS beads and cups with $R_c = 1$ to establish a sharp, single-occupancy distribution. Suspensions with vari-

ous bead concentrations were then introduced into the disc and captured using the following protocol:

1. Spinning at 20 Hz for 4 s clockwise
2. Spinning at 20 Hz for 1 s counterclockwise
3. Shake mode

The capture efficiency was then determined using the following methodology: the total number of all beads (b_T) entering the array was counted in each experiment. Additionally the amount of captured (b_c) and by-passing (b_B) beads was counted. The term by-passing beads describes beads which travel along the side wall of the capturing chamber and cannot be captured due to the absence of V-Cups at the side wall. Introducing cups on the side wall would result in agglomerates of beads in their vicinity. Typically, 3-5% of all beads entering the array bypassed the cups. For applications where high capture efficiency is of paramount importance, bypassing beads could be largely eliminated by increasing the width of the capture array. The capture efficiency was then calculated using the following formula:

$$Capture\,efficiency = b_C/(b_T - b_B)$$

Additionally the array occupancy was also calculated:

$$Array\,occupancy = b_c/n_c$$

Whereas n_c is the total number of cups in the array. For all capture efficiency experiments n_c amounts to 1358. These results show the very high capture efficiency of the stagnant flow scheme. For low bead concentrations, i.e. a ratio of beads to cups (R_{bc}) $\ll 1$, the capture efficiency is close to 100% and even for a ratio of 0.78 the capture efficiency is still above 90%. For $R_{bc} = 0.95$, 86.9% of all beads are captured and 83% of the array are occupied (Fig. 4.5). The fact that the capture efficiency is high for a low bead-to-cup ratio but decreases when the ratio approaches unity underlines the importance of a homogeneous bead distribution over the whole extent of the array. This is necessary to assure that all beads are

trapped because they always encounter an unoccupied cup before leaving the array. With the here presented setup, a R_{bc} of 0.46 results in a capture efficiency of 99.1% which demonstrates the feasibility of performing a full particle count with high accuracy. Methods to improve the particle distribution are currently investigated since increasing R_{bc} while at the same time maintaining a high capture efficiency would allow to reduce the footprint of the array.

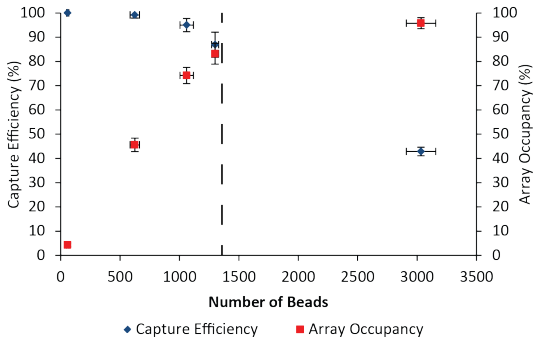

Figure 4.5: Bead capture efficiency and array occupancy depending on the amount of beads presented to the array. The dashed line indicates the total number of cups in the array.

4.4.3 Multiplexed, Bead-Based Immunoassay

Due to the intrinsic advantages of the sedimentation-based V-Cup array technology such as highly reproducible hydrodynamic conditions and the arrayed presentation of beads in a single focal plane, this platform is well suited for bead-based immunoassays with low-complexity instrumentation compared to complex, sheath-flow based commercial flow cytometers. In order to demonstrate this unique capability, a single-step antibody assay has been chosen. 20 μm polystyrene beads have been coated with antibodies and the assay has been performed according to the protocol described previously. Fig. 4.6 represents the results of the assay, where the beads have been captured and subsequently exposed to an analyte solution containing one secondary antibody.

The calibration curve obtained for the assay using beads coated with human IgG and anti-human Ab in the analyte is shown in Fig. 4.7.

Due to the fact that the beads are individually located in a well-defined array within the same focal plane, readout of the assay is straight forward and multiplexing can easily be achieved by using beads of different colors corresponding to the surface-

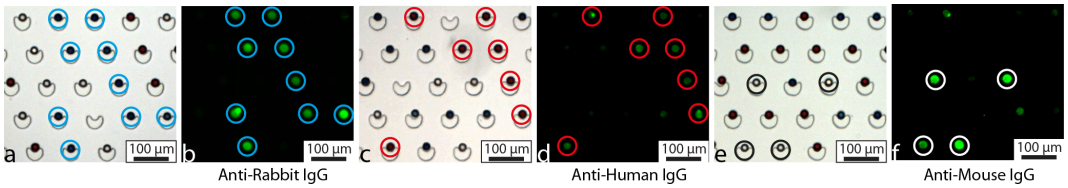

Figure 4.6: Image sequence of a multiplexed immunoassay using colored beads. In each case all beads have been exposed to one secondary IgG (anti-rabbit, anti-human and anti-mouse). a) and b) Beads exposed to anti-rabbit IgG which only attach to the beads coated with rabbit IgG (blue beads). c) and d) Analyte contains anti-human IgG which only attaches to beads coated with human IgG (red beads). e) and f) beads coated with mouse IgG (white) exposed to anti-mouse IgG.

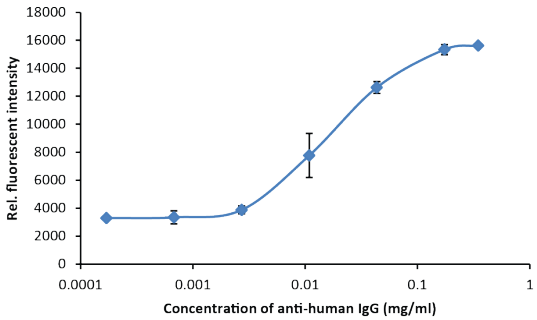

Figure 4.7: Calibration curve for on-disc immunoassay for goat anti-human IgG.

immobilized antibody. The main constraints are that the color of the beads is well distinguishable and that none of the dyes used to color the beads is auto fluorescent at the same wavelength as the fluorophore attached to the detection anti bodies. With this approach only one fluorescent dye, i.e. only one light source and set of filters is needed for the detection and hence the cost for the readout instrument can be notably reduced.

4.5 Conclusion and Outlook

In summary we presented a novel, centrifugal microfluidic platform for highly efficient trapping, distribution and treatment of beads using sedimentation under stagnant flow conditions. The experiments show that our platform is capable of very high capture efficiencies (close to 100%) paired with a high array occupancy. The maximum as well as the width of the particle occupancy distribution are primarily governed by the ratio between the bead diameters and the characteristic length scale of the active capture site as well as the protocols of the rotational frequency. The here presented, arrayed alignment of individual particles in the same

focal plane greatly facilitates detection and readout of signals from the particles. Furthermore, it assures homogeneous assay conditions across the entire bead population. We also demonstrated the capability of our novel platform to perform color-multiplexed, bead-based immunoassays. Future work will concentrate on applying these capabilities to clinically relevant, disease-specific test panels featuring multiplexed immunoassays with integrated sample preparation. Also cell detection and screening will be implemented (see chapter 6).

Chapter 5

Rotationally Controlled Magneto-Hydrodynamic Particle Handling for Bead-Based Microfluidic Assays

This Chapter has been published in:

Robert Burger, Patrick Reith, Victor Akujobi and Jens Ducrée,

***Rotationally controlled magneto-hydrodynamic particle handling for bead-based microfluidic assays*, Microfluidics and Nanofluidics 2012**

This chapter introduces a novel frequency controlled magnetic actuator for releasing particles captured in the V-Cup array as well as for rapid mixing of liquids. The actuation is based on the reciprocating motion of an elastomeric (PDMS) membrane featuring an integrated permanent (on-disc) magnet and a stationary magnet aligned along the orbit of the disc-based chamber. Upon entering the magnetic field of the stationary magnet, the on-disc magnet is deflected such that it compresses the chamber below the on-disc magnet, leading to displacement of the liquid in the chamber. After leaving the magnetic field the PDMS relaxes, thus restoring the original volume of the chamber and hence leading to an inversion of the liquid flow. The magnetic actuator is solely controlled by the rotation frequency of the disc. Below a certain spin speed the residence time in the external magnetic field is long enough to displace the on-disc magnet and hence the actuator is active. Towards higher rotational frequencies the residence time is too short i.e. the actuator is inactive, thus allowing the capturing of particles in the V-Cup array.

This work presents a novel magnetic actuation scheme for advanced particle handling on our previously introduced, centrifugal microfluidic platform for array-based analysis of individual cells and beads. The conceptually simple actuation is based on the reciprocating motion of an elastomeric membrane featuring an integrated permanent magnet and a stationary magnet aligned along the orbit of a disc-based chamber. This compression chamber is placed at the downstream end of the particle capture chamber to induce centripetally directed, hydrodynamic lift forces on particles trapped in V-shaped geometrical barriers. Towards high frequencies of rotation, the on-disc magnet ceases to follow the rapidly oscillating magnetic field, so that the magnetic actuator is disabled during the initial, sedimentation-based filling of the trap array. At reduced spin speeds, the residence time of the magnetic actuator is sufficient to displace the magnetic actuator, resulting in a flow through the V-Cup array that re-distributes, and eventually fully depletes, the previously trapped beads from the array. The same magnetic deflection scheme is also demonstrated to accelerate mixing, e.g. for upstream sample preparation.

5.1 Introduction

Centrifugal microfluidic systems offer many advantages and have attracted considerable interest from academia and industry alike [33, 34, 48]. Advantages of these systems include the wide-ranging tolerance to fluidic properties, such as viscosity, pH or surface tension. Furthermore, the centrifugal actuation principle only requires a spindle motor instead of complex and bulky mechanical displacement pumps. In addition, the capability to use the artificial gravity on the disc readily allows density-based particle separation. However, a disadvantage of the centrifugal platform is the difficulty to integrate on-board actuation. The most convenient approach is to use contact-free methods, e.g. for valving which is pivotal for centrifugal microfluidics. Over recent years, valving schemes for centrifugal and non-centrifugal microfluidic systems employed techniques, such as light switchable polymers [14], heat actuated wax valves [15, 16] , or a laser to connect separate channel pathways [17]. Chen and colleagues recently published a valving scheme for PDMS-based microfluidic chips using permanent magnets. The attraction between the magnets and a ferromagnetic

base plate is used to compress the PDMS, which in turn compresses the microchannels and hence prevents the flow of liquid through the channel [176]. Another very interesting, contact-free method uses magnetic actuation to speed up on-disc mixing through the interplay of an external permanent magnet and on-disc paramagnetic microbeads [45]. Häberle and *et al.* presented an integrated pump for gas sampling in centrifugal microfluidic systems [134]. Another interesting combination of centrifugal microfluidics and magnetic actuation for cell lysis has been demonstrated by Siegrist and co-workers [67].

In this work, we will investigate the combination of on-disc permanent magnets as actuators and stationary off-disc magnets as driving elements. We will show the use of this novel actuator for creating hydrodynamic lift forces leading to the retrieval of previously captured microbeads from an array of V-Cups. The same principle also lends itself to rapid on-disc mixing, which is often an important step in the process chain of immunoassays. The advantage of using the same actuation principle for two different steps of the process (i.e. mixing and particle removal) is that it simplifies the design of the instrumental setup as well as that of the chip itself.

5.2 Array-Based Capture of Individual Particles in V-Cups

The here presented magnetic actuation principle enhances the particle redistribution and retrieval from a previously introduced V-Cup array [104, 106]. In brief, particles sediment into an array of V-shaped cups under stagnant (i.e. no-flow) conditions (Fig. 5.1). The array comprises a staggered arrangement of V-shaped cups with each subsequent line shifted by 1/3 of the center-to-center distance λ between two neighboring cups. This arrangement eliminates free radial pathways between the sample inlet and the bottom of the chamber. Initially, the array is completely filled with pure liquid.

Beads are then introduced radially inwards from the V-Cup array. Rotating the disc induces a radially directed sedimentation of the beads which have a higher density than the surrounding liquid. The capturing chamber is designed to completely

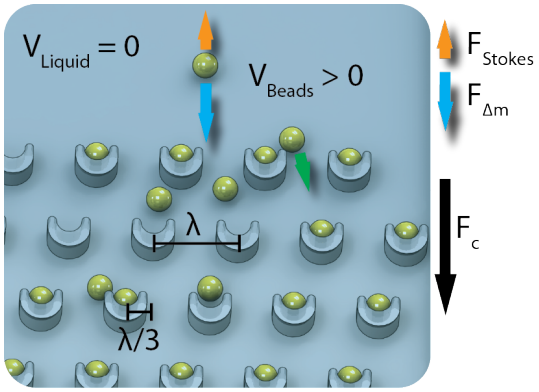

Figure 5.1: Working principle of the V-Cup-based capturing scheme. Particles sediment in a stagnant liquid (i.e. $V_{Liquid} = 0$) due to the centrifugal force F_c into an array of V-Cups. When a bead impacts near the center of an empty cup, it is likely to get trapped. If a bead encounters an already occupied cup, it is deflected since each cup can only hold a single particle.

suppress flow during the capturing process, i.e. trapping occurs with mere particle sedimentation under stagnant conditions. When a bead sedimenting into the array hits sufficiently close to the center of a cup, the bead is mechanically locked by the interaction of shape and centrifugal force. Through scale matching the size of the cups to the size of the particles, the particle distribution can even be adjusted towards sharply peaked, single occupancy. The working principle of this capturing scheme is shown in detail elsewhere [104] and chapter 4. The advantage of this capturing method compared to traditional approaches using pressure-driven flow is the significantly higher capture efficiency (close to 100 %) due to the absence of flow lines that would otherwise drag the particles around the capturing elements and hence reduce the capture efficiency. As shown previously, the liquid in the chamber surrounding the captured particles can then be exchanged several times to expose the particles to various reagents (e.g. antibodies, stains or washing buffer), while retaining the vast majority of the captured particles [104, 106].

5.3 Working Principle

5.3.1 Magnetic Actuator

The magneto-hydrodynamic actuation principle is based on the reciprocating motion of a flexible membrane sealing a compression chamber (Fig. 5.2). To this end, a small disc magnet is attached to the membrane on top of the compression chamber,

and a second stationary magnet is located at the same radial position along its orbit. Both magnets are oriented such that attracting poles are facing each other. During rotation, the on-disc magnet periodically enters the magnetic field of the stationary magnet, resulting in a transient attraction of the on-disc magnet towards the stationary magnet which, in turn, deflects the membrane. This deflection propels a flow from the compression into the array-chamber. After leaving the external field of the stationary magnet, the flexible membrane relaxes, thus restoring the original volume of the compression chamber and generating a reversed flow in the direction of the centrifugal field. The flow generated by the magnetic actuation and (transiently) counteracting the centrifugal field depends on the frequency and amplitude of the magnet displacement, which is related to the effective residence time in the external magnetic field. At quasi-static conditions, i.e. in the regime of low spin rates, the magnetic deflection induces maximum stroke towards the full (static) equilibrium between the elastic restoring force of the membrane and the magnetic attraction. When the rotational frequency is increased, the flow rate initially rises proportional to the increasing number of actuator strokes per unit time. However the inertia of the movable parts, which is equivalent to the inductance in an electric network, leads to an increasing phase lag between the magnetic actuation and deflection. So for high frequencies, the magnetic interaction interval becomes too short to compress the chamber and the phase lag becomes too large to deflect the membrane. Hence, the merely frequency-controlled magnetic actuator is effectively switched off. Essentially, the actuation principle constitutes a magneto-hydrodynamic low-pass filter.

5.3.2 Particle Capture, Re-Distribution and Retrieval

The here-described rotationally induced magneto-hydrodynamic actuation will be combined with the centrifugally induced sedimentation to enable the capture, re-distribution and eventual retrieval of beads in the V-Cup array. By virtue of the low-pass nature of the magnetic actuation, high-frequency sedimentation for trapping incoming beads under hydrostatic conditions is not affected by the (transiently) counteracting magneto-hydrodynamic actuator. For particle retrieval, we combine magnetic actuation and sedimentation. As a consequence of the centripetally di-

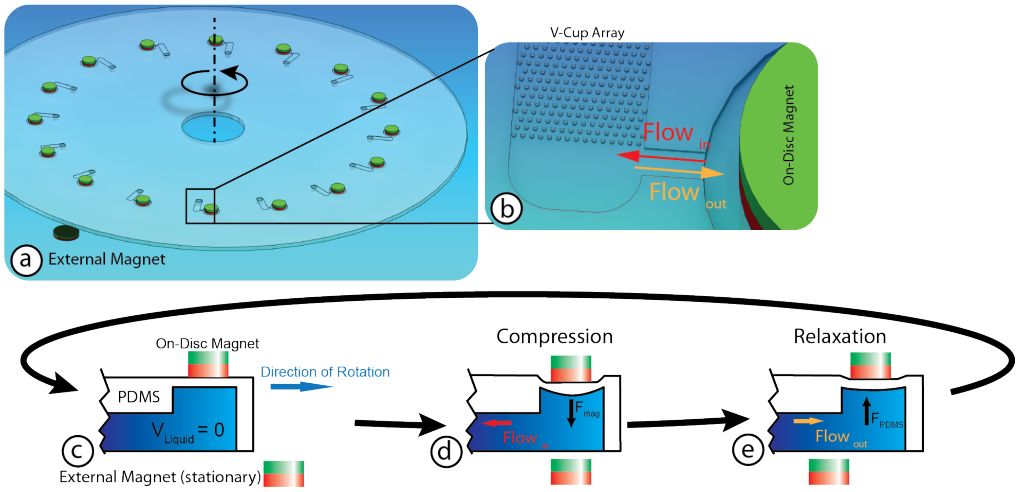

Figure 5.2: The design of the disc used for the bead capturing and release experiments is shown in image a. A detailed view of one capturing structure containing an array of V-Cups for particle capturing and adjacent chamber with attached on-disc magnet is shown in b. The image sequence c - e depicts the working principle of the magnetic actuator. When the on-disc magnet is distant from the external magnet, the actuator remains inactive and the velocity of the liquid residing in the chamber is zero (c). Upon entering the field of the external magnet, the on-disc magnet is attracted, leading to a compression of the chamber which, in turn, results in an essentially centripetal flow into the chamber exhibiting the V-Cup array ($Flow_{in}$) (d). After leaving the magnetic field, the compressed PDMS relaxes and restores the chamber to its original volume, resulting in a flow from the V-Cup array into the actuator chamber ($Flow_{out}$) (e). This process repeats periodically as the disc rotates. If the rotational frequency exceeds a certain threshold, the residence time in the external magnetic field is too short to compress the actuator chamber and to generate flow.

rected, magneto-hydrodynamically induced flow, beads originally trapped in the V-Cups are lifted up while the temporarily reversed flow induced by the relaxation of the membrane drags the beads around the cups and hence prevents re-trapping. Due to the underlying centrifugal force, sedimentation continuously drives the particles towards the edge of the disc. Therefore, a certain fraction of the raised beads will not be able to return to their original trapping position, thus falling through the V-Cup array. Over the course of magnetic actuation, the center of gravity of the bead distribution successively moves towards the peripheral end of the V-Cup array until the beads are retrieved in the outer part of the chamber.

5.3.3 Magnetic Mixer

As a further use of the magneto-hydrodynamic actuation, we implemented an on-disc mixing scheme (Fig. 5.3). The two educts are loaded in separate chambers positioned radially inwards from the mixing chamber. When the disc is spinning, the educts are transferred into the mixing chamber on top of which the magnetic

actuator is mounted. In the presence of external stationary magnet, the on-disc actuator periodically compresses the mixing chamber, resulting in internal advection to accelerate mixing.

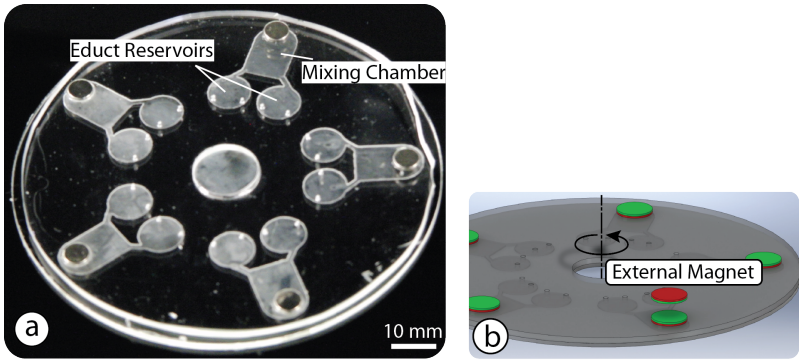

Figure 5.3: Mixing disc made in PDMS with five independent mixing chambers (a). The configuration of the magnets used for the mixing experiments is shown in b. The magnets are oriented such that equal poles are facing each other and the magnets are on the same side of the disc.

5.4 Materials and Methods

All devices used in this work have been fabricated in PDMS (Sylgard 184, Dow Corning GmbH, Germany). Molds for PDMS casting have been manufactured using photolithography. Chips containing V-Cup structures have been manufactured in SU8 (SU8 3025, Microchem, USA), whereas chips for magnetic mixing were fabricated using dry film resist (WBR 2100, DuPont, USA). The reason for using two different processes is that SU8 offers higher resolution, which is mandatory for the replication of the V-Cups, whereas dry film resist (DFR) allows easier fabrication of thick layers which is beneficial for the mixing structures. The molds for the V-Cup chips were manufactured by spin coating a 25 μm thick layer of SU-8 on a silicon wafer followed by lithographic patterning using a mask aligner (MA56, Süss MicroTec, Germany). The molds for the mixing structures were fabricated by laminating two layers of WBR 2100 on a silicon wafer in order to achieve a total thickness of 200 μm. Subsequently, the resist was structured using a mask aligner. In both cases, following removal of the un-exposed areas, the molds were treated with a hydrophobic coating to facilitate the removal of the PDMS from the mold. This was achieved by immersing the wafer in 400 μM octadecyltrichlorosilane (OTS)

(Sigma Aldrich, Ireland) in heptane for 2 h. Subsequently, the wafer was sonicated for 5 min in pure heptane followed by rinsing with methanol. The wafer was then baked on a hot plate for 30 min at 100 °C. This resulted in a coating with a water contact angle $> 108\,°$.

PDMS was mixed in a ratio of 5:1 (base to curing agent by weight), poured on the mold and degassed under vacuum for 20 min. Subsequently, the PDMS was partially cured in an oven at 70 °C for 15 min, removed from the mold and access holes have been punched. The disc was sealed by placing it on a PMMA disc with a spin-coated layer of PDMS in a ratio 20:1 (base to curing agent by weight) which had been cured in the oven for 20 min. The microfluidic structure was bonded to the spin-coated PDMS layer by baking in an oven at 70 °C for at least 3 h [141]. This process resulted in an irreversible bond. The magnetic discs (Supermagnete.de, Germany) for the actuators where subsequently placed on the discs and fixed with PDMS. Magnets for the on-disc actuators had a diameter of 2 mm for the bead release structures and a diameter of 6 mm in the case of the mixing devices. The thickness was 1 mm in both cases. Prior to use, the V-Cup discs have been degassed under vacuum for at least 2 h in order to enable priming of the dead end channels [142], whereas the mixing discs have been used without degassing. All bead release experiments have been carried out using monodisperse polystyrene beads with a diameter of 20 μm (Microparticles GmbH, Germany) and chips have been initially filled with PBS buffer containing 5 % (w/v) Bovine Serum Albumin (BSA) (Sigma Aldrich, Ireland). In the case of the mixing experiments, a colorimetric method has been used to evaluate the efficiency. To this end, 0.2 μM Potassium Thiocyanate and 0.067 μM Iron(III) Chloride (Sigma Aldrich, Ireland) have been used. Both solutions are initially transparent and react to produce a dark red color upon contact. This change in color has been used to quantify the mixing efficiency and time. Mixing efficiency was assessed by the following method. Using ImageJ (NIH, USA) the outline of the region containing the educts was selected. Next, the area containing the magnetic actuator was subtracted from this region and the standard deviation was measured and normalized using the standard deviation measured for a completely mixed sample to assess the mixing efficiency (i.e. a value of 1 signifies complete mixing). Experiments were performed

on a custom made centrifugal test stand, similar to the setup presented by [175]. A computer controlled motor (Faulhaber Minimotor SA, Switzerland) was used to spin the discs and imaging during rotation was achieved using a camera (Pixelfly qe, PCO, Germany) attached to a motorized zoom lens (Navitar, USA) (for more details see chapter 3).

5.5 Results and Discussion

5.5.1 Particle Re-Distribution and Retrieval

We implemented strategies to re-distribute particles in order to optimize conditions and read-out for bead-based assays. Furthermore, we wanted to retrieve all particles from the V-Cup array after completion of the assays, e.g. to further analyze the beads or cells in downstream processes or to regenerate an empty array.

Initially, we looked into ultrasonic treatment where the disc is intermittently placed in an ultrasonic bath to re-distribute captured particles. Subsequent spinning of the disc leads to sedimentation of the beads. Particles which have been redistributed below the last capturing line, or do not hit an empty cup while sedimenting, will leave the array and accumulate at the bottom of the chamber. However, since some particles are trapped during the sedimentation step in empty cups or interstitial locations, the cycle of sonication and spinning has to be repeated several times. The results of these experiments are shown in the ESI (see 5.7). Repeated cycles of ultrasonic treatment lead indeed to the re-distribution of the beads. After eight ultrasonic treatment cycles, $< 10\%$ of the original beads remained trapped in the array. However, the repeated removal of the disc, insertion into the ultrasonic bath and re-mounting onto the spindle motor are quite cumbersome and not readily automatable. To overcome the burdensome handling procedure of the disc, an integrated particle manipulation scheme based on the above-described, magneto-hydrodynamic actuator has been developed. A series of experiments were performed to determine the optimum rotational frequencies for capturing mode (magnetic actuator inactive, movement of particles solely governed by centrifugal force) and for release mode (centrifugal force still prevails but flow induced by the magnetic actuator lifts cap-

tured beads from the cups and prevents re-trapping). It has been found that for frequencies above 30 Hz the system operates in capture mode while a frequency of 8 Hz has been determined as optimum for the release mode (on-disc magnets were positioned at a distance of 27 mm from the center of rotation). Therefore, frequencies of 30 and 8 Hz have been chosen to perform capturing and release, respectively. The successful re-distribution of the beads is illustrated by the frame sequence in Fig. 5.4, while the bead distribution over the rows of the V-Cup array over time is shown in Fig. 5.5.

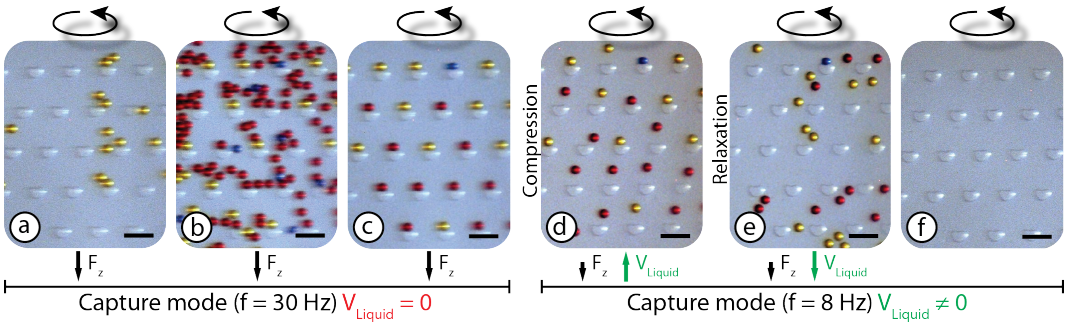

Figure 5.4: The image sequence a – c shows the capturing of 20 μm PS particles in the V-Cup array. Although the external magnet is present, the movement of the beads is solely governed by the centrifugal force since the residence time in the external magnetic field is too short (actuator is off, capture mode). After capturing the particles (c) the rotation frequency is decreased to 8 Hz, resulting in a residence time in the external magnetic field which is long enough to activate the magnetic actuator and also in a reduced centrifugal force acting on the beads. During the compression phase, the liquid flow into the V-Cup array lifts the beads and prevents re-capture of un-trapped beads. When the actuator leaves the magnetic field, the combination of flow and centrifugal force leads to sedimentation of the beads without re-trapping (e). The large majority of all initially trapped beads can be removed from the array using the magnetic actuator (f). Scale bars 50 μm

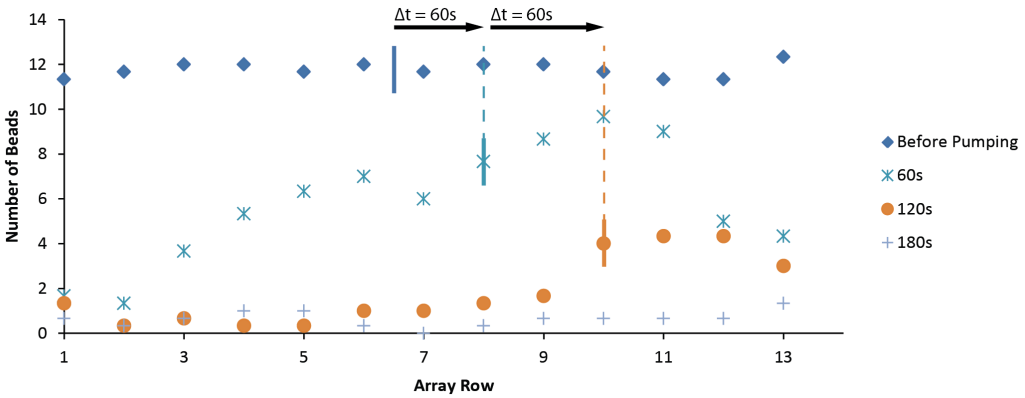

Figure 5.5: Moving average of the bead distribution over three adjacent rows of V-Cups at different times during the magneto-hydrodynamic bead removal process (1 denominates the radially most inwards row). The vertical lines indicate the mean position of the beads in the array. With increasing actuation time, the center of the bead distribution moves to the right side of the graph, i.e. beads are successively leaving the array.

Figure 5.6 shows the statistics of the bead release experiments. 92.6% of all captured beads could be removed in as little as 3.5 min. This is notably faster than the bead release approach using ultrasonic actuation which includes cumbersome manual handling steps.

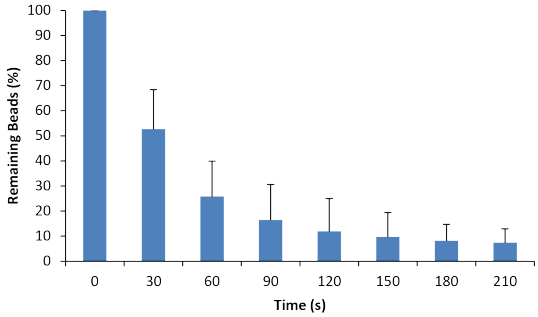

Figure 5.6: The results of the bead release using the magnetic actuator (f = 8 Hz). After 210 s, only 7.4% of all initially trapped particles remain in the array

These results show that our integrated magnetic actuator is capable of removing the large majority of all beads trapped in the array, and the fact that this actuation scheme is solely controlled by the rotation frequency of the disc enables very simple integration in an automated point-of-care system where a minimum of user interaction is desirable.

5.5.2 Magnetic Mixing

To investigate further applications of the magneto-hydro- dynamic actuation, we evaluated agitation of advection in a mixing chamber. This mixing mode might be implemented for upstream sample preparation in a future, integrated, sample-to-answer system for bead-based assays. For these magnetic mixing experiments, the configuration of the disc has been chosen such that the PDMS side of the disc with the on-disc magnets was facing towards the external magnet (magnets were integrated such that repelling poles were facing each other). This allows the on-disc and stationary magnets to be in much closer proximity than they are in the configuration used for the bead retrieval where the distance between the two magnets was larger than the thickness of the disc. The advantage of this configuration is that the force of the magnetic actuator is higher, thus invigorating mixing. The proximity of the two magnets also results in the fact that in this configuration the

magnetic actuator is active even at rotational frequencies above 30 Hz but, as the main objective here is to achieve fast and uniform mixing, this is not considered a disadvantage in this context. Mixing experiments were performed by introducing 6 μl of each educt (Potassium Thiocyanate and Iron(III) Chloride, respectively) in the sample loading chamber, the disc was then mounted on the spindle motor and spun at 20 Hz to transfer the educts into the mixing chamber. After all educts had been transferred, the motor was set to the desired frequency and the external magnet was positioned under the on-disc actuator to start the active mixing process. The mixing time has been measured for frequencies ranging from 5 to 30 Hz. These experiments showed that the rotational frequency has no major impact on the mixing time. In all cases, mixing has been achieved in < 20 s whereas pure diffusion-driven mixing (i.e. without the external magnet) took more than 5 min in all cases. The mixing process for a rotation speed of 10 Hz is shown in Fig. 5.7.

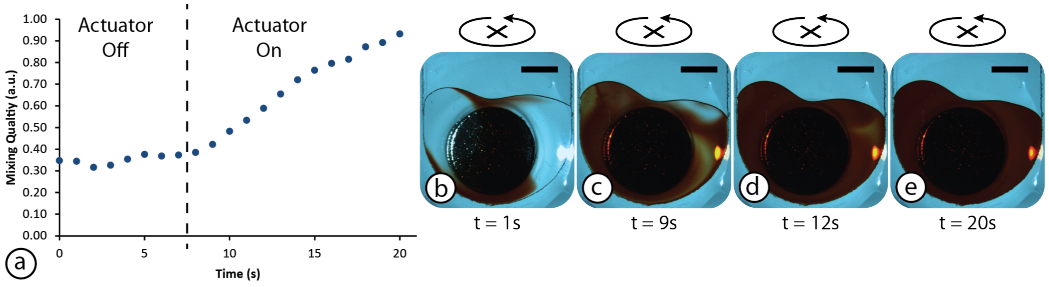

Figure 5.7: Graph a shows the progression of the liquid mixing in the chamber over time. Before the external magnet is positioned below the on-disc actuator (actuator off, *left side of the dashed line*),mixing is only driven by diffusion. After the external magnet has been positioned (actuator on, *right side of the dashed line*), active mixing is initiated and completed in < 20 s. The sequence b - e shows snap shots of the mixing chamber at progressive times during the mixing process. Scale bars 2 mm.

5.6 Conclusion and Outlook

In summary, we present a novel, frequency controlled magneto-hydrodynamic actuator for bead-based centrifugal microfluidic platforms, and demonstrate its application for the retrieval of captured microparticles from an array of V-Cups as well as for rapid liquidliquid mixing. Due to the inertance of its moving parts, the magnetic actuation is restricted to the low-frequency regime, and thereby does not interfere with the sedimentation of microparticles during the high-speed capture

phase. This solely frequency controlled activation enables the design of instrumentally very simple setups, indeed the only component which needs to be added to a standard centrifugal setup is a permanent magnet. Furthermore, the application of this actuator to construct a mixing structure capable of mixing a total volume of 14 μl of liquid in < 20 s has been demonstrated. Our novel magnetic actuator can readily be integrated in the disc to leverage facile automation of liquid handling on a point-of-care device featuring bead-based assays including upstream mixing.

5.7 Supplementary Information

Ultrasonic Re-Distribution and Retrieval of Beads Initially bead retrieval using the ultra-sonic actuation has been studied. The results of these experiments are shown in Fig. 5.8. After 9 cycles of sonication for 30 s and subsequent spinning of the disc at 15 Hz for 90 s, 92% of all captured beads could be removed from the array and collected at the bottom of the capturing chamber. Although this method proved to be efficient, it is labor-intensive, since the disc has to be manually handled to be transferred between the ultrasonic bath and the motor for spinning. Furthermore the ultrasonic actuation might have adverse effects on biological cells. This renders the ultrasonic approach unsuitable for integrated point-of-care devices.

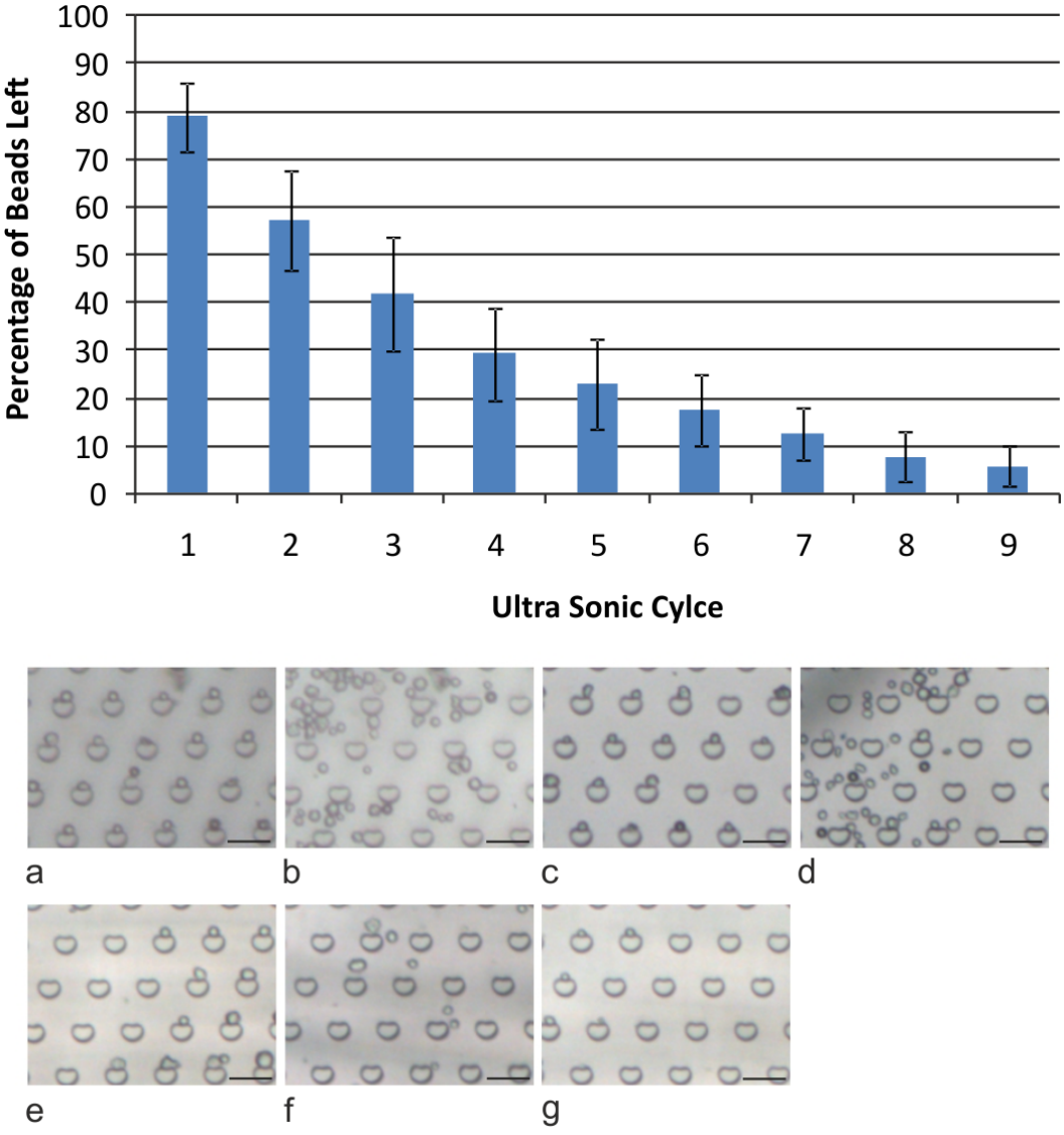

Figure 5.8: The graph illustrates the percentage of remaining beads in the array after each cycle of ultrasonic treatment and spinning. After 8 cycles, less than 10% of the initially captured beads are left in the array. The image sequence shows the array before and after cycles of ultrasonic treatment and spinning. Scale bars are 50 μm.

Chapter 6

Capturing and Analysis of Cells in an Array of V-Cups

This chapter has been published in:

R. Burger, G. Kijanka, O. Sheils, J. OLeary, and J. Ducrée, Arrayed capture, assaying and binary counting of cells in a stopped- flow sedimentation mode. In *Proceedings of the 15th International Conference on Miniaturized Systems for Chemistry and Life Sciences (μTAS 2011)*, 538-540

This chapter demonstrates the application of the V-Cup array to capture cells (HeLa, MCF7 and RPMI-8226) and perform cell discrimination based on markers displayed on the membrane of the cells (EpCAM) as well as on intra-cellular proteins (ESR-1).

6.1 Introduction

Microfluidic systems offer a unique approach to handle biological cells and to perform cell-based assays for biological studies as well as for clinical diagnostics. Devices for single cell capture are of special interest since they allow to study individual cells and their direct responses to various conditions. Single cell capture also allows to discriminate and count individual cells in sub-populations of mixed cells. Several devices for cell capture have been developed in the past, using, for example, capture elements in pressure driven systems to enable cell fusion [170] or centrifugal systems with radially sloped channels and pockets in the side walls [100]. Centrifugal microfluidic systems are especially suited for cell capturing applications since they can take advantage of the density difference between cells and surrounding medium to sediment cells. Furthermore, a wide range of liquid handling functions such as metering, valving and mixing have already been shown in the past [34]. Our system utilizes an array of V-Cup elements to capture cells under stagnant flow conditions on a centrifugal platform, thus overcoming the typically low capture efficiency of pressure driven systems.

6.2 Theory

The system presented here utilizes our previously introduced V-Cup array structure for single cells capture on a centrifugal microfluidic disc (see chapter 4). In brief, cells sediment in a chamber on the disc under stagnant flow conditions due to the centrifugal force into an array of V-shaped capturing elements. Since the sedimentation takes place with the liquid bulk at rest, i.e., in the absence of flow (lines), the capture efficiency of this system is much higher than that of typical flow driven systems. Pressure driven systems are typically characterized by a rather low capture efficiency due to the continuity of streamlines which diverge around obstacles and

hence drag cells around the capturing elements. This can be reduced to a certain extent by introducing gaps in the capturing elements or between capturing elements and the bottom of the chip. However, this approach adds significant complexity to the micromanufacturing process. A sharply peaked single cell occupancy distribution can be achieved by scale-matching of the size of the capture elements to the size of the cells (see chapter 4). Once cells are captured in the V-Cup array, the reagents in the capturing chamber can be easily altered exposing the cells to a variety of conditions (e.g., antibodies, stains or washing buffers).

6.3 Experimental Setup

All discs used for these experiments have been fabricated in PDMS (Dow Corning, USA) using a combination of SU8 and DFR as described in chapter 3.1.1. A 30 μm thick layer SU8 layer was used for the V-Cup array, whereas 200 μm of DFR were used for the reservoirs.The PDMS discs were then bonded to PMMA discs and degassed prior to use (for details see chapter 3) Three different cell lines were used in this work: HeLa, MCF7 and RPMI-8226. The cells were harvested from cultures immediately prior to the experiments. Two different assays have been used in this work. The first is an assay to discriminate cancer cells (MCF7) from a background of plasma cells (RPMI-8226) by detecting the surface protein EpCAM. The second assay uses an intracellular marker (ESR-1 - Estrogen Receptor α) to differentiate cells. The following staining protocol was used: Once captured, cell were fixed using a solution of 4% formaldehyde (Sigma-Aldrich, Ireland) and cell were permeabilized using a solution of 0.05% Triton X100 (Sigma-Aldrich, Ireland) in PBS Buffer. Nuclear DNA was then stained using Propidium Iodide (Invitrogen, USA). For the EpCAM assay, the cells were subsequently exposed to anti-EpCAM antibody from goat (BAF960, R&D Systems, USA) followed by an incubation with a fluorescently labeled anti-goat antibody (F0109, R&D Systems, USA). In the case of the ESR-1 assay, cells were first incubated with anti-ESR-1 antibody from mouse (SC-8002, Santa Cruz Biotech, USA) and then incubated with fluorescently labeled anti-mouse antibody from goat (A11001, Invitrogen, USA). Including the washing and blocking steps, the liquid in the capturing chamber is exchanged 18 times during this assay.

Images have been taken using a fluorescence microscope (IX 81, Olympus, Japan).

6.4 Results and Discussion

Identification of cancer cells among plasma cells: A population of RPMI-8226 plasma cells has been spiked with a small amount of MCF7 breast cancer cells. 2 μl of the cell suspension were then introduced into the disc and cells were captured in the V-Cup array. Next, the cells were stained using the EpCAM staining protocol described above. Figure 6.1 shows the results of these experiments. MCF7 cells can easily be distinguished from the population of plasma cells.

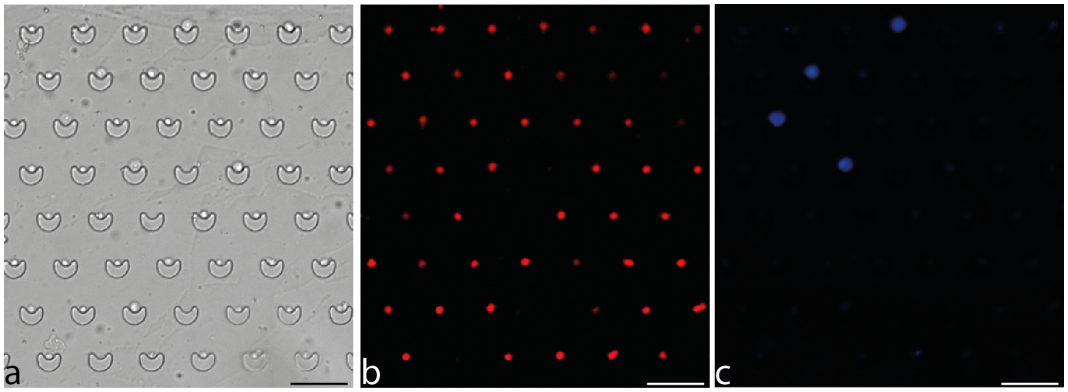

Figure 6.1: RPMI plasma cells spiked with a small quantity of MCF7 cancer cells have been captured in the array (a). The nucleus of all cells has been stained with PI (b). MCF7 cells are identified using anti-EpCAM IgG and a secondary FITC- labeled detection antibody (for better discrimination between anti-EpCAM and anti-ERα, the fluorescent signal from anti-EpCAM IgG has been false colored in blue)(c). All scale bars: 100 μm.

On-chip Estrogen Receptor expression analysis: In order to demonstrate the capability to classify cells based on intra-cellular markers, a population of MCF7 cells has been spiked with HeLa cells. The mixed sample was loaded onto the disc and cells were captured in the V-Cup array. Staining protocols were performed as described above. Figure 6.2 shows the captured cells after staining. MCF7 and HeLa cells can easily be discriminated.

6.5 Conclusion and Outlook

In summary, we demonstrate the capability of our centrifugal V-Cup array platform to capture mixed populations of bio-logical cells and discriminate these based on

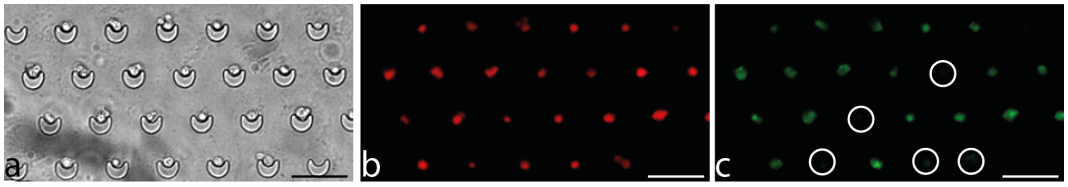

Figure 6.2: A mixed population of HeLa and MCF7 cells has been trapped in the array. Part (a) shows a bright field image of the trapped cells, (b) a fluorescent image of all cells with PI stained nuclei (red), and (c) the ESR-1-expressing MCF7 cells which are selectively stained (green) by a FITC-labeled anti-ESR-1 antibody. By comparing images (b) and (c), the ESR-1- negative (HeLa) cells can easily be identified (white circles). Scale bars: 100 μm.

either membrane proteins such as EpCAM or intracellular proteins such as ESR-1. The arrayed display of single cells in one focal plane greatly facilitates detection and readout. This is only the first step towards an integrated platform for cell analysis for point-of-care applications. Future work will concentrate on applying this platform to answer clinically relevant questions such as performing a full blood count.

Chapter 7

Laser-based Manipulation and Fluorescent Detection of Individual, Centrifugally Arrayed Bioparticles

Parts of this chapter will be published in:

R. Burger, D. Kurzbuch, R. Gorkin, O. Sheils, J. O'Leary, M. Glynn and J. Ducrée, Laser-based Manipulation and Fluorescent Detection of Individual, Centrifugally Arrayed Bioparticles. In *Proceedings of the 15th International Conference on Miniaturized Systems for Chemistry and Life Sciences (μTAS 2012)*

In this work we for the first time present a technology which pairs up fluorescence based detection and manipulation of individual particles using optical tweezers with our highly efficient, array-based centrifugal particle trapping in scale-matched V-Cups under stagnant flow conditions. To the best of our knowledge, this is the first time that centrifugal microfluidics and optical tweezers have been combined to perform single particle manipulations.

7.1 Introduction

Centrifugal microfluidics for lab-on-a-chip applications is a field which has attracted considerable interest in recent years, both from academia as well as from industry [48]. The novel, here presented instrumental setup significantly expands state-of-art microfluidics to sophisticated particle-manipulation and detection, thus for the first time enabling applications involving multiplexed, bead- and cell-based counting, ID, and cherry-picking of individual target particles. In particular the integration of fluorescence detection comprises a seminal improvement of our preceding work, where the disc had to be cumbersomely moved to a separate microscope [106]. Furthermore we demonstrated in our previous work a magnetic actuator for the simultaneous retrieval of all captured particles [177]. In this work we significantly improved the particle manipulation capabilities by adding an optical tweezers module to the setup, thus allowing manipulation of individual particles in the array.

7.2 Working Principle

This work is based on our previously introduced V-Cup based particle capturing platform. In brief, particles (beads or cells) sediment under stagnant flow conditions into an array of scale matched V-Cups, where they are mechanically trapped with a single-occupancy distribution. Earlier we demonstrated the very high (close to 100%) capture efficiency of this approach and the suitability of the system to perform bead-based immunoassays [104]. The major novelty of this work is the integration of an optical module which provides fluorescence detection as well as an optical tweezers function. The manipulation of particles using a laser has first been presented by

Askin and co-workers in 1970 [143], followed by the demonstration of the trapping of living cells [150]. In brief, a laser beam is focused through a microscope objective with a high numerical aperture in order to create a highly focused spot with a steep filed gradient. Dielectric particles such as polystyrene (PS) beads or cells are drawn towards this energy well where they are trapped. The captured particles can then be moved by displacing the laser, thus forcing the particle to follow in order to remain in the focus of the laser. For detailed description of the working principle in the ray optics regime (i.e. $d_{Particle} \gg \lambda_{Laser}$) see [159] and Chapter 3.3.2.

7.3 Materials and Methods

The centrifugal test stand setup consists of standard components such as a computer controlled motor, camera and illumination. Furthermore it features an optical module. This module incorporates the optical tweezers to manipulate individual microparticles on disc using a 1-W, 1064-nm infrared laser (Roithner Lasertechnik, Austria). The laser is focused through a 40x oil immersion microscope objective with a numerical aperture of 1.3 (Zeiss, Germany). This setup allows a working distance of 200 μm. The module also features a fluorescence detection part at an excitation wavelength of 488 nm and up to six emission filters. Additionally, this module includes a secondary camera (TXG 14f, Baumer, Germany) which utilizes the same optical path as the laser to facilitate particle manipulation and acquisition of fluorescent images. The whole module is mounted on a computer controlled X-Y stage.

The microfluidic chips used in this work were manufactured in PDMS by casting on a lithographically structured SU-8 master. Following curing, the PDMS chips were cut to size, inlet holes were punched and the chips were irreversibly bonded to glass cover slides (thickness #1, VWR, Ireland) using O_2 plasma activation. The design of the chips and the holder used to mount them on the test stand is outlined in Fig. 7.1.

For the experiments involving PS particles, we used FITC loaded beads with a diameter of 12.5 μm (PS FluoGreen) and non-fluorescent beads with a diameter of 20 μm (both from Microparticles, Germany). Cell experiments were performed

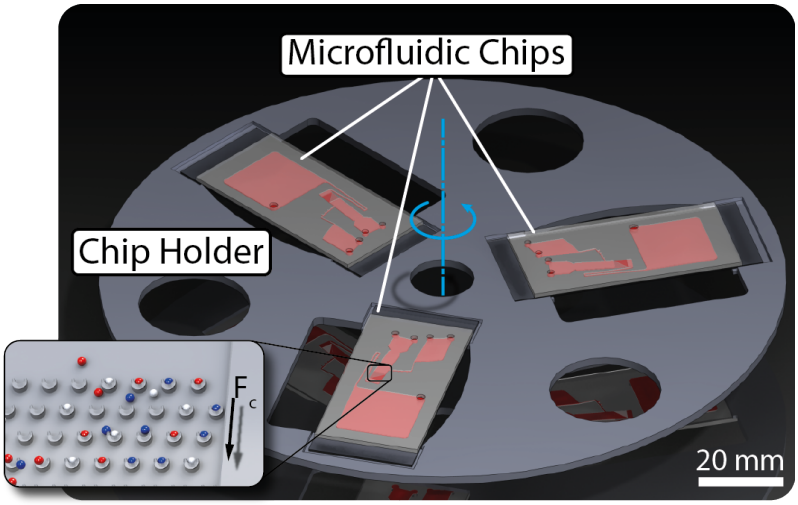

Figure 7.1: Microfluidic chips used in this work, attached to a holder to enable mounting on the centrifugal test stand. The insert shows the V-Cup based capturing principle.

using HL-60. The cells were fixed off-disc using 4% (v/v) formaldehyde (Sigma-Aldrich, Ireland). Cells were then captured and subsequently stained by incubation Propidium Iodide (PI) (4 μl/ml, Invitrogen, Ireland) for 15 min. Subsequently the cells were washed twice with PBS containing 5% (v/v) FBS.

7.4 Results and Discussion

First, the manipulation of a captured PS particle using the optical tweezers is demonstrated. To this end 20 μm beads were captured in the array and subsequently one bead has been selected and translated (Fig. 7.2 a-d). The optical tweezers were then used to re-arrange captured fluorescently labeled beads to represent the letters BDI (Fig. 7.2 e-g).

The main application of this platform is to capture cells from a suspension to identify and count sub populations. This has been demonstrated by introducing a sample containing HL60 cells, capturing them in the V-Cups and staining them with PI. The stained cells were then imaged using the integrated optical module (Fig. 7.3). Furthermore, captured cells were then manipulated using the optical tweezers. The displacement of a trapped cell to a neighboring cup is shown in Fig. 7.2

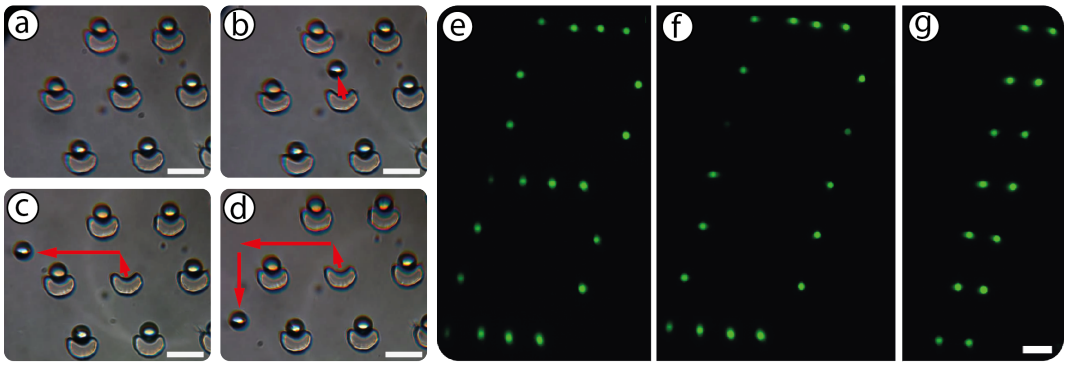

Figure 7.2: Single-bead manipulation using the optical tweezers module. After selecting a bead, the laser is turned on to trap the bead and lift it from the capturing element (a, b). The bead is then carried to the side and can be removed from the array for downstream analysis (c, d). Fluorescent PS beads with a diameter of 12.5 m have been captured in the array and subsequently been re-arranged using the optical tweezers setup to display the letters BDI (e-g). Scale bars are 50 μm.

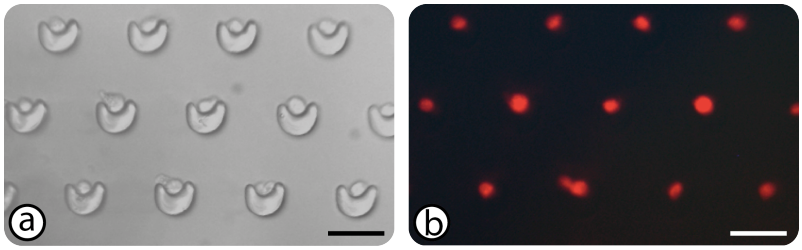

Figure 7.3: HL 60 cells have been captured in the V-Cup chip, stained with PI and subsequently imaged using the optical module. Bright field image (a) and fluorescent image (b) of the same area. Scale bars are 50 μm.

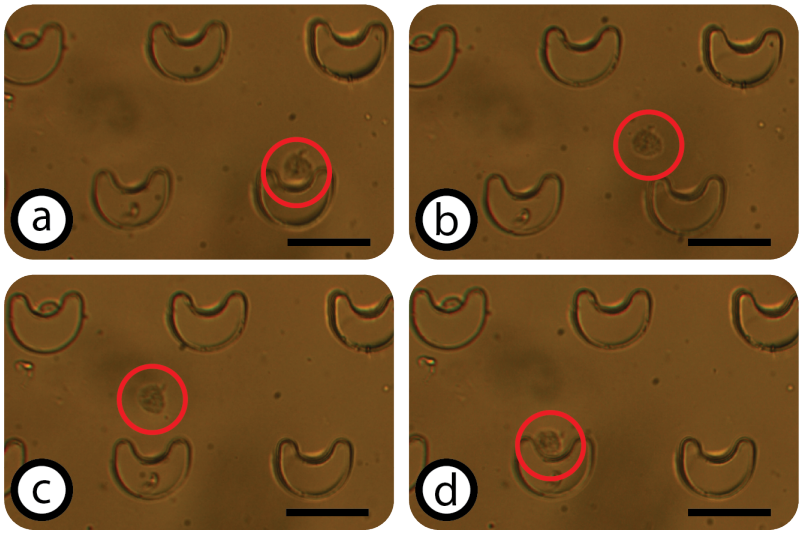

Figure 7.4: A captured HL60 cell is displaced from the initial capturing element to a neighboring V-Cup using the optical tweezers module (a-d). Scale bars are 50 μm.

7.5 Conclusions and Outlook

In summary we present a decisively improved microfluidic platform which integrates centrifugal particle trapping, multi-color fluorescence detection and the capability to translocate single particles using optical tweezers. After demonstrating the successful on-disc capturing, staining, imaging and manipulation of PS beads and cells, work is currently under way to implement a complete cell screening assay using this platform.

Chapter 8

Summary, Conclusions and Outlook

This work added novel methods for the capturing and handling of particles (such as beads or biological cells) to the centrifugal microfluidic toolbox. The centrifugal platform is predestined for applications involving particle handling due to the centrifugal force present within the rotating system. In the past, research has mainly been focused on developing methods to remove cells from a sample such as blood, and to provide cell-free plasma for downstream assay steps. Only recently has research concentrated on developing strategies to separate cells for subsequent analysis.

In Chapter 2, a comprehensive review of centrifugal microfluidic systems for cell and particle handling was presented (note: also see Appendix A for another published review on this topic.). Furthermore, the physical basics governing liquid and particle behavior on centrifugal platforms were introduced.

Chapter 3 introduced the methods used for fabricating the microfluidic chips used in this work. Masters were manufactured by photo lithography and subsequently replicated in PDMS or PMMA. Additionally, this chapter introduced the two generations of centrifugal test stands which I designed and built during the course of this work. Especially the 2^{nd} generation spin stand is novel and noteworthy since it offers unprecedented capabilities including fluorescence detection and single particle manipulation using optical tweezers.

Chapters 4 – 7 presented the original work performed during the course of this the-

sis. The V-Cup based particle capturing scheme which I developed, designed and characterized was presented first (Chapter 4). This novel platform for particle capturing is highly efficient, with a capturing efficiency close to 100 %. Furthermore, it has been shown that the occupancy of each cup can be tailored such as to achieve a sharply peaked single occupancy distribution by scale matching the size of the V-Cups to the diameter of the particles. For a ratio of particle diameter to cup size of 1, a single occupancy of 99.7 % was achieved. Additionally, the application of the V-Cup array to perform bead based immunoassasys was demonstrated. Chapter 5 introduced a novel frequency controlled magnetic actuator which I designed to retrieve captured beads from the V-Cup array. It comprises of an on-disc magnet mounted on an elastic membrane and a stationary off-disc magnet. When the on-disc magnet enters the magnetic field of the off-disc magnet it gets attracted, thus compressing the chamber below the elastic membrane. The compression in turn leads to a liquid flow through the array which lifts the captured particles from the V-Cups. The advantage of this actuator is its simplicity since it is solely controlled by the rotational frequency of the disc. At frequencies above 30 Hz the residence time in the external magnetic field is too short to displace the magnet (actuator is off) and particle movement is solely governed by the centrifugal force (capturing mode). Below 8 Hz the residence time is long enough to displace the magnet and create the flow (actuator is on, release mode). Furthermore, this actuator can also be used for rapid mixing of liquids e.g. for upstream sample prep steps. In Chapter 6 I conducted experiments to demonstrated the capabilities of this platform to capture cells and perform cell discrimination assays based on intra-cellular (ESR-1) as well as membrane (EpCAM) based markers. These experiments confirmed that cells can successfully be captured and rather complex assays with up to 18 medium exchange steps can be conducted. Finally Chapter 7 demonstrated the capabilities of the optical tweezers setup to manipulate individual particles which had been captured in the V-Cup array. Appendix B.1 shows a siphon based droplet mixer which I developed. This mixer enables rapid mixing of liquids (10 μl were mixed in less than 20 s) and also dilution of PBS buffer and human plasma has been successfully demonstrated. This manuscript has been submitted to *Microfluidics and*

Nanofluidics and is currently under review.

Outlook

The V-Cup platform developed within this work is very promising and forms the basis of two on-going research projects within our group. The first one is focused on implementing a 5-part differential white blood cell count on a disc. The aim of the second project is to develop a CD4 cell count for HIV diagnostics in resource poor settings. While it has already been demonstrated that cell capture and assaying is possible, there still remain some challenges to overcome:

1. Removal of red blood cells such that only white blood cells enter the V-Cup array
2. Transfer of the fluidic structures from PDMS to standard polymers such as PMMA or PC
3. Development of a cost-effective read-out method

Removal of red blood cells Since the capturing principle is based on mechanical trapping, for performing an absolute cell count it is necessary to ensure that the number of V-Cups is larger than the number of cells in the sample. Blood typically contains between 4.5 and 5.5 million red blood cells per microliter, and only between 4000 and 11000 white blood cells. Therefor red blood cells need to be removed before forwarding the white blood cells into the V-Cup array. This could be achieved by chemical lysis of the red blood cells or by density gradient based separation / band extraction like the one which is currently under development in our group [8].

Transfer from PDMS to PMMA or PC PDMS is a very good material for rapid prototyping but it is not a viable option for mass production of microfluidic discs. For mass production polymers like PMMA or PC which are well amenable to injection molding are more suitable. The main challenge will be to ensure bubble-free filling of the V-Cup array since the degas-driven priming method is not applicable. This problem could be overcome by using so-called phaseguides to ensure bubble-

free filling even in rigid polymers [178]. Possibly, the V-Cups themselves could be used as part of the phaseguide design.

Cost efficient read-out In particular for market- compliant point-of-care applications, it is imperative to keep the cost of the instrument low. To achieve this ambitious goal, I believe that it would be beneficial to use off-the-shelf components, e.g. from conventional optical disc drive technologies. For example, read-out could be performed using a standard laser pickup from a CD or DVD drive [113, 114, 122] to scan the array and detect individual cells in the cups. The highly ordered arrangement of the V-Cups (and hence the captured cells) in a defined focal plane would greatly facilitate readout. Several projects have sparked off from my work in the group to investigate these options.

Possible future applications and limitations

Building on this technology, there are several strands which could be explored:

1. Within this work only uniform arrays have been used, i.e. all cups had the same size. It would certainly be promising to investigate the use of heterogeneous arrays with varying cup dimensions to enable size filtration of particles, i.e. small cups radially inwards and larger cups radially outwards. The idea would be that small particle get captured in the small cups (which have to be sufficiently small so as not to allow stable trapping of large particles) whereas larger particles are captured in the radially outwards section of the array.

2. It would also be worth investigating the possibility to coat the V-Cups with specific capturing probes (e.g. antibodies) to add another capturing condition besides size. In this configuration the cups would have to be designed such that they are smaller than the particles, i.e. no stable, purely mechanical trapping is possible. Therefore particles would only be trapped if the hit a cup and express the antigen which binds to the antibody immobilized on the cup. Ultimately the cups could be replaced by an array of pillars similar to the system presented by Toner *et al.* [131]. A homogeneous coating of the

array with one antibody would certainly be no problem. However it would be very interesting to selectively coat specific areas of the array with different antibodies. This may be achieved by a microarray printer.

The approaches mentioned in 1 and 2 are currently being investigated by one of the PhD students in the group.

3. Another method to tackle this immunocapture challenge could be to coat color coded beads with antibodies (similar to the beads used for the immunoassay in chapter 4), capture the bead ensemble in the array (at statistical positions) and, in a subsequent step, introduce the cell suspension to be investigated into the array. Thus the color-coded, immuno-functionalized beads would act as capturing elements for the incoming cells.

4. The IR laser of the second generation test stand which has been used to implement the optical tweezers capability could also be used for other tasks. For example, it would be possible to use the laser to open sacrificial wax valves. By using a different objective with a larger working distance and synchronizing the laser with the rotation of the disc, this could even be carried out during rotation. I believe this would be very straightforward to implement in the current setup.

   Furthermore the laser could be used to heat small amounts of liquids (this would require that the top of the chamber is coated with an IR absorbing material). If the heating is controlled precisely this could be used to perform PCR within a chip. The necessary temperature cycles could be achieved by rotating the disc such that the chamber is only heated while hit by the laser and after leaving the impact zone the liquid in the chamber would cool down (this setup could be similar to the Qiagen Rotor-Gene Q system). This setup could also include a fan to achieve more rapid cooling and hence faster temperature cycling.

   It would certainly also be very interesting to build a system where a mixed population of cells is trapped and stained in the V-Cup array and subsequently one or more cells of interest are transferred to a side chamber containing PCR mix using the optical tweezers. This chamber could then be sealed off using

the wax valves and a PCR or isothermal amplification could be performed on the isolated, cherry-picked cells. Detection of the PCR products could then be performed using the fluorescence detection capabilities already implemented into the setup.

5. The optical tweezers could be used to spike a cell sample with an exactly known amount of cells. This could be very beneficial for testing and developing devices for the detection of circulating tumor cells (CTCs) where it is necessary to detect very low numbers of target cells.

Like most technologies, the V-Cup array also has some drawbacks and limitations. The major ones are:

1. The system works best under stagnant flow conditions. Therefor it is necessary to completely fill the array without entrapping gas bubbles. Using PDMS this can easily be assured by degassing the bulk material, but bubble-free priming is challenging for rigid polymers such as PMMA or PC (see above).

2. A homogeneous distribution of the particles across the whole width of the array is essential to ensure a high efficiency trapping. Hence the inlet into the capturing chamber should not be too narrow since under stagnant flow conditions there is only the merely radial centrifugal force field which cannot establish a lateral spreading.

3. It has been observed that some particles got stuck on the step at the inlet of the V-Cup array due to the difference in height between the upstream reservoir on top of the array ($\approx 200\ \mu$m) and the cups ($\approx 30\ \mu$m) themselves. This could easily be avoided by creating a sloped transition from the reservoir to the V-Cup array, either by using a 5-axis milling machine or greyscale lithography. Unfortunately none of these technologies has been available during the course of this work.

4. Since the system relies purely on mechanical trapping of particles, a sharply peaked single occupancy can only be achieved by closely matching the size of the cups to the size of the particles. This implies that in the case of a

polydisperse suspension it will be difficult to avoid multi-particle occupancy or loss of particles. This could be solved using the inhomogeneous array approach discussed above.

In summary I believe that there is a large potential in this platform for various applications in biological research and biomedical diagnostics. Some of the potential applications mentioned above are currently being investigated within this group.

Chapter 9

Acknowledgments

The past years here in Dublin, and at DCU in particular, have been very interesting, challenging and fun. Of course there are a lot of people who contributed to this work in one way or another.

First, I would like to thank Prof. Jens Ducrée for all his help and support during the last years, not only during my PhD thesis but also during my time as an undergrad in Freiburg. Thank you for all the advice and that you gave me the opportunity to work in your group.

I would also like to thank all the guys at Biosurfit, especially my co-supervisor Nuno and João, for valuable discussions at the beginning of this project.

During my stay here I had the fortune to work in the amazing Microfluidics group and I really learned a lot from everyone. Thanks to all the current members, Gerson, Charles, Daniel, Mary, Liza, Dave, Maria, Chandra, Niko, Lorcan and especially Macdara (who was always there to proof read my papers and thesis and probably some times despaired because of my grammar (he also very patiently answered all my questions on biology)). I'm also very grateful to the former members of the group: Jon, Robin, Neus, Ana and Patrick.

A big thank you also goes to Gregor for all his help with the experiments involving cells. Furthermore, our advanced centrifugal test stand would have never been the same without the hard work and expertise of Dirk and Robin.

There are also many other people who helped me a lot along the way: Des in the physics workshop who was always available to manufacture the mechanical parts for

my experimental setups; Pat, who answered all my questions on electronics, built a lot of circuits for me and usually always had exactly the piece I was looking for lying around in one of his many drawers and of course Alan who was always fighting to keep the nitrogen supply going. Without you guys this would not have been possible.

Another thank you goes to everyone in the umbrella office (Barry, Brian, Stephen and Lorcan), the administration team in BDI and Lisa in physics who always did an amazing job.

Of course there are also many people outside of DCU who made my time here truly amazing and helped me to think about other things than microfluidics from time to time.

Last but not least I'm also very grateful to my family, they were always there for me and supported me every step of the way.

Thanks to all of you!

Bibliography

[1] K. A. Erickson and P. Wilding. Evaluation of a novel point-of-care system, the i-stat portable clinical analyzer. *Clinical chemistry*, 39:283–287, 1993.

[2] C. Papadea, J. Foster, S. Grant, S. A. Ballard, J. C. Cate, M. Southgate, and D. M. Purohit. Evaluation of the i-stat portable clinical analyzer for point-of-care blood testing in the intensive care units of a university children's hospital. *Annals of Clinical and Laboratory Science*, 32:231–243, 2002.

[3] A. Inc. www.abaxis.com.

[4] R. Diagnostics. www.radisens.com.

[5] B. SA. www.biosurfit.com.

[6] Abbott. www.abbottpointofcare.com.

[7] C. D. Chin, V. Linder, and S. K. Sia. Commercialization of microfluidic point-of-care diagnostic devices. *Lab. Chip*, 12:2118–2134, 2012.

[8] D. J. Kinahan, M. T. Glynn, and J. Ducrée. Concentration of white blood cells from whole blood by centrifugo-pneumatic siphoning with density gradient medium. In *The 16th International Conference on Miniaturized Systems for Chemistry and Life Sciences (μTAS 2012)*, 2012 (Accepted).

[9] D. Kirby, J. Siegrist, G. Kijanka, L. Zavattoni, R. Burger, and J. Ducrée. Centrifugo-magnetophoretic particle separation. *Microfluidics and Nanofluidics*, 2012.

[10] D. D. Nolte. Invited review article: Review of centrifugal microfluidic and bio-optical disks. *Review of Scientific Instruments*, 80:101101, 2009.

[11] R. Gorkin, S. Soroori, W. Southard, L. Clime, T. Veres, H. Kido, L. Kulinsky, and M. Madou. Suction-enhanced siphon valves for centrifugal microfluidic platforms. *Microfluidics and Nanofluidics*, 12:345–354, 2012.

[12] J. Siegrist, R. Gorkin, L. Clime, E. Roy, R. Peytavi, H. Kido, M. Bergeron, T. Veres, and M. Madou. Serial siphon valving for centrifugal microfluidic platforms. *Microfluidics and Nanofluidics*, 9:55–63, 2010.

[13] N. Godino, R. G. III, A. V. Linares, R. Burger, and J. Ducreée. A centrifugo-pneumatic cascade for fully integrated and multiplexed biological analysis. In *Proceedings of IEEE MEMS*, pages 989–992, 2012.

[14] F. Benito-Lopez, R. Byrne, A. M. Raduta, N. E. Vrana, G. McGuinness, and D. Diamond. Ionogel-based light-actuated valves for controlling liquid flow in micro-fluidic manifolds. *Lab on a Chip*, 10:195–201, 2010.

[15] K. Abi-Samra, R. Hanson, M. Madou, and R. A. G. III. Infrared controlled waxes for liquid handling and storage on a cd-microfluidic platform. *Lab on a Chip*, 11:723–726, 2011.

[16] J.-M. Park, Y.-K. Cho, B.-S. Lee, J.-G. Lee, and C. Ko. Multifunctional microvalves control by optical illumination on nanoheaters and its application in centrifugal microfluidic devices. *Lab on a Chip*, 7:557–564, 2007.

[17] J. L. Garcia-Cordero, D. Kurzbuch, F. Benito-Lopez, D. Diamond, L. P. Lee, and A. J. Ricco. Optically addressable single-use microfluidic valves by laser printer lithography. *Lab on a Chip*, 10:2680–2687, 2010.

[18] R. Gorkin III, C. E. Nwankire, J. Gaughran, X. Zhang, G. G. Donohoe, M. Rook, R. O'Kennedy, and J. Ducrée. Centrifugo-pneumatic valving utilizing dissolvable films. *Lab on a Chip*, 2012.

[19] D. L. Englert, M. D. Manson, and A. Jayaraman. Flow-based microfluidic device for quantifying bacterial chemotaxis in stable, competing gradients. *Applied and Environmental Microbiology*, 75:4557–4564, 2009.

[20] H. M. Yu, I. Meyvantsson, I. A. Shkel, and D. J. Beebe. Diffusion dependent cell behavior in microenvironments. *Lab on a Chip*, 5:1089–1095, 2005.

[21] D. Reyes, D. Iossifidis, P. Auroux, and A. Manz. Micro total analysis systems. 1. introduction, theory, and technology. *Analytical Chemistry*, 74:2623–2636, 2002.

[22] T. Vilkner, D. Janasek, and A. Manz. Micro total analysis systems. recent developments. *Analytical Chemistry*, 76:3373–3385, 2004.

[23] P. Auroux, D. Iossifidis, D. Reyes, and A. Manz. Micro total analysis systems. 2. analytical standard operations and applications. *Analytical Chemistry*, 74:2637–2652, 2002.

[24] D. B. Weibel, W. R. DiLuzio, and G. M. Whitesides. Microfabrication meets microbiology. *Nature Reviews Microbiology*, 5:209–218, 2007.

[25] H. Andersson and A. van den Berg. Microfluidic devices for cellomics: a review. *Sensors and Actuators B-Chemical*, 92:315–325, 2003.

[26] D. Huh, W. Gu, Y. Kamotani, J. Grotberg, and S. Takayama. Microfluidics for flow cytometric analysis of cells and particles. *Physiological Measurement*, 26:R73–R98, 2005.

[27] D. Erickson and D. Li. Integrated microfluidic devices. *Analytica Chimica Acta*, 507:11–26, 2004.

[28] H. A. Svahn and A. van den Berg. Single cells or large populations? *Lab on a Chip*, 7:544–546, 2007.

[29] J. El-Ali, P. K. Sorger, and K. F. Jensen. Cells on chips. *Nature*, 442:403–411, 2006.

[30] S. Lindstrom and H. Andersson-Svahn. Overview of single-cell analyses: microdevices and applications. *Lab on a Chip*, 10:3363–3372, 2010.

[31] C. Yi, C.-W. Li, S. Ji, and M. Yang. Microfluidics technology for manipulation and analysis of biological cells. *Analytica Chimica Acta*, 560:1–23, 2006.

[32] A. A. S. Bhagat, H. Bow, H. W. Hou, S. J. Tan, J. Han, and C. T. Lim. Microfluidics for cell separation. *Medical & biological engineering & computing*, 48:999–1014, 2010.

[33] M. Madou, J. Zoval, G. Jia, H. Kido, J. Kim, and N. Kim. Lab on a cd. *Annual Review of Biomedical Engineering*, 8:601–628, 2006.

[34] J. Ducrée, S. Häberle, S. Lutz, S. Pausch, F. von Stetten, and R. Zengerle. The centrifugal microfluidic bio-disk platform. *Journal of Micromechanics and Microengineering*, 17:S103–S115, 2007.

[35] R. M. Rocco. *Landmark Papers in Clinical Chemistry*. Elsevier, Amsterdam, 2006.

[36] C. Burtis, N. Anderson, J. Mailen, C. SCOTT, T. Tiffany, and W. Johnson. Development of a miniature fast analyzer. *Clinical chemistry*, 18:753–&, 1972.

[37] C. Burtis, W. Johnson, J. Mailen, J. Overton, T. Tiffany, and M. Watsky. Development of an analytical system based around a miniature fast analyzer. *Clinical chemistry*, 19:895–903, 1973.

[38] D. Mark, T. Metz, S. Häberle, S. Lutz, J. Ducrée, R. Zengerle, and F. von Stetten. Centrifugo-pneumatic valve for metering of highly wetting liquids on centrifugal microfluidic platforms. *Lab on a Chip*, 9:3599–3603, 2009.

[39] Y. K. Cho, J. G. Lee, J. M. Park, B. S. Lee, Y. Lee, and C. Ko. One-step pathogen specific dna extraction from whole blood on a centrifugal microfluidic device. *Lab on a Chip*, 7:565–573, 2007.

[40] K. Abi-Samra, R. Hanson, M. Madou, and R. A. G. III. Infrared controlled waxes for liquid handling and storage on a cd-microfluidic platform. *Lab on a Chip*, 11:723–726, 2011.

[41] J. Steigert, T. Brenner, M. Grumann, L. Riegger, S. Lutz, R. Zengerle, and J. Ducrée. Integrated siphon-based metering and sedimentation of whole blood on a hydrophilic lab-on-a-disk. *Biomedical Microdevices*, 9:675–679, 2007.

[42] P. Andersson, G. Jesson, G. Kylberg, G. Ekstrand, and G. Thorsen. Parallel nanoliter microfluidic analysis system. *Analytical Chemistry*, 79:4022–4030, 2007.

[43] J. Ducrée, T. Brenner, S. Häberle, T. Glatzel, and R. Zengerle. Multilamination of flows in planar networks of rotating microchannels. *Microfluidics and Nanofluidics*, 2:78–84, 2006.

[44] J. Ducrée, S. Häberle, T. Brenner, T. Glatzel, and R. Zengerle. Patterning of flow and mixing in rotating radial microchannels. *Microfluidics and Nanofluidics*, 2:97–105, 2006.

[45] M. Grumann, A. Geipel, L. Riegger, R. Zengerle, and J. Ducrée. Batch-mode mixing on centrifugal microfluidic platforms. *Lab on a Chip*, 5:560–565, 2005.

[46] M. Bynum and G. Gordon. Hybridization enhancement using microfluidic planetary centrifugal mixing. *Analytical Chemistry*, 76:7039–7044, 2004.

[47] Z. Noroozi, H. Kido, M. Micic, H. Pan, C. Bartolome, M. Princevac, J. Zoval, and M. Madou. Reciprocating flow-based centrifugal microfluidics mixer. *Review of Scientific Instruments*, 80:075102, 2009.

[48] R. Gorkin, J. Park, J. Siegrist, M. Amasia, B. S. Lee, J.-M. Park, J. Kim, H. Kim, M. Madou, and Y.-K. Cho. Centrifugal microfluidics for biomedical applications. *Lab on a Chip*, 10:1758–1773, 2010.

[49] W. C. Lee, A. A. S. Bhagat, S. Huang, K. J. V. Vliet, J. Han, and C. T. Lim. High-throughput cell cycle synchronization using inertial forces in spiral microchannels. *Lab on a Chip*, 11:1359–1367, 2011.

[50] A. A. S. Bhagat, S. S. Kuntaegowdanahalli, and I. Papautsky. Continuous particle separation in spiral microchannels using dean flows and differential migration. *Lab on a Chip*, 8:1906–1914, 2008.

[51] S. Ookawara, R. Higashi, D. Street, and K. Ogawa. Feasibility study on concentration of slurry and classification of contained particles by microchannel. *Chemical Engineering Journal*, 101:171–178, 2004.

[52] S. Ookawara, D. Street, and K. Ogawa. Numerical study on development of particle concentration profiles in a curved microchannel. *Chemical Engineering Science*, 61:3714–3724, 2006.

[53] A. A. S. Bhagat, S. S. Kuntaegowdanahalli, N. Kaval, C. J. Seliskar, and I. Papautsky. Inertial microfluidics for sheath-less high-throughput flow cytometry. *Biomedical Microdevices*, 12:187–195, 2010.

[54] J. Seo, M. H. Lean, and A. Kole. Membrane-free microfiltration by asymmetric inertial migration. *Applied Physics Letters*, 91:033901–033901–3, 2007.

[55] C. Blattert, R. Jurischka, I. Tahhan, A. Schoth, P. Kerth, and W. Menz. Separation of blood in microchannel bends. In *Engineering in Medicine and Biology Society, 2004. IEMBS '04. 26th Annual International Conference of the IEEE*, volume 1, pages 2627–2630, 2004.

[56] C. Blattert, R. Jurischka, I. Tahhan, A. Schoth, P. Kerth, and W. Menz. Separation of blood cells and plasma in microchannel bend structures. In T. J. K. D. J. Laurell, editor, *8th International Conference on Miniaturized Systems for Chemistry and Life Sciences*, pages 483–485, Sep 26-30 2004 2004.

[57] M. Amasia and M. Madou. Large-volume centrifugal microfluidic device for blood plasma separation. *Bioanalysis*, 2:1701–1710, 2010.

[58] S. Häberle, T. Brenner, R. Zengerle, and J. Ducrée. Centrifugal extraction of plasma from whole blood on a rotating disk. *Lab on a Chip*, 6:776–781, 2006.

[59] J. L. Zhang, Q. Q. Guo, M. Liu, and J. Yang. A lab-on-cd prototype for high-speed blood separation. *Journal of Micromechanics and Microengineering*, 18:125025, 2008.

[60] C. T. Schembri, T. L. Burd, A. R. Kopfsill, L. R. Shea, and B. Braynin. Centrifugation and capillarity integrated into a multiple analyte whole-blood analyzer. *Journal of Automatic Chemistry*, 17:99–104, 1995.

[61] R. Burger, N. Reis, J. G. Fonseca, and J. Ducrée. Blood separation based on pressure driven membrane deflection. In *The 13th International Conference on Miniaturized Systems for Chemistry and Life Sciences (uTAS)*, pages 122–124, 1-5 November 2009 2009.

[62] B. S. Lee, J.-N. Lee, J.-M. Park, J.-G. Lee, S. Kim, Y.-K. Cho, and C. Ko. A fully automated immunoassay from whole blood on a disc. *Lab on a Chip*, 9:1548–1555, 2009.

[63] S. Lutz, P. Lang, B. Faltin, S. Häberle, F. von Stetten, R. Zengerle, and J. Ducrée. Towards a comprehensive centrifugal process integration by rotationally induced lyophilisate dissolution and cell lysis. In *11th International Conference on Miniaturized Systems for Chemistry and Life Sciences*, pages 516–518, 7-11 October 2007 2007.

[64] G. J. Kellogg, T. E. Arnold, B. L. Carvalho, D. C. Duffy, and N. F. Sheppard. Centrifugal microfluidics: Applications. In *4th International Conference on Miniaturized Systems for Chemistry and Life Sciences*, pages 239–242, 14 - 18 May 2000 2000.

[65] K. Kleparnik and M. Horky. Detection of dna fragmentation in a single apoptotic cardiomyocyte by electrophoresis on a microfluidic device. *Electrophoresis*, 24:3778–3783, 2003.

[66] H. Kido, M. Micic, D. Smith, J. Zoval, J. Norton, and M. Madou. A novel, compact disk-like centrifugal microfluidics system for cell lysis and sample homogenization. *Colloids and Surfaces B-Biointerfaces*, 58:44–51, 2007.

[67] J. Siegrist, R. Gorkin, M. Bastien, G. Stewart, R. Peytavi, H. Kido, M. Bergeron, and M. Madou. Validation of a centrifugal microfluidic sample lysis and homogenization platform for nucleic acid extraction with clinical samples. *Lab on a Chip*, 10:363–371, 2010.

[68] J. Kim, S. H. Jang, G. Y. Jia, J. V. Zoval, N. A. D. Silva, and M. J. Madou. Cell lysis on a microfluidic cd (compact disc). *Lab on a Chip*, 4:516–522, 2004.

[69] L. Riegger, M. Grumann, J. Steigert, S. Lutz, C. P. Steinert, C. Mueller, J. Viertel, O. Prucker, J. Ruhe, R. Zengerle, and J. Ducrée. Single-step centrifugal hematocrit determination on a 10-$processing device. *Biomedical Microdevices*, 9:795–799, 2007.

[70] J. L. Garcia-Cordero, L. M. Barrett, R. O'Kennedy, and A. J. Ricco. Microfluidic sedimentation cytometer for milk quality and bovine mastitis monitoring. *Biomedical Microdevices*, 12:1051–1059, 2010.

[71] U. Y. Schaff, A. M. Tentori, and G. J. Sommer. Differential white cell count by centrifugal microfluidics. In *14th International Conference on Miniaturized Systems for Chemistry and Life Sciences (TAS)*, pages 103–105, 3.-7. October 2010 2010.

[72] P. Chen, X. Feng, R. Hu, J. Sun, W. Du, and B.-F. Liu. Hydrodynamic gating valve for microfluidic fluorescence-activated cell sorting. *Analytica Chimica Acta*, 663:1–6, 2010.

[73] L. Wang, L. A. Flanagan, N. L. Jeon, E. Monuki, and A. P. Lee. Dielectrophoresis switching with vertical sidewall electrodes for microfluidic flow cytometry. *Lab on a Chip*, 7:1114–1120, 2007.

[74] J. Voldman, M. L. Gray, M. Toner, and M. A. Schmidt. A microfabrication-based dynamic array cytometer. *Analytical Chemistry*, 74:3984–3990, 2002.

[75] I. Doh and Y. Cho. A continuous cell separation chip using hydrodynamic dielectrophoresis (dep) process. *Sensors and Actuators A-Physical*, 121:59–65, 2005.

[76] B. B. Yellen, R. M. Erb, H. S. Son, R. H. Jr., H. Shang, and G. U. Lee. Traveling wave magnetophoresis for high resolution chip based separations. *Lab on a Chip*, 7:1681–1688, 2007.

[77] D. D. Carlo. Inertial microfluidics. *Lab on a Chip*, 9:3038–3046, 2009.

[78] S. C. Hur, H. T. K. Tse, and D. D. Carlo. Sheathless inertial cell ordering for extreme throughput flow cytometry. *Lab on a Chip*, 10:274–280, 2010.

[79] J. Oakey, R. W. A. Jr., E. Arellano, D. D. Carlo, S. W. Graves, and M. Toner. Particle focusing in staged inertial microfluidic devices for flow cytometry. *Analytical Chemistry*, 82:3862–3867, 2010.

[80] H. Shiono and Y. Ito. Novel method for continuous cell separation by density gradient centrifugation: Evaluation of a miniature separation column. *Preparative biochemistry & biotechnology*, 33:87–100, 2003.

[81] H. Shiono, H. M. Chen, T. Okada, and Y. Ito. Colony-forming cell assay for human hematopoietic progenitor cells harvested by a novel continuous-flow cell separation method. *Journal of Chromatography a*, 1151:153–157, 2007.

[82] H. Shiono, T. Okada, and Y. Ito. Application of a novel continuous-flow cell separation method for separation of cultured human mast cells. *Journal of Liquid Chromatography & Related Technologies*, 28:2071–2083, 2005.

[83] M. Yamada, M. Nakashima, and M. Seki. Pinched flow fractionation: Continuous size separation of particles utilizing a laminar flow profile in a pinched microchannel. *Analytical Chemistry*, 76:5465–5471, 2004.

[84] T. Morijiri, S. Sunahiro, M. Senaha, M. Yamada, and M. Seki. Sedimentation pinched-flow fractionation for size- and density-based particle sorting in microchannels. *Microfluidics and Nanofluidics*, 11:105–110, 2011.

[85] G. Banfalvi. Cell cycle synchronization of animal cells and nuclei by centrifugal elutriation. *Nature Protocols*, 3:663–673, 2008.

[86] K. Donaldson, A. McShea, and A. Wahl. Separation by counterflow centrifugal elutriation and analysis of t- and b-lymphocytic cell lines in progressive stages of cell division cycle. *Journal of immunological methods*, 203:25–33, 1997.

[87] T. Morijiri, T. Hikida, M. Yamada, and M. Seki. Microfluidic counterflow centrifugal elutriation for cell separation using density-gradient media. In *14th International Conference on Miniaturized Systems for Chemistry and Life Sciences (uTAS)*, pages 722–724, 3. - 7. October 2010 2010.

[88] R. Martinez-Duarte, R. A. G. III, K. Abi-Samra, and M. J. Madou. The integration of 3d carbon-electrode dielectrophoresis on a cd-like centrifugal microfluidic platform. *Lab on a Chip*, 10:1030–1043, 2010.

[89] M. Boettcher, M. S. Jaeger, L. Riegger, J. Ducrée, R. Zengerle, and C. Duschl. Lab-on-chip-based cell separation by combining dielectrophoresis and centrifugation. *Biophys. Rev. Lett.*, 1:443–451, 2006.

[90] N. Pamme. Magnetism and microfluidics. *Lab on a Chip*, 6:24–38, 2006.

[91] S. Bronzeau and N. Pamme. Simultaneous bioassays in a microfluidic channel on plugs of different magnetic particles. *Analytica Chimica Acta*, 609:105–112, 2008.

[92] N. Pamme and C. Wilhelm. Continuous sorting of magnetic cells via on-chip free-flow magnetophoresis. *Lab on a Chip*, 6:974–980, 2006.

[93] J. Siegrist, L. Zavattoni, R. Burger, and J. Ducrée. 2-dimensional separation of biomimetic particles by stopped-flow centrifugo-magnetophoresis. In *16th International Solid-State Sensors, Actuators and Microsystems Conference (TRANSDUCERS)*, pages 278–281, 5 - 9 June 2011 2011.

[94] J. Siegrist, R. Burger, D. Kirby, L. Zavattoni, G. Kijanka, and J. Ducrée. Stress-free centrifugo-magnetic 2d-separation of cancer cells in a stopped-flow mode. In *15th International Conference on Miniaturized Systems for Chemistry and Life Sciences (TAS)*, pages 1915–1917, 2 - 6 October 2011 2011.

[95] J. Siegrist, L. Zavattoni, and J. Ducreée. Centrifugo-magnetophoretic separation and routing of particles. In *IEEE 24th International Conference on Micro Electro Mechanical Systems (MEMS)*, pages 1107–1110, 23 - 27 January 2011 2011.

[96] C.-L. Chen, K.-C. Chen, Y.-C. Pan, T.-P. Lee, L.-C. Hsiung, C.-M. Lin, C.-Y. Chen, C.-H. Lin, B.-L. Chiang, and A. M. Wo. Separation and detection of rare cells in a microfluidic disk via negative selection. *Lab on a Chip*, 11:474–483, 2011.

[97] K.-C. Chen, T.-P. Lee, Y.-C. Pan, C.-L. Chiang, C.-L. Chen, Y.-H. Yang, B.-L. Chiang, H. Lee, and A. M. Wo. Detection of circulating endothelial cells via a microfluidic disk. *Clinical chemistry*, 57:586–592, 2011.

[98] S. Häberle, L. Naegele, R. Burger, F. V. Stetten, R. Zengerle, and J. Ducrée. Alginate bead fabrication and encapsulation of living cells under centrifugally induced artificial gravity conditions. *Journal of microencapsulation*, 25:267–274, 2008.

[99] I. Kubo, S. Furutani, and K. Matoba. Use of a novel microfluidic disk in the analysis of single-cell viability and the application to jurkat cells. *Journal of Bioscience and Bioengineering*, 112:98–101, 2011.

[100] S.-W. Lee, J. Y. Kang, I.-H. Lee, S.-S. Ryu, S.-M. Kwak, K.-S. Shin, C. Kim, H.-I. Jung, and T.-S. Kim. Single-cell assay on cd-like lab chip using centrifugal massive single-cell trap. *Sensors and Actuators A: Physical*, 143:64–69, 2008.

[101] S. Furutani, H. Nagai, Y. Takamura, and I. Kubo. Compact disk (cd)-shaped device for single cell isolation and pcr of a specific gene in the isolated cell. *Analytical and Bioanalytical Chemistry*, 398:2997–3004, 2010.

[102] H. Chen, X. Li, L. Wang, and P. C. H. Li. A rotating microfluidic array chip for staining assays. *Talanta*, 81:1203–1208, 2010.

[103] L. Riegger, M. Grumann, T. Nann, J. Riegler, O. Ehlert, W. Bessler, K. Mittenbuehler, G. Urban, L. Pastewka, T. Brenner, R. Zengerle, and J. Ducrée. Read-out concepts for multiplexed bead-based fluorescence immunoassays on centrifugal microfluidic platforms. *Sensors and Actuators A-Physical*, 126:455–462, 2006.

[104] R. Burger, P. Reith, G. Kijanka, V. Akujobi, P. Abgrall, and J. Ducrée. Array-based capture, distribution, counting and multiplexed assaying of beads on a centrifugal microfluidic platform. *Lab on a Chip*, 12:1295, 2012.

[105] R. Burger, P. Reith, P. Abgrall, G. Kijanka, and J. Ducreée. Multiplexing of highly reproducible, bead-based immunoassays on a centrifugal microfluidic platform. In *Micro Electro Mechanical Systems (MEMS), 2011 IEEE 24th International Conference on*, pages 1170–1172, 2011.

[106] R. Burger, G. Kijanka, O. Sheils, J. O'Leary, and J. Ducrée. Arrayed capture, assaying and binary counting of cells in a stopped-flow sedimentation mode. In *15th International Conference on Miniaturized Systems for Chemistry and Life Sciences (μTAS)*, pages 538–540, 2 - 6 October 2011 2011.

[107] R. Burger, P. Reith, P. Abgrall, and J. Ducreée. Integration of high-efficiency capture and magneto-hydrodynamic retrieval of particles on a centrifugal microfluidic platform. In *24th International Conference on Micro Electro Mechanical Systems (MEMS)*, pages 1147–1149, 23.-27. January 2011 2011.

[108] H. Cho and L. P. Lee. A novel integrated microfluidic sers-cd with high-throughput centrifugal cell trapping array for quantitative biomedicine. In *The 10th International Conference on Miniaturized Systems for Chemistry and Life Sciences (uTAS)*, pages 642–644, 5 - 9 November 2006 2006.

[109] A. Rothert, S. K. Deo, L. Millner, L. G. Puckett, M. J. Madou, and S. Daunert. Whole-cell-reporter-gene-based biosensing systems on a compact disk microfluidics platform. *Analytical Biochemistry*, 342:11–19, 2005.

[110] A. Date, P. Pasini, and S. Daunert. Integration of spore-based genetically engineered whole-cell sensing systems into portable centrifugal microfluidic platforms. *Analytical and Bioanalytical Chemistry*, 398:349–356, 2010.

[111] N. Kim, C. M. Dempsey, J. V. Zoval, J.-Y. Sze, and M. J. Madou. Automated microfluidic compact disc (cd) cultivation system of caenorhabditis elegans. *Sensors and Actuators B-Chemical*, 122:511–518, 2007.

[112] K. Fan, C. Lin, and L. Shyu. The development of a low-cost focusing probe for profile measurement. *Measurement Science & Technology*, 11:N1–N7, 2000.

[113] A. Bartoli, P. Poggi, F. Quercioli, and B. Tiribilli. Fast one-dimensional profilometer with a compact disc pickup. *Applied Optics*, 40:1044–1048, 2001.

[114] S. Kostner and M. J. Vellekoop. Cell analysis in a microfluidic cytorneter applying a dvd pickup head. *Sensors and Actuators B-Chemical*, 132:512–517, 2008.

[115] S. M. Imaad, N. Lord, G. Kulsharova, and G. L. Liu. Microparticle and cell counting with digital microfluidic compact disc using standard cd drive. *Lab on a Chip*, 11:1448–1456, 2011.

[116] H. Chen, L. Wang, and P. C. H. Li. Nucleic acid microarrays created in the double-spiral format on a circular microfluidic disk. *Lab on a Chip*, 8:826–829, 2008.

[117] J. L. Clair and M. Burkart. Molecular screening on a compact disc. *Organic & Biomolecular Chemistry*, 1:3244–3249, 2003.

[118] S. Morais, J. Carrascosa, D. Mira, R. Puchades, and A. Maquieira. Microimmunoanalysis on standard compact discs to determine low abundant compounds. *Analytical Chemistry*, 79:7628–7635, 2007.

[119] S. A. Lange, G. Roth, S. Wittemann, T. Lacoste, A. Vetter, J. Grssle, S. Kopta, M. Kolleck, B. Breitinger, M. Wick, J. K. H. Hrber, S. Dble, and A. Bernard. Measuring biomolecular binding events with a compact disc player device. *Angewandte Chemie*, 45:270–273, 2006.

[120] R. Barathur, J. Bookout, S. Sreevatsan, J. Gordon, M. Werner, G. Thor, and M. Worthington. New disc-based technologies for diagnostic and research applications. *Psychiatric genetics*, 12:193–206, 2002.

[121] H. Yu. New chemistry on old cds. *Chemical Communications*, 23:2633–2636, 2004.

[122] F. G. Bosco, E.-T. Hwu, C.-H. Chen, S. Keller, M. Bache, M. H. Jakobsen, I.-S. Hwang, and A. Boisen. High throughput label-free platform for statistical bio-molecular sensing. *Lab on a Chip*, 11:2411–2416, 2011.

[123] T. G. Ltd. www.tecan.com.

[124] Bayer. www.bayer.com.

[125] B. Ingelheim. http://www.boehringer-ingelheim.com.

[126] R. AG. www.roche.com.

[127] Gyros. www.gyros.com.

[128] Samsung. www.samsung.com.

[129] M. Cristofanilli, G. Budd, M. Ellis, A. Stopeck, J. Matera, M. Miller, J. Reuben, G. Doyle, W. Allard, L. Terstappen, and D. Hayes. Circulating tumor cells, disease progression, and survival in metastatic breast cancer. *New England Journal of Medicine*, 351:781–791, 2004.

[130] M. Yu, S. Stott, M. Toner, S. Maheswaran, and D. A. Haber. Circulating tumor cells: approaches to isolation and characterization. *Journal of Cell Biology*, 192:373–382, 2011.

[131] S. Nagrath, L. V. Sequist, S. Maheswaran, D. W. Bell, D. Irimia, L. Ulkus, M. R. Smith, E. L. Kwak, S. Digumarthy, A. Muzikansky, P. Ryan, U. J. Balis, R. G. Tompkins, D. A. Haber, and M. Toner. Isolation of rare circulating tumour cells in cancer patients by microchip technology. *Nature*, 450:1235–U10, 2007.

[132] W. Allard, J. Matera, M. Miller, M. Repollet, M. Connelly, C. Rao, A. Tibbe, J. Uhr, and L. Terstappen. Tumor cells circulate in the peripheral blood of all major carcinomas but not in healthy subjects or patients with nonmalignant diseases. *Clinical Cancer Research*, 10:6897–6904, 2004.

[133] J. L. Garcia-Cordero, L. Basabe-Desmonts, J. Ducrée, and A. J. Ricco. Liquid recirculation in microfluidic channels by the interplay of capillary and centrifugal forces. *Microfluidics and Nanofluidics*, 9:695–703, 2010.

[134] S. Häberle, N. Schmitt, R. Zengerle, and J. Ducrée. Centrifugo-magnetic pump for gas-to-liquid sampling. *Sensors and Actuators A-Physical*, 135:28–33, 2007.

[135] S. Häberle, R. Zengerle, and J. Ducrée. Centrifugal generation and manipulation of droplet emulsions. *Microfluidics and Nanofluidics*, 3:65–75, 2007.

[136] H. Lorenz, M. Despont, N. Fahrni, J. Brugger, P. Vettiger, and P. Renaud. High-aspect-ratio, ultrathick, negative-tone near-uv photoresist and its applications for mems. *Sensors and Actuators A-Physical*, 64:33–39, 1998.

[137] P. Abgrall, C. Lattes, V. Conedera, X. Dollat, S. Colin, and A. M. Gue. A novel fabrication method of flexible and monolithic 3d microfluidic structures using lamination of su-8 films. *Journal of Micromechanics and Microengineering*, 16:113–121, 2006.

[138] P. Abgrall, V. Conedera, H. Camon, A. M. Gue, and N. T. Nguyen. Su-8 as a structural material for labs-on-chips and microelectromechanical systems. *Electrophoresis*, 28:4539–4551, 2007.

[139] D. C. Duffy, J. C. McDonald, O. J. A. Schueller, and G. M. Whitesides. Rapid prototyping of microfluidic systems in poly(dimethylsiloxane). *Analytical Chemistry*, 70:4974–4984, 1998.

[140] J. C. McDonald, D. C. Duffy, J. R. Anderson, D. T. Chiu, H. Wu, O. J. A. Schueller, and G. M. Whitesides. Fabrication of microfluidic systems in poly(dimethylsiloxane). *ELECTROPHORESIS*, 21:27–40, 2000.

[141] T. Thorsen, S. J. Maerkl, and S. R. Quake. Microfluidic large-scale integration. *Science*, 298:580–584, 2002.

[142] K. Hosokawa, K. Sato, N. Ichikawa, and M. Maeda. Power-free poly(dimethylsiloxane) microfluidic devices for gold nanoparticle-based dna analysis. *Lab on a Chip*, 4:181–185, 2004.

[143] A. Ashkin. Acceleration and trapping of particles by radiation pressure. *Physical Review Letters*, 24:156–&, 1970.

[144] A. Ashkin and J. M. Dziedzic. Optical levitation by radiation pressure. *Applied Physics Letters*, 19:283–&, 1971.

[145] A. Ashkin, J. M. Dziedzic, J. E. Bjorkholm, and S. Chu. Observation of a single-beam gradient force optical trap for dielectric particles. *Optics Letters*, 11:288–290, 1986.

[146] S. Chu. Laser manipulation of atoms and particles. *Science*, 253:861–866, 1991.

[147] K. Visscher, M. J. Schnitzer, and S. M. Block. Single kinesin molecules studied with a molecular force clamp. *Nature*, 400:184–189, 1999.

[148] G. J. L. Wuite, S. B. Smith, M. Young, D. Keller, and C. Bustamante. Single-molecule studies of the effect of template tension on t7 dna polymerase activity. *Nature*, 404:103–106, 2000.

[149] M. D. Wang, M. J. Schnitzer, H. Yin, R. Landick, J. Gelles, and S. M. Block. Force and velocity measured for single molecules of rna polymerase. *Science*, 282:902–907, 1998.

[150] A. Ashkin, J. M. Dziedzic, and T. Yamane. Optical trapping and manipulation of single cells using infrared-laser beams. *Nature*, 330:769–771, 1987.

[151] A. Y. Lau, L. P. Lee, and J. W. Chan. An integrated optofluidic platform for raman-activated cell sorting. *Lab on a Chip*, 8:1116–1120, 2008.

[152] M. MacDonald, G. Spalding, and K. Dholakia. Microfluidic sorting in an optical lattice. *Nature*, 426:421–424, 2003.

[153] M. Ozkan, M. Wang, C. Ozkan, R. Flynn, A. Birkbeck, and S. Esener. Optical manipulation of objects and biological cells in microfluidic devices. *Biomedical Microdevices*, 5:61–67, 2003.

[154] J. E. Molloy and M. J. Padgett. Lights, action: optical tweezers. *Contemporary Physics*, 43:241–258, 2002.

[155] D. Grier. A revolution in optical manipulation. *Nature*, 424:810–816, 2003.

[156] K. C. Neuman and S. M. Block. Optical trapping. *Review of Scientific Instruments*, 75:2787–2809, 2004.

[157] J. R. Moffitt, Y. R. Chemla, S. B. Smith, and C. Bustamante. Recent advances in optical tweezers. *Annual Review of Biochemistry*, 77:205–228, 2008.

[158] P. Chaumet and M. Nieto-Vesperinas. Time-averaged total force on a dipolar sphere in an electromagnetic field. *Optics Letters*, 25:1065–1067, 2000.

[159] A. Ashkin. Forces of a single-beam gradient laser trap on a dielectric sphere in the ray optics regime. *Biophysical journal*, 61:569–582, 1992.

[160] K. Neuman, E. Chadd, G. Liou, K. Bergman, and S. Block. Characterization of photodamage to escherichia coli in optical traps. *Biophysical journal*, 77:2856–2863, 1999.

[161] P. S. Dittrich and A. Manz. Lab-on-a-chip: microfluidics in drug discovery. *Nature Reviews Drug Discovery*, 5:210–218, 2006.

[162] J. Nilsson, M. Evander, B. Hammarstrom, and T. Laurell. Review of cell and particle trapping in microfluidic systems. *Analytica Chimica Acta*, 649:141–157, 2009.

[163] A. R. Wheeler, W. R. Throndset, R. J. Whelan, A. M. Leach, R. N. Zare, Y. H. Liao, K. Farrell, I. D. Manger, and A. Daridon. Microfluidic device for single-cell analysis. *Analytical Chemistry*, 75:3581–3586, 2003.

[164] W. H. Tan and S. Takeuchi. A trap-and-release integrated microfluidic system for dynamic microarray applications. *Proceedings of the National Academy of Sciences of the United States of America*, 104:1146–1151, 2007.

[165] S. Kobel, A. Valero, J. Latt, P. Renaud, and M. Lutolf. Optimization of microfluidic single cell trapping for long-term on-chip culture. *Lab on a Chip*, 10:857–863, 2010.

[166] M. Ikami, A. Kawakami, M. Kakuta, Y. Okamoto, N. Kaji, M. Tokeshi, and Y. Baba. Immuno-pillar chip: a new platform for rapid and easy-to-use immunoassay. *Lab on a Chip*, 10:3335–3340, 2010.

[167] R. D. Oleschuk, L. L. Shultz-Lockyear, Y. B. Ning, and D. J. Harrison. Trapping of bead-based reagents within microfluidic systems: On-chip solid-phase extraction and electrochromatography. *Analytical Chemistry*, 72:585–590, 2000.

[168] M. Yang, C.-W. Li, and J. Yang. Cell docking and on-chip monitoring of cellular reactions with a controlled concentration gradient on a microfluidic device. *Analytical Chemistry*, 74:3991–4001, 2002.

[169] D. D. Carlo, L. Y. Wu, and L. P. Lee. Dynamic single cell culture array. *Lab on a Chip*, 6:1445–1449, 2006.

[170] A. M. Skelley, O. Kirak, H. Suh, R. Jaenisch, and J. Voldman. Microfluidic control of cell pairing and fusion. *Nature Methods*, 6:147–152, 2009.

[171] M. Khoury, A. Bransky, N. Korin, L. C. Konak, G. Enikolopov, I. Tzchori, and S. Levenberg. A microfluidic traps system supporting prolonged culture of human embryonic stem cells aggregates. *Biomedical Microdevices*, 12:1001–1008, 2010.

[172] M.-C. Kim, B. C. Isenberg, J. Sutin, A. Meller, J. Y. Wong, and C. M. Klapperich. Programmed trapping of individual bacteria using micrometre-size sieves. *Lab on a Chip*, 11:1089–1095, 2011.

[173] J. Y. Park, M. Morgan, A. N. Sachs, J. Samorezov, R. Teller, Y. Shen, K. J. Pienta, and S. Takayama. Single cell trapping in larger microwells capable of supporting cell spreading and proliferation. *Microfluidics and Nanofluidics*, 8:263–268, 2010.

[174] J. R. Rettig and A. Folch. Large-scale single-cell trapping and imaging using microwell arrays. *Analytical Chemistry*, 77:5628–5634, 2005.

[175] M. Grumann, T. Brenner, C. Beer, R. Zengerle, and J. Ducrée. Visualization of flow patterning in high-speed centrifugal microfluidics. *Review of Scientific Instruments*, 76:25101–25101–6, 2005.

[176] C.-Y. Chen, C.-H. Chen, T.-Y. Tu, C.-M. Lin, and A. M. Wo. Electrical isolation and characteristics of permanent magnet-actuated valves for pdms microfluidics. *Lab on a Chip*, 11:733–737, 2011.

[177] R. Burger, P. Reith, V. Akujobi, and J. Ducrée. Rotationally controlled magneto-hydrodynamic particle handling for bead-based microfluidic assays. *Microfluidics and Nanofluidics*, 2012.

[178] P. Vulto, S. Podszun, P. Meyer, C. Hermann, A. Manz, and G. A. Urban. Phaseguides: a paradigm shift in microfluidic priming and emptying. *Lab on a Chip*, 11:1596–1602, 2011.

[179] P. Dittrich, K. Tachikawa, and A. Manz. Micro total analysis systems. latest advancements and trends. *Analytical Chemistry*, 78:3887–3907, 2006.

[180] H. Craighead. Future lab-on-a-chip technologies for interrogating individual molecules. *Nature*, 442:387–393, 2006.

[181] A. J. DeMello. Control and detection of chemical reactions in microfluidic systems. *Nature*, 442:394–402, 2006.

[182] G. M. Whitesides. The origins and the future of microfluidics. *Nature*, 442:368–373, 2006.

[183] D. Mark, S. Haeberle, G. Roth, F. von Stetten, and R. Zengerle. Microfluidic lab-on-a-chip platforms: requirements, characteristics and applications. *Chemical Society Reviews*, 39:1153–1182, 2010.

[184] T. Arai, S. C. B. Gopinath, H. Mizuno, P. K. R. Kumar, C. Rockstuhl, K. Awazu, and J. Tominaga. Toward biological diagnosis system based on digital versatile disc technology. *Japanese Journal of Applied Physics Part 1-Regular Papers Brief Communications & Review Papers*, 46:4003–4006, 2007.

[185] X. Wang, M. Zhao, and D. D. Nolte. Combined fluorescent and interferometric detection of protein on a biocd. *Applied Optics*, 47:2779–2789, 2008.

[186] S. Lai, S. Wang, J. Luo, L. Lee, S. Yang, and M. Madou. Design of a compact disk-like microfluidic platform for enzyme-linked immunosorbent assay. *Analytical Chemistry*, 76:1832–1837, 2004.

[187] N. Honda, U. Lindberg, P. Andersson, S. Hoffman, and H. Takei. Simultaneous multiple immunoassays in a compact disc-shaped microfluidic device based on centrifugal force. *Clinical chemistry*, 51:1955–1961, 2005.

[188] M. Inganas, H. Derand, A. Eckersten, G. Ekstrand, A. Honerud, G. Jesson, G. Thorsen, T. Soderman, and P. Andersson. Integrated microfluidic compact disc device with potential use in both centralized and point-of-care laboratory settings. *Clinical chemistry*, 51:1985–1987, 2005.

[189] X. Y. L. Peng, P. C. H. Li, H.-Z. Yu, M. P. Ash, and W. L. J. Chou. Spiral microchannels on a cd for dna hybridizations. *Sensors and Actuators B-Chemical*, 128:64–69, 2007.

[190] R. Peytavi, F. Raymond, D. Gagne, F. Picard, G. Jia, J. Zoval, M. Madou, K. Boissinot, M. Boissinot, L. Bissonnette, M. Ouellette, and M. Bergeron. Microfluidic device for rapid (¡ 15 min) automated microarray hybridization. *Clinical chemistry*, 51:1836–1844, 2005.

[191] G. Jia, K. Ma, J. Kim, J. Zoval, R. Peytavi, M. Bergeron, and M. Madou. Dynamic automated dna hybridization on a cd (compact disc) fluidic platform. *Sensors and Actuators B-Chemical*, 114:173–181, 2006.

[192] C. Li, H. Li, J. Qin, and B. Lin. Rapid discrimination of single-nucleotide mismatches based on reciprocating flow on a compact disc microfluidic device. *Electrophoresis*, 30:4270–4276, 2009.

[193] M.-J. Banuls, F. Garcia-Pinon, R. Puchades, and A. Maquieira. Chemical derivatization of compact disc polycarbonate surfaces for snps detection. *Bioconjugate chemistry*, 19:665–672, 2008.

[194] C. Lu, Y. Xie, Y. Yang, M. M. C. Cheng, C.-G. Koh, Y. Bai, and L. J. Lee. New valve and bonding designs for microfluidic biochips containing proteins. *Analytical Chemistry*, 79:994–1001, 2007.

[195] J. M. Chen, P.-C. Huang, and M.-G. Lin. Analysis and experiment of capillary valves for microfluidics on a rotating disk. *Microfluidics and Nanofluidics*, 4:427–437, 2008.

[196] I. Gorkin, Robert, L. Clime, M. Madou, and H. Kido. Pneumatic pumping in centrifugal microfluidic platforms. *Microfluidics and Nanofluidics*, 9:541–549, 2010.

[197] T. Brenner, T. Glatzel, R. Zengerle, and J. Ducrée. Frequency-dependent transversal flow control in centrifugal microfluidics. *Lab on a Chip*, 5:146–150, 2005.

[198] N. Nguyen and Z. Wu. Micromixers - a review. *Journal of Micromechanics and Microengineering*, 15:R1–R16, 2005.

[199] V. Hessel, H. Lowe, and F. Schonfeld. Micromixers - a review on passive and active mixing principles. *Chemical Engineering Science*, 60:2479–2501, 2005.

[200] S. Hardt, K. Drese, V. Hessel, and F. Schonfeld. Passive micromixers for applications in the microreactor and mu tas fields. *Microfluidics and Nanofluidics*, 1:108–118, 2005.

[201] Z. Yang, H. Goto, M. Matsumoto, and R. Maeda. Active micromixer for microfluidic systems using lead-zirconate-titanate(pzt)-generated ultrasonic vibration. *Electrophoresis*, 21:116–119, 2000.

[202] P. Paik, V. K. Pamula, and R. B. Fair. Rapid droplet mixers for digital microfluidic systems. *Lab on a Chip*, 3:253–259, 2003.

[203] I. Glasgow and N. Aubry. Enhancement of microfluidic mixing using time pulsing. *Lab on a Chip*, 3:114–120, 2003.

[204] A. D. Stroock, S. K. W. Dertinger, A. Ajdari, I. Mezic, H. A. Stone, and G. M. Whitesides. Chaotic mixer for microchannels. *Science*, 295:647–651, 2002.

[205] F. G. Bessoth, A. J. deMello, and A. Manz. Microstructure for efficient continuous flow mixing. *Analytical Communications*, 36:213–215, J 1999.

[206] S. W. Lee, D. S. Kim, S. S. Lee, and T. H. Kwon. A split and recombination micromixer fabricated in a pdms three-dimensional structure. *Journal of Micromechanics and Microengineering*, 16:1067–1072, 2006.

[207] F. Schonfeld, V. Hessel, and C. Hofmann. An optimised split-and-recombine micro-mixer with uniform 'chaotic' mixing. *Lab on a Chip*, 4(1):65–69, 2004.

Appendices

Appendix A

Own Publications

COCHBI-974; NO. OF PAGES 6 ARTICLE IN PRESS

Available online at www.sciencedirect.com

SciVerse ScienceDirect

Current Opinion in Chemical Biology

Centrifugal microfluidics for cell analysis

Robert Burger, Daniel Kirby, Macdara Glynn, Charles Nwankire, Mary O'Sullivan, Jonathan Siegrist, David Kinahan, Gerson Aguirre, Gregor Kijanka, Robert A Gorkin III and Jens Ducrée

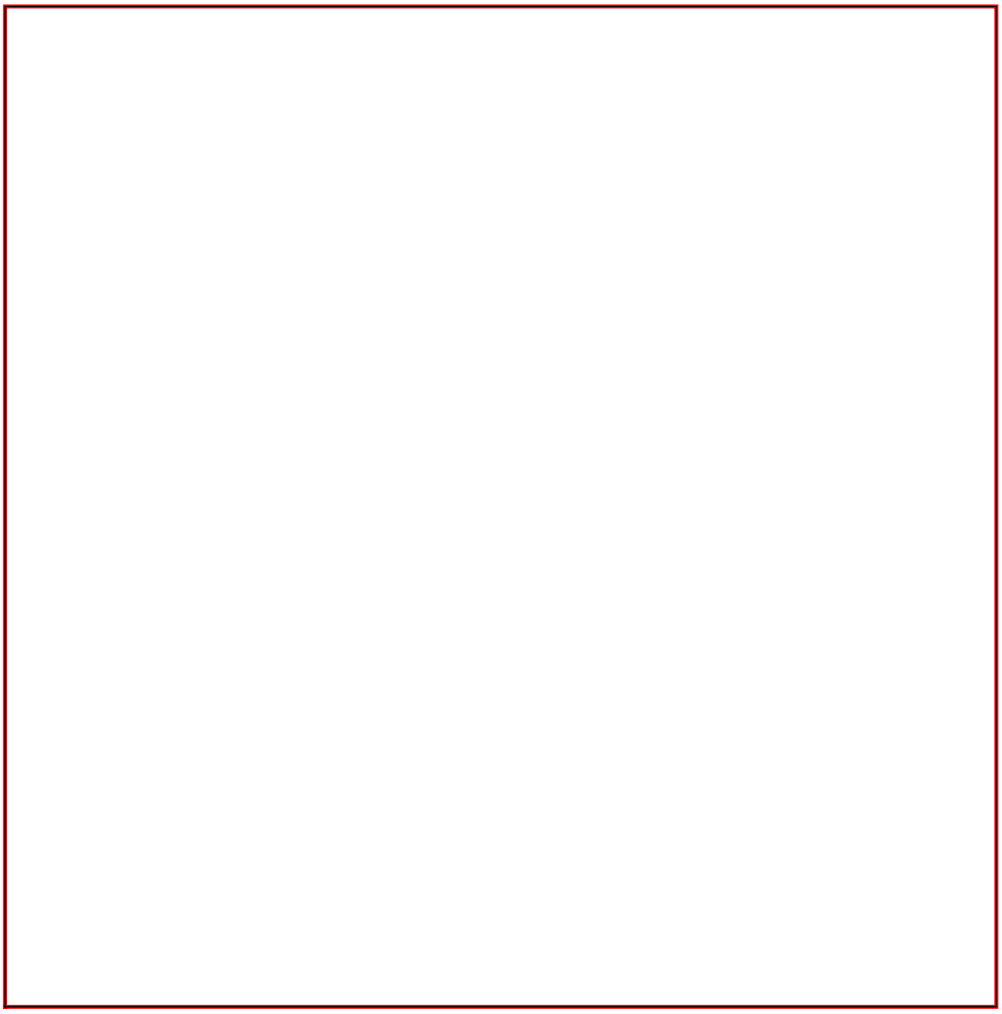

Please cite this article in press as: Burger R, et al.: Centrifugal microfluidics for cell analysis, Curr Opin Chem Biol (2012), http://dx.doi.org/10.1016/j.cbpa.2012.06.002

COCHBI-974; NO. OF PAGES 6 ARTICLE IN PRESS

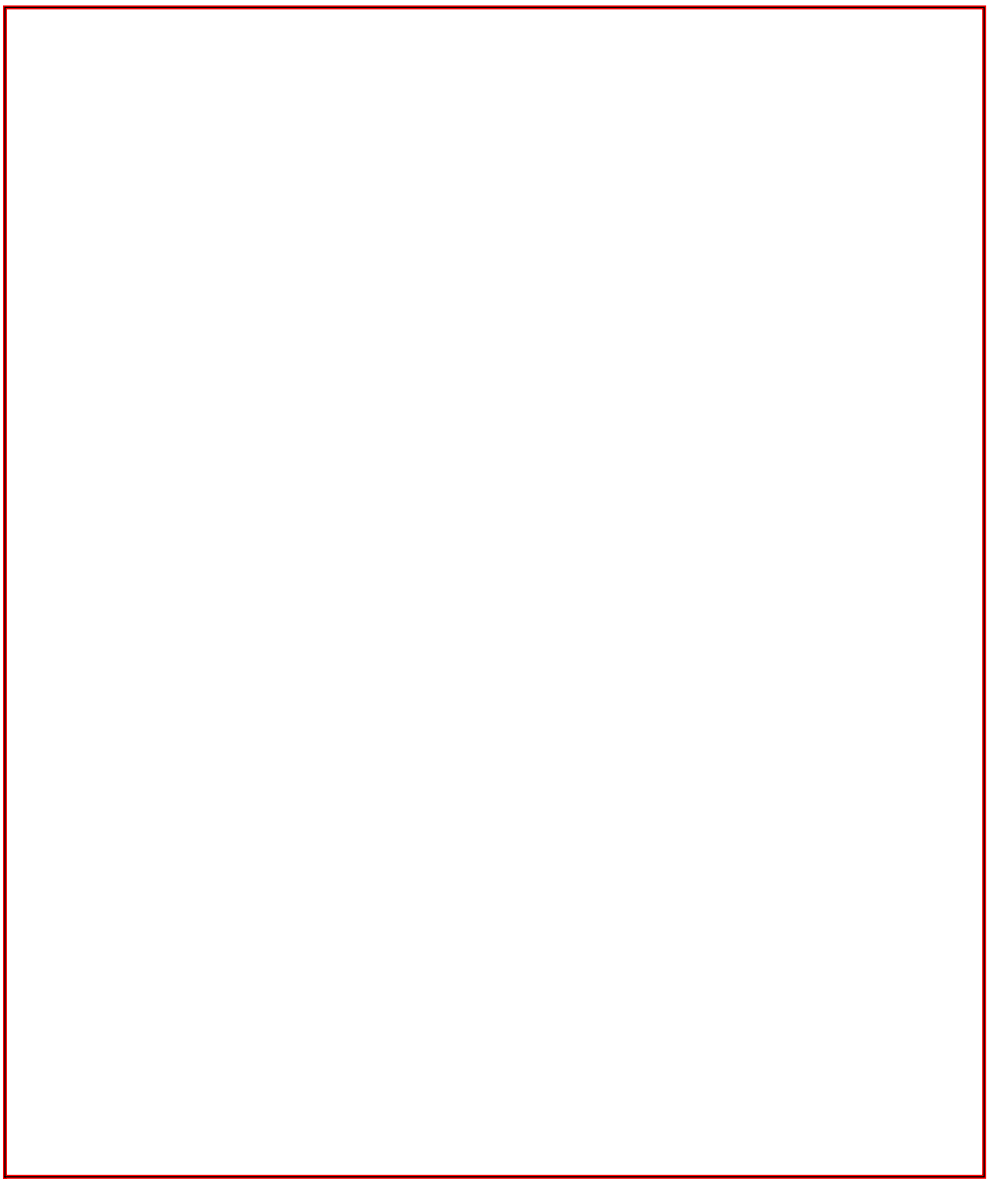

Please cite this article in press as: Burger R, et al.: Centrifugal microfluidics for cell analysis, Curr Opin Chem Biol (2012), http://dx.doi.org/10.1016/j.cbpa.2012.06.002

COCHBI-974; NO. OF PAGES 6 ARTICLE IN PRESS

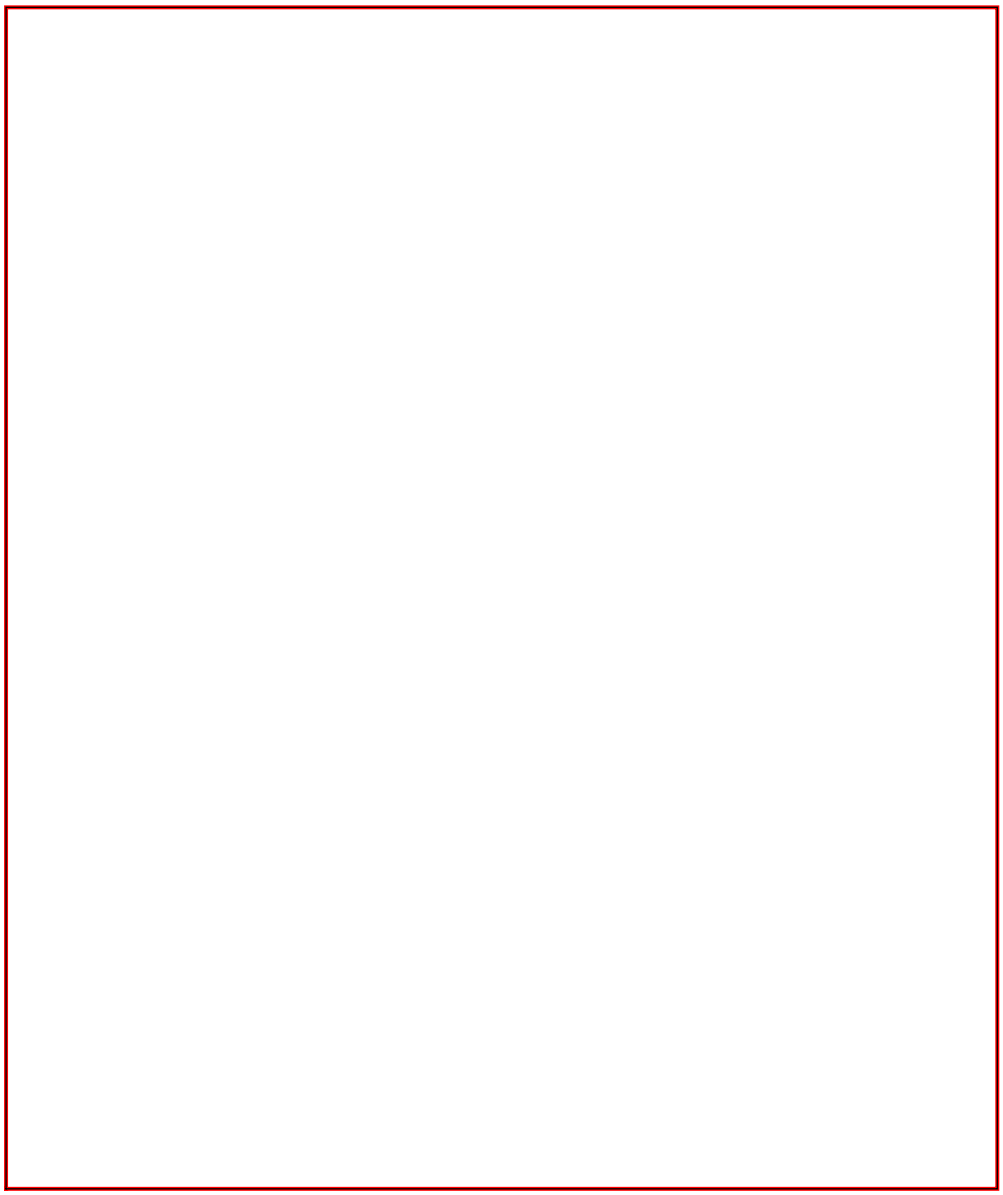

Please cite this article in press as: Burger R, et al.: Centrifugal microfluidics for cell analysis, Curr Opin Chem Biol (2012), http://dx.doi.org/10.1016/j.cbpa.2012.06.002

COCHBI-974; NO. OF PAGES 6 ARTICLE IN PRESS

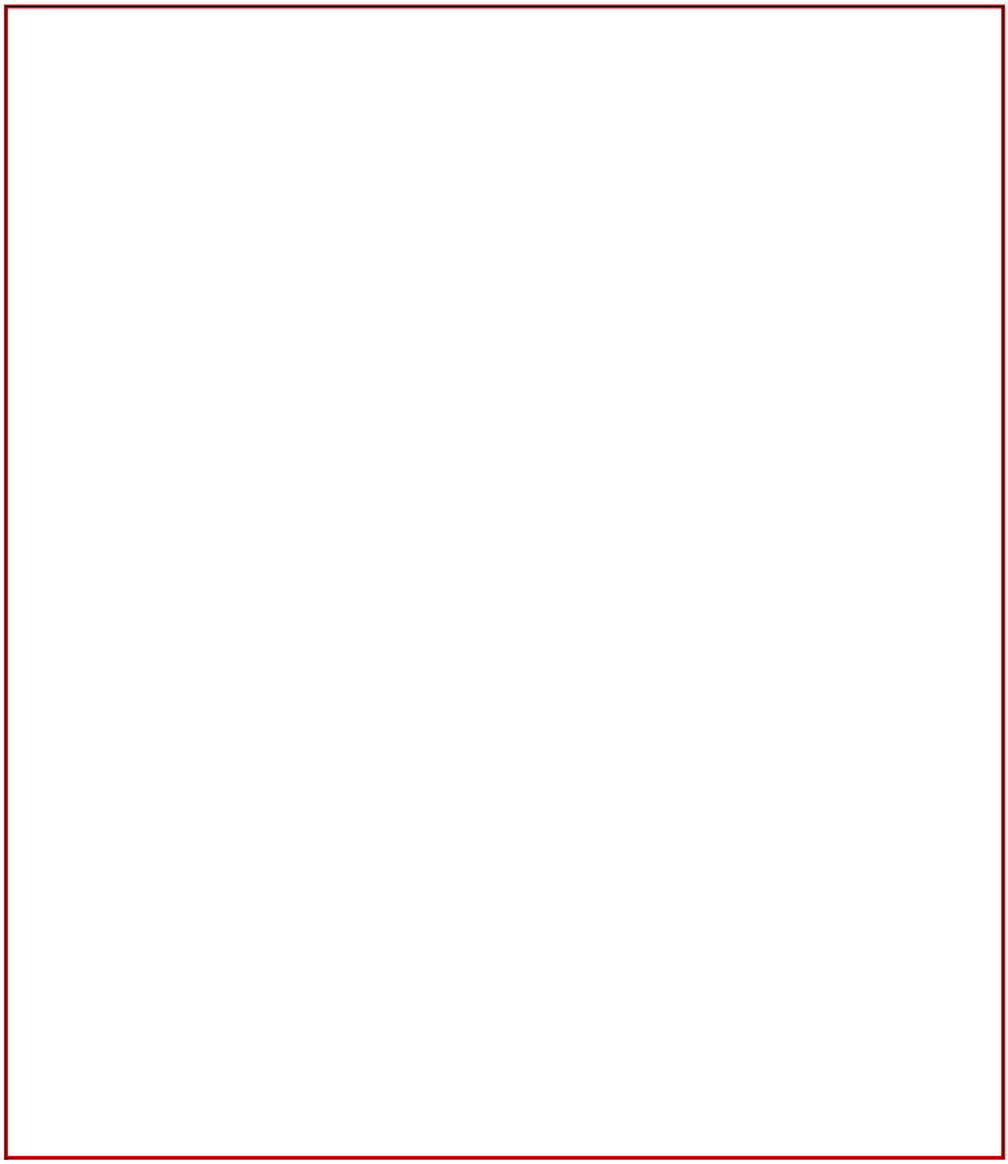

Please cite this article in press as: Burger R, et al.: Centrifugal microfluidics for cell analysis, Curr Opin Chem Biol (2012), http://dx.doi.org/10.1016/j.cbpa.2012.06.002

COCHBI-974; NO. OF PAGES 6 ARTICLE IN PRESS

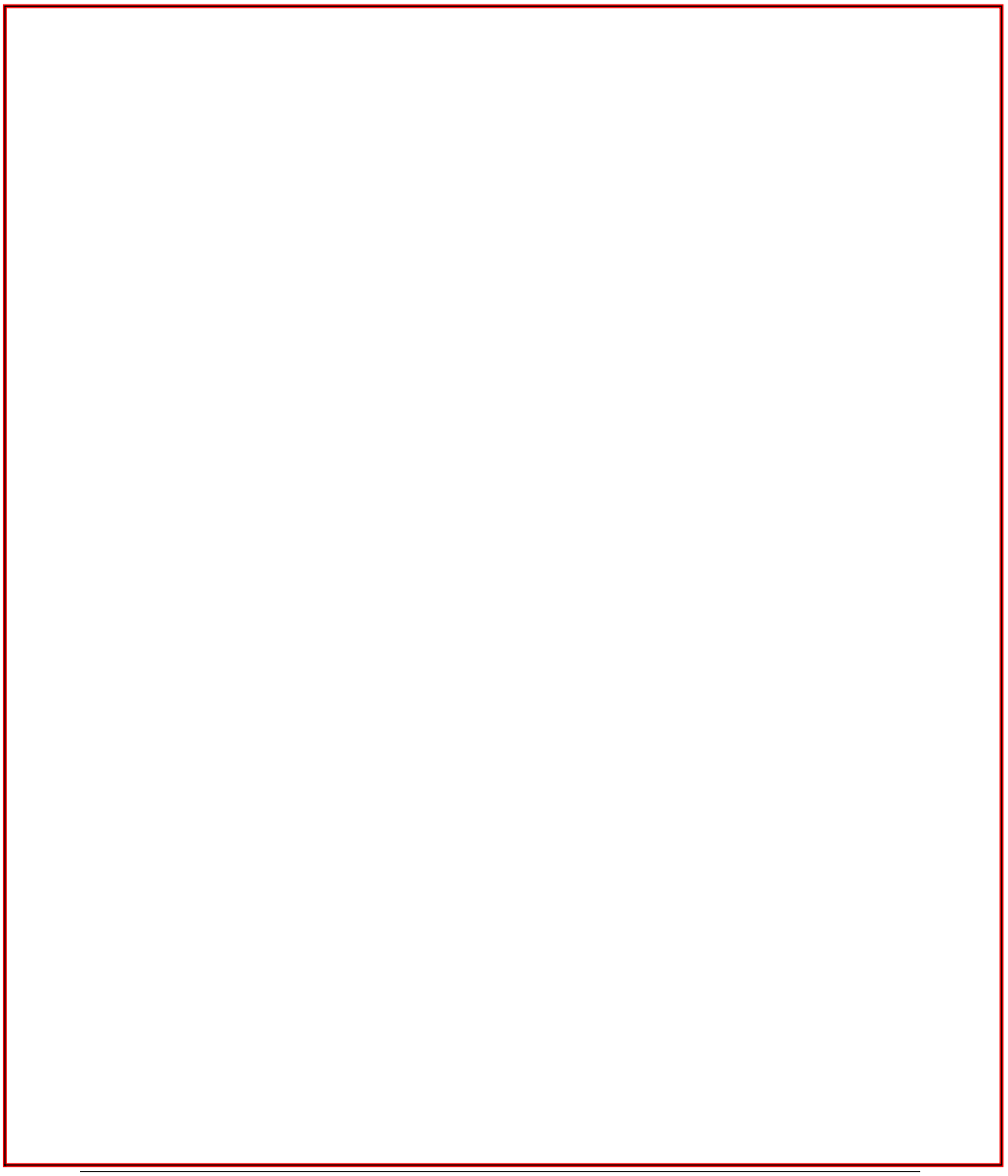

Please cite this article in press as: Burger R, et al.: Centrifugal microfluidics for cell analysis, Curr Opin Chem Biol (2012), http://dx.doi.org/10.1016/j.cbpa.2012.06.002

COCHBI-974; NO. OF PAGES 6 ARTICLE IN PRESS

Please cite this article in press as: Burger R, et al.: Centrifugal microfluidics for cell analysis, Curr Opin Chem Biol (2012), http://dx.doi.org/10.1016/j.cbpa.2012.06.002

Appendix B

Own Publications under Review

B.1 Centrifugally Actuated Mixing Based on Siphon–Induced Droplet Break Off and Phase Shifting

This work has been submitted to Microfluidics and Nanofluidcs and is currently under review. Authors: Robert Burger, Hélène Cayron, Nuno Reis, João Garcia da Fonseca and Jens Ducrée

We present a novel, powerful and compact, batch-mode mixing and dilution technique for centrifugal microfluidic platforms. Siphon structures are designed to disrupt continuous flows into a sequence of droplets, displaying individual volumes as low as 100 nL. Using a passive, self-regulating 4-step mechanism, discrete volumes of the two educts are alternatingly issued into a common intermediate chamber where the educts converge. The joined droplet then runs down a radial nozzle where it is advectively stirred and issued into the final receiving chamber. Upon impact onto the liquid interface, the droplet spreads laterally, resulting in short diffusion distances. Fast and homogeneous mixing is demonstrated for various combinations of liquids such as aqueous solutions as well as saline solutions and human plasma. The mixing quality is assessed on a quantitative scale by using a colorimetric method based on the mixing of potassium thiocyanate and iron(III) chloride, and in the case of human plasma using a spectroscopic method. For instance, volumes of 5 μl been mixed in less than 20 s. Single-step dilutions up to 1 : 5 of plasma in a standard phosphate buffer solution are also demonstrated.

Introduction

The interest in microfluidic technologies has emerged at breath-taking speed since their initial pioneering steps dating back mainly to the 1980s and the early 1990s [179–183]. Initial work overwhelmingly focused on chip-based analytical separations, e.g. capillary electrophoresis (CE) or high-performance liquid chromatography

(HPLC), and the miniaturization of individual fluidic components such as pumps and valves through micromachining. In the recent decade an increasing number of researchers investigated options to assemble sample preparation steps as well the assay and detection on so-called lab-on-a-chip platforms.

Lab-on-a-chip platforms can be categorized on the basis of their underlying liquid handling principles such as electroosmosis, pressure, peristaltics, ultrasonics and electrowetting. Rotational microfluidic systems are a special variant of lab-on-a-chip platforms which have thrived in the academic community as well as in the commercial world. There are two main categories. One of them, which may be referred to as bioanalytical screening CD, derives from commercial optical disc drive (ODD) technology (e.g. Compact Disc, DVD). This technology takes advantage of the high-density data storage capability as well as the favorable pricing for its main constituents, i.e., the optical pickup unit, the spindle drive and the optical disc substrates [118–120, 184, 185]. The lab-on-a-disc technology [33, 34, 48, 60] investigated here performs a much smaller number of more complex bioanalytical assay protocols in a sample-to-answer fashion. The technological precursor of these systems are the centrifugal analyzers which became popular in the 1970s and 1980s [36] for automating a very limited number of simple assay steps on rather macroscopic sample volumes, and readout on a centrifuge based instrument. Currently the main areas of application are immunoassays [186–188], nucleic acid testing [39,67,189–193] and cell sorting / identification [84, 96, 100]. These lab-on- a-disc systems make specific use of the interplay of the frequency controlled centrifugal force and capillary action in a surface-functionalized network of microchannels and cavities. Liquid handling operations such as valving [16,194,195], metering [38,41], mixing [43–45,47,133], pumping [134, 196], switching / routing of flow [197] and sample preconditioning [67, 68] have been successfully demonstrated.

While there is no real technological link to the first category of optical data storage technology, it is still convenient to use the (outer) geometric format of a CD for lab-on-a-disc systems. The nature of the centrifugal field implies an outbound transport of the sample away from the central axis, so the radial space as well as the area near the center is rather precious while more space opens up towards the

outer perimeter. It is therefore an important design goal to reduce the inner area occupied by sample preparation steps like mixing, which occur early in the process chain.

This paper demonstrates a novel, spatially compact structure for mixing on a lab-on-a-disc platform which is a critical step in the workflow of biological assays. In contrast to macroscopic systems where mixing can be achieved by turbulence inducing means such as stirring or shaking, this approach is not feasible in most microfluidic systems, mainly due to limitations on the manufacturability of actuated moving parts and the prevalent laminar flow conditions with Reynolds numbers typically around unity. Hence, mixing in microfluidic systems is mainly driven by chaotic advection, i.e., the flow-driven stretching and thinning of reagent layers, and subsequent diffusion. In general, one can categorize micromixers according to different characteristics [198–200], e.g. batch and continuous flow mode, laminar and turbulent, planar and 3-dimensional geometry, low- or high-aspect-ratio structures, manufacturing technologies or active / passive mixers. Active mixers utilize external forces such as ultrasonic waves [201], electrowetting [202] or periodically changing flow rates [203]. While it is hard to make a general statement, active mixers tend to provide shorter mixing lengths, but they are typically more complicated to fabricate and more complex to control. Their more facile fabrication makes passive mixers preferable for disposable lab-on-a-chip devices.

Passive mixers use the hydrodynamic energy, e.g., provided by a pressure difference created by a pump, gravity or centrifugal force, to restructure the liquid flows in such ways that rapid mixing is promoted. Examples for passive mixing principles are bas/relief structures incorporated in the channel walls to induce advection in a liquid flow [204] and multi-lamination of flow [205], e.g. through split-and-recombine strategies [206, 207]. Mixing principles using the specific effects on centrifugal lab-on-a-disc platforms include Coriolis-force induced split-and-recombine [43], advection [44] and reciprocating flow [47, 133] as well as batch mode mixing by periodically changing angular acceleration and / or magnetic beads [45]. Also, the periodic, centrifugo-capillary driven recirculation of flow has been utilized to mix larger volumes on lab-on-a-disc devices [133].

Interestingly, it is in some cases actually difficult to distinguish these rotational mixers as purely passive or active; on the one hand, the power for the mixing processes is drawn from the same rotational motion as the flow, i.e. in this regard it should be passive. On the other hand, the actuation mechanism for mixing is still to a large extent decoupled from the centrifugal force driving the flow. For instance, the rotationally induced mixing can be implemented by driving a radial flow through the centrifugal force while transverse stirring is agitated by the Coriolis force [43]. As these two pseudo forces are both linked to the rotation, they display a different scaling with the centrifugal frequency and are directed perpendicular to each other. In this paper we for the first time describe and characterize a passive, batch-mode, siphon- based striation mixer on a centrifugal microfluidic lab-on-a-disc platform. The novel principle dissects the centrifugally driven flows originating from two separate educt reservoirs into discrete droplets. In a first step, these droplets are alternatingly issued into a common chamber where the educts are contacted. Next, the joined droplets run through the nozzle at the outlet of the intermediate chamber and are issued as droplets into a final mixing chamber where they are laterally stretched by their impact on the liquid interface. The mixer shows a good mixing performance while requiring a comparatively small footprint, thus saving precious real estate on the disc substrate.

Following this introduction, we briefly survey the hydrodynamic principle underlying our centrifugal striation mixer. In the subsequent experimental sections, we describe the materials and fabrication of our mixer, as well as the methods used to experimentally characterize its mixing performance. Finally we conclude and give an outlook to future work.

Operational Principle

We pursue a novel, 4-step concept to create alternating lamellae for rapid mixing on a centrifugal microfluidic platform:

1. Discretization of continuous flow by siphon mechanism into droplets

2. Contacting of educt droplets in an intermediate chamber

3. Flow-based pre-mixing of educts in a nozzle channel

4. Mixing by droplet impact on liquid interface in the outer chamber

The droplet formation in the first step is implemented by siphon-induced flow discretization as schematically outlined in Fig. B.1. Liquid is centrifugally driven into a retention chamber at a flow rate, Q_i, scaling with the square of the rotational frequency (Fig. B.1 a). The outlet of this first chamber is connected to a siphon. Given that the frequency dependent centrifugal force is able to suppress capillary priming of the siphon channel, liquid will continuously fill the chamber (Fig. B.1 b) until the liquid level rises beyond the crest point of the siphon. At this instance, the siphon based valve yields to release the transiently stored liquid at an outgoing flow rate, Q_o (Fig. B.1 c). If the respective flow resistances of the inlet and outlet sections of the siphon are properly chosen, i.e., Q_o exceeds Q_i, the retention chamber empties and the intrusion of gas disrupts the continuous liquid column which results in a droplet being issued into the mixing chamber (Fig. B.1 d). At this point, the flow-discretization cycle starts over and the siphon acts again as a closed valve until the crest point is reached.

The size of the individual droplets is determined by the aggregate volume of the retention chamber V_c and the connected siphon up to the crest point V_s (Fig. B.2). These volumes can easily be adjusted in the layout to deliver the desired droplet volumes. The smallest droplet volumes can be obtained by completely eliminating the chamber and connecting the siphon directly to the inlet channel. The droplet volumes studied in this paper range from 100 nL to 890 nL.

In the second step, droplets emerging from the two educt feeds are dispensed into a common contacting reservoir (Figure B.3). It is very difficult to identify the exact mechanism for the phase shift. However, empirical evidence shows that efficient mixing is always achieved. We speculate that the introduction of a droplet into the common mixing chamber creates a slight back pressure on the other siphon resulting in alternating droplet dispensing. The joined droplets then continue into a single nozzle outlet where they are agitated by hydrodynamically induced advection. Finally, these pre-mixed droplets are issued again from the common nozzle into the common receiving chamber, where they spread upon impact on the surface of the

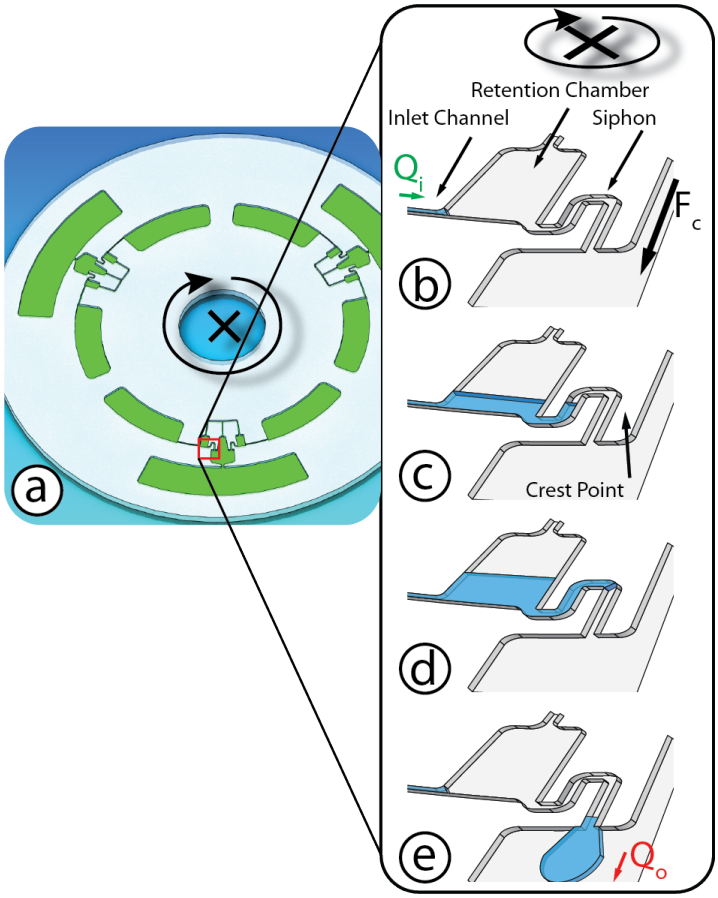

Figure B.1: Working principle of the flow discretization structure. Image (a) shows a typical disc containing 3 identical mixing structures. The insert illustrates the flow break-up principle. Under the impact of the centrifugal field liquid flows through an inlet channel at a flow rate Q_i into the retention chamber (b) where it accumulates (c). Once the liquid level has passed the crest point of the siphon, the valve opens and liquid exits at a flow rate Q_o (d). When the chamber is empty, the liquid column breaks and the cycle resumes (e).

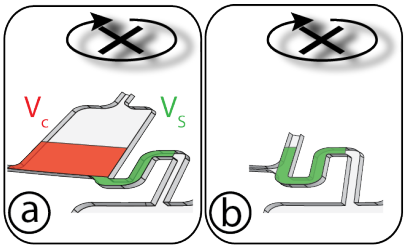

Figure B.2: Relation of the droplet volume with the geometry of the retention chamber. (a) Chamber with attached outlet siphon. (b) The chamber is eliminated to minimize the droplet volume.

resident mixture.

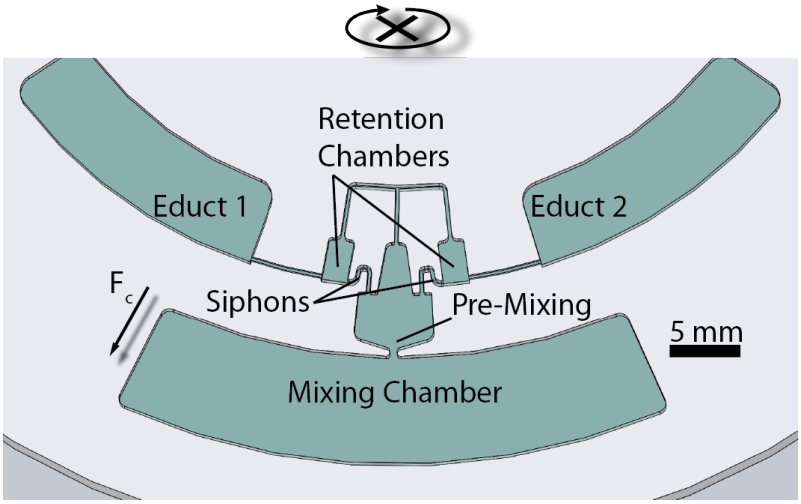

Figure B.3: Mixing structure for generating 420 nL droplets. Educt streams are discretized into droplets and dispensed through the siphons into the premixing chamber, from where the droplets are dispensed into the mixing chamber.

The key impact parameters of the centrifugal mixer are the statically defined volume of the siphon and connected chamber, the flow resistances of the inlet and outlet sections of the retention chamber and the nozzle channel, the lateral cross section of the common mixing chamber as well as the dynamically adjustable rotational frequency ω. Assuming laminar conditions in the common mixing chamber, Fick's law implies that the mixing time

$$t_{mix} \propto l^2/D$$

scales with the square of the layer thickness l and the inverse of the diffusion coefficient D. Assuming ideal, planar spreading upon impact, the layer thickness, l, depends on the droplet volume and the lateral extension (i.e., the width and the depth) of the mixing chamber. The mixing performance is not directly linked to the volume flow rate as long as the time period between two subsequent droplets is sufficiently large to allow lateral spreading. To avoid the formation of a large single layer with long diffusion lengths at the end of the lamination process, it is important that both educt reservoirs are depleted at roughly the same instant in time. The

time for the delivery of the entire liquid volume

$$t = V_{educt}/Q_i$$

corresponds to the quotient of the initial volume V_{educt} and the discharge flow rate Q_i, which in turn is given by the equivalent hydrostatic pressure difference ΔP_ω divided by the flow resistance of the inlet section R_{hd}.

$$Q_i = \Delta P_\omega / R_{hd}$$

The hydrostatic pressure difference ΔP_ω is given by

$$\Delta P_\omega = \rho \bar{r} \Delta r \omega^2$$

with the density ρ, the mean radial position $\bar{r}$ and radial length Δr of the liquid volume in the educt chamber. Finally, the hydraulic resistance of a square channel can be approximated by:

$$R_{hd} = \frac{8(1 + A_r)^2 \ \eta_l \ l}{A_r \ A^2}$$

With η_l being the viscosity of the liquid, A_r the aspect ratio of the channel and A its cross sectional area.

Experimental

Materials and Fabrication

Discs have been manufactured using two different methods, hot embossing and direct fabrication in dry film resist (DFR).

The masters for hot embossing have been created using SU8. To this end first a layer of SU-8 3005 (Microchem, USA) has been spin coated on a silicon wafer at 2500 RPM and subsequently been flood exposed (MA 56, Karl Süss, Germany). This layer serves to improve the adhesion of the subsequent layers and hence increase the life time of the master. A second layer of SU8 3025 was then spin coated with a thickness of 30 μm, baked for 15 min at 95 °C and structured with an exposure energy of 240 mJ cm^{-2}. Following a post exposure bake of 3 min at 95 °C a third

layer of SU8 3050 with a thickness of 170 μm was spin-coated in two steps. After each step the resist was baked on a hot plate at 95 °C for 20 min. The resist was then structured using an exposure intensity of 300 mJ cm^{-2}. Subsequently post exposure bake was performed at 95 °C for 6 min, followed by removal of unexposed resist in standard developer solution. The resist was then hard baked at 150 °C for 90 min. To facilitate demoulding of the master after hot embossing the surface of the master was coated with a layer of Octadecyltrichlorosilane (OTS) (Sigma-Aldrich, Ireland). The coating has been created by immersing the wafer in a solution of 400 μM of OTS in heptane (Sigma- Aldrich, Ireland) for 120 min. Subsequently the master was sonicated in heptane for 5 min, followed by rinsing with methanol and finally baked on a hot plate at 100 °C for 20 min. This resulted in a hydrophobic surface coating with a water contact angle of approximately 108° and significantly facilitated demoulding as compared to untreated masters. Discs were embossed in 2 mm thick PMMA sheets (Radionics, Ireland) using a HEX-02 hot embosser (Jenoptik, Germany) at a pressure of 2.85 MPa and an embossing temperature of 123 °C. The best pattern transfer was achieved with an embossing time of 310 s. The total cycle time was 15 min, only. Figure B.4 shows a comparison of the master profile and the replicated PMMA disk.

After embossing, fluidic inlets were drilled and the discs were sealed by bonding to a PMMA disc using pressure sensitive adhesive (Adhesive Research, Ireland).

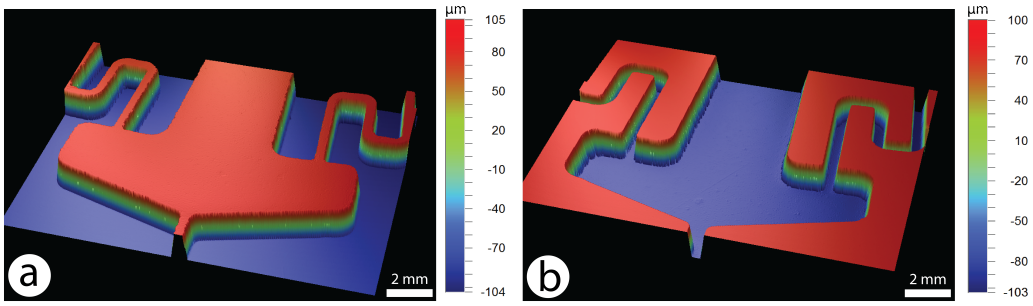

Figure B.4: Profile of SU8 master used for embossing (left) and profile of embossed PMMA mixing structure (right).

Discs for the asymmetric mixing of PBS buffer and plasma were manufactured using dry film resist (DFR). A CO_2 laser (Epilog, USA) was used to cut the PMMA substrates to disc shape and create fluidic I/O ports. Subsequently a layer of 120 μm

thick DFR (Ordyl P50120, Elga Europe, Italy) was laminated onto the PMMA disc and structured with the reservoirs and mixing structure by exposure to UV light. The connecting channels between initial reservoirs and discretization chambers were created in 55 μm thick DFR (SY 350, Elga Europe, Italy) laminated on a 600 μm thick polycarbonate disc. After removing unexposed areas of DFR, both parts were aligned and bonded by lamination at 80 °C.

Methods

The experimental setup used to perform the fluidic experiments consists of a computer controlled motor for spinning the discs (Faulhaber Minimotor SA, Switzerland), a stroboscopic illumination (Drello, Germany) and a highly sensitive colour camera (Pixelfly qe, PCO, Germany) attached to a motorized 12x zoom lens (Navitar, USA). The quality of the mixing of potassium thiocyanate and iron(III) chloride was evaluated using a colorimetric method. Subsequent to mixing, an image of the resulting mixture was acquired using the camera of the test point setup. Using an image processing software (ImageJ, NIH, USA), the area containing the mixture was selected and the standard deviation of the histogram was calculated. Since the supply reservoirs did not always empty at the same time, the area where droplets were issued into the mixing reservoir was excluded from this analysis when it only contained one type of educt. To compensate systematic errors due to the measurement setup, the standard deviation of a reference mixture was recorded and later used to normalize the standard deviations measured during the experiments. The reference solution was prepared by mixing equal volumes of potassium thiocyanate and iron(III) chloride solution using a vortex mixer. Then the same amount of reference solution used in the mixing experiments was pipetted into an identical disk device and an image was acquired.

In experiments where plasma and PBS were mixed, a modified version of the mixing structure was used (Fig. B.5). The mixing chamber is connected to a siphon which in turn leads to a sample collection reservoir. After performing the mixing, the disc is stopped to prime the siphon. The disc is then spun again and a part of the mixture is transferred to the sample collection reservoir while monitoring the

liquid level in the collection reservoir using the camera. The disc is stopped after a sample of 1.5 mul has been collected. This sample is then collected from the reservoir and stored for further analysis. The sampling step is repeated until all mixed liquid is collected. The mixing quality of each 1.5 μl sample was then assessed using a spectrophotometer (Nanodrop 1000, Thermo Scientific, USA). The concentration of plasma proteins in each of these aliquots was determined by measuring the absorbance at 280 nm. A perfect mixture would display the same concentration of proteins in all aliquots. Typically 7 to 9 aliquots were collected per mixing trial.

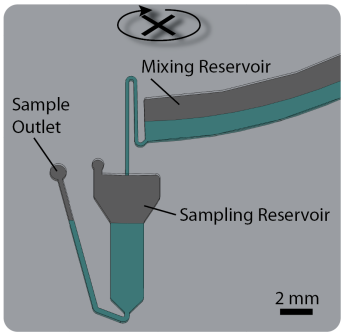

Figure B.5: Structure used to aliquot samples of plasma/PBS mixture.

Results and Discussions

All mixing experiments presented in this work have been carried out at rotation frequencies between 40 and 50 Hz. The mixing quality was evaluated immediately after mixing. At first, mixing of symmetric droplet volumes has been examined using 4 different structures which allow dispensing of different liquid volumes $V_c + V_s$ (Fig. 2): 170 nL, 240 nL, 420 nL and 890 nL. All experiments have been performed with 5 μl of each educt and mixing has been performed in less than 20 s.

A frame sequence obtained while dispensing discrete 170 nL volumes is shown in Figure B.6. The photos visualize the alternating dispensing of educt droplets from the flow discretization siphons, pre-mixing and dispensing of the droplets into the mixing chamber. A movie showing the mixing process is also available as electronic supplementary information.

The results of the mixing experiments with potassium thiocyanate and iron(III)

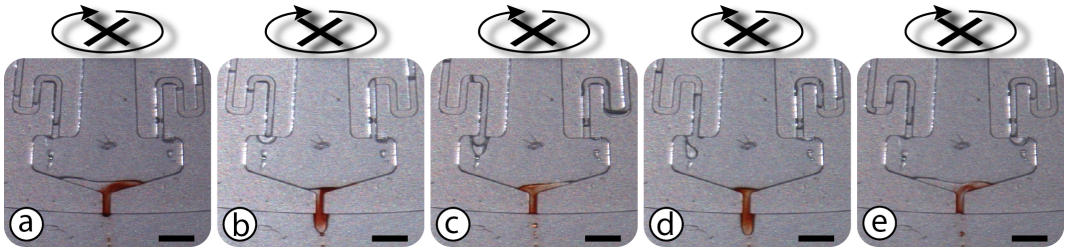

Figure B.6: The image sequences show the droplet dispensing and pre-mixing process. Educts enter the siphon channels (a). The liquids are alternatingly issued into the common chamber with the nozzle outlet where the educts are pre-mixed before being dispensed through the nozzle into the mixing chamber (b – e). Scale bar is 2 mm. A movie of the mixing is provided as ESI.

chloride is shown in Fig. B.7. These results confirm that, as expected, a reduced droplet size results in a faster and more homogenous mixing due to shorter diffusion distances.

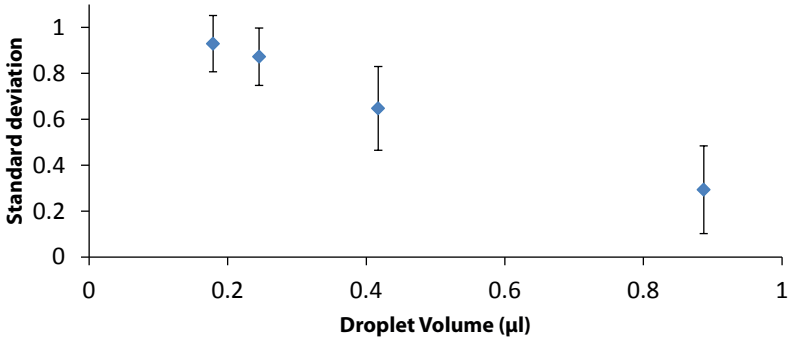

Figure B.7: Normalized standard deviation of mixed aqueous solutions as a function of the droplet size provided by the two disc-based siphons. A value of unity corresponds to perfect mixing. The measured standard deviations were calibrated against the standard deviation of a sample processed by a conventional vortex mixer.

As expected, decreasing the droplet volumes leads to an increased homogeneity of the mixing. Furthermore, the mixing quality obtained with the smallest droplet volumes is close to the reference mixture.

Based on the outcomes of these experiments, mixing structures for the dilution of plasma have been designed. Since the smallest droplets delivered the best mixing quality, a discretization volume of 100 nL was chosen for the plasma dilution structure. We examined dilutions of plasma in PBS in ratios of $1:2.6$ and $1:5$, whereas the hydraulic resistance of the connecting channels were adjusted such that both liquid reservoirs emptied at the same time. Hydraulic resistances have been calculated based on the theory detailed above and channel parameters have been optimized experimentally. Fig. B.8 shows the results obtained for several experiments with

these structures. The histograms show the distribution of the protein concentration in the aliquots. Ideally, the concentration of all aliquots would be identical. These results demonstrate that the here proposed approach is well suitable for diluting human blood plasma in PBS.

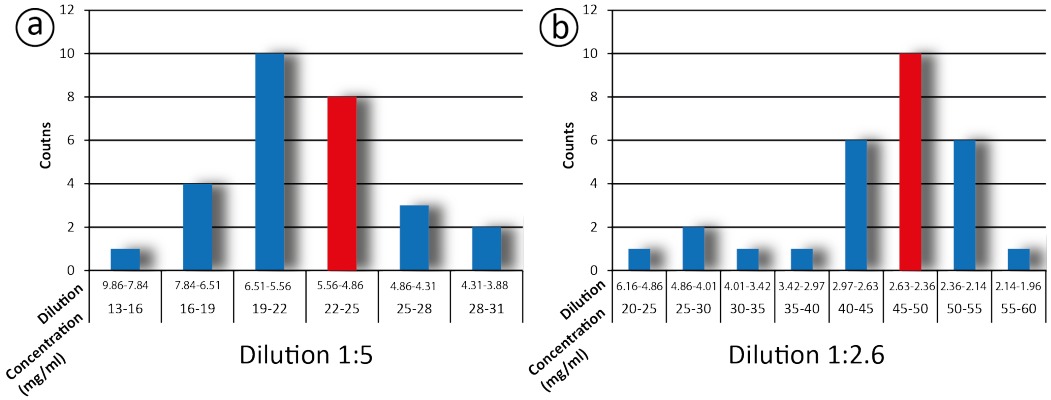

Figure B.8: Results of mixing experiments with blood plasma and PBS buffer for two different mixing ratios. Histogram (a) shows the concentration distribution for a dilution of $1:5$, while histogram (b) displays the distribution for a mixing ratio of $1:2.6$. The red bars indicate the populations with the target dilution.

Conclusion and Outlook

This work for the first time exploits siphon-induced flow discretization to perform batch-mode mixing and dilution of liquids in a compact, small-footprint structure on a centrifugal microfluidic lab-on-a-disc platform. The here presented technology is suitable for mixing liquids at ratios between unity and $1:5$. Higher mixing ratios may be realized through a cascading strategy. Furthermore, our structure has proven to be suitable for mixing liquids with considerably different hydrodynamic properties, such as human blood plasma and standard buffer solutions. Moreover, our new mixing technique obviates surface modifications and runs at a constant spin rate. The fact that the structures have successfully been prototyped using hot embossing suggests that this mixing scheme is well amenable to large scale production techniques such as injection moulding.

Appendix C

Co-Authored Work

C.1 Centrifugo-Magnetophoretic Particle Separation

This Paper has been accepted for publication in Microfluidics and Nanofluidics

Microfluid Nanofluid
DOI 10.1007/s10404-012-1007-6

RESEARCH PAPER

Centrifugo-magnetophoretic particle separation

Daniel Kirby · Jonathan Siegrist · Gregor Kijanka · Laëtitia Zavattoni · Orla Sheils · John O'Leary · Robert Burger · Jens Ducrée

Received: 13 February 2012 / Accepted: 14 May 2012

Published online: 08 July 2012

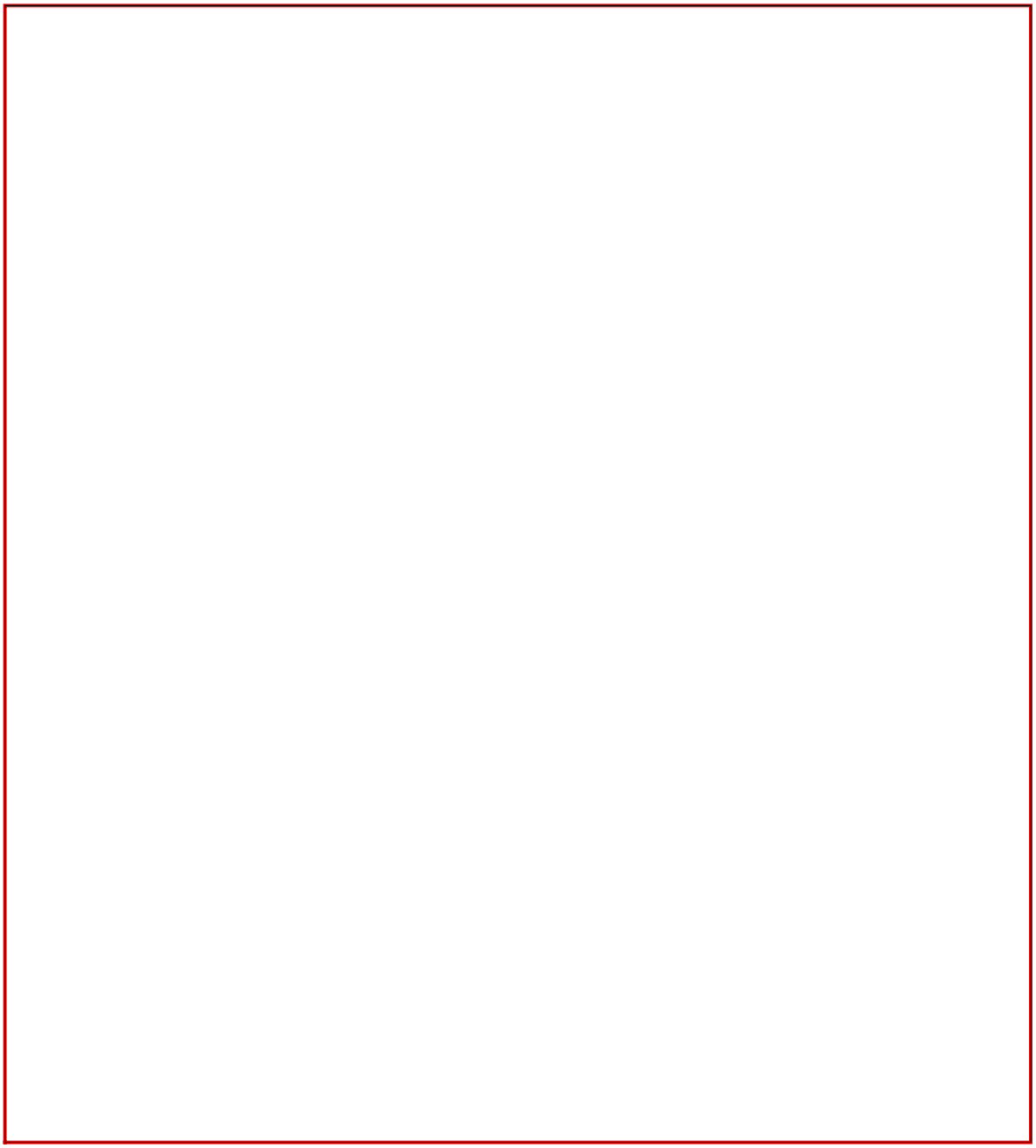

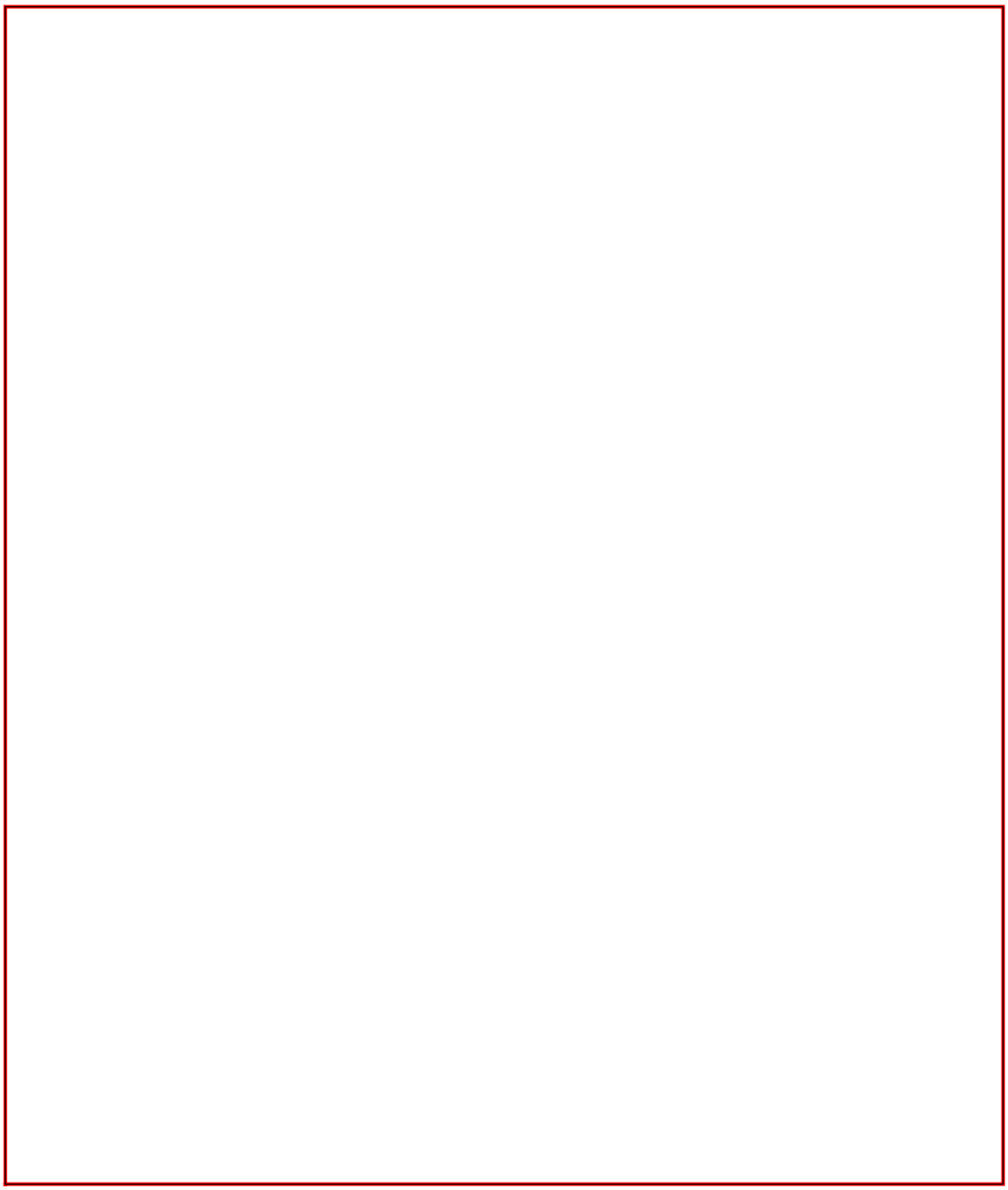

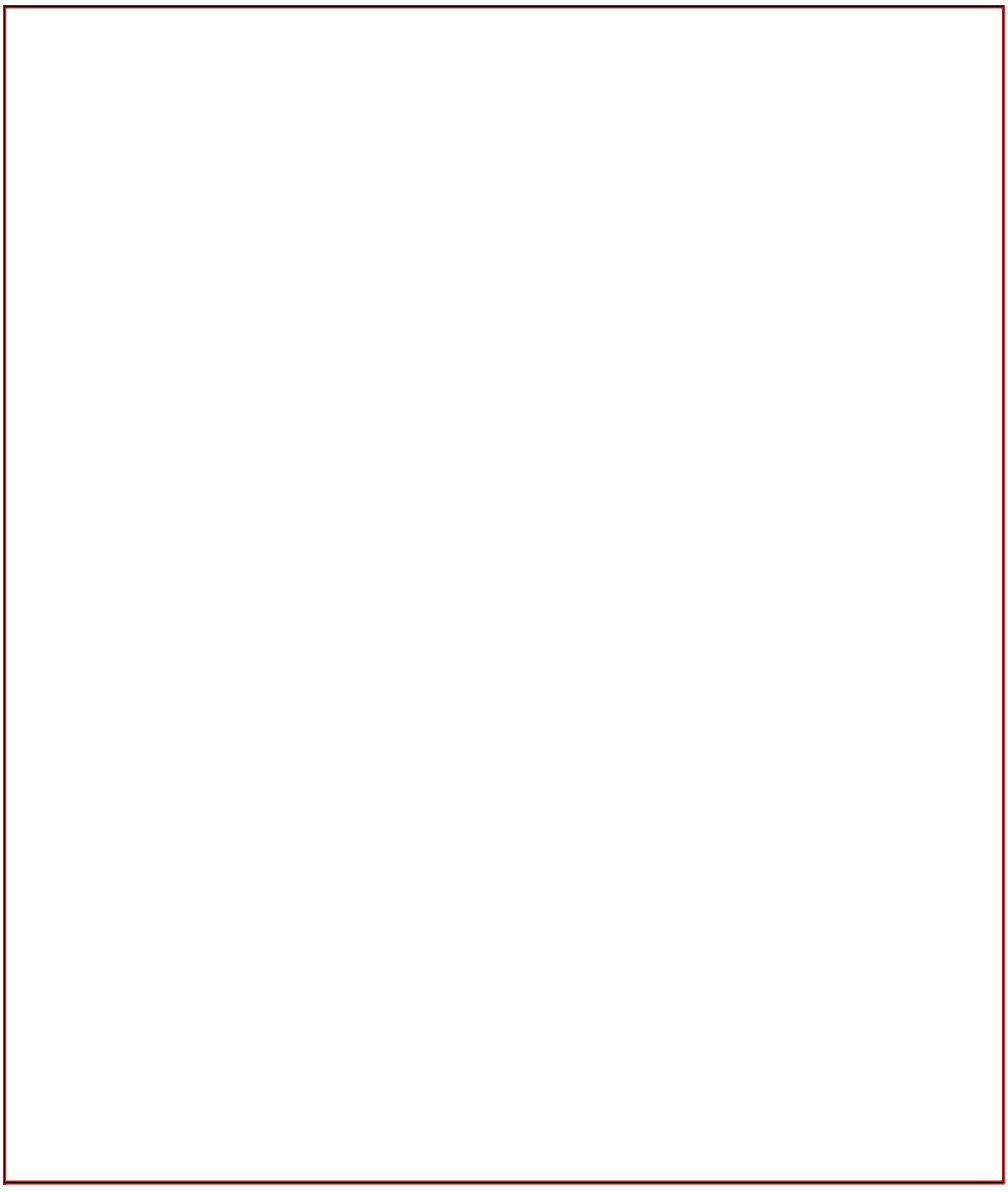

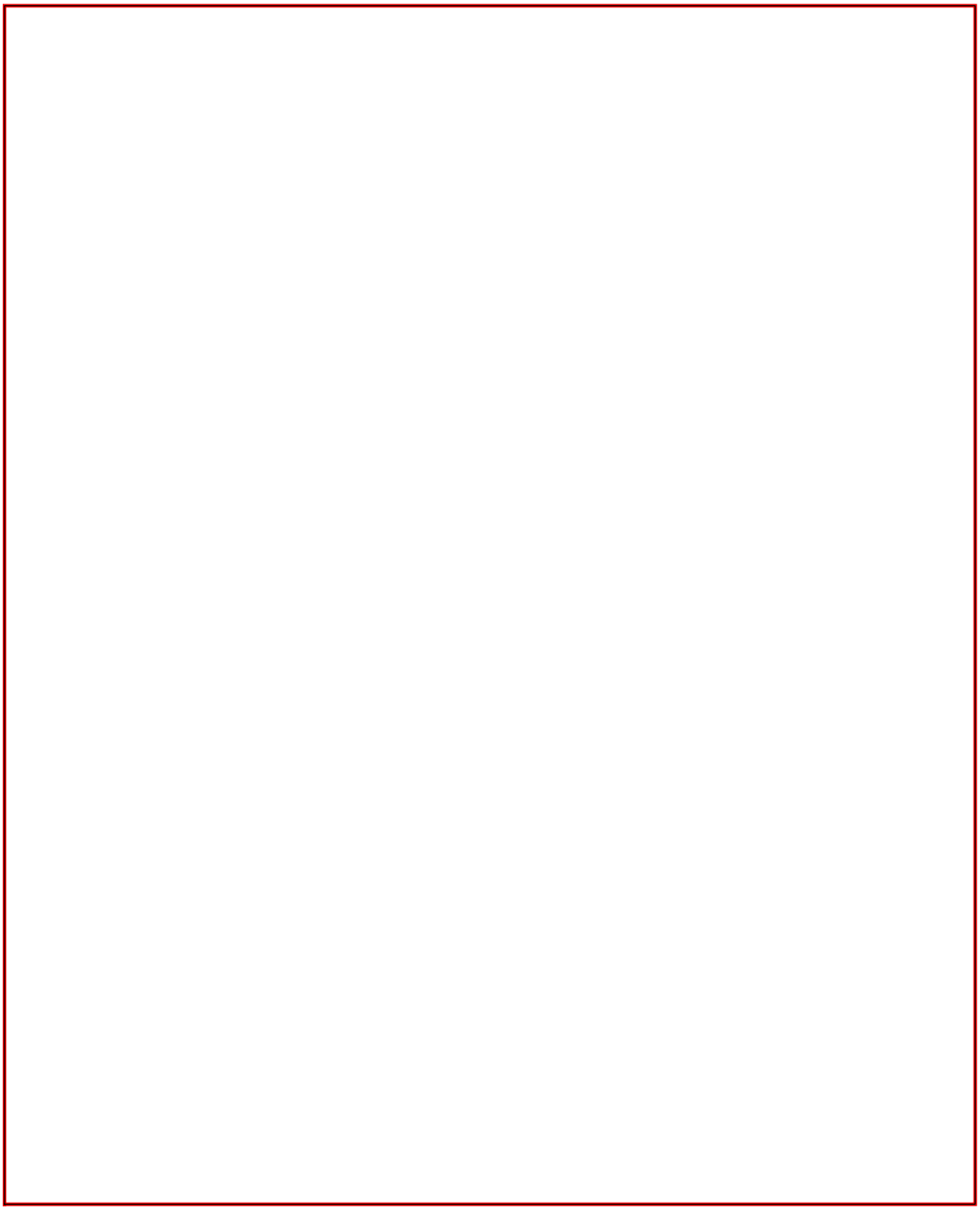

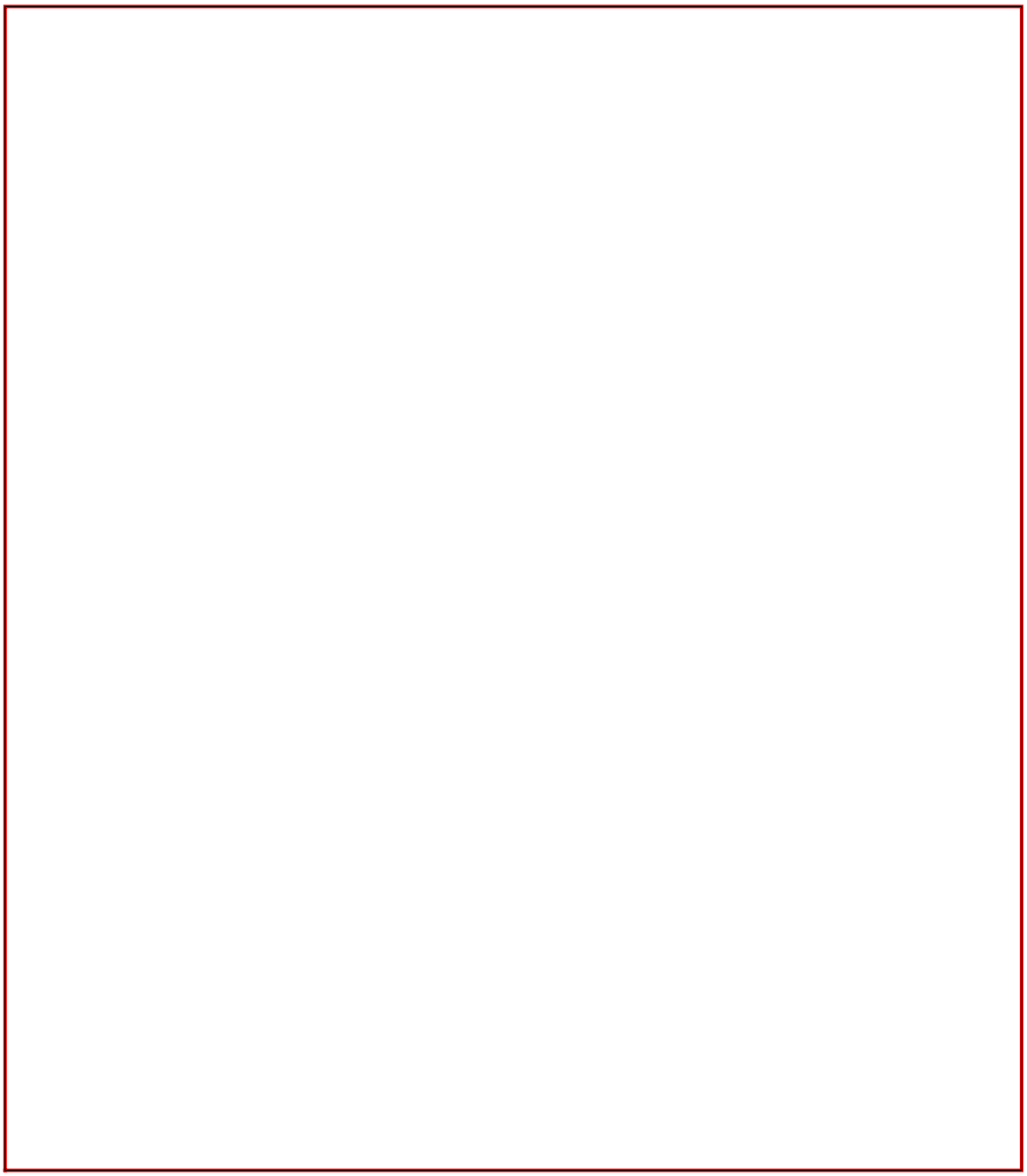

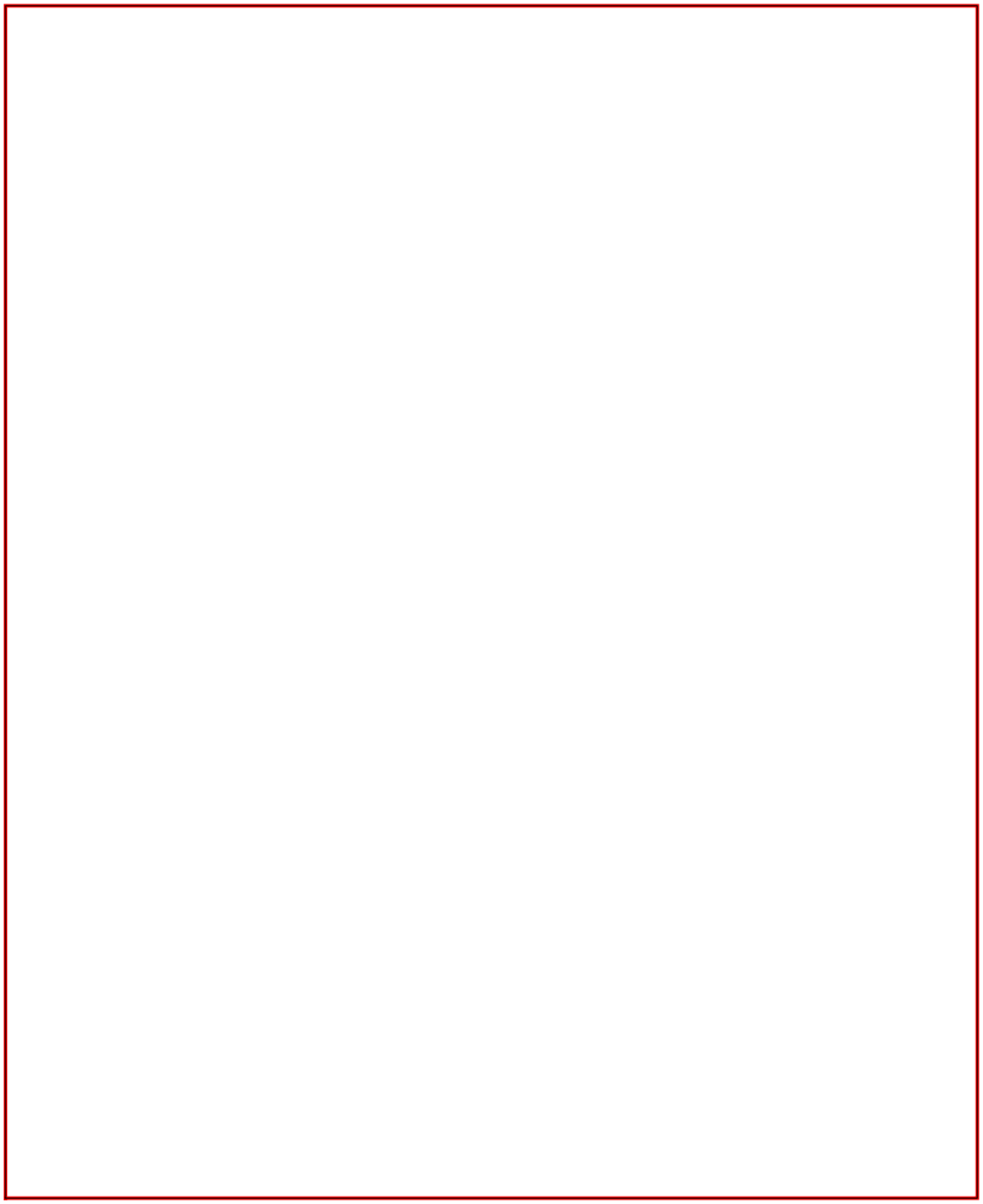

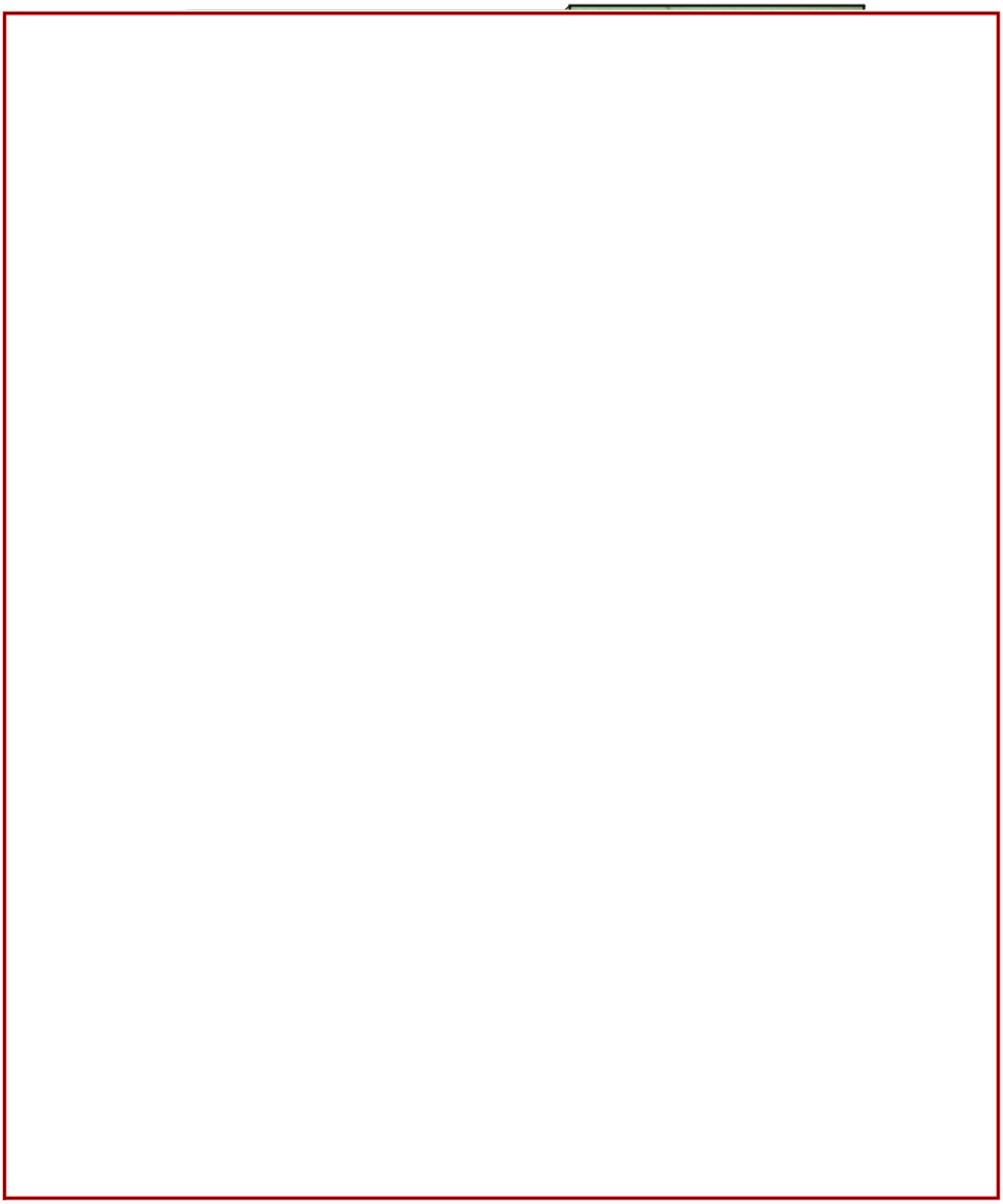

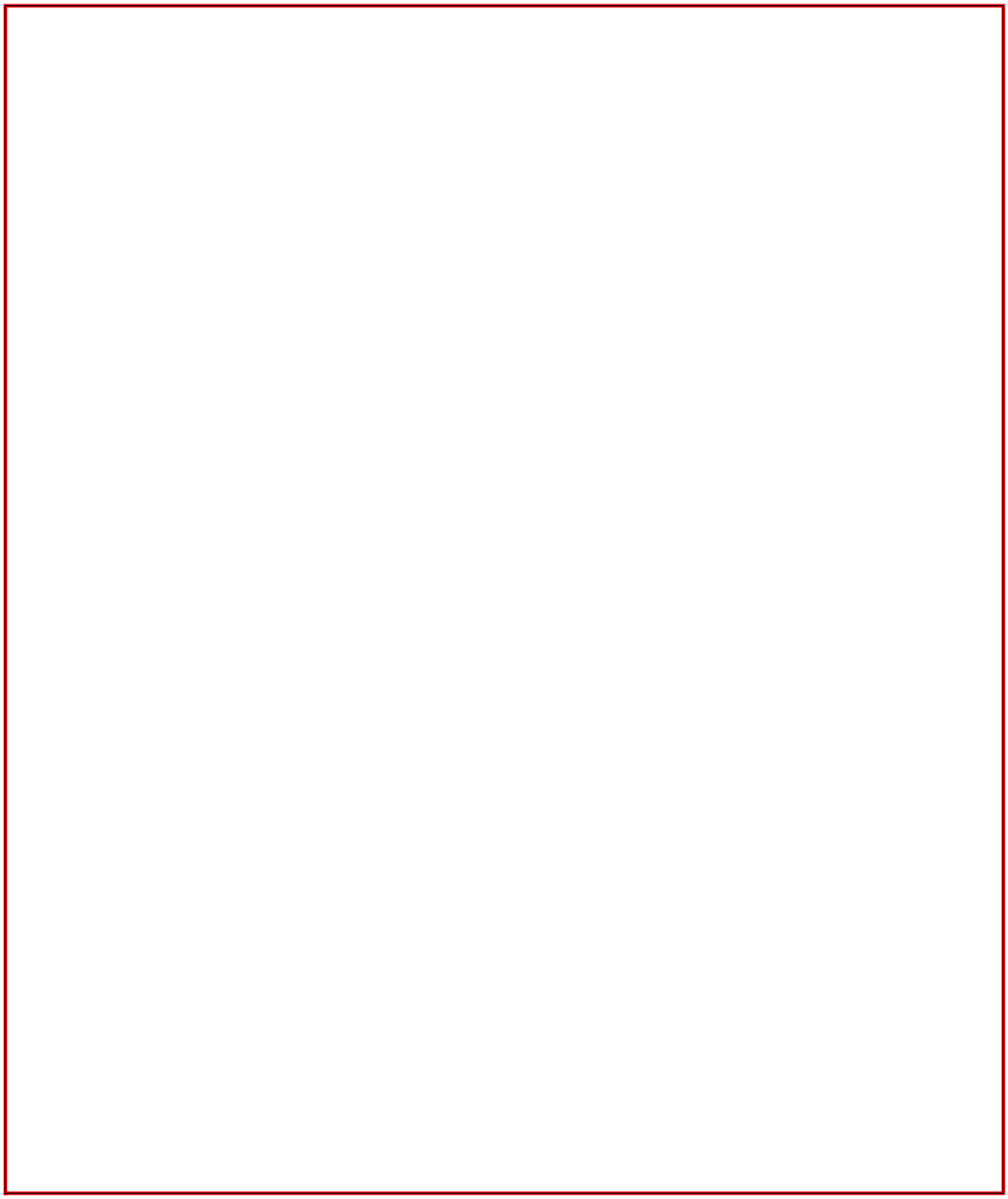

C.2 Comprehensive Integration of Homogeneous Bioassays via Centrifugo-Pneumatic Cascading

This manuscript has been re-submitted to Lab on a Chip and is currently under review

Lab on a Chip

Dynamic Article Links ►

Cite this: DOI: 10.1039/c0xx00000x

www.rsc.org/loc

PAPER

Comprehensive Integration of Homogeneous Bioassays via Centrifugo-Pneumatic Cascading†

Neus Godino♣, Robert Gorkin III, Ana V. Linares, Robert Burger, and Jens Ducrée*

Received (in XXX, XXX) Xth XXXXXXXXX 20XX, Accepted Xth XXXXXXXXX 20XX

DOI: 10.1039/b000000x

This work for the first time presents the full integration and automation concept for a range of bioassays leveraged by a centrifugo-pneumatic valving scheme. After sample and reagent loading, a high level of flow control and synchronization is achieved during the sequential movement of several liquids through shared channel segments for multi-step sample preparation into the detection zone. This novel, centrifugo-pneumatic cascading significantly simplifies system manufacture by obviating the need for complex surface functionalization procedures or hybrid materials integration as it is common in conventional valving methods like siphoning, capillary burst valves, or sacrificial valves. Based on the centrifugo-pneumatic valving scheme, this work presents a toolkit of operational elements implementing liquid loading/transfer, metering, mixing and sedimentation in a microstructured polymer disc. As a proof of concept for the broad class of homogeneous bioassays, the full integration and automation of a colorimetric nitrate/nitrite test for the detection of clinically relevant nitric oxide (NO) in whole blood is implemented. 40 µL of plasma is extracted from a 100-µL sample of human blood, incubated for one hour with the enzymatic mixture (60 µL), and finally reacted with 100 µL of colorimetric (Greiss) reagents. Following single loading phase at the beginning of the process, all of these steps are automated through the centrifugo-pneumatic cascade. Our system shows good correlation with controls up to 50 µM of nitrate, which well covers the healthy human range (4 µM to 45.3 µM).

Introduction

Since their inception in the 1990s, centrifugal microfluidic platforms have been developed in numerous academic and corporate groups[1, 2]. By now, a comprehensive set of laboratory unit operations (LUOs) such as metering, mixing, diluting, reagent storage, and cell lysis has been created and exploited for integrating assay protocols and detection.

Recently pneumatically assisted pumping was shown to overcome limitations in centrifugal microfluidics by allowing manipulation of fluids back towards the disc centre[3, 4]. This ability to pump fluids inverse to the direction of the centrifugal field while additionally providing a new valving mechanism optimizes the use of real estate on a disc which is typically scarce for highly integrated processing[2]. The technique is based on transient compression and relaxation of an air volume actuated by rotation. Specifically, liquids are initially driven into designated pneumatic chambers which trap the air. The air is then compressed through further high-speed centrifugation. By consecutively lowering spin speeds, the centrifugally induced hydrostatic pressure reduces to relax the air volume to its original state. If the chamber is designed appropriately, the expansion of the air will drive the liquids through conduits back towards the center of rotation. The radially inbound fluid movement can even occur in the presence of a reversely directed centrifugal field which points towards the edge of the disc[3].

While various methods exist to create such counter-centrifugal flows, the pneumatic method ranks amongst the least demanding in terms of design, fabrication, actuation and instrumentation. For example, the use of pneumatic pumping avoids the need for hydrophilic surface modification to generate inbound capillary flows towards the center of the disc. Traditionally, hydrophilic treatments[5, 6] and materials[7] are necessary to enable capillary action as many plastics used for centrifugal microfluidic devices are innately hydrophobic[8]. Often hydrophilic modifications introduce inherent difficulties regarding fabrication and assembly as well as long-term stability; hydrophilization induced by plasma treatment fades over time, causing reduced and irreproducible wicking behaviour; and hydrophilic coating steps add to the cost and complexity of device manufacture and assembly.

Also new, active pneumatic pumping methods have been developed around the original concept. Variations on the theme include the application of pressurized air[9] to disc ports or on-disc pressure generation through thermal energy[10] and electrolytic gas production[11]. By providing external energy to the system, fluids can be driven more vigorously; however, these techniques come with the drawback of requiring add-ons components, e.g. compressed air, peripheral heating and electrical power. These add-ons notably raise the complexity of the conceptually very simple centrifugal instrumentation composed of a spindle motor and a readout unit. Furthermore, the use of such equipment alludes to known issues when interfacing with the rotating platform, e.g. contamination prone, open fluid interfaces, and, for

the electrolytic method, embedding (metal) electrode layers in the device itself. On the other hand, our here presented, purely pneumatic system is completely self-contained without physical fluid or electrical interfaces to the instrument.

In terms of liquid handling operations, pneumatically assisted pumping has been utilized for reciprocal fluid flows[4], volume aliquoting[12] and for priming of siphon valves[3] on a disc. However, these previous LUOs were designed to function in an isolated, stand-alone fashion, i.e. centripetal pumping[3] and mixing[4] without connecting them with downstream elements. The centrifugo-pneumatic cascade presented in this work is based on the same pneumatic principles while additionally allowing the integration of a fully automated, multi-step assay which is key for many applications. Lately, Noroozi *et al.*[13] also created a simple

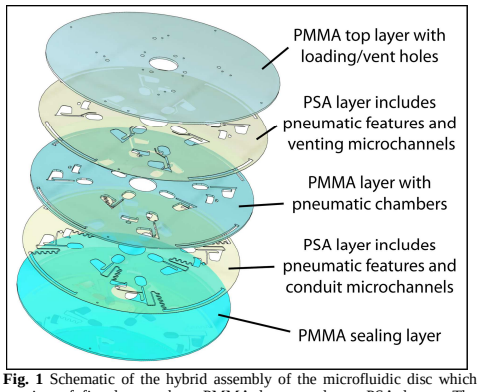

Fig. 1 Schematic of the hybrid assembly of the microfluidic disc which consists of five layers: three PMMA layers and two PSA layers. The chambers are defined in the central PMMA substrate and the two adjacent PSA layers. The first layer of PSA also contains the venting microchannel to allow part of the air to escape when the liquid is pushed to the pneumatic chamber. The second layer of PSA contains the siphon microchannel to concatenate the different pneumatic chambers.

tool for advanced microarray studies. In their system, immunoassay reagents were introduced to a pneumatic chamber coupled to an area functionalized with a microarray. Modulating the speed of rotation initiated pneumatic pumping which drove the reciprocal flow. By repeatedly passing liquid samples over the target surface, volume usage was reduced and efficient analyte capture and washing enabled rapid processing. An adjoining conduit to the chamber acted as a siphon which allowed for removal of liquids from the array after each assay step. In general, while manual introduction of each assay reagent was necessary, the fluidic structures showed the ability to process the material and temporarily restrict and release (valve) fluids.

This report introduces a network of functional structures based on centrifugo-pneumatic actuation that improves liquid loading / transfer, metering, mixing and sedimentation on a polymer disc. The main objective is to develop a pneumatically actuated microfluidic tool kit able to carry out the most fundamental liquid handling processes necessary for the a great variety of applications. For instance, the present colorimetric application concatenates a sequence of LUOs such as plasma extraction, reagent storage, mixing and incubation. In addition, due to the implementation of flow control without the need for local or global hydrophilic / hydrophobic coatings, microscale constrictions or sacrificial valves, the pneumatic cascade significantly reduces the complexity of manufacture and operation. Including pneumatic valving[3], the novel cascade designs use such valves for serial and sequential release of reagents without the need for hybrid embedding / actuating of gating materials (e.g., PDMS restrictions)[14], sacrificial materials such as wax[15] or the use of external instrumentation other than the spindle motor itself. Therefore, pneumatic valving allows for a direct transfer from the prototype stage to production techniques, such as hot embossing or injection moulding.

As a proof-of-concept application of centrifugo-pneumatic cascading, a ready-to-use colorimetric assay kit for the indirect detection of nitric oxide (NO) in whole blood was fully integrated and automated. Nitric oxide is a fundamental biomarker related with several biological processes such as neurotransmission, tumour cell killing, immunity and inflammatory processes[16-18]. It constitutes a highly relevant parameter for fields such as neuroscience, physiology or immunology.

Experimental methods

Disc fabrication

Standard CAD software was used for the microfluidic design of the centrifugo-pneumatic cascade. The multi-layer polymer substrates featuring the 120-mm diameter disc format akin to a conventional CD (Fig. 1) were manufactured by the following prototyping techniques: Initially, a CO_2 laser ablation system (Zing 16 Laser, Epilog, USA) machines the large chambers in 1.5-mm thick poly(methylmethacrylate) (PMMA) (Radionics, Ireland) discs. Then a standard knife plotter (ROBO Pro cutter/plotter, Graphtec, USA) cuts the microfluidic channels in 86-µm thick pressure sensitive adhesive layers (PSA, Adhesive Research, Ireland). Utilizing established polymer lamination techniques, the PMMA and PSA layers were consecutively stacked and press assembled to create the final device. Figure 1 depicts the hybrid, five-layer assembly composed of three PMMA discs and two interspersed PSA layers. However, it is important to mention that the pneumatic chambers only extend across the three central layers while the connecting microchannels are merely patterned in the PSA film.

Assay and reagents

Direct determination of nitric oxide is difficult due to its short lifetime, so it has to be detected indirectly by the measurement of end products like nitrate (NO_3^-) and nitrite (NO_2^-)[19, 20]. Colorimetric methods have been used for detection of nitric oxide levels in biosamples such as urine, culture media or even plasma[20, 21]. In this work, we integrate nitrate/nitrite colorimetric detection by following the protocol and using the reagents of a commercial kit (Nitrate/Nitirite Colorimetric Assay kit from Sigma Aldrich). This kit contains $NaNO_2$ stock solution ([NO_2^-] = 0.1 mM), KNO_3 stock solution ([NO_3^-] = 0.1 mM), Phospate Buffer Solution (50 mM, pH 7.5), Nitrate Reductase (lyophilized), Nitrate Reductase cofactor (lyophilized),

colorimetric dye solution A (Greiss Reagent A) and colorimetric dye solution B (Greiss Reagent B).

All chemical were used as purchased without further modification. For the calibration experiments shown in this work we used dilutions of food colouring ink (Goodall's, Ireland) in DI water. The red, 20-µm polystyrene (PS) beads were purchased from Microparticles (Germany). Human blood samples were collected from a healthy volunteer into BD Vacutainer K3EDTA tubes (BD, USA). The blood was used within 24 hours after the extraction.

Instrumental set-up

Experiments were performed on a custom made centrifugal test stand using a computer controlled motor (Faulhaber Minimotor SA, Switzerland) to spin the discs[22]. High-resolution imaging, even during fast rotation, was achieved by a sensitive camera with short exposure time (Sensicam qe, PCO, Germany) and mounted on a motorized, 12x zoom lens (Navitar, USA).

For the colorimetric measurements, we used the Nanodrop 2000c spectrophotometer from Thermo Fisher Scientific (Thermo Fisher Scientific Inc., USA).

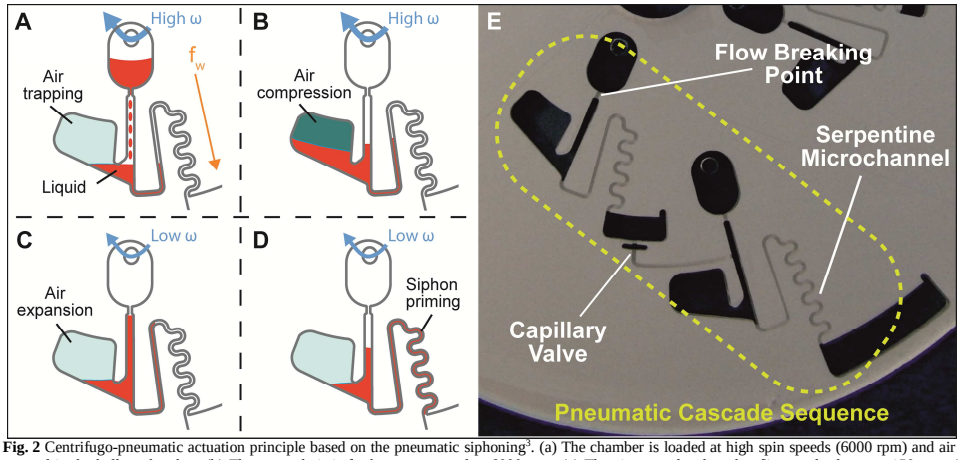

Fig. 2 Centrifugo-pneumatic actuation principle based on the pneumatic siphoning[3]. (a) The chamber is loaded at high spin speeds (6000 rpm) and air is trapped in the ballast chamber. (b) The trapped air is further compressed at 6000 rpm. (c) The air expands when the s[in speed relaxes to 150 rpm. (d) Siphon priming. (e) Sequence of centrifugo-pneumatic cascading elements on a disc. Several microfluidic features (flow breaking point, capillary valve and serpentine channel) playing a pivotal role in the sequence are highlighted.

Results and discussion

This section is divided in two main parts. The first part is an introduction to the advanced pneumatic functionality, where the concepts of siphoning and centrifugo-pneumatic cascading as well as the pneumatic tool kit are described. The second section covers the integration and automation of a standard colorimetric assay for nitrate/nitrite detection in whole blood.

Centrifugo-pneumatically triggered siphon valving

Valving mechanisms are key in microfluidics, in particular in centrifugal "lab-on-a-disc" systems where all on-board liquids are subject to the same, rotationally induced driving force. There are operations requiring valves that yield towards high frequencies of rotation, e.g. for synchronizing parallel flows on the same system. Common examples are hydrophobic constrictions or hydrophilic expansions which are also termed capillary burst valves. Other LUOs require valves to be able to sustain high centrifugal pressures, e.g. for controlling the release of plasma following a high-speed centrifugal sedimentation process.

The most common variant of these "low-pass" valves in centrifugal microfluidics are siphons. In such siphons, a conduit connects an upstream chamber with a receiving chamber that is located more radially outward. The siphon features a crest point above the maximum liquid level in the upstream chamber. Once the meniscus in the wound siphon channel has advanced past the crest point and then below the liquid level in the upstream chamber, the liquid is "pulled" by the centrifugal field through the siphon into the downstream chamber. Siphon flow ceases when the upstream chamber is emptied and / or the integrity of the force-transmitting liquid column in the siphon is disrupted[5, 6, 23].

There are two main mechanisms to prime the siphon, i.e. to fill the siphon channel beyond its crest point. The first "overflow" mechanism employs the principle of interconnected tanks by adding volume to the upstream chamber until its liquid level surpasses the crest point. The second, more commonly used principle in "lab-on-a-disc" systems relies on the interplay between centrifugal and capillary force in a hydrophilic siphoning channel. Only at low frequencies of rotation, the capillary pressure supersedes the centrifugal force so the liquid meniscus can protrude past the crest point of the siphon.

However, as common polymers are rather hydrophobic, hydrophilization is then either induced (transiently) by plasma treatment or for the longer term using coating. Both hydrophilization techniques increase the number of fabrication steps and thus the complexity of device manufacture. The here

used pneumatic siphoning structure is composed of three interconnected vessels: the inlet channel, the outlet siphon channel and a compression chamber (Fig. 2). This chamber is sealed by the liquid itself to entrap air ballast (Fig. 2a) which is compressed according to the centrifugally induced hydrostatic pressure. The liquid needs to be loaded at very high frequency (and rotational acceleration) for various reasons: to trap and then compress as much air as much as possible within the ballast compartment; to achieve a fast hydrostatic equilibrium between the liquid in the pneumatic chamber and the liquid in the siphoning channel; and to suppress the priming of the siphon during loading. In hydrostatic equilibrium at a given frequency of rotation, the (radial height of the) liquid levels in the inlet and siphon channel are equal and positioned below the crest point of the siphon. Due to the centrifugally induced pressurization, the level in the gas ballast chamber remains lower (Fig. 2b). After reducing the spinning rate, the entrapped gas expands (Fig. 2c), thus acting as a pressure-controlled pump powered by the (hydrostatic) energy

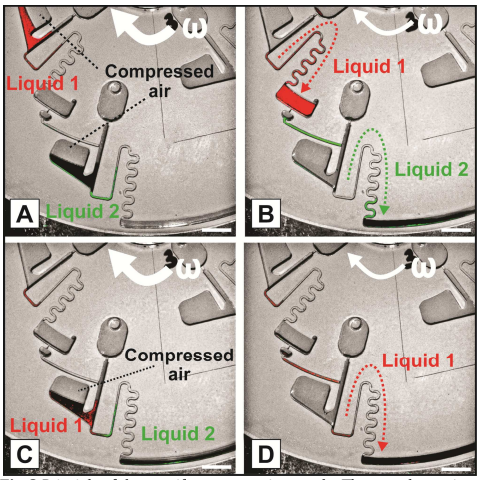

Fig. 3 Principle of the centrifugo-pneumatic cascade. The cascade consists on the concatenation of pneumatic structures based on the pneumatic siphoning mechanism[3]. Two liquids (50 µL of red and green diluted inks, respectively) are moved simultaneously in the downstream direction. a) Air trapped in both chambers (6000 rpm). (b) Expansion of air (150 rpm) and emptying of both chambers. (c) Loading the second structure in the cascade with the first liquid (6000 rpm). (d) Re-expansion of the air (150 rpm) and mixing of both liquids in the last chamber. Scale bars: 5 mm

stored in the pressure chamber during high-speed rotation. Hence, liquid is pushed out from the ballast chamber into the inlet and siphon channels where the meniscus is lifted beyond the crest point of the siphon (Fig. 2d). This siphoning mechanism therefore represents a merely rotationally actuated valve yielding towards low frequencies of rotation. An analytical description of the pneumatic siphoning is found in the ESI.

Compared to the above described, overflow-primed siphon, no liquid volume needs to be added to prime the siphon. In contrast to the hydrophilic variant common in microfluidics, no (hydrophilic) surface treatment of the siphon channel which tends to be unstable over time[5], is required. Notably, the siphon channel may be reused - a feature we will deliberately exploit later in this paper to realize a multi-step bioassay with the pneumatic cascade.

Centrifugo-pneumatic cascade

Our disc-based cascade which will eventually implement the full process integration and automation of bioanalytical assays consists of a series of radially aligned, centrifugo-pneumatic valving elements[3]. In order to coordinate the proper fluid communication between the succeeding liquid-handling elements, several microfluidic features have been implemented.

In Figure 2e, each of the two ballast chambers is valved by a pneumatic siphon. This way, each liquid volume introduced in its inlets will partially occupy the ballast chamber until the frequency is reduced to trigger the siphon. In order to avoid that the liquid passes through the siphoning channel during the loading phase, a cut-off element for the flow is placed between the loading chamber and the subsequent radial channel.

This break-off point gives high flexibility in the design of the siphoning channel as the continuity between the liquid in the loading chamber and the liquid residing in the pneumatic chamber is disrupted. The serpentine shape of the channel after the crest point of the siphon raises the resistance of the channel and consequently throttles the speed of flow. This way the flow does not possess sufficient momentum to immediately open the burst valve which transiently seals the intermediate chamber[24, 25]. This interposed chamber is necessary as at the high frequencies necessary to properly prime the subsequent element of the cascade tend to disrupt the liquid column in the siphon, leaving a sizeable fraction of the volume behind. So the optimum way to reliably transfer a volume between pneumatic modules is to fill an intermediate, “buffer” chamber at moderate frequencies and then accelerate the rotation to swiftly burst the capillary valves and fill the subsequent structure.

Liquid handling

We have supplemented the portfolio around the basic centrifugo-pneumatically triggered siphon with common LUOs such as a particle retention chamber for plasma extraction from whole blood, an overflow restriction to enable metering and a mixer. The idea is to have a pneumatic tool-kit based on which, by configuring a set of basic components, we are able to tailor the sequence of LUOs in order to process integrate and automate a broad range of bioassays on a disc. The ESI contains a table (Table 1) with the fundamental geometrical and operation parameters regarding of LUOs presented below.

Synchronous transfer of liquid aliquots

Sequential or parallelized handling several reagents is a common requirement for the integration of bioassays on microfluidic platforms[1, 26]. We now focus on a general case of transferring two different liquids simultaneously. However, the design can be modified for handling an even higher number of liquids in parallel.

Figure 3 demonstrates the potential for concurrent liquid handling in the same fluidic pathway which represents a unique, core principle of the pneumatic cascade. The sequence establishes the simultaneous control of two liquids along the cascade (50 µL of red diluted ink and 50 µL green diluted ink). All liquids (i.e., representatives of sample and reagents) are loaded into the main inlet chambers before the spin protocol commences (first step). Next, the volumes are moved from the loading chamber to the main pneumatic chamber at a very high frequency of rotation (6000 rpm). Both liquids pressurize the air trapped at the respective ballast compartments until the spin speed is reduced to 150 rpm (Fig. 3a).

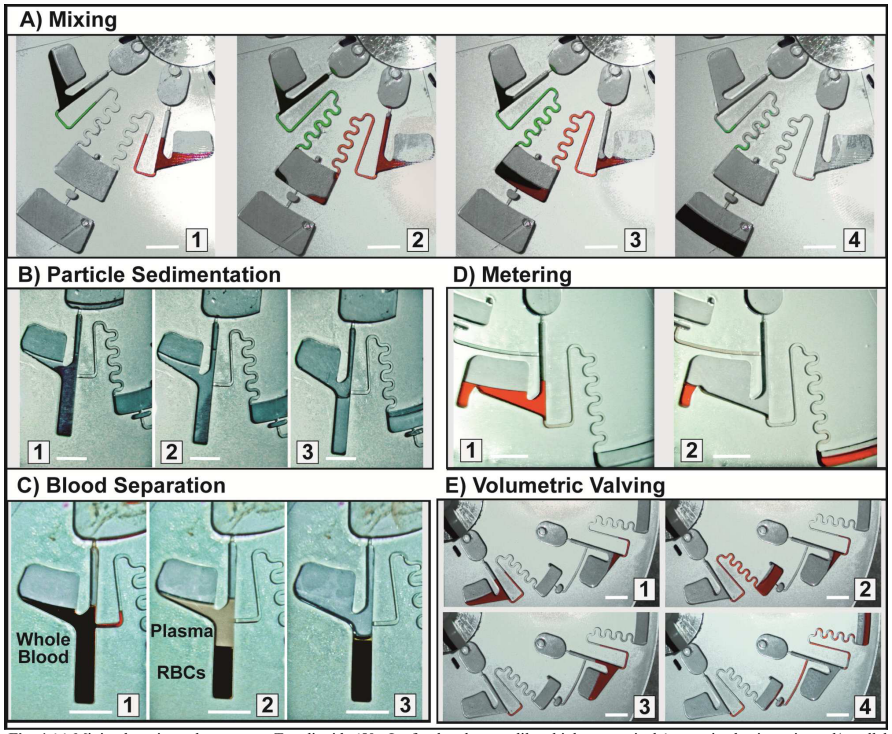

Fig. 4 (a) Mixing by mirrored structures. Two liquids (50 µL of red and green diluted ink, respectively) are mixed using mirrored/parallel structures. (1) Trapping of air in both chambers (6000 rpm). (2) Expansion of air (150 rpm) pushing the liquids towards the mixing chamber (3) While maintaining a low frequency of rotation, the pneumatic chambers are emptied and the liquids moved to the mixing chamber. (4) After oscillating between higher and lower frequencies, the capillary valve bursts and the mixed solution proceeds towards the final chamber. (b) Particle sedimentation. (1) 100 µL of 20-µm PS red particles in DI water is loaded and pushed to the pneumatic chamber at 6000 rpm. (2) Due to the high frequency of rotation, air is trapped and compressed at the pneumatic ballast while also the particles (with higher density than DI water) are pushed toward the bottom of the sieve where they form a pellet. (3) The frequency of rotation is reduced to 150 rpm and part of the liquid is moved to the subsequent chamber without affecting the integrity of the particle pellet. (c) Blood separation. (1) 100 µL of blood is loaded and moved to the pneumatic chamber at 6000 rpm. (2) Due to the high frequency of rotation, the air is trapped and compressed in the pneumatic ballast chamber at the same time as the denser blood cells are pushed down to the bottom of the sieve. (3) Once the frequency is relaxed to 450 rpm, purified plasma (liquid phase) is moved to the following chamber and the red blood cell pellet remains trapped at the sieve. (d) Pneumatic metering. (1) 50 µL of diluted red ink is loaded at 6000 rpm. The excess volume is recovered in a waste chamber (2) Once the frequency is lowered to 150 rpm, the volume remains within the overspill chamber without further affecting the pneumatic actuation. (e) Volumetric valving. (1) 50 µL and 10 µL of diluted red ink are loaded into the two different pneumatic chambers in the cascade at 6000 rpm. (2) The spinning is slowed to 150 rpm and only the 50-µL volume is moved to the following chamber as in the second pneumatic chamber the volume is not sufficient to trap and compress air. (3) Ramping the frequency again up to 6000 rpm, the volume in is moved from the central chamber to the second pneumatic chamber, where some air is trapped and compressed in the ballast chamber. (4) Once the frequency reaches 150 rpm, the whole volume is pushed to the following chamber due to the air expansion in the pneumatic ballast. Scale bars: 5 mm

At this point both volumes are pushed through the siphons into the downstream chambers (Fig. 3b). While staying this low frequency regime, both pneumatic chambers are completely emptied. The red ink (first liquid) is intermittently retained in the midway chamber by a capillary valve to allow the full discharge of the upstream chamber at roughly 450 rpm. Afterwards, the compress/release cycle is repeated in order to still move the red ink to the compression chamber where the second liquid (green ink) already resides. Figure 3c shows how at subsequent, high-frequency rotations the liquid pressurizes the air compression ballast. Finally, after decreasing the frequency of rotation back to 150 rpm, the second siphon valve yields (again) and both liquids are mixed in the outermost chamber (Fig. 3d).

As it is possible to distinguish in Figure 3b-d there is a tiny residual volume in the structure, mainly in the microchannel communicating the different structures. In the pneumatic cascade shown in Figure 3, the total residual volume amounts to about 1.2 µL of an initial loading volume of 50 µL, hence less than 2.5%.

The capability to simultaneously control separately introduced liquid volumes provided in the initial loading step is highly relevant to the vast majority of real-world applications. This is because sample preparation and detection typically involve the handling of several liquid aliquots in parallel. Using centrifugo-pneumatic actuation, we have shown for the first time that several volumes can even be introduced at different stages of the cascade, and then (partially) share the same fluidic pathway. This would be impossible for capillary-action controlled centrifugal microfluidic systems where wetted surfaces cannot be reused after they have been primed[5, 6]. For instance, when using hydrophilic functionalization of the siphon, once the transfer channel has been wetted, it cannot be re-used for opening the same siphon for another, subsequently introduced liquid. However, using centrifugo-pneumatic actuation for which the pneumatic energy remains stored in the compression/expansion of air in the ballast compartment, the following siphon valve can be used recurrently.

Mixing by mirrored structures

Mixing of two or more reagents is a fundamental process in most bioassays. In the micro-scale, the flow is laminar due to the low Reynolds numbers, so mixing by turbulence effects is hardly achievable[1, 26]. However, this drawback is easily overcome using centrifugal platforms where different approaches can be implemented, e.g. by using the Coriolis force[1] or by rapid oscillations of the disc (either clockwise and counter-clockwise, or by alternating between two different spin speed values in a "macroscopic" chamber)[2, 27].

In our case, we use this second approach (rapid oscillations of the disc), and the pneumatic actuation is used to hold the two liquids in previously to the mixing step in mirrored structures to perform the mixing at a precise desired moment. For that purpose, two mirrored pneumatic structures are placed at the same radial position on the disc to parallelize the liquid transfer to the mixing chamber (Fig. 4a). The two liquids (red and green diluted ink), 50 µL each, are pipetted into the loading chambers and expelled to the bottom of the pneumatic chamber at rapid spinning (6000 rpm) to simultaneously trap and compress the air residing in the ballast chamber (Fig. 4a-1). When the speed of rotation is slowed to 150 rpm, the air expansion in each chamber pushes both liquids radially inwards, thus opening the two siphon valves (Fig. 4a-2). The liquids proceed towards the mixing chamber where they are retained by a capillary valve confining the exit of the chamber. During the initial, slow filling of this chamber, the liquid is still inhomogeneous (Fig. 4a-3). Advective mixing is then induced by ramping between two different frequencies of revolution while staying below the threshold frequency that breaks the capillary valve. Finally, the spin speed is elevated to break the capillary valve and issue the mixed solution into the outer chamber (Fig. 4a-4).

It is important to highlight at this point that mixing using mirrored structures demonstrates that the pneumatic valving principle works independently of the position of the air-compression ballast and independent of the sense of rotation. Working with mirrored structures introduces the option of parallel liquid handling, and not just sequential operation as shown in Figure 3.

Particle sedimentation

Particle sedimentation, i.e. the density-based separation of particles suspended in a liquid matrix, constitutes a fundamental process in sample preparation, e.g. for plasma extraction from whole blood as an initial step of many clinical assays. Centrifugal microfluidic platforms lend themselves particularly well to fast particle sedimentation[1, 2]. Various groups have already successfully demonstrated a spectrum of plasma extraction schemes[15, 28-31].

To enable centrifugally induced particle separation, we supplement the fundamental pneumatic module (Fig. 2) by another chamber designated to receive the cellular pellet (Fig. 4b/c). The arrangement does not interfere with the previous pneumatic siphoning mechanism. In the experiment portrayed in Figure 4b, red, 20-µm PS beads suspended in 100 µL of DI water are loaded to the inlet port. Figure 4c shows the same mechanism but now with the aim of red blood cell separation to form a pellet in the sieve.

For that purpose, 100 µL of blood is loaded at a high frequency of rotation (6000 rpm). The same, 6000-rpm spin speed interval imposed for the proper filling of the siphoning structure pellets the cells (Fig. 4c-1). After several minutes, the entire solid phase is retained in the sedimentation chamber (Fig. 4c-2). Once the centrifugal pressure relaxes at 450 rpm, the plasma residing above the siphon outlet is extracted (Fig. 4c-3). As the sequences in Fig. 4b/c demonstrate, adding the sedimentation compartment does neither impair the pneumatic actuation nor does it compromise the trapping of air when compressing at high speed or the expansion of air when lowering the spin speed. The volume capacity of the sedimentation chamber must be sufficient to take up the whole solid phase. Also, the sedimentation chamber must exhibit a minimum length so the integrity of the pellet is not affected by the subsequent pneumatic pumping phase.

Metering

Accurate metering is pivotal for assay precision, flow control and quantification[1]. On centrifugal platforms, it is normally achieved by an overflow at the top of a geometrically well-defined chamber into a waste[2,21]. In this section, we show the adaptions of

the main pneumatic chamber in order to implement a simultaneous metering step (Fig. 4d). The excess volume is diverted to an overflow (small waste chamber on the left) during the air compression (Fig. 4d-1) where it remains during the extraction of the particle-free phase (Fig. 4d-2). By virtue of the centrifugo-pneumatic valving principle, the left overflow chamber will always be filled after metering as the meniscus rises at initially high frequencies always above the crest point and lowers as the spin rate is reduced. So, for instance, enlarging the volume of the overflow would not interfere with the effect.

The introduction of the waste chamber for metering purposes does not compromise the pneumatic compress-release cycle. As in the previous cases, this pneumatic metering chamber can be placed at different stages of the pneumatic cascade.

Parallel handling of liquids by volumetric valving

We now want to extend the valving (Fig. 2) to coordinate the transport of separate liquid volumes residing in two subsequent centrifugo-pneumatic siphon structures (Fig. 4e). To this end we make use of the fact that if the volume loaded in the pneumatic chamber stays below a critical level, air in the ballast compartment will not be trapped and compressed. Hence, there will not be any force to push the liquid towards the siphoning channel.

In Figure 4e-1, the first structure is filled at 6000 rpm with a 50-µL volume above the critical liquid level while the subsequent structure is loaded with 10 µL, only. This volume falls short of the volume threshold enabling the entrapment of the air ballast. Once the spin speed is lowered (Fig. 4e-2), the air trapped in the first pneumatic ballast chamber expands and pushes the liquid to the intermediate chamber. However, all liquid is held back in the second pneumatic chamber as, in absence of capillary action in the hydrophobic siphon, there is no other force to move the liquid radially inwards. Next, we ramp the spin speed up back to 6000 rpm (Fig. 4e-3) in order to break the capillary valve and forward the liquid into the outer pneumatic chamber. In this chamber, sufficient volume has now accumulated to enable the centrifugo-pneumatic siphoning mechanism. Finally, after the spin speed is slowed back to 150 rpm (Fig. 4e-4), the entire volume proceeds to the final chamber.

This volumetric valving principle assumes a paramount role for the integration of reagent storage and release. It can also control incubation times at specific points of the pneumatic cascade. The volumetric valving principle can be understood as a frequency-synchronized mixing of discrete liquid volumes traveling through the same fluidic pathway.

Automation of colorimetric assay

The level of nitric oxide (NO) is commonly determined by the end products of a conversion reaction, i.e. nitrate (NO_3^-) and nitrite (NO_2^-)[20]. There are several commercial kits for the colorimetric detection of nitrate/nitrite for use in standard well plates and detection by absorbance by a plate reader. In this work, we integrate and automate the full range of sample preparation steps, i.e. LUOS, necessary to carry out the colorimetric detection of nitrate/nitrite in blood using the versatility of the centrifuge pneumatic cascade technology.

First, we extract plasma from whole blood. Resident nitrate is converted by nitrate reductase into nitrite. The reaction between nitrite and the Greiss Reagents subsequently changes the colour of the solution from transparent to purple. Following the manufacturer's manual, the sample preparation steps for the nitrate/nitrite detection in blood are:

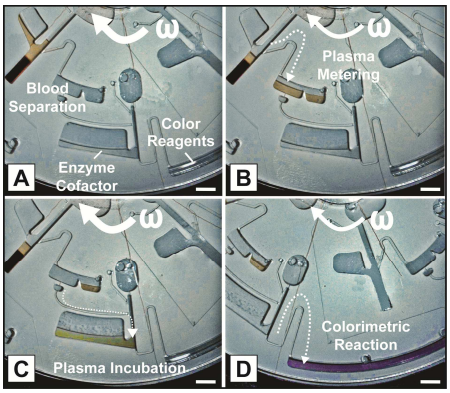

Fig. 5 Sequence of the NO colorimetric detection. (a) Before the starting the frequency protocol, blood and all reagents are loaded. Plasma is separated from red blood cells. (b) Following the protocol, the plasma is metered to 40 µL and incubated with the enzyme. (c) Incubation of plasma with 10 µL of enzyme, 10 µL of cofactor and 40 µL of buffer for 1 hour (following the commercial protocol). (d) Reaction with the colorimetric reagents to obtain a purple color with an intensity depending on the initial concentration of nitrate. Scale bars: 5 mm

1. Blood separation
2. Dilution of 40 µL of plasma in 40 µL of buffer
3. Addition of 10 µL of enzyme (nitrate reductase) cofactor
4. Addition of 10 µL of enzyme (nitrate reductase)
5. Incubation for one hour at room temperature
6. Addition of 50 µL of Greiss Reagent A
7. Addition of 50 µL of Greiss Reagent B
8. Incubation for ten minutes
9. Absorbance measurement at 550 nm

Based on the concept of the centrifugo-pneumatic cascade, we integrate all steps (from 1 to 8) in a polymeric microfluidic disc (Fig. 5). Note that blood sample and reagents are loaded in a single run prior to starting the centrifugal protocol, thus leveraging full sample-to-answer automation of the entire assay. This specific test requires four main sample preparation processes: plasma extraction, subsequent metering, incubation with reagents and reaction. It is important to note that previous tests were carried out with the kit on the lab bench to ensure functionality during early experimentation. Once we verified the use of the commercial kit – we then ran systematic tests with the modified assay in the disc.

Figure 5 displays how these four main steps are cascaded. Initially, whole (patient) blood is separated with the sedimentation structure from Fig. 4c. In the second step, plasma is metered by an overflow structure in the intermediate chamber. In the subsequent chamber, the so defined plasma volume is incubated with reagents using the concept of volumetric valving.

The volume occupied by the enzymatic solution (enzyme, cofactor and buffer) is not sufficient to compress air and lift the liquid high enough beyond the crest point to initiate the siphon valving.

However, after incubation, once the metered plasma is added to the mixture, the volume is sufficiently large to leverage a complete pneumatic cycle and advance to the following chamber. In the most outward positioned reaction chamber the Greiss reagents mix with the sample (see movie in the ESI for whole view of the complete assay).

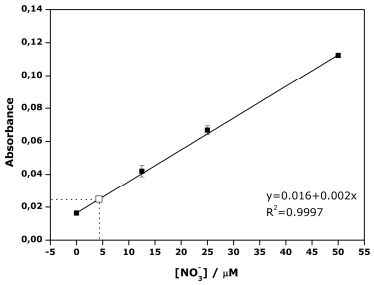

Fig. 6(■) Absorbance values for the calibration points, using the standard reagents in the kit and following the protocol for the calibration curve. The error bar is calculated using the standard deviation of 3 measurements. (—) Linear fit of the calibration points with $R^2 = 0.997$. (□) Absorbance measurement on the real sample. The error bar is calculated using the standard deviation of 3 measurements.

The assay sequence shown in Figure 5 starts with all reagents loaded (with the disc at rest) through their corresponding inlets: 100 µL of blood is loaded in the most inward loading chamber, 10 µL of enzyme plus 10 µL of cofactor and 40 µL of buffer in the second loading chamber, and finally, 50 µL of Greiss Reagent A and 50 µL of Greiss Reagent B at the reaction chamber (most outward position respect to the center of the disc). Setting a high frequency of revolution (6000 rpm), both blood and enzymatic mixture are propelled to their corresponding pneumatic chambers where they are retained to compress air in the ballast chamber (pneumatic actuation). As mentioned in Figure 4c, the sieve must be sufficiently long to retain all the blood cells (dimensions described in Table 1 in ESI). Moreover, to ensure a proper separation, this process needs to run for about 2 minutes.

At the same time, due to the centrifugal force, the red blood cells are pelleted in the sedimentation chamber (Fig. 5a) to enable the plasma separation. Afterwards, the frequency is reduced to 450 rpm and the air expansion pushes the now particle-free liquid phase (plasma) into the subsequent middle chamber (Fig. 5b) where it is metered. This process lasts around 5 minutes at 450 rpm. The chamber volumes are dimensioned to provide the amount of plasma necessary for the detection (40 µL). As expected, the solid fraction of the blood remains in the sedimentation sieve. Also the volume of the enzyme mixture in the incubation chamber is not large enough to break the corresponding siphon valve.

When the frequency elevated to 6000 rpm, the metered plasma (40 µL) moves to the main incubation chamber where it is mixed with the enzymatic solution (10 µL of enzyme, 10 µL of cofactor and 40 µL of buffer) as shown in Figure 5c. Now the extracted plasma is incubated with the enzymatic cofactor buffer for 1 hour. According to the manufacturer's recommendation, this step ensures that all nitrate present in the solution is transformed to nitrite. Finally, at 450 rpm, the mixture is transferred to the detection chamber where the pre-loaded (Greiss) reagents induce purple coloring with an absorbance correlating to the initial concentration of nitrate/nitrite in blood (Fig. 5d).

In this proof-of principle of the fluidically fully integrated and automated bioanalytical assay, we pipette a 2-µL aliquot from the detection chamber to a spectrophotometer to measure the absorbance. Various schemes are known to integrate a detector unit for absorption measurements with the instrument[28, 30, 32-34]. However, we chose to focus this article on the fluidic implementation rather than instrumentation aspects.

For absolute quantification of nitrate/nitrite concentrations in blood, we calibrated with nitrate dilution series (0, 12.5 µM, 25 µM and 50 µM) in buffer using the same, previously described assay structure for whole blood (Fig. 5). The assay protocol is similar to the one for the blood sample, but we injected 100 µL of buffer in the first loading chamber which is subsequently metered to 40 µL. In the second chamber, the enzyme and the cofactor as well as a certain amount of 100-µM nitrate solution is added, depending on the corresponding dilution. The incubation time again amounts to 1 hour. The product is then mixed with the colorimetric reagents (Greiss reagent A and Greiss reagent B) for 10 minutes. The liquid transfer between each of the previously mentioned steps for the calibration curve is performed using the same pneumatic cycle (high frequency for air compression and low frequency for air expansion) as described for whole blood. Figure 6 shows the 550-nm absorbance peak values for each dilution aliquot. The linear correlation for the calibration points is high ($R^2 = 0.9997$).

Based on the so obtained standard calibration curve, it is possible to quantify the absolute nitrate/nitrite concentration level in whole blood. As depicted in Fig. 5 for the entire process, 100 µL of a free donor blood as well as the assay reagents were loaded to the disc prior to the spinning. We measured the absorbance for each concentration in triplicate. As shown in Figure 6, our donor presents a 7.4-µM nitrate level (the corresponding value in Figure 6 corresponds with a dilution 1:2 of the initial plasma). The range of nitrate concentrations in healthy population varies from 4.0 to 45.3 µM[20], so our donor enjoys a good health (at least regarding his nitrate levels).

Summary, conclusions & outlook

In this work, a novel centrifugo-pneumatic valving principle is introduced. The valving concept enables a powerful toolbox comprising modules for plasma extraction from whole blood, metering, coordination of parallel volume transfers, mixing and incubation with reagents. We successfully implemented a pilot assay by serial and parallel cascading of these modules on a centrifugal lab-on-a-disc platform. Liquid volumes can even share the same fluidic pathway. The centrifugo-pneumatic cascading obviates the need for surface treatment and hybrid

materials integration compared to conventional valving schemes, thus decisively reducing the complexity of system manufacture and assembly. This simplicity allows an easy transfer from the prototyping stage to production, using techniques such as hot embossing or injection molding.

As a proof of concept, the liquid handling protocol of a commercial nitrate/nitrite colorimetric detection was successfully implemented in a fully automated fashion. All the reagents, including blood are loaded in a single step prior to the start of the centrifugal spinning protocol. By customizing the chamber volumes and spinning frequencies, it is evident that the here presented, centrifugo-pneumatic toolkit will also leverage the implementation of a range of other assays on whole blood.

For proceeding towards a full-fledged, sample-to-answer point-of-care device, a low-cost optical detection unit can be added to the instrument.

Acknowledgment

This work has been supported in part by the FP-7 ENIAC programme CAJAL4EU, Enterprise Ireland under Grant No IR/2010/0002 and the Science Foundation of Ireland (Grant No 10/CE/B1821).

Notes and references

Biomedical Diagnostics Institute, National Centre for Sensor Research, School of Physical Sciences, Dublin City University, Ireland. Fax: +353-1-700-7873 ; Tel: +353-1-700-5377 ; E-mail:, jens.ducrée@dcu.ie, neus.godino@gmail.com

‡ Neus Godino is currently working at Fraunhofer IBMT, Potsdam, Germany; E-mail: neus.godino@ibmt.fraunhofer.de

†Electronic supplementary information (ESI) available: Analytical description, Geometry and operational parameters, Movie (Pneumatic cascade. mp4).

1. J. Ducrée, S. Haeberle, S. Lutz, S. Pausch, F. von Stetten and R. Zengerle, *Journal of Micromechanics and Microengineering*, 2007, **17**, S103-S115.
2. R. Gorkin, J. Park, J. Siegrist, M. Amasia, B. S. Lee, J. M. Park, J. Kim, H. Kim, M. Madou and Y. K. Cho, *Lab on a Chip*, 2010, **10**, 1758-1773.
3. R. Gorkin Iii, L. Clime, M. Madou and H. Kido, *Microfluidics and Nanofluidics*, 2010, **9**, 541-549.
4. Z. Noroozi, H. Kido, M. Micic, H. Pan, C. Bartolome, M. Princevac, J. Zoval and M. Madou, *Review of Scientific Instruments*, 2009, **80**.
5. J. Siegrist, R. Gorkin, L. Clime, E. Roy, R. Peytavi, H. Kido, M. Bergeron, T. Veres and M. Madou, *Microfluidics and Nanofluidics*, 2010, **9**, 55-63.
6. J. Steigert, T. Brenner, M. Grumann, L. Riegger, S. Lutz, R. Zengerle and J. Ducrée, *Biomedical Microdevices*, 2007, **9**, 675-679.
7. J. L. Garcia-Cordero, L. Basabe-Desmonts, J. Ducrée and A. J. Ricco, *Microfluidics and Nanofluidics*, 2010, **9**, 695-703.
8. H. Becker and C. Gärtner, *Analytical and Bioanalytical Chemistry*, 2008, **390**, 89-111.
9. M. C. R. Kong and E. D. Salin, *Analytical Chemistry*, 2010, **82**, 8039-8041.
10. K. Abi-Samra, L. Clime, L. Kong, R. Gorkin Iii, T. H. Kim, Y. K. Cho and M. Madou, *Microfluidics and Nanofluidics*, 2011, **11**, 643-652.
11. Z. Noroozi, H. Kido and M. J. Madou, *Journal of the Electrochemical Society*, 2011, **158**, P130-P135.
12. D. Mark, S. Metz, S. Haeberle, S. Lutz, J. Ducrée and R. Zengerle, *Lab on a Chip*, 2009, **9**, 3599-3603.
13. Z. Noroozi, H. Kido, R. Peytavi, R. Nakajima-Sasaki, A. Jasinskas, M. Micic, P. L. Felgner and M. J. Madou, *Review of Scientific Instruments*, 2011, **82**, 064303.
14. H. Hwang, H. H. Kim and Y. K. Cho, *Lab on a Chip*, 2011, **11**, 1434-1436.
15. B. S. Lee, Y. U. Lee, H. S. Kim, T. H. Kim, J. Park, J. G. Lee, J. Kim, H. Kim, W. G. Lee and Y. K. Cho, *Lab on a Chip* , 2011, **11**, 70-78.
16. A. Goch, M. Banach, D. P. Mikhailidis, J. Rysz and J. Henryk Goch, *Clinical and Experimental Hypertension*, 2009, **31**, 20-30.
17. R. G. Knowles and S. Moncada, *Biochemical Journal*, 1994, **298**, 249-258.
18. V. Matei, A. Rodríguez-Vilarrupla, R. Deulofeu, D. Colomer, M. Fernández, J. Bosch and J. C. Garcia-Pagán, *Hepatology*, 2006, **44**, 44-52.
19. H. Moshage, P. L. M. Jansen, G. Giovannoni and S. J. R. Heales, *Annals of Clinical Biochemistry*, 1998, **35**, 154-155.
20. H. Moshage, B. Kok, J. R. Huizenga and P. L. M. Jansen, *Clinical Chemistry*, 1995, **41**, 892-896.
21. H. Moshage, C. A. Stegeman and P. L. M. Jansen, *Clinical Chemistry*, 1998, **44**, 1780-1781.
22. M. Grumann, T. Brenner, C. Beer, R. Zengerle and J. Ducrée, *Review of Scientific Instruments*, 2005, **76**, 025101.
23. C. T. Schembri, T. L. Burd, A. R. Kopf-Sill and B. Braynin, *J. Autom. Chem.*, 1995, **17**, 99.
24. S. Haeberle and R. Zengerle, *Lab on a Chip*, 2007, **7**, 1094-1110.
25. S. Lai, S. Wang, J. Luo, L. J. Lee, S. T. Yang and M. J. Madou, *Analytical Chemistry*, 2004, **76**, 1832-1837.
26. D. Mark, S. Haeberle, G. Roth, F. von Stetten and R. Zengerle, *Chemical Society Reviews*, 2010, **39**, 1153-1182.
27. M. Grumann, A. Geipel, L. Riegger, R. Zengerle and J. Ducrée, *Chemical Engineering & Technology*, 2005, **28**, 613-616.
28. M. Grumann, J. Steigert, L. Riegger, I. Moser, B. Enderle, K. Riebeseel, G. Urban, R. Zengerle and J. Ducrée, *Biomedical Microdevices*, 2006, **8**, 209-214.
29. L. Riegger, M. Grumann, J. Steigert, S. Lutz, C. P. Steinert, C. Mueller, J. Viertel, O. Prucker, J. Rühe, R. Zengerle and J. Ducrée, *Biomedical Microdevices*, 2007, **9**, 795-799.
30. J. Steigert, T. Brenner, M. Grumann, L. Riegger, R. Zengerle and J. Ducrée, Design and fabrication of a centrifugally driven microfluidic disk for fully integrated metabolic assays on whole blood, *19th IEEE International Conference on Micro Electro Mechanical Systems (MEMS 2006)*, Istanbul, 2006.
31. J. Zhang, Q. Guo, M. Liu and J. Yang, *Journal of Micromechanics and Microengineering*, 2008, **18**, 125025.
32. R. Gorkin, M. Czugala, C. Rovira-Borras, J. Ducree, D. Diamond and F. Benito-Lopez, A wireless paired emitter detector diode device as an optical sensor for Lab-on-a-disc applications, *16th International Conference on Solid-State Sensors, Actuators & Microsystems (Transducers 2011)*, Beijing, 2011.
33. M. Grumann, M. Dube, T. Brefka, J. Steigert, L. Riegger, T. Brenner, K. Mittmann, R. Zengerle and J. Ducrée, Direct hemoglobin measurement by monolithically integrated optical beam guidance, *13th International Conference on Solid-State Sensors, Actuators & Microsystems (Transducers 2005)*, Seoul, 2005.
34. J. Steigert, M. Grumann, T. Brenner, L. Riegger, J. Harter, R. Zengerle and J. Ducrée, *Lab on a Chip*, 2006, **6**, 1040-1044.

C.3 Full Integration and Automation of Whole-Blood Bioassays by Centrifugo-Pneumatically Actuated Dissolvable Film Valves

This manuscript has been submitted to Lab on a Chip and is currently under review

Journal Name

Dynamic Article Links ►

Cite this: DOI: 10.1039/c0xx00000x

www.rsc.org/xxxxxx

ARTICLE TYPE

Full Integration and Automation of Whole-Blood Bioassays by Centrifugo-Pneumatically Actuated Dissolvable Film Valves

Charles E. Nwankire, Di-sien S. Chan, Jennifer Gaughran, Tríona O'Connell, Robert Burger, Robert Gorkin III, and Jens Ducrée[1]

Received (in XXX, XXX) Xth XXXXXXXXX 20XX, Accepted Xth XXXXXXXXX 20XX
DOI: 10.1039/b000000x

This paper presents a fully integrated and automated centrifugal microfluidic platform for multi-step, multi-reagent enzyme-linked-immunosorbent assays (ELISAs) based on advanced flow control by a novel valving scheme. These dissolvable film (DF) valves are merely rotationally actuated. At rest and under slow rotation, the sacrificial DF valves provide permanent liquid and vapour barriers. Once a critical burst pressure, that can be individually tuned in a typical range of equivalent spin rates between 1000 RPM and 5500 RPM, has been passed, the valves yield. This burst frequency is mainly defined by the radial position, geometry and volume of valve chamber and its inlet channel. We have successfully tested the barrier properties of the DF valves. Our novel DF valves thus also provide an advanced technique for on-board storage and well-controllable, complete release of liquid reagent volumes. As a proof of concept, we first show that these DF valves enable the full integration and automation of a 7-step ELISA for quantifying nitrate and nitrite levels in whole blood within about 15 minutes. The assay protocol encompasses the extraction of metered plasma, the controlled release of on-board stored reagents (enzymes, co – factors and fluorescent labels), incubation and detection. As a second application, we demonstrate a liver assay panel (LAP) for the detection of four liver function biomarkers on a single disc.

1. Introduction

Centrifugal microfluidic platforms have predominantly been applied in biomedical diagnostics, environmental monitoring and food safety testing[1-3]. A prominent advantage of these "lab-on-a-disc" systems is their robust liquid handling which is widely independent of the sample properties. The systems also excel with their comprehensive repertoire of high-performance laboratory unit operations (LUOs) for sample preparation such as sedimentation, lysis, metering, decanting, aliquoting, mixing and reagent storage[1-4]. Testing procedures such as common immunoassays consist of a multi-step sequence of such LUOs. In order to coordinate the timing of these protocols as well as to allow on-board storage and gating of several liquids handled in parallel, a sophisticated valving strategy needs to be implemented.

Such valving schemes are typically classified as passive or active. Common passive valves on centrifugal platforms are capillary barriers such as hydrophobic constrictions and hydrophilic expansions. These capillary burst valves yield once the surface-tension mediated capillary retention mechanism is superseded by the centrifugal force at enhanced spin rates[5]. While conceptually rather simple, the range of practically achievable burst frequencies is quite narrow, thus severely limiting the number of independently controllable LUOs, i.e. assay steps, which can be concatenated on a disc substrate. Another frequently used passive valving scheme on centrifugal platforms is siphoning. While able to withstand high centrifugal frequencies, siphoning relies on the hydrophilicity for priming the siphon channel. Long-term stable hydrophilization is an issue in polymer microfabrication. It is also hard to selectively open a specific siphon in a parallel arrangement, so a more complex serial siphoning approach has been proposed[6]. Overall, capillary burst valves as well as siphoning lack the barrier properties required to suppress vapour spreading of on-board stored reagents during shelf life.

Hwang *et al* evaluated the use of elastomeric membrane valves[7]. The elastomeric membrane was formed by spin coating PDMS onto a polycarbonate sheet. It was shown that as the rotational frequency of the disc is increased the membrane valves deflect, thus allowing liquid flow through the valve site. The ability of these passive valves to be merely actuated by the disc rotation gives them an edge over other types of active valves. However, a challenging issue is how to assure complete release of the reagent aliquot stored upstream of the valve as the centrifugally induced pressure head driving the membrane deflection vanishes with the depletion of the reservoir. Also the behaviour of the membranes when in contact with liquids for longer periods of time might be problematic. If the membranes prematurely absorb liquid, they may alter the elastic properties of the valve. Active valves are controlled by second control mechanism which is independent of the rotational motion. Active valving schemes often used in lab-on-a-disc systems involve a sacrificial material like a polymer film or wax[2, 3]. This way valves can be actuated independently from transient spin rates and locations of the valves with respect

to the centre of rotation. The sacrificial membrane even provides a liquid and vapour barrier during shelf-life. However, the actuation of these valves may necessitate stopping the disc and requires additional, typically instrument-based components, such as strong lasers, to melt the barrier material, thus making the instrumentation more complex and costly.

The eventual choice of the valving strategy is guided by the level of process integration and automation that can be pursued. The simplest approach is to load reagents on demand as they are needed in the assay protocol[1]. The valves in this case need to function during the rather short, minute-scale processing routine, only. Nevertheless, as reagents are hard to add to disc-based inlet ports during rotation, this method implies a stop-and-go rotational protocol which would involve a number of interspersed, rather cumbersome manual pipetting steps or advanced liquid handling automation on the instrumentation side. Furthermore, uncontrolled spreading of on-board liquids, e.g. through prevalent capillary action, is difficult to contain during the halt of the disc. So while this approach is feasible during development of the microfluidic chip, it lacks the user-friendliness and cost-efficiency typically imposed on point-of-care platforms.

The second level of process automation is to preload the sample and all reagents just before starting the centrifugal protocol. This scheme clearly enhances the ease of operation as, once the disc is furnished with the sample and reagents, the assay can run unattended. Also unwanted liquid spreading is suppressed as all on-board liquids may continuously be exposed to the centrifugal control force. The requirements on the involved valving mechanism are somewhat enhanced compared to the previous stop-and-go protocol as the valves need to hold back reagents during the initial sample processing phase, which typically involves high-frequency centrifugation. Furthermore, this approach still leaves issues of error prone reagent logistics and system setup procedures which are undesirable in a typical point-of-care environment.

Some fully integrated and automated centrifugal platforms have been proposed over the years[1, 2, 8, 9]. For example, Steigert *et al*[3] showed a fully automated assay protocol on a disc for the detection of alcohol in whole blood. The authors implemented passive valving (capillary and hydrophobic stops) techniques which accurately determined the level of alcohol from a metered, 500-nL blood volume. However, while working in this simple assay protocol, the surface-tension based valving principle limits storage time of the disposable microfluidic cartridge and, even more, restricts the number of discrete burst frequencies required for concatenating more complex assay protocols. Similar issues arise in the above mentioned serial siphoning approach which also involves the highly reliable hydrophilization of channels including intermittent geometrical expansions[6].

Therefore active valves based on sacrificial barrier materials are increasingly employed for bioassay protocols on a disc[2, 4, 7, 10]. Recently, Lee *et al* demonstrated a fully integrated and automated centrifugal platform for the detection of Hepatitis B virus[2]. The authors implemented active ferrowax valves, which were sequentially opened using a low intensity laser light. Immunoassays and other biochemical tests from whole blood were carried out within minutes. Although this system is highly innovative, a laser is necessary to actuate the valves and wax has to be introduced into the microfluidic disposable, thus adding further complexity to the system concept.

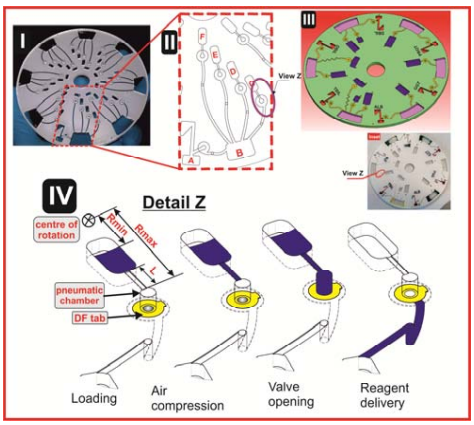

Fig. 1: I) Image of a fully assembled nitrite/nitrate assay disc platform showing the 8 parallel assay structures on the disc, 1 for the sample plus 7 co-running calibration standards. II) Enlarged segment of a single-assay structure featuring blood separation (A), reaction chamber (B) and (C – F) reagent storage chambers. III) 3D rendered illustration of the liver assay panel (LAP) disc platform showing the six independent assay structures (Inset shows a fully assembled LAP disc) IV) Schematic of the DF valving technique with a sequence of sample loading, air compression, layer inversion / valve opening and reagent delivery through valve site.

Lately, Godino *et al*[11] have fully integrated and automated a multi-step bio-assay through a so-called centrifugo-pneumatic cascade on a lab-on-a-disc platform. Multi-liquid flow control of the sample and several pre-loaded reagents is achieved solely through rotational actuation of siphons, i.e. without the need for surface modification or geometrical microfeatures. Instead, the siphons are primed by the expansion of centrifugally compressed air pocket upon reduction of the spin speed. While the centrifugo-pneumatic platform boasts very simple flow control, the open-channel structure does not provide a vapour barrier for on-disc reagent storage.

We will here introduce a “plug-and-play” strategy which widely eliminates the need for cumbersome manual or instrumentally complex pipetting. For the first time, all assay reagents are stored on the disc and released on-demand by the system-intrinsic rotational actuation. This will on the one hand guarantee direct, off-the-shelf use for maximum user convenience. On the other hand, we will keep the complexity of instrumentation at a minimum as the reagents are released upon a simple change of the frequency of rotation.

Our assay integration is based on a recently developed, centrifugo-pneumatic valving technique based on water-dissolvable films (DFs)[12] that provides the physical, vapour-proof gating of sacrificial valves while being actuated through mere passive rotation. Here we present two fully integrated and automated centrifugal microfluidic platforms. The first platform (Fig 1I) performs blood separation and sequential release of four

different reagents. In addition to blood separation, the second platform also carries out the sequential release of eight assay reagents (Fig. 1III). Below a critical burst pressure scaling with the square of the spinning frequency, liquid is kept at bay from the valve site by means of a flow induced air pocket above the gas sealing valve until a critical burst pressure is reached. Beyond critical burst frequency, the metastable inverse gas-liquid stack flips to its low-energy state, i.e. the heavier liquid resides farther away from the centre of rotation than the gas. The liquid then enters the pneumatic compression chamber to contact and dissolve the DF membrane and then protrude into the downstream reaction chamber (see Fig. 1IV). All the assay steps were purely controlled by automatically varying the rotational frequency of the disc.

2. Materials and methods

2.1 Design and fabrication of the disc platform

We documented the details of fabricating, assembling and embedding DF plugs in our previous work[12]. In brief, the disc consists of 5 layers: 3 layers of 1.5-mm thick poly (methylmethacrylate) (PMMA) sheets (Radionics, Ireland) and 2 layers of ~90-µm thick pressure sensitive adhesives (PSA) from Adhesives Research, Ireland. A series of design iterations was assisted by the CAD software SolidWorks (Solid Solutions, Ireland). The optimised disc design with chambers and access holes was machined using a Zing CO_2 laser cutter (Epilog Laser, USA).

The chambers were tailored to the desired reagent volume. The pneumatic chambers are 4 mm in diameter. The exit channel from the blood separation chamber (Chamber A, Fig. 1II) has been designed so as to fundamentally prevent leakage of whole blood into the pneumatic chamber. The microchannels were defined in the PSA using a Craft ROBO knife cutter (Graphtec Corp, USA). The microchannels are 0.6 mm wide. The hybrid DF valve tabs were fabricated by firstly cutting 1-mm diameter through holes in the PSA, and then rolling the ~20-µm DFs (also supplied by Adhesives Research, Ireland) on the PSA, in order to cut out a ∅3.5-mm outline. After placing the DF tabs at the designated valve locations, the 5-layered discs (Fig 1I) are assembled using a standard hydraulic laminator.

2.2 Biological assays

We demonstrate the high application potential of this new centrifugal valving technique by fully automating two homogeneous assays through a rotational frequency protocol. The first assay is a fluorometric nitrate / nitrite assay (Cambridge Biosciences, UK), the second a colorimetric liver assay panel.

One motivation of the nitrate/nitrite assay is that it has been shown that elevated nitrate level in infants (< 6 months old) could lead to shortness of breath and blue baby syndrome[13]. Another motivation is that in the event of an accident, increased nitrate levels in the blood plasma and some tissues may also indicate traumatic brain injury[14].

Nitric oxide (NO) undergoes a series of reactions with several biological fluids. The final products of NO *in vivo* are nitrate (NO^-_3) and nitrite (NO^-_2). However, their proportion in whole blood is small, so it is more common to determine the total NO^-_3 + NO^-_2 and then NO^-_2 separately; and then calculate NO^-_3 from the difference. This assay kit we used provides an accurate measurement of total nitrate / nitrite concentration in a 2-step process. The first step is the conversion of NO^-_3 to NO^-_2 utilising nitrate reductase. The second step is the addition of diaminonapthalene (DAN), provided as an acidic solution forming a product known as 1(H) naphthotriazole. NaOH solution is then added to the 1(H) naphthotriazole in order to enhance its fluorescence and to stop the enzymatic reaction.

Measurement of the fluorescence of this compound accurately determines the NO^-_2 concentration. Similarly, upon addition of the enzyme cofactor, the total NO^-_2 + NO^-_3 content was determined. The NO^-_3 content was then obtained by subtracting the NO^-_2 content from the total NO^-_2 + NO^-_3 content. Both calibration curves were generated by following the user manual of the commercial assay protocol. A simplified schematic representation of this homogeneous assay is given in Fig. 2.

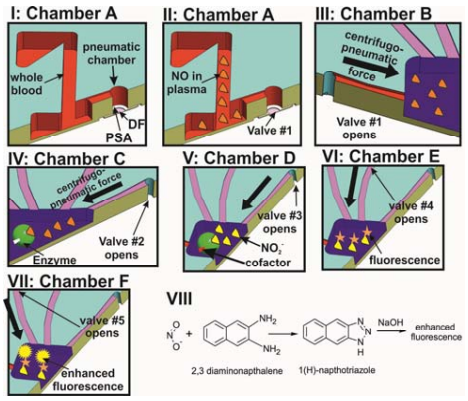

Fig.2: Schematic illustration of the homogeneous nitrate/nitrite assay showing the liquid-handling protocol and actuation of the DF valves I) the pneumatic air compression chamber, DF tab with PSA support II) blood plasma separation and plasma containing NO III) valve #1 opens and releases the extracted plasma with NO to the reaction (rxn) chamber IV) valve #2 opens, delivering the enzyme (nitrate reductase) to the rxn chamber. The enzyme is involved in the "key and lock" enzymatic reaction with NO V) valve #3 opens, delivering the enzyme cofactor to the rxn chamber. The enzyme cofactor activates the enzyme, thus triggering the conversion of NO to NO_2^- VI) valve #4 opens, releasing DAN reagent to the rxn chamber. This reagent reacts with NO_2^- to form a fluorescent product VII) valve #5 opens and releases NaOH to the rxn chamber, which then stops the enzymatic reaction and also enhances the fluorescence VIII) the reaction equation of the nitrate / nitrite formation chemistry.

In a homogeneous immunoassay, the antibodies, antigens and labelled antigens are mixed. The unbound and antibody-bound marked antigens can be distinguished by a change of activity of the marker when coupled. In this assay, the nitrate reductase reagent reduces the nitrate in the plasma to nitrite, when they are mixed. After this reduction reaction, the enzyme cofactor cross-links with the nitrite and makes it an active enzyme which is fluorescently tagged by the DAN reagent. Addition of the NaOH solution enhances the fluorescence and the analyte is ready for detection. This reaction equation is given in Fig. 2VIII. A read-

out is then performed off-chip on a fluorescence analyser (NanoDrop 3300 Fluorospectrometer, Thermo Scientific, Ireland). The excitation wavelength was set at 360 nm – 365 nm, and emission wavelengths at 430 nm.

A vital motivation for integrating the LAP on this new platform is a recent report that shows a marked increase in medication-induced liver toxicity[15]. It was also suggested that the death risk of patients taking antiretroviral medicines due to drug toxicity was similar to that from AIDS itself. In this work, we have integrated this common LAP on our DF–based centrifugal microfluidic platform (see Fig. 1III). A range of four bio-markers is run concurrently for monitoring liver function: Albumin (ALB), alkaline phosphatase (ALP), total (TBIL) and direct (DBIL) bilirubin. A conventional assay kit was purchased (Randox Life Sciences, UK), the volumes downscaled and the protocol optimised for our DF–based lab-on-a-disc platform. To comply with the assay kit, blood samples were collected in serum vacuum tubes.

2.3 Testing of the lab-on-a-disc platform

For the nitrate/nitrite assay, the microfluidic discs are designed to concurrently run eight simultaneous tests (see Fig. 1I), e.g. seven calibration standards, and one biological sample. All samples and reagents are pre-loaded on the disc before taking it to the centrifugal test stand. The disc also holds 70 µl of assay buffer and whole blood in chambers A and B, respectively. 10 µl of nitrate reductase, enzyme cofactor and DAN reagents are loaded into chambers C, D and E, respectively, and finally 20 µl of NaOH solution is loaded in chamber F.

For the LAP comprising of four concurrent assays, the calibration curves for the assays are obtained from different discs. A 50-µl aliquot of whole blood is loaded into each of the four blood separation chambers. These separation chambers have been designed so as to release 10 µl of serum through the DF valve site into the reaction chambers.

The centrifugal test stand, which has been fully described in previous work[12, 16] comprises of a computer-controlled motor and a stroboscopic light for imaging a chosen area on the disc during rotation. The steps involved in these assays are sample metering, blood separation, plasma metering and extraction, sequential reagent delivery, mixing and, again, reagent delivery. The centrifugal force provides the pumping pressure for the liquid reagents.

2.4 Centrifugo – pneumatic actuation of the DF valves

The normally-closed DF valve follows a centrifugo-pneumatic principle[12]. While the disc is at rest, liquid reagent in the reservoir is restrained by a combination of the capillary and surface tension forces at the entrance of the microchannel. Rotation at the angular velocity ω induces a pressure head

$$\Delta p_\omega = \rho \bar{r} \Delta r \omega^2 \qquad (1)$$

(see Fig. 1IV) where ρ is the liquid density, ω is the angular velocity of the rotating disc, $\bar{r} = (R_{\max} + R_{\min})/2$ is the characteristic distance of the liquid element from the centre of rotation, while $\Delta r = R_{\max} - R_{\min}$, is the radial height of the liquid column. The advancing meniscus stops as Δp_ω is balanced by pressure in the valve chamber

$$p = p_0 \frac{1}{1 - \Delta V / V_0} \qquad (2)$$

as obtained by Boyle's law. In equation (2), p_0 is the ambient pressure, V_0 is the (full) chamber volume and ΔV is the gas volume reduction due to the protruding liquid meniscus[17].

The meniscus in this metastable, inverted-layer configuration is stabilized by the surface tension. As the centrifugal pressure head Δp_ω (1) increases, the liquid plug can proceed farther into the compression chamber, thus making it more difficult for the surface tension to sustain the "hanging" liquid volume ΔV. At the so-called burst frequency, the liquid plug disrupts to invert the metastable liquid-gas configuration. Liquid thus penetrates unimpeded into the pneumatic chamber to dissolve the DF and hence fully open the valve.

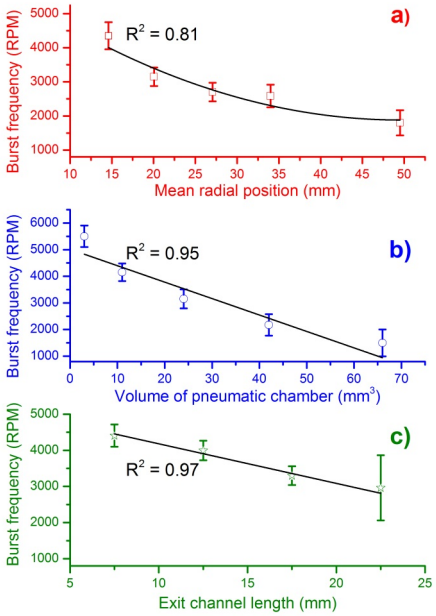

Fig. 3: Graph demonstrating: Decrease in burst frequency as (a) the radial position of the DF valve on the disc platform increases, (b) as the volume of the compressed air increases (2) and (c) as the exit channel length increases (2).

For a given, rotationally induced pressure head Δp_ω (1), the distance the plug can protrude into the compression chamber (and the displaced air volume ΔV) until Δp_ω (1) balances the counter pressure p (2) increases with the dead volume of the chamber V_0. In other words, the fluidic capacitance defined by volume change ΔV induced by a given pressure change p (2) increases with V_0. As the "burst" is induced towards increasing ΔV, the burst frequency tends to shrink with increasing chamber volume V_0.

3. Results and Discussion

3.1 Rotational automation of bio-assays

All valves are initially in a closed state until their individual centrifugal critical burst pressure is reached, at which the valve yields and liquid is pumped onward for further processing. The measurements in Fig. 3 verify the three main experimental impact parameters on the burst frequency:

a) Mean radial position $\bar{r}$ of the liquid plug (and thus also the valve) on the disc. According to (1), the centrifugal force increases with the radial distance from the centre of rotation, thus the valves which are located more radially outward are slated to be actuated first (Fig. 3a).

b) Volume of the pneumatic chamber V_0. According to (2), the larger the volume of the compressed air, the lower the centrifugal burst pressure as illustrated in Fig. 3b.

c) Exit channel length, L (see Fig 1III). According to (1), extending the length of the liquid plug acting on the pneumatic chamber will decrease the burst frequency, and thus the burst pressure of the DF valve as shown in Fig 3c. It should be noted that at increased channel lengths (e.g. 22.5 mm), the DF valve actuation became unstable.

Consequently, the rotational burst frequency as the central control parameter for all (liquid bearing) valves on the centrifugal platform can be specifically tailored over a wide range. Figure 4 for the first time demonstrates the spin protocol of a fully integrated, merely rotationally actuated, 7-step bio-assay protocol. Each valve is colour-coded in order to highlight the time course of the rotational burst frequency and the pressure head as deduced from (1). The plot in Fig. 4a references the pressure heads of each valve (1) to their respective burst pressures. The sequential crossing of the horizontal ($y = 1$)-line, corresponds to a valve opening, i.e. the point where p (1) exceeds the critical pressures $p_{i,\mathrm{crit}}$ of each valve i.

Figure 4a demonstrates the sequential actuation of the DF valves 1 to valve 5 to fully integrate and rotationally automate the homogeneous nitrate/nitrite bioassay including blood separation, plasma extraction and sequential release of four different reagents. Figures 4b shows the absolute pressure heads as a function of the spin protocol expressed in terms of rotations per minute (RPM) displayed in Fig. 4c.

The first step is to meter the whole blood sample, by spinning the disc at 600 RPM for 1 min, leaving 65 µl of blood in chamber B. The disc is then spun at 1200 RPM for 3 min to sediment the red blood cells and separate plasma. After this plasma separation step, the rotational frequency is increased to 2100 RPM in order to open valve #1, thus releasing 10 µl of plasma into chamber B (reaction chamber), which has already been preloaded with 70 µl of assay buffer (see Fig 1ii & Fig. 2). The enzyme in chamber C is released into the reaction chamber at 2700 RPM, while the cofactor is added to the same chamber at 2850 RPM. At this stage the assay requires an incubation step to sufficiently mix plasma + assay buffer + enzyme cofactor + nitrate reductase. To this end the disc was alternatingly spun in a clockwise and anticlockwise sense of rotation at an amplitude of 600 RPM for 3 min[18].

Upon increasing the rotational frequency to 3300 RPM, the DAN reagent was released from chamber E into the reaction chamber. Subsequently, NaOH was added to the same reaction chamber at a frequency of 3900 RPM from chamber F. The NaOH solution terminates the enzymatic reaction and also amplifies the fluorescence signal.

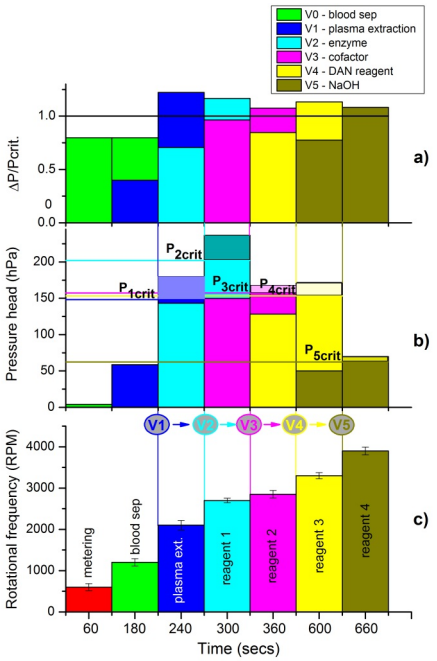

Fig. 4: A graph demonstrating for each DF valve: a) ratio of the pressure to the burst pressure b) rotationally induced pressure heads and burst pressures indicated as horizontal lines and c) corresponding rotational burst frequencies. The crossings of the same-coloured horizontal lines an (a) and (b) illustrate the sequential opening of the valves.

The procedure for the nitrite assay is very similar. In this case, only 10 µl of the DAN reagent and 20 µl of NaOH are used. The DAN reagent and NaOH solution are sequentially released into the reaction chamber while the disc spun at 2700 RPM and 2900 RPM, respectively, after which 3 minutes of on-disc incubation is carried out by using the vigorous, "shake-mode" mixing at ±600 RPM.

A schematic representation of the liquid handling procedure and the image frame sequence of this process are detailed in Fig. 5A – B. In order to enhance the contrast, coloured food dye was used for this demonstration. The full video of this centrifugally automated immunoassay with all assay reagents including blood separation and plasma extraction processes can be found in **ESI.1**. As a proof-of-concept for the LAP platform, we were able to run four assays in parallel – ALB (1 reagent), ALP, DBIL (2 reagents each) and TBIL (3 reagents). All assay reagents and the blood samples are preloaded into their respective chambers (Fig 1III).

Journal Name

Dynamic Article Links ►

Cite this: DOI: 10.1039/c0xx00000x

www.rsc.org/xxxxxx

ARTICLE TYPE

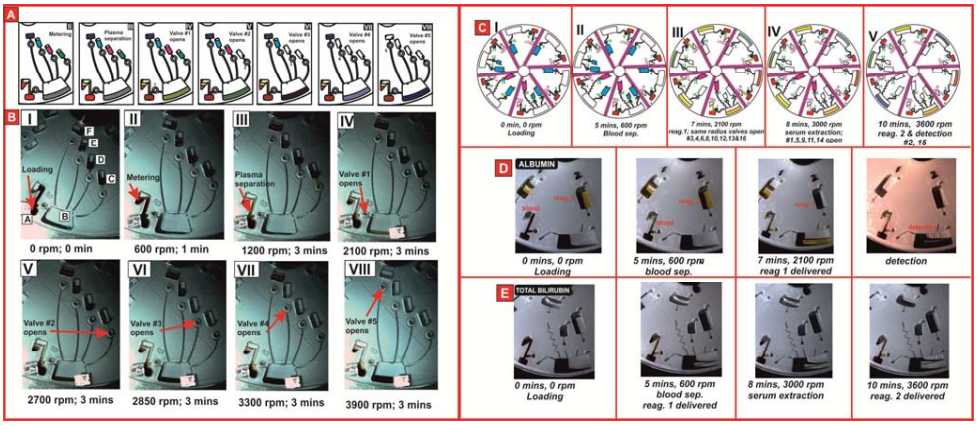

Fig 5: A) Nitrate/Nitrite assay platform – schematic representation of the blood plasma separation and sequential reagent delivery B.i) frame sequence of the DF valving technique demonstrating pre-loaded reagents and fresh whole blood sample ii) metering iii) blood plasma separation iv) valve #1 opening and plasma extraction v) valve #2 opens after 10 mins vi) valve #3 opens after 13 mins vii) valve #4 opens after 16 mins viii) valve #5 opens after 19 mins and then detection C. i) Liver assay panel platform - schematic representation demonstrating the sample loading ii) blood sep. iii - iv) sequential reagent release at 40-mm and 20-mm radii, respectively. D - E) frame sequence of ALB and TBIL assays.

The disc has been designed such that the reagents delivered simultaneously are placed at the same radius (Fig. 5C). A schematic representation and frame sequence of the disc operation are given in Fig. 5C – E. Briefly, the disc is spun at 600 rpm for 5 min for blood separation, after which the disc rotation is increased to 2100 rpm for another 2 min to release the assay reagents located at the 40-mm radius. After ramping up to 3000 rpm, serum is released into the reaction chamber. Incubation is then advectively enhanced by spinning the disc in a clockwise and anti-clockwise direction between ±600 rpm for 3 min. The rotational frequency is then increased to 3600 rpm and spun for another 2 min to release the reagents located at the 20-mm radius. At this stage of development focusing primarily on the microfluidic assay integration, colorimetric detection is carried out off-chip on a UV-Vis analyser. At a later stage, common techniques for on-chip absorption measurements may be implemented through known concepts[3, 19].

3.2 Assay results

As this paper focuses on the fluidic automation aspect of a multi-step assay protocol, we decided to leave separate issue of the integration of an optical detector onto the instrument to a later stage. For now the final detection steps are carried out off-chip on the NanoDrop Fluorospectrometer and NanoDrop UV-Vis spectrophotometer (both Thermo Scientific, Ireland) for the nitrate/nitrite assay and the LAP panel, respectively. A 2-µl sample of the end product is taken from the disc-based reaction chamber, placed on the NanoDrop pedestal for analysis.

As shown in Figure 6I, the unknown concentration of nitrate and nitrite in the blood of two anonymous donors has been determined. A fresh whole blood sample was obtained and used on the same day. The control assay was initially carried out on a 96-well plate, and later implemented on the automated disc platform. For blood donor A, the levels of nitrite and nitrate are 8.7 µM and 20.7 µM respectively. For blood donor B, the nitrate and nitrite levels are 5.4 µM and 10.7 µM, respectively. These levels of nitrite and nitrate are well within the normal reported clinically relevant range of 1.3 – 13 µM for nitrite and 4 µM – 45.4 µM for nitrate[20]. As further shown in Fig. 6I, the high R^2 of the linear regression indicates a good correlation between the data obtained from the standard well plate and that obtained from this innovative automated disc platform. The calibration curves for the LAP on the DF–based centrifugal platform are given in Fig. 6II. For validation purposes, this liver assay was also carried out on whole blood from the same donor on the same day on a well plate and in a local hospital. The results detailed in Table 1 demonstrate a 6.8% CV between the three test platforms.

Table 1 Comparison of liver assay on different platforms

	Well plate	Disc platform	Hospital	Normal range
ALB (g/L)	48.8 ± 3.1	48.1 ± 3.7	43	35 - 50
ALP (U/L)	113.7 ± 7	112.7 ± 9	109	30 - 130
TBIL (µM)	6.4 ± 0.5	7.5 ± 0.9	5	5 - 24.0

Journal Name

Dynamic Article Links ►

Cite this: DOI: 10.1039/c0xx00000x

www.rsc.org/xxxxxx

ARTICLE TYPE

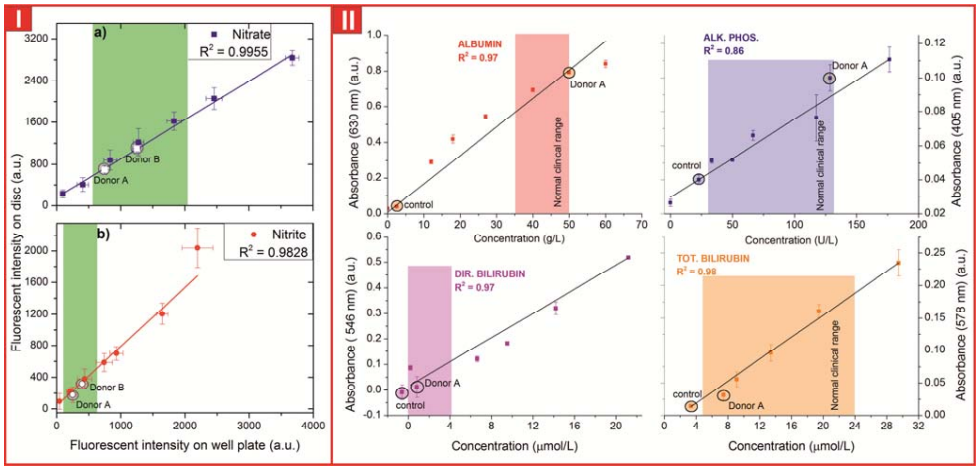

Fig. 6: Calibration curves for I) (a) Nitrate and (b) nitrite assays obtained from a standard 96-well plate and the automated disc platform showing the good correlation between both results. The highlighted region is the normal range of nitrite and nitrate levels for adults, and the results obtained using this assay from two anonymous blood donors (A & B) are also indicated on this graph. II) Calibration curves for the ALB, ALP, DBIL and TBIL. Control tests and whole blood sample result from an anonymous donor is also shown.

3.3 Reagent storage with the DF valves

In order to validate the potential of the DF barriers for reagent storage, liquids have been placed in the chambers, and the disc was enclosed in a heat seal bag and stored in the fridge at ~4 ˚C for a period of 7 days (**ESI.2**). The aim is to assess the integrity of the valving technique after this storage period. After 7 days of storage, the disc was taken out, examined and spun on the spin stand. It was observed that liquid droplets had leaked into the pneumatic chamber of the section of the disc without the centrifugo-pneumatic DF valves, while the sections with DF valves remained sealed.

4. Conclusion and Outlook

Leveraged by the broad range and sharp definition of burst frequencies, we have for the first time integrated and automated a comprehensive, 7-step bioassay protocol including plasma separation and the sequential release of 4 on-board stored liquid reagents by our novel, merely rotationally actuated DF-based centrifugo-pneumatic valving scheme. We experimentally verified that the DF valves yield at a well-defined burst pressure which can be tailored over a wide range of equivalent spin rates by the radial position of the valve on the disc, the volume of the entrapped air in the pneumatic compression chamber and the geometry of their inlet channel.

As a pilot application, we chose the detection of nitrate/nitrite and a liver assay panel starting at clinically relevant concentrations in whole blood. The results were in good quantitative agreement with the same assay carried out on a regular well plate and in a clinical lab.

Regarding the potential use of DF valves for on-board storage of liquid reagents, we successfully validated the vapour-barrier properties of the DF valves. Further studies are to be undertaken in order to test and optimize the long-term stability of the DF valves which might be further enhanced, e.g. by optimizing their formulation or common (surface) treatments. Future work will focus on integrating and parallelizing a range of multi-step assay protocols based on this novel, rotationally controlled centrifugal valving scheme and integrating the on-chip readout.

Acknowledgement

This work was supported by the Science Foundation Ireland under grant 10/CE/B1821.

References

1. S. Lai, S. Wang, J. Luo, J. L. Lee, S.-T. Yang and M. Madou, *Analytical Chemistry*, 2004, **76**, 1832 - 1837.
2. B. S. Lee, J.-N. Lee, J.-M. Park, J.-G. Lee, S. Kim, Y.-K. Cho and C. Ko, *Lab on a Chip*, 2009, **9**, 1548-1555.
3. J. Steigert, M. Grumann, T. Brenner, L. Riegger, J. Harter, R. Zengerle and J. Ducree, *Lab on a Chip*, 2006, **6**, 1040-1044.

4. J. L. Garcia-Cordero, F. Benito-Lopez, D. Diamond, J. Ducree and A. J. Ricco, *IEEE*, 2009.
5. J. Ducrée, S. Haeberle, S. Lutz, S. Pausch, F. v. Stetten and R. Zengerle, *Journal of Micromechanics and Microengineering*, 2007, **17**, S103-S115.
6. J. Siegrist, R. Gorkin, L. Clime, E. Roy, R. Peytavi, H. Kido, M. Bergeron, T. Veres and M. Madou, *Microfluidics and nanofluidics*, 2010, **9**, 55-63.
7. H. Hwang, H.-H. Kim and Y.-K. Cho, *Lab on a Chip*, 2011, **11**, 1434-1436.
8. H. He, Y. Yuan, W. Wang, N.-R. Chiou, A. J. Epstein and L. J. Lee, *Biomicrofluidics*, 2009, **3**, 022401-022417.
9. N. Honda, U. Lindberg, P. Andersson, S. Hoffmann and H. Takei, *Clinical chemistry*, 2005, **51**, 1955.
10. J. L. Garcia-Cordero, D. Kurzbuch, F. Benito-Lopez, D. Diamond, L. P. Lee and A. J. Ricco, *Lab on a Chip*, 2010, **10**, 2680-2687.
11. N. Godino, R. Gorkin, A. Linares, V. and J. Ducrée, *Lab on a Chip*, 2012, **under review**.
12. R. A. Gorkin, C. Nwankire, J. Gaughran, X. Zhang, G. Donohoe, G., M. Rook, R. O'Kennedy and J. Ducree, *Lab on a Chip*, 2012, **DOI: 10.1039/c2lc20973j**.
13. C.-W. Liu, C.-N. Lin, C.-S. Jang, M.-P. Ling and J.-W. Tsai, *Environmental Geochemistry and Health*, 2011, **33**, 503-514.
14. A. M. Rao, A. Dogan, J. F. Hatcher and R. J. Dempsey, *Brain Research*, 1998, **793**, 265-270.
15. S. J. Vella, P. Beattie, R. Cademartiri, A. Laromaine, A. W. Martinez, S. T. Phillips, K. A. Mirica and G. M. Whitesides, *Analytical Chemistry*, 2012.
16. M. Grumann, T. Brenner, C. Beer, R. Zengerle and J. Ducree, *Rev Sci Instrum*, 2005, **76**, 025101-025101-025106.
17. D. Mark, T. Metz, S. Haeberle, S. Lutz, J. Ducrée, R. Zengerle and F. von Stetten, *Lab on a Chip*, 2009, **9**, 3599.
18. M. Grumann, A. Geipel, L. Riegger, R. Zengerle and J. Ducree, *Lab on a Chip*, 2005, **5**, 560-565.
19. M. Grumann, J. Steigert, L. Riegger, I. Moser, B. Enderle, K. Riebeseel, G. Urban, R. Zengerle and J. Ducrée, *Biomedical Microdevices*, 2006, **8**, 209-214.
20. H. Moshage, B. Kok, J. R. Huizenga and P. Jansen, *Clinical chemistry*, 1995, **41**, 892.